



BRNO UNIVERSITY OF TECHNOLOGY

VYSOKÉ UČENÍ TECHNICKÉ V BRNĚ

FACULTY OF ELECTRICAL ENGINEERING AND COMMUNICATION

FAKULTA ELEKTROTECHNIKY A KOMUNIKAČNÍCH TECHNOLOGIÍ

DEPARTMENT OF PHYSICS

ÚSTAV FYZIKY

COMPREHENSIVE ANALYSIS AND EXPERIMENTAL STUDIES ON POLYMERS WITH EMPHASIS ON PVDF

KOMPLEXNÍ ANALÝZA A EXPERIMENTÁLNÍ STUDIE POLYMERŮ S DŮRAZEM NA PVDF

HABILITATION THESIS

HABILITAČNÍ PRÁCE

AUTHOR

AUTOR PRÁCE

Mgr. et Mgr. Rashid Dallaev, Ph.D.

BRNO 2024

Abstract

This habilitation thesis explores the dynamic and evolving field of polymer science, with a particular emphasis on polyvinylidene fluoride (PVDF) materials and their modifications. The thesis is structured into two primary sections. The first section comprises comprehensive reviews of self-healing polymers and their mechanisms, such as microcapsules and crack healing, as well as an overview of epoxies in electronics, highlighting their significance and applications.

The bulk of the thesis is dedicated to the in-depth study of PVDF materials. This includes a series of experimental investigations where PVDF is modified with various additives, including carbon nanotubes, nitrate salts, and carbon flakes. These modifications aim to enhance the properties of PVDF for diverse applications. The modified PVDF samples are subjected to thorough characterization using advanced analytical techniques such as X-ray Photoelectron Spectroscopy (XPS), Scanning Electron Microscopy (SEM), Raman Spectroscopy, X-ray Diffraction (XRD), Secondary Ion Mass Spectroscopy (SIMS), and Fourier Transform Infrared Spectroscopy (FTIR).

The findings provide valuable insights into the structural, chemical, and physical changes induced by these additives, offering a deeper understanding of how such modifications can optimize PVDF for specific uses. This thesis not only advances the current knowledge of PVDF-based materials but also contributes to the broader field of polymer science by exploring the integration of functional additives and their impact on polymer performance.

Abstrakt

Tato habilitační práce zkoumá dynamickou a rozvíjející se oblast vědy o polymerech se zvláštním důrazem na polyvinylidenfluoridové (PVDF) materiály a jejich modifikace. Práce je strukturována do dvou hlavních částí. První část obsahuje komplexní přehledy samoopravných polymerů a jejich mechanismů, jako jsou mikrokapsle a hojení trhlin, a také přehled epoxidů v elektronice, zdůrazňující jejich význam a aplikace.

Převážná část práce je věnována hloubkovému studiu PVDF materiálů. To zahrnuje řadu experimentálních výzkumů, kde je PVDF modifikován různými přísadami, včetně uhlíkových nanotrubic, dusičnanových solí a uhlíkových vloček. Cílem těchto úprav je zlepšit vlastnosti PVDF pro různé aplikace. Modifikované PVDF vzorky jsou podrobeny důkladné charakterizaci pomocí pokročilých analytických technik, jako je rentgenová fotoelektronová spektroskopie (XPS), rastrovací elektronová mikroskopie (SEM), Ramanova spektroskopie, rentgenová difrakce (XRD), sekundární iontová hmotnostní spektroskopie (SIMS), a infračervená spektroskopie s Fourierovou transformací (FTIR).

Zjištění poskytují cenné poznatky o strukturálních, chemických a fyzikálních změnách vyvolaných těmito přísadami a nabízejí hlubší pochopení toho, jak takové modifikace mohou optimalizovat PVDF pro konkrétní použití. Tato práce nejenže rozšiřuje současné znalosti o materiálech na bázi PVDF, ale také přispívá k širší oblasti vědy o polymerech zkoumáním integrace funkčních přísad a jejich vlivu na výkonnost polymerů.

Keywords: PVDF, modification, doping, characterization, self-healing polymers, epoxies

Klíčová slova: PVDF, modifikace, doping, charakterizace, samoopravné polymery, epoxidy

Preface

Over the past several years, the applicant has authored or co-authored a significant number of papers on the topic of this habilitation thesis. Thus, it was decided that this thesis would be best presented as a compilation of these papers. Each paper will be prefaced with a brief one-page commentary discussing the motivation behind the study, the conclusions drawn, the author's contributions, and relevant paper metrics. Given that each paper already includes specific and comprehensive introductions and state-of-the-art discussions, additional text outside the papers will be kept to a minimum. This format ensures that the thesis remains focused and cohesive, leveraging the detailed and specific content already present in the individual publications.

This comprehensive body of work spans a wide range of polymeric materials, with a primary focus on polyvinylidene fluoride (PVDF). Hence, the thesis is divided into two major parts, each comprising four papers, for a total of eight papers. The first part consists of extensive review papers authored by the applicant, covering a broad spectrum of polymeric materials, with a particular emphasis on PVDF in the last two papers. These reviews provide a thorough exploration of current knowledge and advancements in the field. The second part is dedicated entirely to original research papers presenting novel experimental results on PVDF, conducted by the applicant and his colleagues. These papers offer new insights and contributions to the research of PVDF and its modifications.

Furthermore, the appendix contains an educational conference paper that offers a summary of recommendations and new methods for training newcomers in scanning probe microscopy. This appendix aims to guide learners effectively, ensuring a comprehensive understanding of the system's operation, advantages, and limitations. This paper highlights the author's commitment to enhancing the pedagogical process.

It is also worth mentioning, that all eight papers included in the main body of this thesis were published in high-impact Open Access journals. Most of these papers have garnered a significant number of citations in a relatively short period, underscoring the relevance and significance of the thesis topic.

Finally, the author hopes that the comprehensive nature of the provided published work, coupled with the dual focus of the thesis, will present a thorough and engaging exploration of polymeric materials, in particular PVDF.

Acknowledgements

First and foremost, I would like to express my heartfelt gratitude to my immediate colleagues, with whom I collaborate closely on a regular basis. This list includes (but not limited to): Ing. Pavel Kaspar, Ph.D., doc. Ing. Petr Sedlák, Ph.D., Ing. Nikola Papež, Ph.D., and doc. Mgr. Dinara Sobola, Ph.D. Their professional expertise and support were invaluable in creation of this work.

Additionally, I extend my sincere appreciation to doc. Ing. Vladimír Holcman, Ph.D., Head of the Physics Department at the Faculty of Electrical Engineering and Communication, Brno University of Technology, for his supportive attitude and continuous encouragement.

I also acknowledge Brno University of Technology (BUT) and Central European Institute of Technology (CEITEC) for providing the necessary conditions to conduct the research presented in this work. The research described in this thesis was supported by the Ministry of Education, Youth and Sports of the Czech Republic under the project CEITEC 2020 (LQ1601). The CzechNanoLab project LM2018110, funded by MEYS CR, is gratefully acknowledged for the financial support of the measurements and sample fabrication at the CEITEC Nano Research Infrastructure.

Finally, I am deeply thankful to my family and friends for their unwavering emotional support throughout this journey.

Table of contents

Motivation	8
PART I	9
Chapter 1. Advances in Self-Healing Polymers	10
1.1 Motivation of the article	10
1.2 Conclusion on the article.....	10
1.3 Contribution	10
1.4 Article 1	10
Chapter 2. Epoxies in Electronics: Properties, Applications, and Modifications	33
2.1 Motivation of the article	33
2.2 Conclusion on the article.....	33
2.3 Contribution	33
2.4 Article 2	33
Chapter 3. PVDF Properties and Applications Potential	55
3.1 Motivation of the article	55
3.2 Conclusion on the article.....	55
3.3 Contribution	55
3.4 Article 3	58
Chapter 4. Current State of PVDF as an Energy Harvester	85
4.1 Motivation of the article	85
4.2 Conclusion on the article.....	85
4.3 Contribution	85
4.4 Article 4	85
PART II	110
Chapter 5. PVDF Fibers Modified by Carbon Nanotubes	111
5.1 Motivation of the article	111
5.2 Conclusion on the article.....	111
5.3 Contribution	111
5.4 Article 5	111
Chapter 6. PVDF Fibers Modified by Carbon Flakes	123
6.1 Motivation of the article	123
6.2 Conclusion on the article.....	123
6.3 Contribution	123
6.4 Article 6	123

Chapter 7. PVDF Fibers Modified by Nitrate Salts	139
7.1 Motivation of the article	139
7.2 Conclusion on the article.....	139
7.3 Contribution	139
7.4 Article 7	139
Chapter 8. Analysis of PVDF/NMP/[EMIM][TFSI] Solid Polymer Electrolyte	155
8.1 Motivation of the article	155
8.2 Conclusion on the article.....	155
8.3 Contribution	155
8.4 Article 8	155
Conclusion	172
List of abbreviations	173
Appendix	174
Applicant's CV	178

Motivation

The pursuit of advanced materials with enhanced properties is a cornerstone of modern scientific research and industrial application. This habilitation thesis is motivated by the need to explore and expand the capabilities of polymers, focusing on their structural, electrical, and mechanical enhancements through innovative modifications. The thesis presents a comprehensive study of polyvinylidene fluoride (PVDF) materials, self-healing polymers, and epoxies used in electronics, aiming to contribute significantly to the field of material science. The initial chapters of this thesis delve into self-healing polymers, a fascinating area of research dedicated to materials that can autonomously repair damage. By exploring microcapsules and crack-healing mechanisms, these chapters provide a thorough overview of the current state and future potential of self-healing polymers. These materials promise to enhance the durability and longevity of products in various industries, from aerospace to consumer electronics, by reducing maintenance costs and improving safety. Another crucial aspect covered in the early chapters is the role of epoxies in electronics. Epoxy resins are indispensable in the electronics industry due to their excellent adhesive properties, thermal stability, and electrical insulation. This section reviews the latest advancements in epoxy formulations and their applications in electronic devices, highlighting the importance of these materials in ensuring the reliability and performance of electronic components.

The core of this thesis is dedicated to PVDF, a polymer known for its exceptional chemical resistance, thermal stability, and unique piezoelectric and pyroelectric properties. The research presented involves the modification of PVDF with various additives, including carbon nanotubes, nitrate salts, and carbon flakes. These modifications aim to enhance the intrinsic properties of PVDF, making it more suitable for a wide range of applications such as sensors, actuators, and energy storage devices. Experimental results are thoroughly characterized using a suite of analytical techniques. X-ray photoelectron spectroscopy (XPS) is employed to analyze the surface chemistry and bonding states of modified PVDF. Scanning electron microscopy (SEM) provides detailed images of the material's morphology and structural changes. Raman spectroscopy and Fourier-transform infrared spectroscopy (FTIR) are used to investigate the vibrational modes and chemical structure of the polymers. X-ray diffraction (XRD) reveals the crystalline phases and degree of crystallinity, while secondary ion mass spectrometry (SIMS) offers insights into the depth profiling and elemental composition of the samples. By integrating these advanced analytical techniques, the thesis provides a comprehensive understanding of how various additives influence the properties of PVDF. The findings demonstrate significant improvements in the material's performance, opening up new possibilities for its application in high-tech industries. This habilitation thesis aims to bridge the gap between fundamental research and practical applications, offering new insights into the development of advanced polymer materials. By focusing on both theoretical reviews and experimental studies, it seeks to contribute to the scientific community's knowledge and provide a foundation for future innovations in the field of polymers. The motivation behind this work is to push the boundaries of material science, developing polymers that can meet the ever-evolving demands of modern technology and industry.

PART I

*Overviews of current advances in polymer
science*

Chapter 1. Advances in Self-Healing Polymers

1.1 Motivation of the article

The motivation for this review article stems from the growing significance of self-healing materials (SHMs) (which are essentially polymers) in extending the lifespan and improving the resilience of engineering and structural applications. Despite the substantial progress made in SHM research, a comprehensive synthesis of recent advancements across different material types—polymers, ceramics, metals, and composites—is lacking. This review seeks to fill this gap by providing a detailed overview of state-of-the-art developments in SHMs, highlighting the distinct self-repair mechanisms of each material type and addressing specific challenges. By exploring the latest research on crack healing processes and identifying future research directions, this review aims to offer valuable insights and guide the ongoing efforts to innovate and develop sustainable materials with superior self-healing capabilities. Through this extensive exploration, the review aspires to contribute significantly to the understanding and advancement of SHMs, ultimately fostering the creation of materials that can autonomously repair and maintain their integrity over time.

1.2 Conclusion on the article

In summary, this review has thoroughly examined self-healing materials (SHMs), focusing on their mechanisms, applications, and material types. Various self-healing mechanisms, from intrinsic chemical reactions to stimuli-triggered processes, essential for designing and optimizing SHMs for specific uses were explored.

The broad applications of SHMs in industries such as biomedical, aerospace, and construction were highlighted. These materials provide innovative solutions for improving durability, safety, and performance, from medical implants and prostheses to coatings and structural components in aerospace and construction. Additionally, different types of SHMs were reviewed, including hydrogels, gels, polymers, ceramics, concretes, and cements, each offering unique benefits and challenges, underscoring the need for tailored fabrication and optimization approaches

Finally the importance of understanding crack healing and microcapsules mechanisms in SHMs to enhance their efficiency and reliability was stressed. This review emphasizes the transformative potential of SHMs in addressing societal challenges and advancing various industries. By deepening our understanding of self-healing mechanisms and materials, researchers can continue to innovate and develop impactful solutions for the future.

1.3 Applicant's contribution

The applicant is the sole author and thus is responsible for the entirety of the manuscript.

1.4 Article 1

The paper "*Advances in Materials with Self-Healing Properties: A Brief Review*" was published in July 2022 in "*Materials*" journal (IF: 3.8; Q2). Due to the recency of the paper no information on citation is available for now.

Advances in Materials with Self-Healing Properties: A Brief Review

Rashid Dallaev 

Department of Physics, Faculty of Electrical Engineering and Communication, Brno University of Technology, Technická 2848/8, 61600 Brno, Czech Republic; rashid.dallaev@vut.cz

Abstract: The development of materials with self-healing capabilities has garnered considerable attention due to their potential to enhance the durability and longevity of various engineering and structural applications. In this review, we provide an overview of recent advances in materials with self-healing properties, encompassing polymers, ceramics, metals, and composites. We outline future research directions and potential applications of self-healing materials (SHMs) in diverse fields. This review aims to provide insights into the current state-of-the-art in SHM research and guide future efforts towards the development of innovative and sustainable materials with enhanced self-repair capabilities. Each material type showcases unique self-repair mechanisms tailored to address specific challenges. Furthermore, this review investigates crack healing processes, shedding light on the latest developments in this critical aspect of self-healing materials. Through an extensive exploration of these topics, this review aims to provide a comprehensive understanding of the current landscape and future directions in self-healing materials research.

Keywords: self-healing; polymers; crack healing; microcapsules; implants; hydrogels; ceramics; concrete

1. Introduction

In response to the growing demands for increased durability, reliability, and safety, composite materials with self-healing abilities have been developed, drawing inspiration from the innate healing abilities observed in plants and animals. These self-healing materials (SHMs) have found widespread application in aerospace, marine, biomedical, and structural fields, with advancements extending to numerous other domains. In the works [1–3], the applications of self-healing polymers and nanocomposites, along with their recent developments across various sectors are discussed, offering insights into product-based outcomes and future prospects of these materials. The ability of artificial materials to self-heal any properties can increase their service life, reduce the cost of maintaining them in working condition and repairs, and also increase the level of safety of the structure or product as a whole. For this reason, SHMs are currently the subject of one of the most researched areas of materials science [4–6]. The advancement of self-healing effects finds its pinnacle in polymer materials, owing to their capacity to swiftly restore not only intermolecular bonds but also, under specific conditions, generate new ones during the cross-linking process. The presence of cross-links within polymers dictates relatively elevated diffusion rates, while the nature of interactions (covalent versus non-covalent) determines the mechanism for consolidating damaged boundaries and reestablishing bonds.

Self-healing is the capacity of a material to naturally and autonomously recover from damages without external interference. Various terms like self-repair, autonomic healing, and automatic repair are used to describe such characteristics in materials. Some products necessitate external intervention to initiate self-healing properties [7,8], resulting in two modes of self-healing processes: autonomic (no external intervention required) and non-autonomic (requires human or external triggering). The effect of self-healing (self-healing) in artificial materials is a complete or partial reduction in the surface area of damaged material due to mass transfer and combining boundaries (consolidation) with full or partial restoration of the functional characteristics of the material.



Citation: Dallaev, R. Advances in Materials with Self-Healing Properties: A Brief Review. *Materials* **2024**, *17*, 2464. <https://doi.org/10.3390/ma17102464>

Received: 23 April 2024

Revised: 17 May 2024

Accepted: 18 May 2024

Published: 20 May 2024



Copyright: © 2024 by the author. Licensee MDPI, Basel, Switzerland. This article is an open access article distributed under the terms and conditions of the Creative Commons Attribution (CC BY) license (<https://creativecommons.org/licenses/by/4.0/>).

integrity. Even minute pinholes can undergo filling and restoration processes, ultimately bolstering the mechanical performance of the materials. Inspired by biological systems, the development of this innovative class of smart materials takes cues from nature, where many materials exhibit inherent self-healing properties. In essence, self-healing materials (SHMs) possess the innate capacity to substantially regain their mechanical properties post-damage. This recovery process can occur autonomously or be triggered by specific stimuli like heat, radiation, or pressure. As a result, these materials are poised to significantly enhance the safety and durability of polymeric components without necessitating costly active monitoring or external repairs [15].

In self-healing materials (SHMs), the process of “healing” relies on the consolidation of damaged boundaries, which occurs subsequent to their reduction through mass transfer. Mass transfer, within the context of self-healing materials, involves the movement or diffusion of healing agents throughout the material to mend damage. When a self-healing material experiences damage, such as cracking or fracturing, the healing agents housed within it are released and conveyed to the site of damage via mass transfer mechanisms. This transport mechanism can take various forms, including diffusion, capillary action, or flow within the material matrix. Upon reaching the damaged area, the healing agents react or recombine to restore the material’s integrity, effectively repairing the damage. Mass transfer is pivotal in enabling the self-healing capacity of these materials by facilitating the transport of healing agents to the areas in need of repair [16].

These processes can occur autonomously, such as through the flow of material, or non-autonomously, when healing is triggered by external influences like increased temperature or ultraviolet radiation. Self-healing mechanisms in artificial materials are categorized into “external” and “internal” based on how the healing process is organized. The “external” mechanism relies on restorative components embedded within the base material’s matrix, such as microcapsules containing healing substances (discussed further in the next sub-chapter), while “internal” self-healing mechanisms operate without the need for additional restorative compounds [17].

In contrast to the microcapsule self-healing method, the vascular network self-healing system does not rely on storing healing agents within capsules. Instead, the healing agents are housed within microchannels designed to mimic the structure of blood vessels found in the human body, as demonstrated in a biomimetic vascular network pioneered by C. Dry [18]. This approach, illustrated in Figure 2, operates on the principle of a vascular network facilitating self-healing processes.

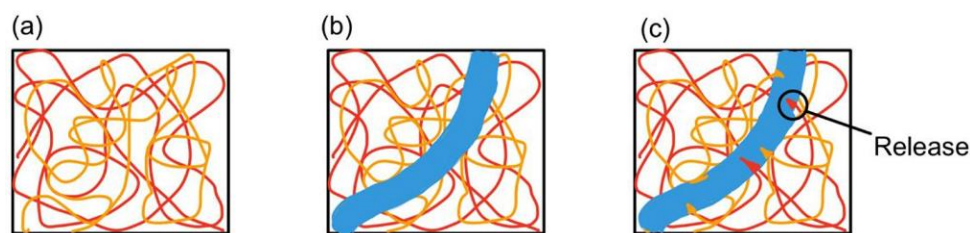


Figure 2. (a) The polymer composite matrix contains a vascular network, (b) depicted by the blue region, where a cut is made, and (c) monomers from the microchannel seep into the matrix [19]. (The figure is available in Open Access).

Dynamic covalent chemistry, encompassing reactions like imine formation, boronate ester complexation, catechol-iron coordination, Diels–Alder reaction, and disulfide exchange, plays a significant role in crafting self-healing hydrogels. These bonds exhibit a stronger yet slower dynamic equilibrium compared to non-covalent interactions [20].

1.3. Composite SHMs and Microcapsules

The development of composite systems based on SHMs makes it possible to use and improve the self-healing characteristics of the materials from which they are composed. The

introduction of various fibers, chemical components, etc., reduces the degree of destruction of the original material and also accelerates the complete healing of the defect. Thus, the presence of elastic fibers in the matrix helps to reduce the boundaries of the damaged area of the polymer after deformation, accelerating the healing process. A large number of works are devoted to the study of materials with inert, fragile capsules with a healing substance introduced into the main matrix [21–23]. When a defect occurs, the capsule breaks, releasing a healing agent that spreads to the site of the defect. At the same time, it either interacts with the matrix or the external environment, or is mixed with a catalyst—a hardener, also embedded in the matrix, hardens and restores the damaged area [22,24–26]. The design development of new materials based on the genetic code has entered the stage of active implementation, having a serious impact on our lives. The functional characteristics of materials capable of autonomously detecting damage and repairing it after complete destruction of the structure provide long-term performance characteristics for products based on them. Artificial “self-healing” materials would open up enormous possibilities, especially in cases where the reliability of materials needs to be ensured for as long as possible in difficult-to-reach areas [27].

In the literature, one can find a description of SHMs with microcapsules that act as a healing agent when the microcapsule of a polymer material is destroyed, both with the introduction of a thermoplastic into a polymer matrix and the use of the principle of hydrogen bond rearrangement. Thus, the authors of the work [15] describe synthesized acrylic copolymers with introduced carbon nanotubes. The introduction of nanomodifiers makes it possible to increase the elastic modulus and strength of the copolymer. External self-healing mechanisms, considered as autonomous self-healing, are usually classified based on the type of storage vessels used, although the concept of self-healing is similar. Capsule-based self-healing and vasculature self-healing are two types of extrinsic self-healing mechanisms.

In [28], a mechanism is used in which a mixture of monomers and a photoinitiator of the polymerization reaction are encapsulated in silicon dioxide microcapsules. Taking into account the high thermal stability of silicon dioxide, such materials have great prospects for use in the aerospace industry. To impart self-healing properties to materials, filled microtubes are used. In [29], the authors present an elastomeric composite containing hollow glass microtubes, which are filled with a healing system containing an alkyne, a thiol, and a photoinitiator. When such material is damaged, photoactive healing agents are released from the tube and, under the influence of ultraviolet radiation, the polymer crosslinks at the site of damage.

Another example of capsule systems suitable for space applications is a material developed by the Smart Materials and Sensors for Space Missions Division of MPB Technologies (Montreal, Canada), which is intended to protect against impacts from micrometeoroids and space debris particles [30,31].

The primary self-repair mechanism in microcapsule-based materials involves two key steps: (i) as cracks develop, they rupture nearby capsules, and (ii) the released rejuvenator flows into the cracks to effect repairs. Specifically, these microcapsules, containing rejuvenating agents, are embedded within building materials [32]. Figure 3 depicts the self-healing process in polymer coatings, which is utilized here to demonstrate the general self-repair process involving microcapsules, applicable across various materials such as asphalt or cementitious mixtures.

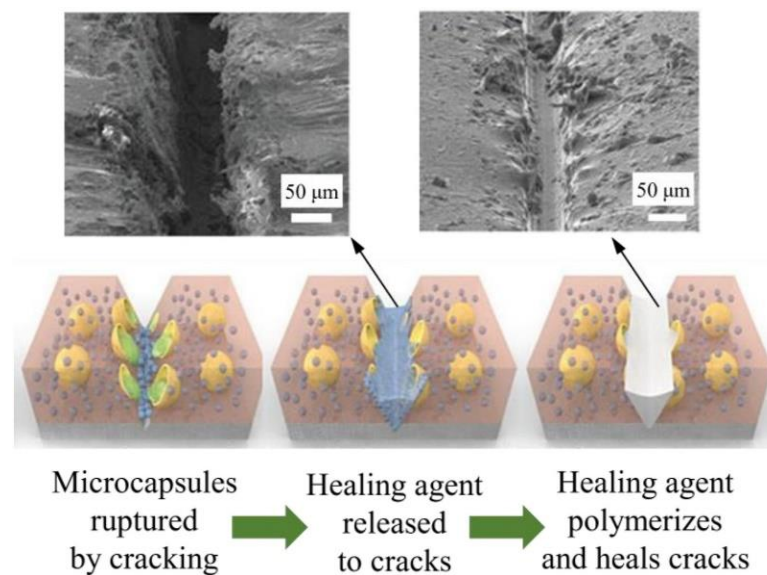


Figure 3. The self-repair mechanism triggered by microcapsules [32] (The figure is available in Open Access).

1.4. SHMs in Biomedicine

The discovery of the basic laws of polymerization and polycondensation of organic compounds with the subsequent development and industrial production of synthetic polymers marked the beginning of their widespread use in medicine. Currently, modern reconstructive surgery of the heart and blood vessels (replacing defects in the walls and septa of the heart, providing artificial circulation) is unthinkable without polymers [33]. In radiation therapy, an important aspect of therapeutic and diagnostic measures is the use of elastic and easily formed materials, which ensure the safe and reliable mounting of radiation sources on the patient's body and their targeted transportation to the treatment object [34].

The range of biomedical materials that have managed to reach the level of clinical implementation is steadily expanding. These materials include, for instance, polymers such as polyvinyl alcohol (PVA), polyacrylamide, and polyethylene glycol (PEG) [35]. Recently, superelastic alloys with a shape memory effect have attracted the close attention of researchers and clinicians. Developments in this direction lie in related areas of various sciences at the intersection of medicine and technology and affect the interests of representatives of various specialties—from physicists and engineers to practicing doctors. An important feature of today's medicine is the increased importance of the quality of treatment. This largely determines the progress in the field of medical equipment. The development and implementation of new-generation bioinert materials and original designs made from them are becoming an integral feature of modern medical materials science and medical technology. New long-term functioning products and devices that are similar in behavior to body tissues meet a higher level of medical and technical requirements than “conventional” materials and designs [36].

1.5. SHMs in Implants and Prostheses

While current artificial systems still fall short of emulating biological skin and analogs, a similar healing approach is emerging, known as the “vascular system”. Analogous to the circulatory system in living organisms, this approach relies on pumps to circulate “healing” components through a network of “vessels”. These vessels can take the form of both 2D and 3D vascular systems, with various configurations available. Self-healing occurs through the simultaneous rupture of fibers (“vessels”) containing different reagents, which, upon mixing, undergo hardening akin to two-component epoxy resins [37–39].

In recent years, there has been a significant increase in the number of polymers used for the production of medical devices, particularly tubing [40,41]. Examples of such polymers include poly(ϵ -caprolactone) (PCL), polyether ether ketone (PEEK), and polyurethane (PUs), which exhibit a shape memory effect where the material regains its original shape at the defective area. Medical-grade materials must possess good resistance to surrounding tissues and body fluids, as well as high physical and mechanical properties, and chemical resistance to sterilization agents [42,43].

Ultra-high molecular weight polyethylene holds a special place among polyethylenes, being one of the optimal materials for cup liners for joint endoprostheses [44]. From an environmental standpoint, polyethylenes are considered harmless as they do not release hazardous substances into the environment. They find application in various medical devices such as packaging and adhesive films, catheters, drainage and irrigation devices, support plates for semi-permeable membranes in hemodialyzers and heme oxygenators, connecting elements, syringe tubes, droppers, and laboratory glassware [45].

Modern surgical practice widely utilizes various types of implanted foreign bodies to replenish structures or functions lost due to injury or disease. These include suture materials, prostheses, and technological devices aimed at restoring impaired organ functioning. This review [46] focuses on Russian import-substituting products, offering comparative characteristics and parameters of implants, highlighting their advantages and disadvantages, modern development approaches, and the requirements placed on them by practical surgeons. Implants should mainly perform the strength functions of the tissues and organs being replaced, at least in the immediate postoperative period [47].

General requirements for polymer implants:

- Biocompatibility (ideally bioinert);
- Certain physical and mechanical properties;
- Resistance to infection;
- Ability/resistance to biodegradation;
- Minimum material consumption;
- Ease of use;
- Economic accessibility.

2. State-of-the-Art

Undoubtedly, SHMs have many advantages. One of the most notable is the development of realistic artificial manipulators and other types of soft robotics. Now, as part of Project SHERO, researchers at the University of Cambridge have created low-cost salt and gelatin materials that can sense strain, temperature, and humidity using soft sensors and self-heal at room temperature [14]. This discovery is set to revolutionize the field of robotics and perhaps some other fields. These new materials differ from their previous counterparts in that they do not need to be heated to heal themselves. They can autonomously (without human intervention) detect the extent and location of damage, then self-regenerate and return to work again.

A group of scientists from the University of Texas at Austin, USA, under the leadership of Yu. Guihua, has created a flexible electrical circuit based on a special gel, which, if cut into two parts, is completely self-healing and resumes its original electrical conductivity. The new gel has a combination of properties that previously have never been seen together, these are flexibility, high electrical conductivity, and the ability to self-heal at room temperature. This solution opens up a wide range of possible applications: flexible electronics, robotics, electric batteries, and even soft artificial skin and biomimetic prostheses [48].

Singaporean researchers have invented a new foam material, AiFoam, which mimics skin for a robotic prosthesis. The main features of this material are the ability to regenerate and the ability to transmit tactile sensations. According to scientists from the National University of Singapore, the foam is created by mixing a fluoropolymer with a compound that reduces surface tension. This allows the artificial leather to literally “heal” damage—the

foam itself fills cuts and other voids. As the inventors of the material note, it can be used both in robotics and to create high-quality prosthetics [49].

The creation of new artificial “self-healing” materials with a certain set of physical and chemical properties is steadily growing. The industry produces several types of polymers that meet basic medical requirements. These include polylactides (for implants of various types), ultra-high molecular weight polyethylene (for joint endoprostheses) [50], polyamides (for surgical threads), polyurethanes (for artificial heart chambers) [51], silicone polymers with high chemical and physiological inertness and thermal stability (for cosmetic surgeries on the face and mammary glands, the manufacture of catheters, heart valves, films to protect the skin surface during burns) [52], polyisobutylene in combination with natural polymers (adhesive compositions), polyparaxylene (for suture materials), polyacrylates (for use in bone grafting as tubes for drainage of the lacrimal sac, maxillary cavity, prosthetic blood vessels, heart valves, esophagus, stomach, bladder, bile ducts, urethra, eye lens; pins and plates for fixing bones during fractures, polymer mesh “frames” for connecting intestines, tendons, trachea, etc.). Particularly high demands are placed on polymers and composites for orthopedic dentistry and maxillofacial surgery [53].

Prostheses made from polyester fibers have been successfully used for more than 20 years to replace damaged areas of the vascular system. The material is used to produce blister packaging for instruments, surgical threads, synthetic blood vessels, and implants [54]. In some cases, antimicrobial and multilayer implants with anti-adhesive (anti-adhesive) properties are of particular interest [55,56]. Endoprostheses made of polypropylene monofilaments are currently the most common. Polypropylene has high biological inertness and resistance to biodegradation [57]. Of the acrylic polymers, polymethyl methacrylate (plexiglass or plexiglass) has found the greatest use in medicine—for optical systems of endoscopes [58] structural elements of medical devices [59], spectacle and contact lenses [60], droppers for blood transfusion systems [54], prostheses [61], preservation containers [62] dentistry (artificial jaws teeth and fillings) [61,63].

Studies on the implantation of various materials into the body have proven that it is polyurethane foam that “takes root” best. At the same time, an inflammatory process is observed in the tissues, during which granulation tissue is formed in the pores of the elastomer—young, rich in blood vessels and necessary for healing. Today, polyurethane is used to relieve a wide variety of health problems.

Promising barrier agents that effectively prevent intra-abdominal adhesion are gels made from absorbable polymers [64,65]. The gel is able to separate desulfurized surfaces for the time necessary for their remesothelization.

Self-healing hydrogels are of particular interest due to their high water content and controlled rheological properties [26,66]. Due to these properties, self-healing hydrogels mimic the extracellular matrix, making this class of smart polymers competitive candidates for biomedical applications [20]. Hydrogel layered composites, each layer of which has different sensitivity, make it possible to create new types of sensors, membranes, etc. based on them [67]. Hydrogels are proposed to be used in medicine as biocompatible materials [68], for example, for drug delivery systems [69–71] or bactericidal coatings of medical instruments [72]. Self-healing hydrogels are three-dimensional chemical or physical reversible networks that can restore the original morphology after damage. Dynamic bonds dominate the processes of dissociation and recombination and impart self-healing properties similar to the restoration of human tissues [20]. The best anti-adhesion effect was obtained using gels based on cellulose ethers (methylcellulose, sodium salt of carboxymethylcellulose, etc.), which have high biological inertness [73].

An aggravating factor complicating recovery after surgery may be caused by the formation of adhesions. Taking into account the etiological factors, a wide variety of anti-adhesive agents (barriers) in the form of membranes, films, and gels are considered to prevent and reduce postoperative adhesions and eliminate the mechanisms of their formation.

The gel acts as an artificial temporary “barrier” between damaged serous surfaces, ensuring their effective separation during healing, and then dissolves. Reducing the

adhesion of the surfaces of organs and tissues helps maintain their mobility and prevents the formation of adhesions [74,75].

The tunable properties and environmental responses of smart polymer materials provide the opportunity to develop personalized biomedical products. The authors of [76] focus on three typical polymer smart materials, including stimulus-responsive, self-healing, and shape memory materials. The review also discusses some recent applications in precision medicine, such as 3D bioprinting, cell therapy, and tissue engineering. The unique mechanism of regeneration of a number of materials opens up great prospects for further development, depending on the solution to the assigned problems: modeling the structure of the material will open up the possibility of obtaining composites with the properties of this effect (self-healing, self-healing), which are unattainable in other materials.

At the stages of design and development of products made from polymer materials, comprehensive materials science analysis acquires particular importance. Toxicological assessment of polymer materials used in medicine under conditions of direct contact with a living organism is important [77].

There are compounds that are derived from polyorganosiloxanes (silicones, siloxanes) containing the Si-O-B group. These compounds are sometimes referred to as “BS” compounds due to the presence of boron (B) in their chemical structure. Mechanically, BS behaves as a non-Newtonian fluid, exhibiting fluidic properties under static loads and elasticity under short-term or shock loads. This unique characteristic enables BS-based materials, when integrated into composite systems under low-speed loads, to facilitate mass transfer to the damaged area and affect the healing of defects [78]. Notably, the properties of this nanomaterial, which serves both protective and structural roles, bear resemblance to the biological process of blood clotting.

Materials featuring covalent bonds exhibit greater strength, as reduction occurs through cross-linking reactions (e.g., Diels–Alder). Consequently, the incorporation of microinclusions becomes necessary to facilitate cross-linking and substance healing, albeit imposing constraints on the material’s longevity due to the gradual depletion of the introduced substance. Conversely, repairing damage via non-covalent interactions (such as the formation of hydrogen bonds, complex compounds, ionic interactions, and van der Waals forces) is characterized by facile bond rupture and restoration, thus amplifying the potential for repeated healing and, consequently, enhancing material durability. However, such systems are sensitive to reduced loads and temperatures [22,25,26,79].

In contrast to covalent bonds, weak interactions such as hydrogen bonds offer greater potential for creating SHMs. A remarkable example of such an autonomous self-healing polymer is an oligomeric thermoplastic elastomer. Upon damage, simply pressing the fractured surfaces together allows the material to regenerate [80,81].

Another type of material that should be mentioned is photofluidic materials. Photofluidic materials refer to substances or composites that exhibit changes in fluidic behavior, such as flow or viscosity, under the influence of light. These materials are often engineered to respond to specific wavelengths or intensities of light, enabling precise control over their fluidic properties [82].

For the development of wearable ultraviolet (UV) detection technologies, photochromic materials have garnered significant attention lately. These materials offer the advantage of not needing electronic components, leading to systems and devices that change color upon irradiation. Their application in wearable technology, however, is currently constrained by the properties of the materials, particularly in meeting requirements for lightweight, compliance, and durability, especially under mechanical stress [83].

In [84], the authors fabricated a photochromic elastomer composed of diarylethene, PDMS, and toluene which demonstrated dual capabilities in self-formation and healing. These attributes were harnessed to realize signal transmission dependent on pulse frequency. Given that the device operates without necessitating high-powered pulses or ultra-fast signal sources, it holds promise for the development of an efficient smart signal transmission system.

3. Methodology and Relevance of the Review

3.1. Methodology

The methodology employed in conducting the review paper titled “Advances in Materials with Self-Healing Properties: A Review” involved a systematic and comprehensive literature search to identify relevant studies, research articles, review papers, and patents related to self-healing materials (SHMs). The search was conducted using academic databases such as PubMed, Scopus, Web of Science, and Google Scholar, utilizing keywords such as “self-healing materials”, “self-repairing polymers”, “self-healing composites”, and “autonomous repair mechanisms”.

The inclusion criteria for selecting studies encompassed publications that focused on recent advances, developments, and innovations in materials with self-healing properties across various fields, including but not limited to aerospace, automotive, construction, biomedical, and electronics. Both experimental studies and theoretical analyses were considered, with a preference for peer-reviewed articles published within the last decade.

Upon identification of relevant literature, the retrieved articles were screened based on their relevance to the review topic, and duplicates were removed. The selected articles underwent thorough examination and analysis to extract key findings, methodologies, experimental techniques, and future implications related to SHMs. Additionally, citation tracking and reference chaining techniques were employed to identify additional relevant studies not captured in the initial search.

3.2. Relevance

SHMs have garnered significant attention in recent years due to their potential to revolutionize various industries by enhancing the durability, reliability, and safety of structural components. As the demand for advanced materials capable of autonomously repairing damage continues to grow, understanding the latest developments and emerging trends in SHMs is crucial for researchers, engineers, and industry stakeholders. A comprehensive review of recent advances in materials with self-healing properties is essential to provide insights into state-of-the-art technologies, identify key challenges, and explore future directions for research and development in this rapidly evolving field.

Despite the rapid progress in the field of SHMs, there remain several knowledge gaps and unresolved challenges that warrant further investigation. While numerous studies have focused on developing novel self-healing mechanisms and materials, there is a need for a systematic review that gathers relevant information and noteworthy results from existing literature and identifies the most promising approaches. Additionally, the scalability, cost-effectiveness, and environmental impact of self-healing technologies require deeper exploration to facilitate their widespread adoption in real-world applications. Furthermore, the integration of SHMs into existing infrastructure and manufacturing processes presents unique engineering and design challenges that need to be addressed. By addressing these knowledge gaps, future research endeavors can contribute to the advancement and commercialization of SHMs for diverse applications.

4. Experimental Data on SHMs

4.1. Self-Healing in Polymers

Self-healing polymers represent a classic category of smart materials capable of autonomously restoring their structure and original functionality following repeated damage [85]. These materials, known as “self-healing” substances or systems, are engineered to partially or fully recover their initial characteristics after sustaining damage, ideally without requiring external intervention or particularly human involvement [26,86]. In nature, self-healing phenomena manifest at various scales, ranging from molecular-level repairs, such as DNA restoration, to macroscopic processes like the healing of fractures and damaged blood vessels. Recent studies by authors [87,88] demonstrate the efficacy of producing self-healing Phase Change Materials (PCMs) by incorporating thermoplastics into the polymer matrix, utilizing methyl acrylate copolymers as the thermoplastic healing

agents. This innovative approach obviates the need for monitoring reaction completeness, and the healing agents do not have expiration dates. Encapsulation of healing agents can be used not only in the PCM industry but also for protective coatings of metals, where the top layer, consisting of fibers, acts in the same way as therapeutic capsules in a polymer matrix [89].

Despite the higher cost associated with polyurethane, its remarkably brief curing time could potentially justify the expense by minimizing downtime [90], ensuring swift preparation enables rapid coating of the substrate, minimizing downtime to maintain continuous substrate protection. However, delayed healing of microcracks can lead to unintended side reactions on the fracture surface, such as disulfide bond reduction or hydrogen bond saturation, hindering subsequent self-healing processes. Therefore, expediting the self-healing process and improving its efficiency are paramount. Consequently, the capacity of polyurethane to self-heal quickly while achieving satisfactory mechanical strength recovery is crucial for mitigating substrate corrosion [91]. All small scratches that appear on the surface disappear. The self-healing film also repels dirt and water, so gadget owners do not have to worry about streaks and greasy fingerprints appearing on the display [92].

The self-healing effect can be realized in various types of materials, both in “pure” substances (polymers and prepolymers, ceramics, cements, and metals) and in complex composite systems (reinforced, layered, encapsulated materials, systems with fibers, vascular systems, sandwich panels with liquid reagents, etc.) [22,24–26].

Self-healing polymer composites represent a completely new class of materials endowed with the ability to regenerate. They are able to independently repair minor mechanical damage due to their structure. Today, there are two fundamental methods for producing self-healing composites: with and without admixtures. In the first case, special healing additives are used in the form of spherical capsules or tubes. The polymer is a material in itself, initially well adapted to the introduction of various additives into it. To ensure self-healing, thin-walled inert fragile capsules with a healing substance are introduced into it [93,94].

Figure 4 illustrates the self-healing studies conducted on copolymer P5 (butyl methacrylate). The scratch was completely healed at 140 °C within 5 min and nearly disappeared after 48 h at 80 °C. Similarly, copolymer P6 (poly(2-(dimethylamino)ethyl methacrylate) exhibited self-healing behavior at temperatures exceeding 120 °C within a 5-min timeframe. However, the surface of the coating appeared less smooth compared to copolymer P5. Both copolymers P5 and P6 demonstrated superior self-healing properties in terms of scratch size and lower healing temperatures.

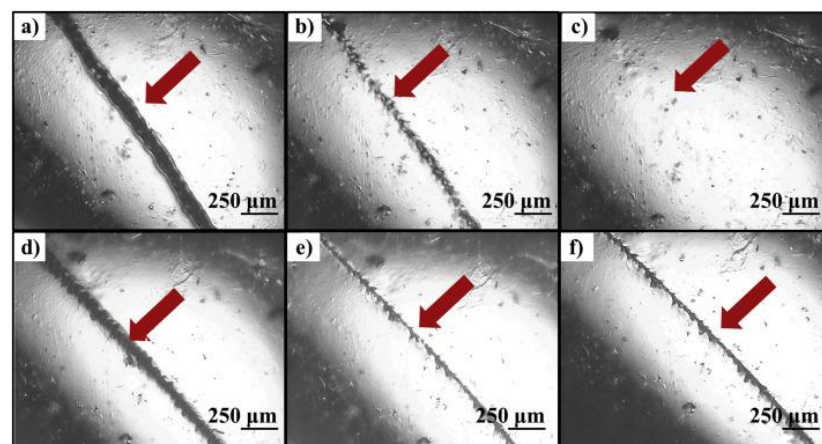


Figure 4. The self-healing experiment conducted on copolymer P5, with visualization using a microscope. Panels (a–c) depict healing experiments performed at 140 °C, showcasing the scratch before annealing (a), after annealing for 2 min (b), and after annealing for 5 min (c). Panels (d–f) display healing experiments conducted at 80 °C, showing the scratch before annealing (d), after annealing for 2 h (e), and after annealing for 48 h (f) [95]. (Permission to use was granted by Elsevier).

Furthermore, in [89] the authors demonstrate the healing process of polymer coatings after being exposed to a corrosive environment. The coatings, both the self-healed and control ones, were visually inspected after being subjected to a corrosive aqueous salt solution during electrochemical testing. Optical images of the coatings taken four months post-exposure to the corrosive environment are depicted in Figure 5. Before the electrochemical analysis, the scribed coatings showed no visible signs of corrosion. However, subsequent exposure to the corrosive environment resulted in significant corrosion damage and undercutting in the three control cases: type A (PDMS) fibers only, type B (DBTL catalyst) fibers only, and those with no fibers. Conversely, the healed coating exhibited minimal signs of corrosion, primarily localized to the scribed region.

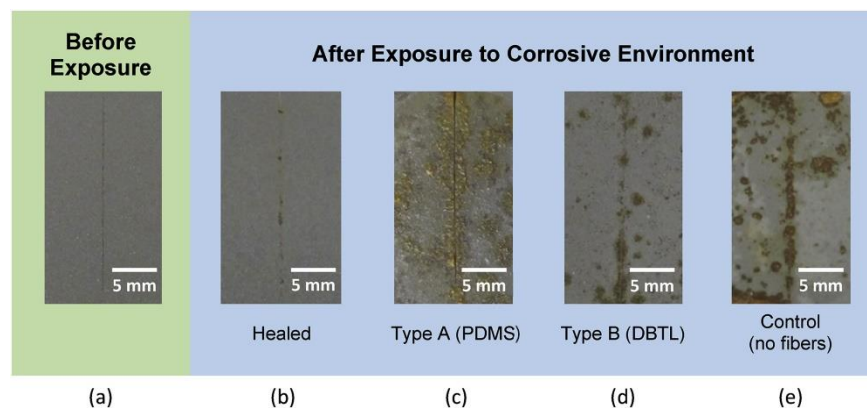


Figure 5. Optical images of both healed and control coatings captured four months post-exposure to a corrosive aqueous salt solution during electrochemical characterization: (a) before exposure, (b) healed, (c) Type A (PDMS), (d) Type B (DBTL), (e) Control (no fibers). Comparing the healed coating before and after corrosion exposure reveals similarity in appearance. Conversely, the control cases comprising type A (PDMS) fibers only, type B (DBTL catalyst) fibers only, and no fibers (silicone binder only) exhibit unmistakable signs of corrosion damage [89] (Permission to use was granted by Elsevier).

The paramount property of self-healing polymers is their healing efficiency. The self-healing behavior of Diels–Alder polyurethane (DAPU) samples was evaluated using a POM test in [96]. In this study, self-healing tests were conducted at various temperatures (100, 110, 120, and 130 °C) for 5 min, and POM images corresponding to each condition are depicted in Figure 6. To simulate intentional damage, samples were deliberately incised using a blade. As illustrated in Figure 6a, DAPU exhibited minimal self-healing capability after 5 min at 100 °C, while a slight self-healing effect was observed after the same duration at 110 °C (Figure 6b). Upon increasing the heating temperature to 120 °C, the extensive cracks in DAPU following damage were notably repaired, with only a slim line remaining visible after 5 min (Figure 6c), indicating a high self-healing efficiency. Furthermore, the pre-existing damage in DAPU was almost entirely restored at 130 °C after 5 min (Figure 6d). However, it is noteworthy that the sample exhibited darkening at this elevated temperature. These findings suggest that this furan-maleimide-based polymer necessitates a critical temperature (e.g., 120 °C) to demonstrate its self-healing capability effectively.

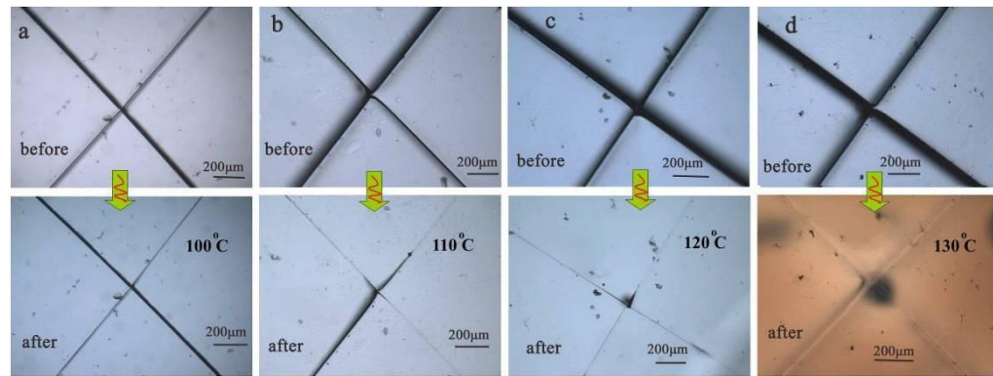


Figure 6. Presents POM images of DAPU films before and after annealing for 5 min at various temperatures: (a) 100 °C, (b) 110 °C, (c) 120 °C, and (d) 130 °C [96] (Permission to use was granted by Elsevier).

4.2. Self-Healing in Composites

The development of layered composite materials (sandwich panels) is promising. In such a scheme, each layer performs its specific function and also contains at least one layer with self-healing properties. When assembled, such material is able to minimize damage and quickly restore its original macro-characteristics. Sandwich panels can include various reinforcing components that impart rigidity and stability to the structure, solid, viscous, and liquid fillers, which, when a material defect occurs, react with each other, forming a viscous or solid phase [31,97].

To effectively harness the self-healing effect in layered composite materials, it is essential to incorporate at least one layer capable of fluidity for facilitating mass transfer. One promising candidate meeting this criterion is a borosiloxane (BS)-based material [98–100].

In [101], the self-repair process underscores the significance of Al_2O_3 dissolution into SiO_2 , pivotal for effectively filling gaps with a low-viscosity supercooled melt and for depositing reinforcing crystals essential for complete strength restoration. Drawing inspiration from bone regeneration, the authors have categorized this mechanism into three primary stages: inflammation, repair, and remodeling (Figure 7) Therefore, through the strategic design and integration of a healing activator that fosters these processes, there exists the potential to augment self-healing capabilities further.

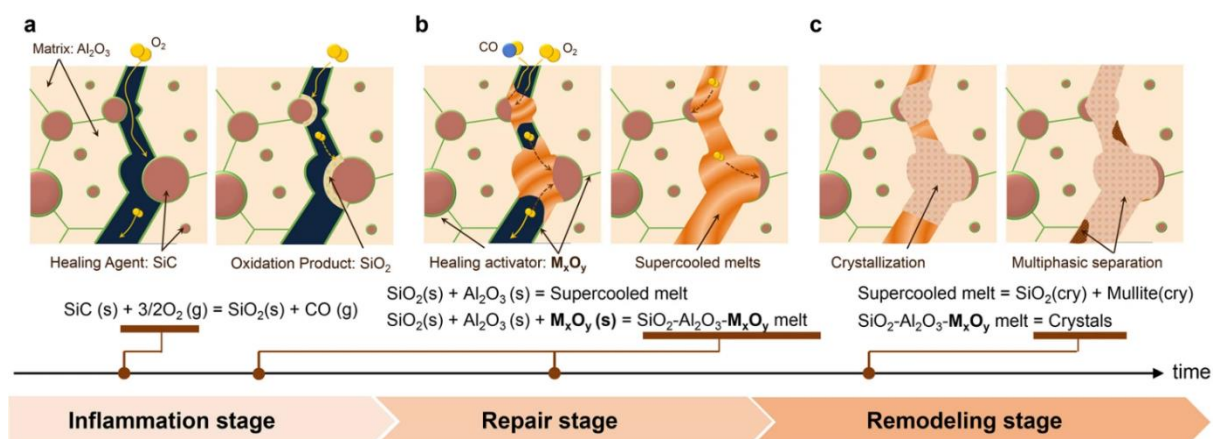


Figure 7. Self-repair mechanisms in $\text{Al}_2\text{O}_3/\text{SiC}$ composites and the influence of healing activator networks. (a) Oxygen infiltration occurs on cracked surfaces, initiating the oxidation of SiC to SiO_2 , termed the inflammation stage. (b) Al_2O_3 and M_xO_y dissolve into SiO_2 , creating a mechanically frail, low-viscosity supercooled melt that effectively occupies uneven gaps, referred to as the repair stage. (c) Robust crystals begin to nucleate and expand within the supercooled melt, marking the remodeling stage [101] (Figure is available in Open Access).

Authors of [102] demonstrate the self-healing functionality of a composite film. Half of the sample undergoes artificial damage via manual cleaving of the material stack between the layers of glass fiber fabric. This results in opacity in the damaged area due to reflections from air-fiber and air-resin interfaces occurring at resin cracks and fiber-resin delamination sites (Figure 8). Following this, the damaged substrate is rotated 90 degrees and inserted halfway into the hot press (with the other half sticking out). Pressing at elevated temperatures restores fiber-resin delamination and heals cracks, thereby fully restoring transparency to the sample. Three-quarters of the sample (pristine, pristine-pressed, and pristine-cleaved-pressed) exhibit the same optical appearance, distinctly contrasting with the pristine-cleaved quarter. From this, it can be inferred that self-healing can be successfully achieved without major side effects.

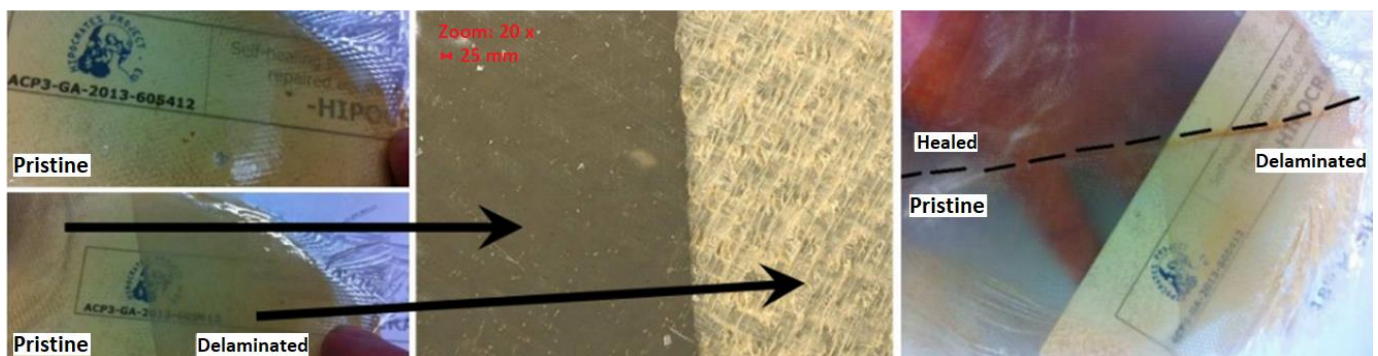


Figure 8. The glass fiber-reinforced epoxy composite functionalized with Diels–Alder undergoes fabrication (**top left**). The woven glass fiber fabrics are separated until halfway into the specimen ((**bottom left**) and microscopic image). Subsequently, half of the damaged area is healed using a hot press (**right**) [102] (The figure is available in Open Access).

4.3. Self-Healing in Ceramics

In addition to polymers, ceramic SHMs are currently being developed. Self-healing ceramic materials often use oxidation reactions, with the volume of oxide exceeding the volume of the starting material. As a result, the products of these reactions, due to the increase in volume, can be used to fill small cracks [103].

The manifestations of self-healing in ceramic materials are not as pronounced or widespread as those observed in polymers. Typically, self-healing in ceramics is limited to addressing small defects, usually on the scale of hundreds of micrometers. However, the phenomenon of “self-ensuring” microcracks, induced by mechanical wear or thermal stress in ceramic materials, offers significant improvements in their operational characteristics [104,105].

For instance, in self-healing Ti_2AlC ceramics, the mechanism involves the filling of cracks with $\alpha-Al_2O_3$ and TiO_2 , which form at high temperatures in air (see Figure 9) [106].

An additional instance of ceramic “self-healing” is exemplified by the self-healing oxidation observed in SiC ceramics. In this process, active SiC filler particles within the matrix undergo oxidation upon exposure to penetrating oxygen. Consequently, SiO_2 is formed, effectively filling the crack [107,108].

In contrast, achieving the self-healing effect in metallic materials poses greater challenges due to their unique properties. One such obstacle stems from the nature of the atomic bonds and their limited mobility at operational temperatures. Essentially, defects in metals are rectified through the introduction of more fusible and ductile phases into the primary matrix or via the accelerated formation of agglomerates from phases that precipitate under specific conditions within the base material at defect sites. These melted or precipitated phases have the capacity to fill defects and halt the further propagation of damage.

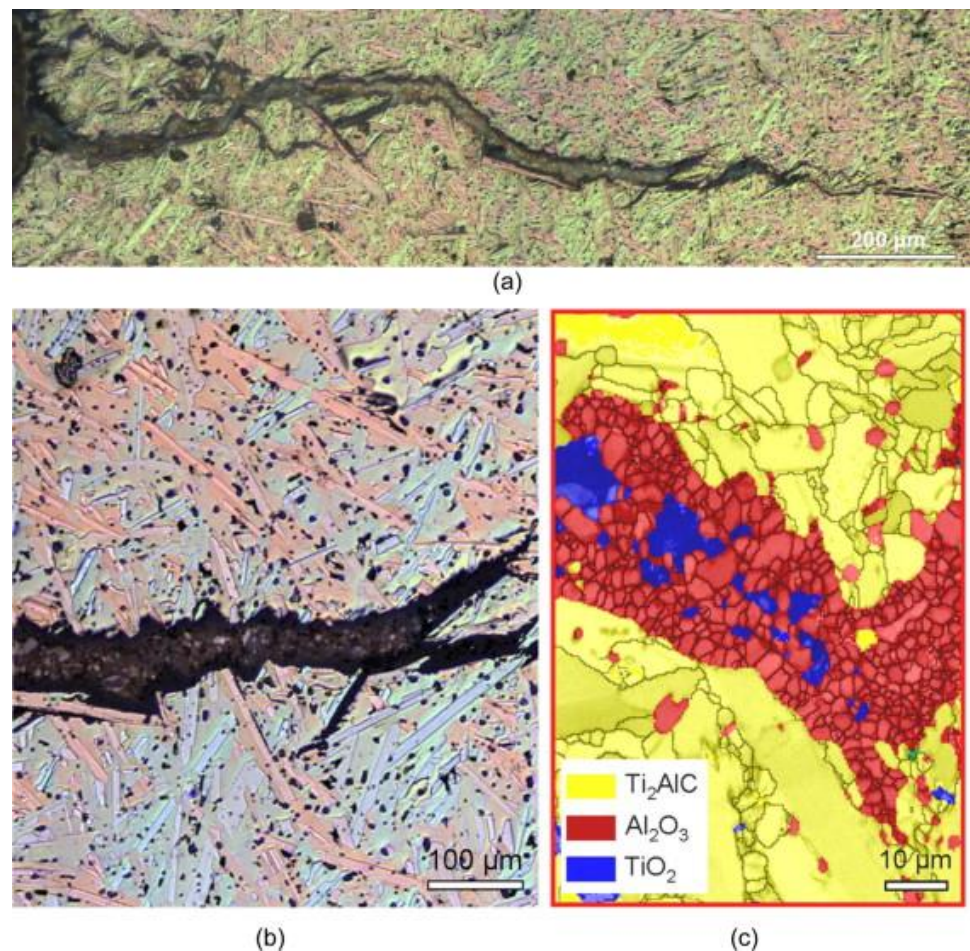


Figure 9. Low- and high-magnification images depict a crack that has been completely filled in the sample following the 8th fracture and subsequent annealing at 1200 °C for 100 h. (a) An optical overview image provides a glimpse of the healed crack; (b) an enlarged optical image, derived from (a), reveals that two opposing fracture surfaces are coated with the same Al_2O_3 layer (depicted in black), while the gap between these surfaces is entirely filled with a mixture of Al_2O_3 (black) and TiO_2 (large white particles); (c) a detailed micrograph of the healed-damage zone, obtained using scanning electron microscopy with electron backscatter diffraction, offers further insight into the healing process [106] (Permission to use was granted by Elsevier).

4.4. Self-Healing in Concrete and Cement

The primary mechanisms underlying the self-healing of cementitious materials can be categorized into three main types: natural or autogenous healing, involving hydration and carbonization reactions; bio-based healing; and activation, achieved through methods such as the application of chemical additives, reactions utilizing fly ash, special expanding agents, and incorporation of geopolymer materials [109–111].

Collectively referred to as self-healing concrete, these approaches encompass a range of modern developments and innovative solutions aimed at altering material structures to enhance recovery and resistance to various stresses. Given that concrete stands as one of the most ubiquitous materials in the construction and repair industries today, the demand for novel production methods is more pronounced than ever [112]. Notably, researchers at Delft University of Technology, under the leadership of Hank Jonkers, have conducted experiments on bioconcrete, a material capable of autonomously repairing cracks and damage through the action of embedded bacteria. These experimental studies were conducted to validate theoretical findings and further advance the understanding of self-healing mechanisms in concrete [113,114].

Additionally, recent research [115] demonstrates the self-healing capabilities of cementitious composite materials incorporating geopolymer materials. Figure 10 shows the healing process of cracked self-healing concretes followed similar patterns to conventional concrete when subjected to the same mixing conditions. A crack measuring 0.15 mm in width exhibited self-healing after 3 days of re-curing, as depicted. Subsequently, after 7 days of re-curing, the crack width decreased from 0.22 mm to 0.16 mm. Furthermore, by the 33rd day, it had almost completely self-healed. This recovery process appeared to involve various self-healing phenomena, including swelling, expansion, and re-crystallization. However, it is important to note that cracked aggregates did not self-heal autonomously. Instead, self-healing initially occurred in the cementitious paste area between cracks, facilitating healing between the cementitious paste and the aggregate surface.

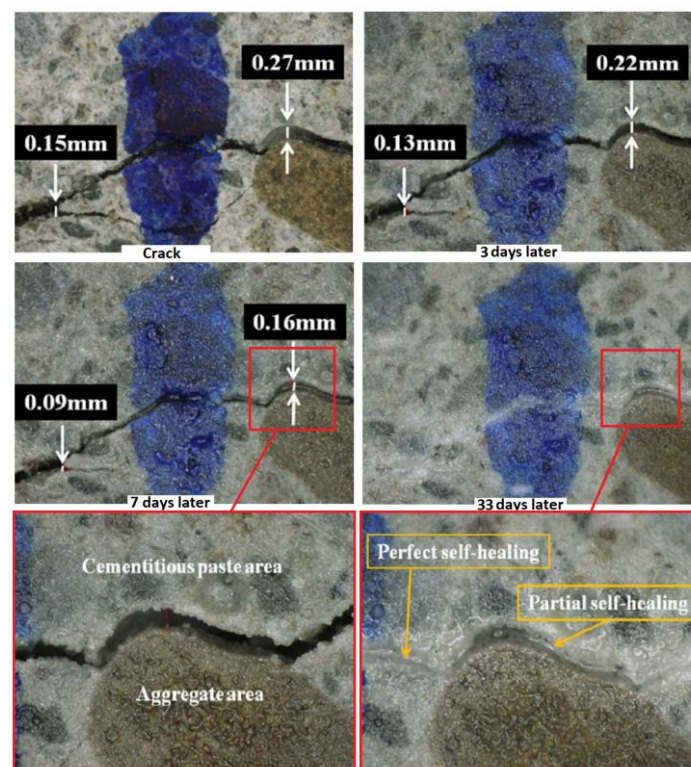


Figure 10. Self-healing of cracks in concrete with mineral fillers [115] (The figure is available in Open Access).

A technique has been devised [116] to computationally and experimentally validate the parameters of transition zones surrounding the anti-filtration element (PFE) to facilitate crack self-healing in clay-cement concrete diaphragms (GCBD). By adhering to the prescribed methodology, which includes considerations such as soil granulometry, reverse filter thickness, and layer count, the filtration strength of the system comprising the upper prism, upper transition layer, healing layer, GCBD, lower transition layer, and lower prism can be effectively ensured. The authors propose, in relation to the healing layer, using sandy soil with a particle size of less than 5 mm as a material.

The authors of the article [117] introduced novel techniques aimed at enhancing the strength and self-healing properties of porous composites within concrete structures through both internal and external factors. The method involves two key steps: firstly, establishing a dense and robust material structure, and secondly, incorporating a chemically active mineral, specifically iron sulfide, into the fine filler. This approach facilitates the formation of ettringite-like iron-containing calcium hydrates within the concrete matrix upon cracking, resulting in an expansion of the solid and condensed phases.

World experience in the development of biomodifying additives includes a fairly wide list of used gram-positive and gram-negative cells (*Sporosarcina pasteurii*, *Bacillus pasteurii*, *B. cohnii*, *B. sphaericus*, *B. pseudofirmus*, *B. cohnii*, *B. halodurans*, *B. subtilis*, *B. megaterium*, *B. alkalinitrilicus*, *Pseudomonas putida*, *Escherichia coli*) [118].

The authors in [119] suggest employing ion-plasma treatment to regulate the sorption capacity of natural zeolites intended for use as carriers of active biomodifiers, such as *Bacillus pasteurii* bacteria, which facilitate self-healing in concrete. The research demonstrates the superior effectiveness of the proposed sorbent modification method over the conventional heat treatment approach. In subsequent studies, findings regarding the capacity of building materials containing Portland cement and gypsum binder to self-repair using capsules containing aerobic bacteria are presented [120]. It was subsequently demonstrated [121] that employing highly porous zeolite as a carrier for an active biomodifier enables the integration of self-healing technology into cement composites. This enables the sealing of defects through the utilization of bacterial byproducts. The enhancement in sample strength is directly linked to the saturation of the microdefect structure within the cement–sand matrix with reinforcing calcium carbonate, as shown in Figure 11.

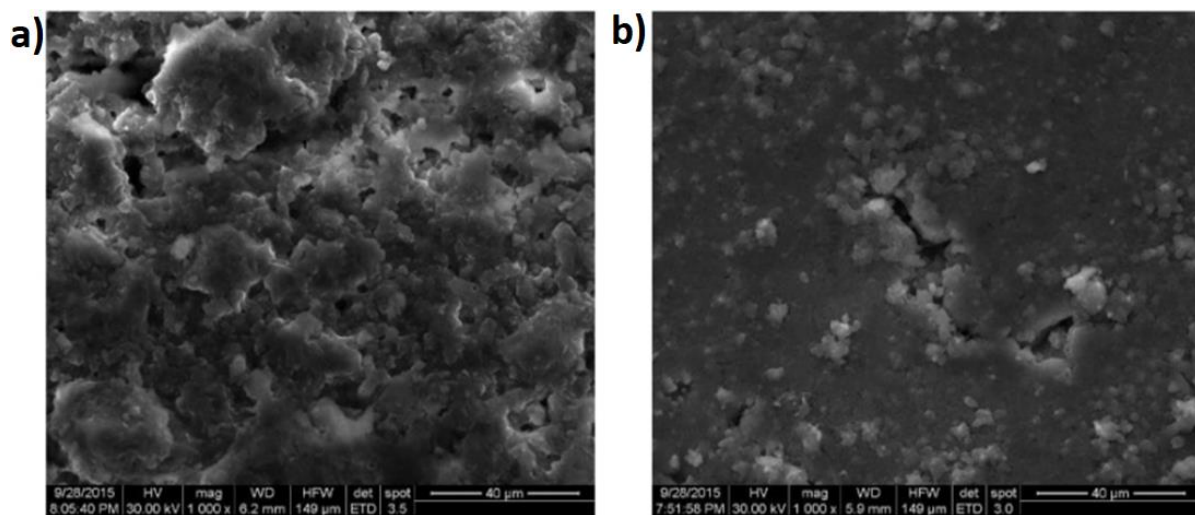


Figure 11. (a) The surface of the control sand-cement specimen without the bioadditive at a hardening age of 28 days; (b) the surface of the sand-cement specimen with a cell concentration of 0.05% by weight of the cement binder at the same hardening age of 28 days [121]. (The figure is available in Open Access).

Employing the developed method of biomodification involving bacteria with urease activity enables the preservation of structural integrity in building constructions, which autonomously repair microstructural defects by sealing them with calcium carbonate at their nascent stages. This biomodification method, aimed at instilling self-healing capabilities, offers numerous advantages, including environmental friendliness, cost-effectiveness, reduced labor requirements for repair and restoration tasks, applicability to structures of varying complexity, and suitability for the restoration of valuable architectural landmarks.

5. Key Findings and Future Implications

5.1. Key Findings

- **Mechanisms of Self-Healing:** This review elucidates various mechanisms underlying self-healing processes, spanning from microcapsules and intrinsic chemical reactions to external stimuli-triggered responses. Understanding these mechanisms is fundamental for the development of advanced SHMs.
- **Applications Across Industries:** SHMs hold immense potential for diverse applications across industries such as implants, prostheses, biomedicine, aerospace, and construc-

tion. These materials offer innovative solutions for enhancing durability, safety, and performance in various contexts.

- **Material Diversity:** This review explores the characteristics and applications of different types of SHMs, including hydrogels, self-healing gels, polymers, ceramics, concretes, and cements. Each material type presents unique advantages and opportunities for advancement.
- **Importance of Crack Healing:** Crack healing mechanisms play a crucial role in the performance of SHMs, influencing factors such as efficiency and reliability. Understanding and optimizing crack healing processes are essential for maximizing the effectiveness of these materials.

5.2. Future Implications

- **Tailored Material Design:** Future research should focus on developing SHMs tailored to specific applications, considering factors such as environmental conditions, mechanical properties, and biocompatibility requirements.
- **Multifunctionality and Integration:** There is potential for the integration of self-healing capabilities with other functionalities, such as sensing or antimicrobial properties, to create multifunctional materials with enhanced performance and versatility.
- **Sustainable Solutions:** Further efforts are needed to explore sustainable sources and manufacturing processes for SHMs, with an emphasis on reducing environmental impact and promoting circular economy principles.
- **Translational Research:** Continued collaboration between researchers, industry partners, and healthcare professionals is essential for translating advances in SHMs into practical applications, ultimately benefiting society and improving quality of life.

6. Conclusions

In conclusion, this review has provided a comprehensive overview of SHMs, covering various aspects including mechanisms, applications, and material types. Throughout this review, we explored the diverse mechanisms of self-healing, ranging from intrinsic chemical reactions to stimuli-triggered processes. Understanding these mechanisms is crucial for the design and optimization of SHMs tailored to specific applications.

We also discussed the wide-ranging applications of SHMs across numerous industries, including biomedical, aerospace, construction, and beyond. From self-healing implants and prostheses in the medical field to self-healing coatings and structures in aerospace and construction, these materials offer innovative solutions for enhancing durability, safety, and performance. Furthermore, we examined the characteristics and applications of various self-SHM types, including hydrogels, self-healing gels, polymers, ceramics, concretes, and cements. Each material type presents unique advantages and challenges, highlighting the importance of tailored approaches for fabrication and optimization. Lastly, we delved into the significance of crack healing mechanisms in SHMs, emphasizing the need to understand factors influencing crack propagation and healing to enhance efficiency and reliability.

Overall, this review underscores the transformative potential of SHMs in addressing a wide range of societal challenges and advancing various industries. By furthering our understanding of self-healing mechanisms and materials, researchers can continue to innovate and develop novel solutions with profound implications for the future.

Funding: This research received no external funding.

Institutional Review Board Statement: Not applicable.

Informed Consent Statement: Not applicable.

Data Availability Statement: Data are contained within the article.

Conflicts of Interest: The author declares no conflict of interest.

References

1. McDonald, S.A.; Coban, S.B.; Sottos, N.R.; Withers, P.J. Tracking capsule activation and crack healing in a microcapsule-based self-healing polymer. *Sci. Rep.* **2019**, *9*, 17773. [CrossRef] [PubMed]
2. Balasubramanian, M.; Jayabalakrishnan, D. Influence of Pin offset and Weave Pattern on the Performance of Al-Cu Joints Reinforced with Graphene Particles. *Int. J. Automot. Mech. Eng.* **2020**, *17*, 8186–8196. [CrossRef]
3. Ramesh, G.; Jayabalakrishnan, D.; Rameshkumar, C. Mechanical and thermal characterization of heat/surface treated egg shell filler diffused natural rubber green composite. *J. Optoelectron. Biomed. Mater.* **2018**, *10*, 21–28.
4. Mashkoo, F.; Lee, S.J.; Yi, H.; Noh, S.M.; Jeong, C. Self-Healing Materials for Electronics Applications. *Int. J. Mol. Sci.* **2022**, *23*, 622. [CrossRef] [PubMed]
5. Yang, Y.; Ding, X.; Urban, M.W. Urban Chemical and physical aspects of self-healing materials. *Prog. Polym. Sci.* **2015**, *49–50*, 34–59. [CrossRef]
6. Meraz, M.M.; Mim, N.J.; Mehedi, M.T.; Bhattacharya, B.; Aftab, M.R.; Billah, M.M.; Meraz, M.M. Self-healing concrete: Fabrication, advancement, and effectiveness for long-term integrity of concrete infrastructures. *Alexandria Eng. J.* **2023**, *73*, 665–694. [CrossRef]
7. Yue, H.; Wang, Z.; Zhen, Y. Recent Advances of Self-Healing Electronic Materials Applied in Organic Field-Effect Transistors. *ACS Omega* **2022**, *7*, 18197–18205. [CrossRef]
8. Ding, Q.; Xu, X.; Yue, Y.; Mei, C.; Huang, C.; Jiang, S.; Wu, Q.; Han, J. Nanocellulose-mediated electroconductive self-healing hydrogels with high strength, plasticity, viscoelasticity, stretchability, and biocompatibility toward multifunctional applications. *ACS Appl. Mater. Interfaces* **2018**, *10*, 27987–28002. [CrossRef]
9. Jayabalakrishnan, D.; Muruga, D.N.; Bhaskar, K.; Pavan, P.; Balaji, K.; Rajakumar, P.S.; Priya, C.; Deepa, R.A.B.; Sendilvelan, S.; Prabhakar, M. Self-Healing materials—A review. *Mater. Today Proc.* **2020**, *45*, 7195–7199. [CrossRef]
10. Uguzzoni, A.M.P.; Fregonara, E.; Ferrando, D.G.; Anglani, G.; Antonaci, P.; Tulliani, J.-M. Concrete Self-Healing for Sustainable Buildings: A Focus on the Economic Evaluation from a Life-Cycle Perspective. *Sustainability* **2023**, *15*, 13637. [CrossRef]
11. Reda, M.A.; Chidiac, S.E. Performance of Capsules in Self-Healing Cementitious Material. *Materials* **2022**, *15*, 7302. [CrossRef]
12. Choi, K.; Noh, A.; Kim, J.; Hong, P.H.; Ko, M.J.; Hong, S.W. Properties and Applications of Self-Healing Polymeric Materials: A Review. *Polymers* **2023**, *15*, 4408. [CrossRef] [PubMed]
13. Wen, N.; Song, T.; Ji, Z.; Jiang, D.; Wu, Z.; Wang, Y.; Guo, Z. Recent advancements in self-healing materials: Mechanicals, performances and features. *React. Funct. Polym.* **2021**, *168*, 105041. [CrossRef]
14. Hardman, D.; Thuruthel, T.G.; Iida, F. Self-healing ionic gelatin/glycerol hydrogels for strain sensing applications. *NPG Asia Mater.* **2022**, *14*, 11. [CrossRef]
15. Rehman, H.U.; Chen, Y.; Guo, Y.; Du, Q.; Zhou, J.; Guo, Y.; Duan, H.; Li, H.; Liu, H. Stretchable, strong and self-healing hydrogel by oxidized CNT-polymer composite, Self-healing nanocomposite materials: A review. *Compos. Part A Appl. Sci. Manuf.* **2016**, *90*, 250–260. [CrossRef]
16. Cerdan, K.; Thys, M.; Cornella, A.C.; Demir, F.; Norvez, S.; Vendamme, R.; Van Puyvelde, P.; Brancart, J. Progress in Polymer Science Sustainability of self-healing polymers: A holistic perspective towards circularity in polymer networks. *Prog. Polym. Sci.* **2024**, *152*, 101816. [CrossRef]
17. Thakur, V.K.; Kessler, M.R. Self-healing polymer nanocomposite materials: A review. *Polymer* **2015**, *69*, 369–383. [CrossRef]
18. Dry, C. Passive tuneable fibers and matrices. *Int. J. Mod. Phys. B* **1992**, *6*, 2763–2771. [CrossRef]
19. Luo, J.; Wang, T.; Sim, C.; Li, Y. Mini-Review of Self-Healing Mechanism and Formulation Optimization of Polyurea Coating. *Polymers* **2022**, *14*, 2808. [CrossRef]
20. Liu, Y.; Hsu, S.-H. Synthesis and Biomedical Applications of Self-healing Hydrogels. *Front. Chem.* **2018**, *6*, 449. [CrossRef]
21. Liu, B.; Wu, M.; Du, W.; Jiang, L.; Li, H.; Wang, L.; Li, J.; Zuo, D.; Ding, Q. The Application of Self-Healing Microcapsule Technology in the Field of Cement-Based Materials: A Review and Prospect. *Polymers* **2023**, *15*, 2718. [CrossRef] [PubMed]
22. Zhu, D.Y.; Rong, M.Z.; Zhang, M.Q. Self-healing polymeric materials based on microencapsulated healing agents: From design to preparation. *Prog. Polym. Sci.* **2015**, *49–50*, 175–220. [CrossRef]
23. Jiang, S.; Lin, Z.; Tang, C.; Hao, W. Preparation and Mechanical Properties of Microcapsule-Based Self-Healing Cementitious Composites. *Materials* **2021**, *14*, 4866. [CrossRef] [PubMed]
24. Urdl, K.; Kandelbauer, A.; Kern, W.; Müller, U.; Thebault, M.; Zikulnig-Rusch, E. Self-healing of densely crosslinked thermoset polymers—A critical review. *Prog. Org. Coat.* **2017**, *104*, 232–249. [CrossRef]
25. Scheiner, M.; Dickens, T.J.; Okoli, O. Progress towards self-healing polymers for composite structural applications. *Polymer* **2016**, *83*, 260–282. [CrossRef]
26. Bekas, D.; Tsirka, K.; Baltzis, D.; Paipetis, A. Self-healing materials: A review of advances in materials, evaluation, characterization and monitoring techniques. *Compos. Part B Eng.* **2016**, *87*, 92–119. [CrossRef]
27. Sitnikov, N.N.; Mostovaya, K.S.; Khabibullina, I.A.; Mashchenko, V.I. Self-healing materials: A review of self-healing mechanisms and their applications. *Video Sci.* **2018**, *1*, 2–30. Available online: <https://cyberleninka.ru/article/n/samovosstanavlivayuschiesya-materialy-obzor-mehanizmov-samovosstanovleniya-i-ih-primeneniya> (accessed on 4 January 2023).
28. Guo, W.; Jia, Y.; Tian, K.; Xu, Z.; Jiao, J.; Li, R.; Wu, Y.; Cao, L.; Wang, H. UVtriggered Self-healing of a Single Robust SiO₂ Microcapsule Based on Cationic Polymerization for Potential Application in Aerospace Coatings. *ACS Appl. Mater. Interfaces* **2016**, *8*, 21046–21054. [CrossRef]

29. Yue, H.-B.; Fernández-Blázquez, J.P.; Beneitoac, D.F.; Vilatela, J.J. Real time monitoring of click chemistry self-healing in polymer composites. *J. Mater. Chem. A* **2014**, *2*, 3881–3887. [CrossRef]
30. Pernigoni, L.; Lafont, U.; Grande, A.M. Self healing materials for space applications: Overview of present development and major limitations. *CEAS Space J.* **2021**, *13*, 341–352. [CrossRef]
31. Aïssa, B.; Tagziria, K.; Haddad, E.; Jamroz, W.; Loiseau, J.; Higgins, A.; Asgar-Khan, M.; Hoa, S.V.; Merle, P.G.; Therriault, D.; et al. The Selfhealing capability of carbon fibre composite structures subjected to hypervelocity impacts simulating orbital space debris. *Int. Sch. Res. Not.* **2012**, *2012*, 351205.
32. Ma, E.; Chen, X.; Lai, J.; Kong, X.; Guo, C. Self-healing of microcapsule-based materials for highway construction: A review. *J. Traffic Transp. Eng.* **2023**, *10*, 368–384. [CrossRef]
33. Hu, K.; Li, Y.; Ke, Z.; Yang, H.; Lu, C.; Li, Y.; Guo, Y.; Wang, W. History, progress and future challenges of artificial blood vessels: A narrative review. *Biomater Transl.* **2022**, *3*, 81–98. [CrossRef] [PubMed]
34. Los, D.M.; Shapovalov, V.M.; Zotov, S.V. Application of polymer materials for medical products. *Probl. Health Ecol.* **2020**, *2*, 5–12. Available online: <https://cyberleninka.ru/article/n/primenenie-polimernyh-materialov-dlya-izdeliy-meditsinskogo-naznacheniya> (accessed on 5 January 2023).
35. Del Prado-Audelo, M.L.; Caballero-Florán, I.H.; Mendoza-Muñoz, N.; Giraldo-Gomez, D.; Sharifi-Rad, J.; Patra, J.K.; González-Torres, M.; Florán, B.; Cortes, H.; Leyva-Gómez, G. Current progress of self-healing polymers for medical applications in tissue engineering. *Iran. Polym. J.* **2021**, *31*, 7–29. [CrossRef]
36. Muslov, S.A.; Yarema, I.V.; Danilevskaya, O.V. Nitinol—A new generation medical material. *Mod. Sci. Intensive Technol.* **2007**, *11*, 55–56. Available online: <https://top-technologies.ru/ru/article/view?id=25600> (accessed on 10 April 2024).
37. Lee, M.W.; An, S.; Yoon, S.S.; Yarin, A.L. Advances in self-healing materials based on vascular networks with mechanical self-repair characteristics. *Adv. Colloid Interface Sci.* **2017**, *252*, 21–37. [CrossRef]
38. Hansen, C.J.; Wu, W.; Toohey, K.S.; Sottos, N.R.; White, S.R.; Lewis, J.A. Self-healing materials with interpenetrating microvascular networks. *Adv. Mater.* **2009**, *21*, 4143–4147. [CrossRef]
39. Hamilton, A.R.; Sottos, N.R.; White, S.R. Self-healing of internal damage in synthetic vascular materials. *Adv. Mater.* **2010**, *22*, 5159–5163. [CrossRef] [PubMed]
40. Cho, S.; Hwang, S.Y.; Oh, D.X.; Park, J. Recent progress in self-healing polymers and hydrogels based on reversible dynamic B-O bonds: Boronic/boronate esters, borax, and benzoxaborole. *J. Mater. Chem.* **2021**, *9*, 14630–14655. [CrossRef]
41. Rumon, M.H.; Akib, A.A.; Sultana, F.; Moniruzzaman; Niloy, M.S.; Shakil, S.; Roy, C.K. Self-Healing Hydrogels: Development, Biomedical Applications, and Challenges. *Polymers* **2022**, *14*, 4539. [CrossRef]
42. Pathan, N.; Shende, P. Strategic conceptualization and potential of self-healing polymers in biomedical field. *Mater. Sci. Eng. C* **2021**, *125*, 112099. [CrossRef] [PubMed]
43. Shirokova, E.S.; Vesnin, R.L.; Khusainov, A.D. Materials based on thermoplastic elastomers for use in medicine and the pharmaceutical industry. *Bull. Kazan Technol. Univ.* **2016**, *11*, 106–110. Available online: <https://cyberleninka.ru/article/n/materialy-na-osnove-termoelastoplastov-dlya-primeneniya-v-meditsine-i-farmatsevticheskoy-promyshlennosti> (accessed on 5 January 2023).
44. Wolf, C.; Lederer, K.; Pfragner, R.; Schauenstein, K.; Ingolic, E.; Siegl, V. Biocompatibility of ultra-high molecular weight polyethylene (UHMW-PE) stabilized with α -tocopherol used for joint endoprostheses assessed in vitro. *J. Mater. Sci. Mater. Med.* **2007**, *18*, 1247–1252. [CrossRef] [PubMed]
45. Paxton, N.C.; Allenby, M.C.; Lewis, P.M.; Woodruff, M.A. Biomedical applications of polyethylene. *Eur. Polym. J.* **2019**, *118*, 412–428. [CrossRef]
46. Zhukovsky, V.A. Polymer Implants for Reconstructive Surgery. *Innova.* 2016. No. 2 (3). Available online: <https://cyberleninka.ru/article/n/polimernye-implantaty-dlya-rekonstruktivnoy-hirurgii> (accessed on 5 January 2023).
47. Zhukovsky, V.A. *Polymer Endoprostheses for Hernioplasty: Production, Properties, Possibilities for Improvement*; Surgery Bulletin: Saint Petersburg, Russia, 2011; Volume 170, pp. 82–86. Available online: <https://cyberleninka.ru/article/n/polimernye-endoprotezy-dlya-gernioplastiki-poluchenie-svoystva-vozmozhnosti-sovershenstvovaniya> (accessed on 10 April 2024).
48. Shi, Y.; Wang, M.; Ma, C.; Wang, Y.; Li, X.; Yu, G. A Conductive Self-Healing Hybrid Gel Enabled by Metal–Ligand Supramolecule and Nanostructured Conductive Polymer. *Nano Lett.* **2015**, *15*, 6276–6281. [CrossRef] [PubMed]
49. Guo, H.; Tan, Y.J.; Chen, G.; Wang, Z.; Susanto, G.J.; See, H.H.; Yang, Z.; Lim, Z.W.; Yang, L.; Tee, B.C.K. Artificially innervated self-healing foams as synthetic piezo-impedance sensor skins. *Nat. Commun.* **2020**, *11*, 5747. [CrossRef]
50. Szarek, A.; Postawa, P.; Stachowiak, T.; Paszta, P.; Redutko, J.; Mordal, K.; Kalwik, A.; Łukomska-Szarek, J.; Gzik, M.; Jozsko, K.; et al. The Analysis of Polyethylene Hip Joint Endoprostheses Strength Parameters Changes after Use inside the Human Body. *Materials* **2021**, *14*, 7091. [CrossRef] [PubMed]
51. Kütting, M.; Roggenkamp, J.; Urban, U.; Schmitz-Rode, T.; Steinseifer, U. Polyurethane heart valves: Past, present and future. *Expert Rev. Med. Devices* **2011**, *8*, 227–233. [CrossRef]
52. Zare, M.; Ghomi, E.R.; Venkatraman, P.D.; Ramakrishna, S. Silicone-based biomaterials for biomedical applications: Antimicrobial strategies and 3D printing technologies. *J. Appl. Polym. Sci.* **2021**, *138*, 50969. [CrossRef]
53. On, S.-W.; Cho, S.-W.; Byun, S.-H.; Yang, B.-E. Bioabsorbable Osteofixation Materials for Maxillofacial Bone Surgery: A Review on Polymers and Magnesium-Based Materials. *Biomedicines* **2020**, *8*, 300. [CrossRef]

54. Vasnetsova, O.A. *Meditinskoye i Farmatsevticheskoye Tovarovedeniye*, 3rd ed.; pererab. i dop; Avtorskaya Akademiya: Moscow, Russia, 2016; 424p. (In Russian)
55. Gazazjan, M.G.; Ponomarjova, S.V.; Lipatov, V.A.; Pugachjova, A.P. Heskiy Vestnik “Chelovek i ego Zdorov’e”. 2012. No. 1. Available online: <http://cyberleninka.ru/article/n/eksperimentalnoe-obosnovanie-primeneniya-implantata-mezogel-dlya-profilaktikivnutrimatochnoy-adgezii> (accessed on 2 October 2016).
56. Lipatov, V.A.; Indrkhov, M.A.; Yarmamedov, D.M.; Lysanskaya, K.V. Morphological and physical-mechanical properties of polymer film implants in in vitro experiments. *Transbaikal Med. Bull.* **2015**, *2*, 67–73.
57. Rana, A.K.; Thakur, M.K.; Saini, A.K.; Mokhta, S.K.; Moradi, O.; Rydzkowski, T.; Alsanie, W.F.; Wang, Q.; Grammatikos, S.; Thakur, V.K. Recent developments in microbial degradation of polypropylene: Integrated approaches towards a sustainable environment. *Sci. Total. Environ.* **2022**, *826*, 154056. [[CrossRef](#)] [[PubMed](#)]
58. Shim, D.; Yeon, J.; Yi, J.; Park, J.; Park, S.N.; Lee, N. A wide-angle camera module for disposable endoscopy. *Opt. Rev.* **2016**, *23*, 596–600. [[CrossRef](#)]
59. Kim, S.J.; Choi, B.; Kim, K.S.; Bae, W.J.; Hong, S.H.; Lee, J.Y.; Hwang, T.K.; Kim, S.W. The potential role of polymethyl methacrylate as a new packaging material for the implantable medical device in the bladder. *Biomed Res. Int.* **2015**, *2015*, 852456. [[CrossRef](#)] [[PubMed](#)]
60. Kantarci, Z.; Aksoy, S.; Hasirci, N. Estimation of Monomer Content in Polymethyl Methacrylate Contact Lens Materials by Raman Spectroscopy. *Int. J. Artif. Organs* **1997**, *20*, 407–411. [[CrossRef](#)] [[PubMed](#)]
61. Zafar, M.S. Prosthodontic Applications of Polymethyl Methacrylate (PMMA): An Update. *Polymers* **2020**, *12*, 2299. [[CrossRef](#)]
62. Özdemir, T.; Usanmaz, A. Use of poly(methyl methacrylate) in radioactive waste management: I. Radiation stability and degradation. *Prog. Nucl. Energy* **2009**, *51*, 240–245. [[CrossRef](#)]
63. Vargas, K.F.; Borghetti, R.L.; Moure, S.P.; Salum, F.G.; Cherubini, K.; de Figueiredo, M.A.Z. Use of polymethylmethacrylate as permanent filling agent in the jaw, mouth and face regions—Implications for dental practice. *Gerodontology* **2011**, *29*, e16–e22. [[CrossRef](#)]
64. Allègre, L.; Le Teuff, I.; Leprince, S.; Warembourg, S.; Taillades, H.; Garric, X.; Letouzey, V.; Huberlant, S. A new bioabsorbable polymer film to prevent peritoneal adhesions validated in a post-surgical animal model. *PLoS ONE* **2018**, *13*, e0202285. [[CrossRef](#)]
65. Cai, J.; Guo, J.; Wang, S. Application of Polymer Hydrogels in the Prevention of Postoperative Adhesion: A Review. *Gels* **2023**, *9*, 98. [[CrossRef](#)]
66. Taylor, D.L.; In Het Panhuis, M. Self-Healing Hydrogels. *Adv Mater.* **2016**, *28*, 9060–9093. [[CrossRef](#)] [[PubMed](#)]
67. Sobczyk, M.; Wallmersperger, T. Modeling and simulation of the electro-chemical behavior of chemically stimulated polyelectrolyte hydrogel layer composites. *J. Intell. Mater. Syst. Struct.* **2016**, *27*, 1725–1737. [[CrossRef](#)]
68. Nonoyama, T.; Gong, J.P. Double-network hydrogel and its potential biomedical application: A review. *J. Eng. Med.* **2015**, *229*, 853–863. [[CrossRef](#)] [[PubMed](#)]
69. Zhang, D.; Di, F.; Zhu, Y.; Xiao, Y.; Che, J. Electroactive hybrid hydrogel: Toward a smart coating for neural electrodes. *J. Bioact. Compat. Polym.* **2015**, *30*, 600–616. [[CrossRef](#)]
70. MJaiswal, V. Koul. Assessment of multicomponent hydrogel scaffolds of poly(acrylic acid-2-hydroxy ethyl methacrylate)/gelatin for tissue engineering applications. *J. Biomater. Appl.* **2013**, *27*, 848–861. [[CrossRef](#)] [[PubMed](#)]
71. Nistor, M.T.; Vasile, C.; Chiriac, A.P.; Tarțău, L. Biocompatibility, biodegradability, and drug carrier ability of hybrid collagen-based hydrogel nanocomposites. *J. Bioact. Compat. Polym.* **2013**, *28*, 540–556. [[CrossRef](#)]
72. Cometa, S.; Iatta, R.; Ricci, M.A.; Ferretti, C.; De Giglio, E. Analytical characterization and antimicrobial properties of novel copper nanoparticle-loaded electrosynthesized hydrogel coatings. *J. Bioact. Compat. Polym.* **2013**, *28*, 508–522. [[CrossRef](#)]
73. Zhang, Y.; Gao, C.; Li, X.; Xu, C.; Zhang, Y.; Sun, Z.; Liu, Y.; Gao, J. Thermosensitive methyl cellulose-based injectable hydrogels for post-operation anti-adhesion. *Carbohydr. Polym.* **2014**, *101*, 171–178. [[CrossRef](#)] [[PubMed](#)]
74. Park, H.; Baek, S.; Kang, H.; Lee, D. Biomaterials to Prevent Post-Operative Adhesion. *Materials* **2020**, *13*, E3056. [[CrossRef](#)]
75. Lazarenko, V.A.; Sukovatyh, B.S.; Bezhin, A.I.; Lipatov, V.A.; Dubonos, A.A.; Zhukovskij, V.A. Chelovek i Ego Zdorov’e”. 2011. No. 1. Available online: <http://cyberleninka.ru/article/n/pervyy-opyt-primeneniya-protivospaehnogorassasyvayuschegosya-polimernogo-sredstva-mezogel-pri-ostrom-appenditsite> (accessed on 26 September 2016).
76. Huang, H.-J.; Tsai, Y.-L.; Lin, S.-H.; Hsu, S.-H. Smart polymers for cell therapy and precision medicine. *J. Biomed. Sci.* **2019**, *26*, 1–11. [[CrossRef](#)]
77. Sheftel’, V.O.; Dyshinevich, N.E.; Sova, R.E. *Toksikologiya Polimernykh Materialov; Izdaniye “Zdorov’ye”*: Moscow, Russia, 1988; 216p.
78. Mashchenko, V.I.; Shashkova, Y.O.; Solomatin, A.C.; Belyaev, V.V. Features of the formation of the microstructure of borosiloxane-based liquid crystal composites. *Bull. MGOU. Ser. Phys. Math.* **2017**, *2*, 34–45.
79. Kuhl, N.; Bode, S.; Hager, M.D.; Schubert, U.S. Self-Healing Polymers Based on Reversible Covalent Bonds. In *Self-healing Materials. Advances in Polymer Science*; Hager, M., van der Zwaag, S., Schubert, U., Eds.; Springer: Cham, Switzerland, 2015; Volume 273. [[CrossRef](#)]
80. Xie, Z.; Hu, B.-L.; Li, R.-W.; Zhang, Q. Hydrogen Bonding in Self-Healing Elastomers. *ACS Omega* **2021**, *6*, 9319–9333. [[CrossRef](#)] [[PubMed](#)]
81. Guo, H.; Han, Y.; Zhao, W.; Yang, J.; Zhang, L. Universally autonomous self-healing elastomer with high stretchability. *Nat. Commun.* **2020**, *11*, 2037. [[CrossRef](#)]

82. Kar, A.K. Photofluidics—A New Platform for Biophotonics. In Proceedings of the 2012 International Conference on Fiber Optics and Photonics (PHOTONICS), Chennai, India, 9–12 December 2012.
83. Yimyai, T.; Crespy, D.; Pena-Francesch, A. Self-Healing Photochromic Elastomer Composites for Wearable UV-Sensors. *Adv. Funct. Mater.* **2023**, *33*, 2213717. [[CrossRef](#)]
84. Saito, M.; Sakiyama, K. Self-healable photochromic elastomer that transmits optical signals depending on the pulse frequency. *J. Opt.* **2013**, *15*, 105404. [[CrossRef](#)]
85. Wang, S.; Lee, J.M.; Yeong, W.Y. Smart hydrogels for 3D bioprinting. *Int. J. Bioprinting* **2015**, *1*, 3–14. [[CrossRef](#)]
86. El Choufi, N.; Mustapha, S.; Tehrani, B.A.; Grady, B.P. An Overview of Self-Healable Polymers and Recent Advances in the Field. *Macromol. Rapid Commun.* **2022**, *43*, e2200164. [[CrossRef](#)]
87. Champagne, J.; Pang, S.; Li, G. Effect of Confinement Level and Local Heating on Healing Efficiency of Self-healing Particulate Composites. *Compos. Part B* **2016**, *97*, 344–352. [[CrossRef](#)]
88. Lee, J.; Bhattacharyya, D.; Zhang, M.Q.; Yuan, Y.C. Mechanical properties of mendable composites containing self-healing thermoplastic agents. *Compos. Part B* **2014**, *62*, 10–18.
89. Doan, T.Q.; Leslie, L.S.; Kim, S.Y.; Bhargava, R.; White, S.R.; Sottos, N.R. Characterization of core-shell microstructure and self-healing performance of electrospun fiber coatings. *Polymer* **2016**, *107*, 263–272. [[CrossRef](#)]
90. Rong, Z.; Li, Y.; Lim, R.Z.; Wang, H.; Dong, Z.; Li, K.; Wang, X. Fire-retardant effect of titania-polyurea coating and additional enhancement via aromatic diamine and modified melamine polyphosphate. *Npj Mater. Degrad.* **2022**, *6*, 38. [[CrossRef](#)]
91. Shen, X.; Dong, Z.; Sim, C.; Li, Y. A Comparative Study on the Self-Healing Characterizations and Formulation Optimization of Polyurea Coating. *Polymers* **2022**, *14*, 3520. [[CrossRef](#)]
92. Ma, J.; Porath, L.E.; Haque, F.; Sett, S.; Rabbi, K.F.; Nam, S.; Miljkovic, N.; Evans, C.M. Ultra-thin self-healing vitrimer coatings for durable hydrophobicity. *Nat. Commun.* **2021**, *12*, 5210. [[CrossRef](#)] [[PubMed](#)]
93. Zhu, D.Y.; Chen, F.; Rong, M.Z.; Zhang, M.Q. Chapter 5—Capsules-based self-healing polymers and polymer composites. In *Recent Advances in Smart Self-Healing Polymers and Composites*, 2nd ed.; Li, G., Feng, X., Eds.; Woodhead Publishing: Shaston, UK, 2022; pp. 113–140. [[CrossRef](#)]
94. Kosarli, M.; Bekas, D.; Tsirka, K.; Paipetis, A.S. *Capsule-Based Self-Healing Polymers and Composites*; Thomas, S., Surendran, A., Eds.; Self-healing polymer-based systems; Elsevier: Amsterdam, The Netherlands, 2020; pp. 259–278. [[CrossRef](#)]
95. Kötteritzsch, J.; Hager, M.D.; Schubert, U.S. Tuning the self-healing behavior of one-component intrinsic polymers. *Polymer* **2015**, *69*, 321–329. [[CrossRef](#)]
96. Li, Y.; Yang, Z.; Zhang, J.; Ding, L.; Pan, L.; Huang, C.; Zheng, X.; Zeng, C.; Lin, C. Novel polyurethane with high self-healing efficiency for functional energetic composites. *Polym. Test.* **2019**, *76*, 82–89. [[CrossRef](#)]
97. Zavada, S.R.; McHardy, N.R.; Gordon, K.L.; Scott, T.F. Rapid, Puncture-Initiated Healing via Oxygen-Mediated Polymerization. *ACS Macro Lett.* **2015**, *4*, 819–824. [[CrossRef](#)]
98. Hia, I.L.; Vahedi, V.; Pasbakhsh, P. Self-Healing Polymer Composites: Prospects, Challenges, and Applications. *Polym. Rev.* **2016**, *56*, 225–261. [[CrossRef](#)]
99. Wang, J.; Xu, W.; Li, Z.; Zhou, Z. Damping and Self-Healing Properties of Polyborosiloxane Composites. *Polym. Mater. Sci. Eng.* **2018**, *34*, 84–90.
100. Wu, T.; Chen, B. Synthesis of Multiwalled Carbon Nanotube-Reinforced Polyborosiloxane Nanocomposites with Mechanically Adaptive and Self-Healing Capabilities for Flexible Conductors. *ACS Appl. Mater. Interfaces* **2016**, *8*, 24071–24078. [[CrossRef](#)]
101. Osada, T.; Kamoda, K.; Mitome, M.; Hara, T.; Abe, T.; Tamagawa, Y.; Nakao, W.; Ohmura, T. A Novel Design Approach for Self-Crack-Healing Structural Ceramics with 3D Networks of Healing Activator. *Sci. Rep.* **2017**, *7*, 17853. [[CrossRef](#)]
102. Turkenburg, D.H.; Fischer, H.R. Reversible cross-linking in composite binders—In-situ repair options and recyclability. *Adv. Mater. Lett.* **2018**, *9*, 861–866. [[CrossRef](#)]
103. Yoshioka, S.; Nakao, W. Methodology for evaluating self-healing agent of structural ceramics. *J. Intell. Mater. Syst. Struct.* **2015**, *26*, 1395–1403. [[CrossRef](#)]
104. Nakao, W.; Abe, S. Enhancement of the self-healing ability in oxidation induced self-healing ceramic by modifying the healing agent. *Smart Mater. Struct.* **2012**, *21*, 025002. [[CrossRef](#)]
105. Farle, A.S.; Kwakernaak, C.; van der Zwaag, S.; Sloof, W.G. A conceptual study into the potential of Mn+1AX_n-phase ceramics for self-healing of crack damage. *J. Eur. Ceram. Soc.* **2015**, *35*, 37–45. [[CrossRef](#)]
106. Li, S.; Song, G.; Kwakernaak, K.; van der Zwaag, S.; Sloof, W.G. Multiple crack healing of a Ti₂AlC ceramic. *J. Eur. Ceram. Soc.* **2012**, *32*, 1813–1820. [[CrossRef](#)]
107. Ghosh, S.K. *Self-Healing Materials: Fundamentals, Design Strategies, and Applications* Edited by Swapan Kumar Ghosh; WILEY-VCH Verlag GmbH & Co.: Weinheim, Germany, 2009; p. 306.
108. Ono, M.; Nakao, W.; Takahashi, K.; Nakatani, M.; Ando, K. A new methodology to guarantee the structural integrity of Al₂O₃/SiC composite using crack healing and a proof test. *Fatigue Fract. Eng. Mater. Struct.* **2007**, *30*, 599–607. [[CrossRef](#)]
109. Zhang, S.; Kwakernaak, C.; Sloof, W.; Brück, E.; van der Zwaag, S.; van Dijk, N. Self healing of creep damage by gold precipitation in iron alloys. *Adv. Eng. Mater.* **2015**, *17*, 598–603. [[CrossRef](#)]
110. Al-Fakih, A.; Mahamood, M.A.A.; Al-Osta, M.A.; Ahmad, S. Performance and efficiency of self-healing geopolymer technologies: A review. *Constr. Build. Mater.* **2023**, *386*, 131571. [[CrossRef](#)]

111. Laha, K.; Kyono, J.; Shinya, N. An advanced creep cavitation resistance Cu-containing 18Cr–12Ni–Nb austenitic stainless steel. *Scr. Mater.* **2007**, *56*, 915–918. [[CrossRef](#)]
112. Kodzoev, M.-B.K.; Isachenko, S.L. Self-healing concrete [Electronic resource]. *Sci. J. Bull. Sci. Pract.* **2018**, *4*, 287–290. Available online: <http://www.bulletennauki.com/kodzoev-isachenko-1> (accessed on 18 April 2024).
113. Jonkers, H.M.; Schlangen, E. Development of a bacteria-based self healing concrete. *Tailor Made Concr. Struct.* **2008**, *1*, 425–430. [[CrossRef](#)]
114. Stefanidou, M.; Tsardaka, E.-C.; Karozou, A. Nanoparticles controlling self-healing properties in cement pastes. *Mater. Today Proc.* **2021**, *54*, 22–27. [[CrossRef](#)]
115. Ahn, T.H.; Kishi, T. Crack self-healing behavior of cementitious composites incorporating various mineral admixtures. *J. Adv. Concr. Technol.* **2010**, *8*, 171–186. [[CrossRef](#)]
116. Soltskiy, S.V.; Orlova, N.L.; Velichko, A.S. Crack self-healing in clay-cement concrete diaphragm of embankment dam. *Mag. Civ. Eng.* **2018**, *77*, 3–12.
117. Tolstoy, A.; Gridchin, A.; Glagolev, E.; Lesovik, R.; Shapovalov, N. Efficient Construction Composites for Construction in the North and the Arctic. *Lect. Notes Civ. Eng.* **2021**, *147*, 15–22.
118. Terzis, D.; Laloui, L. A decade of progress and turning points in the understanding of bio-improved soils: A review. *Géoméch. Energy Environ.* **2019**, *19*, 100116. [[CrossRef](#)]
119. Bruyako, M.; Grigorieva, L.; Grigorieva, A.; Ivanova, I. Treatment of natural zeolites for increasing the sorption capacity. *Solid State Phenom.* **2016**, *871*, 70–75. [[CrossRef](#)]
120. Bruyako, M.; Grigoryeva, L. Bioactive additives for self-healing of concrete microstructure. *Mater. Sci. Forum* **2018**, *945*, 36–41. [[CrossRef](#)]
121. Bruyako, M.; Grigor'eva, A.; Stepina, I.; Golotenko, D.; Podsevalova, A. Biomodified building materials on the base of mineral binders. In Proceedings of the IOP Conference Series: Materials Science and Engineering, 7th International Scientific Conference on Integration, Partnership and Innovation in Construction Science and Education, Tashkent, Uzbekistan, 11–14 November 2020; Volume 1030, p. 012005.

Disclaimer/Publisher's Note: The statements, opinions and data contained in all publications are solely those of the individual author(s) and contributor(s) and not of MDPI and/or the editor(s). MDPI and/or the editor(s) disclaim responsibility for any injury to people or property resulting from any ideas, methods, instructions or products referred to in the content.

Chapter 2. Epoxies in Electronics: Properties, Applications, and Modifications

2.1 Motivation of the article

The motivation behind this review article stems from the critical and multifaceted role epoxy resins (ERs) play in modern materials science. Epoxies are not only foundational materials across various industries due to their diverse characteristics and versatile applications but also essential in the realm of electrical insulation. This review seeks to consolidate current knowledge on ERs, encompassing their wide-ranging properties, chemical modifications, and curing processes. By exploring the mechanisms of dielectric breakdown and strategies to enhance dielectric strength, this paper aims to highlight the significance of epoxies in ensuring reliable electrical insulation. Additionally, the inclusion of recent research and advancements offers readers an updated perspective on the innovations driving this field. The examination of electrical resistance and conductivity, particularly their frequency-dependent behavior, underscores the importance of understanding these properties to optimize the performance of epoxy-based materials. This comprehensive overview serves as a valuable resource for researchers and industry professionals, providing insights into the multifaceted nature of epoxies and their pivotal role in advancing materials science. Through this review, we aim to foster a deeper understanding and appreciation of ERs, encouraging further research and development in this dynamic field.

2.2 Conclusion on the article

In conclusion, this review provides a comprehensive examination of epoxy ER, focusing on their dielectric strength distribution, thermal conductivity, specific conductivity, frequency-dependent dielectric constant, transmittance, electrical conductivity, and bending strength. The dielectric strength distribution in modified ERs highlights their robust insulation properties, making them essential in electrical and electronic applications. Advances in thermal conductivity demonstrate the potential of ERs to efficiently manage heat dissipation, enhancing their suitability for high-performance environments. Specific conductivity studies reveal the adaptability of ERs in various applications, ranging from insulating to semi-conductive roles, depending on the modification techniques employed. The dependence of the dielectric constant on frequency underscores the dynamic behavior of ERs under different electrical conditions, which is crucial for optimizing their performance in specific applications. Transmittance properties of modified ERs open avenues for their use in optical and photonic technologies, while their electrical conductivity showcases their versatility in applications requiring precise control of electrical properties.

2.3 Applicant's contribution

As the first author the applicant is responsible for the majority of the manuscript.

2.4 Article 2

The paper "*A Brief Overview on Epoxies in Electronics: Properties, Applications, and Modifications*" was published in September 2023 in "*Polymers*" journal (IF: 5.0; Q1). It is very recent but already has 6 citations (as of 02.06.2024).

Review

A Brief Overview on Epoxies in Electronics: Properties, Applications, and Modifications

Rashid Dallaev *, Tatiana Pisarenko, Nikola Papež , Petr Sadovský * and Vladimír Holcman

Department of Physics, Faculty of Electrical Engineering and Communication, Brno University of Technology, Technická 2848/8, 61600 Brno, Czech Republic; 177722@vut.cz (T.P.); papez@vut.cz (N.P.); holcman@vut.cz (V.H.)
* Correspondence: rashid.dallaev@vut.cz (R.D.); sadovsky@email.cz (P.S.)

Abstract: This paper offers a short overview of epoxy resins, encompassing their diverse characteristics, variants, chemical modifications, curing processes, and intriguing electrical properties. Epoxies, valued for their multifunctional attributes, serve as fundamental materials across industries. In the realm of dielectric strength, epoxy resins play a crucial role in electrical insulation. This paper discusses the mechanisms governing dielectric breakdown, strategies to enhance dielectric strength, and the impact of various fillers and additives on insulation performance. Through an exploration of recent research and advancements, this paper delves into the spectrum of epoxy properties, the array of subspecies and variants, their chemical adaptability, and the intricacies of curing. The examination of electrical resistance and conductivity, with a focus on their frequency-dependent behavior, forms a pivotal aspect of the discussion. By shedding light on these dimensions, this review provides a concise yet holistic understanding of epoxies and their role in shaping modern materials science.

Keywords: epoxy resins; thermal conductivity; dielectric strength; chemical modifications; electrical conductivity; curing



Citation: Dallaev, R.; Pisarenko, T.; Papež, N.; Sadovský, P.; Holcman, V. A Brief Overview on Epoxies in Electronics: Properties, Applications, and Modifications. *Polymers* **2023**, *15*, 3964. <https://doi.org/10.3390/polym15193964>

Academic Editor: Keon-Soo Jang

Received: 6 September 2023

Revised: 25 September 2023

Accepted: 27 September 2023

Published: 30 September 2023



Copyright: © 2023 by the authors. Licensee MDPI, Basel, Switzerland. This article is an open access article distributed under the terms and conditions of the Creative Commons Attribution (CC BY) license (<https://creativecommons.org/licenses/by/4.0/>).

1. Introduction

1.1. Properties of Epoxy Resins

The evolving landscape of electronics and microprocessor technology, characterized by increasingly potent components within devices, necessitates the advancement of highly efficient composite materials. This also calls for the innovation of robust resins (polymeric materials) that are capable of performing reliably under extreme conditions, including elevated temperatures, exposure to solar radiation, and high humidity levels. These materials are essential for effectively sealing electronic devices that are made from diverse substrates such as plastic, brass, aluminum, copper, and carbon steels. Additionally, they play a vital role in providing protective coatings for structural materials, safeguarding them against various forms of impact and shock [1,2].

The range of use is determined by the parameters of epoxy resins (ERs): thermal conductivity and electrical conductivity. Ensuring reliable adhesion on boards formed from fiberglass with plastic and metal, as well as a combination of dielectric properties with light transmission, are in demand in microelectronics and electrical engineering [3].

The widespread use of epoxy resins in the production of electronic components is due to their high manufacturability and the unique set of performance characteristics of their curing products [4–7]:

- Excellent dielectric/electrical insulating properties;
- Ultra-high water resistance;
- Chemical resistance (resistance to a number of aggressive chemicals, alkalis, acids, salts, solvents);
- High mechanical properties (ideal tensile strength, wear resistance, hardness, impact resistance);

- The highest adhesion (high-quality glue connection);
- Low shrinkage during curing (minor deformations);
- High stability;
- Increased heat resistance (withstands temperatures up to 150–200 °C. High coefficient of thermal conductivity);
- The absence of volatile products and the release of side substances during curing;
- A low coefficient of shrinkage in the course of hardening;
- Minimum creep under load;
- Low odor;
- Ease of production and versatility of processing processes;
- Small weight of the finished product;
- Durability and shelf life;
- Environmental friendliness;
- Safety.

The complex of unique physicochemical (hardness, elasticity, tensile strength, density, conductivity) and physicochemical properties (solubility, reactivity, pH level, heat of combustion, electronegativity) of epoxy resin allows products based on them to cover a wide range of applications in various fields of electrical and radio engineering. Scientific and technical research that focuses on the development of the most specialized coatings (epoxy fills) that are resistant to highly aggressive environments, improving the properties of epoxy resin as a dielectric (electrical conductivity and insulation strength), and satisfying certain operating conditions is steadily growing [8].

At the present stage of the development of space technology, it has been established that the most dangerous factor for existing spacecraft is the functional damage to on-board radio-electronic equipment from ionizing and secondary electromagnetic radiation. The impact of such radiation leads to structural changes in materials, the occurrence of ionization, heating, the appearance of induced radioactivity, and other phenomena that disrupt physical and chemical processes in technical devices [9].

After curing, epoxy resins act as a high-quality insulator that provides the sealing (low hygroscopicity and electrical insulation) of conductive circuits from the effects of electrostatic discharge, high temperatures, vibrations, moisture, chemicals, and shocks in electrical and radio engineering products.

1.2. Applications of Epoxy Resins

Epoxy resin hold significant importance within the electronics industry and find applications in a range of equipment including motors, generators, transformers, switchgear, bushings, and insulators. These epoxy resins offer outstanding electrical insulation properties, effectively shielding electrical components from potential issues like short circuits, dust ingress, and moisture exposure [10].

In addition, metal-filled polymers are widely adopted for electromagnetic interference shielding [11]. Epoxy molding compounds (EMCs) are favored as encapsulation materials for semiconductor devices, safeguarding integrated circuit components against environmental challenges such as moisture, mobile-ion contaminants, temperature variations, radiation, and humidity, as well as mechanical and physical damage. Furthermore, epoxy composites, enriched with particulate fillers like fused silica, glass powder, and mineral silica, have seen extensive use as substrate materials in electronic packaging applications [12].

As sealants, epoxy resins (compounds) remain popular among polymeric materials in terms of application. To date, due to the thermodynamic and reactive compatibility of epoxy oligomers, a huge number of compounds have been synthesized, and various hardeners have been successfully used to turn thermoplastic resins into infusible ones [13].

ERs are one of the most important class of thermoplastics and the following broad areas of their application are listed below [14–17]:

- Radio, electrical industry, electronics, and microelectronics (chip assembly and printed circuit board assembly, which is an epoxy–fiberglass composite);

- The rocket and space industry;
- The energy industry;
- The engineering industry (production of components);
- Construction (paints and varnishes for interior and exterior decoration of buildings; polishes; the production of durable impregnations and structural materials (PCM); sealants; adhesives; the waterproofing of floors, walls of basements, and swimming pools; the impregnation of concrete, brick, wood, and mortar; the successful replacement of bitumen—bitumen–epoxy composition);
- The textile and leather industries;
- The furniture industry (designer furniture);
- Arts and crafts (the production of unique costume jewelry; the production of artificial amber; models; crafts; dioramas; and in bench modeling);
- The domestic sphere and household (home decor; bar counters).

Their implementations, specifically in the production of electronic components, are the following [18–20]:

1. Printed circuit boards (PCBs): epoxy resin is used as a substrate material for printed circuit boards, providing insulation between board layers and protecting components from environmental influences;
2. Sealing: epoxy resin is used to seal electronic components, protecting them from environmental influences such as moisture and dust;
3. Adhesives: epoxy resin is used as an adhesive in the production of electronic components, and is a sensitive strong bond between components and substrates;
4. Coatings: epoxy resin is used as a coating material for electronic components, providing protection against moisture, chemical compounds, and abrasion.

1.3. Curing and Modification of Epoxy Resins

The use of epoxy resin in the manufacturing of electronic components typically involves a curing process, in which the resin is mixed with hardener and then subjected to heating or ultraviolet radiation to initiate a curing reaction. Amines were among the first epoxy resin hardeners, and they have retained a leading position among all reagents of this type [21,22].

The curing process can be carried out using various technologies, including the following [18]:

- Vacuum impregnation: this involves placing the electronic component within a vacuum chamber, where epoxy resin is drawn into the component under vacuum pressure;
- Pouring: in this method, an electronic component is situated in a mold and epoxy resin is poured over it, effectively sealing the component;
- Dispensing: epoxy is administered onto an electronic component using a dispensing machine;
- Spray coating: here, epoxy resin is applied onto an electronic component via a spray gun.

The cross-linking or curing process is usually slow, especially when small volumes of resin are involved. Fast curing hardeners can be used, but they generate a lot of heat during the process, resulting in a strong exothermic reaction that can damage electronic components and cause high mechanical stress not only on them, but also on the circuit [23].

The process of curing epoxy polymers involves the utilization of a hardening agent, typically a primary or secondary amine or an acid anhydride. This agent serves as a binding element among the distinct macromolecules. In order to facilitate the creation of a three-dimensional network, which is crucial for conferring the ultimate product with the characteristics of an impenetrable and non-soluble material (as depicted in Figure 1), it is imperative that the hardening agent possesses a functionality of two or greater [24].

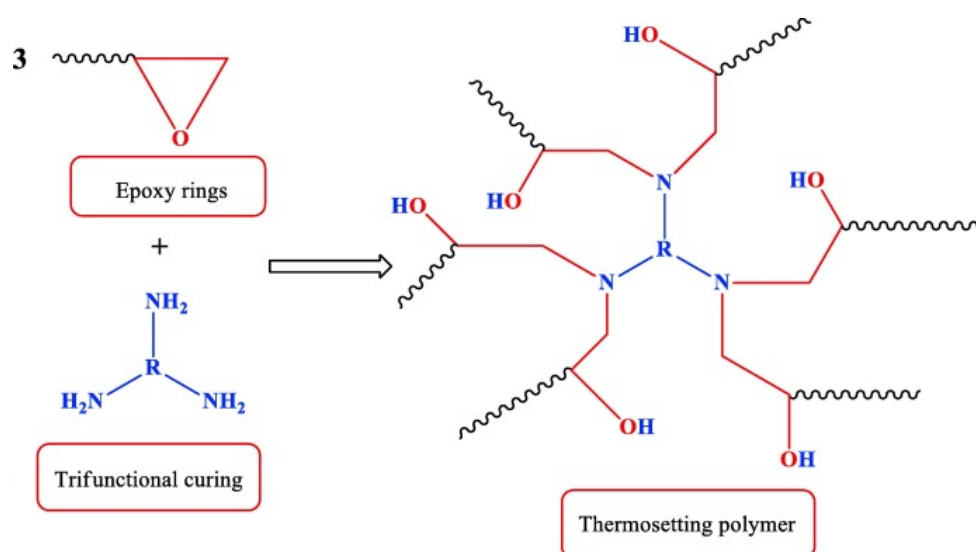


Figure 1. Illustration of the formation process of a polymer with a three-dimensional structure. (Figure from [24], permission granted by “Elsevier”).

Epoxy oligomers and polymers are widely used as matrices for the production of carbon plastics, which are characterized by a combination of high strength and rigidity with low density, a low temperature coefficient of friction, high thermal and electrical conductivity, wear resistance, and resistance to thermal and radiation effects [25].

Epoxy polymers are polar materials, and dipole polarization plays an important role in the dielectric relaxation spectrum. In such polymers, the formation and relaxation of the electrical state is controlled by the interaction of homo- and heterocharges. After polarization, molecular dipoles are oriented in the direction of the polarizing field, and the spatial structure of the polymer is fixed by a three-dimensional network of chemical bonds; as a result, charge carriers are permanently “frozen” in the structure of the network curing product [26].

Studies on the influence of the chemical structure on the properties of epoxy polymers show that a change in the entire complex of polymer properties can be achieved by changing the nature of the initial oligomers and hardeners, as well as their ratio [27].

Epoxy resin is chemically inert; there is a cold, hot, and combined curing. In the liquid state, epoxy resin is extremely vulnerable to high humidity; the cured resin is not toxic.

Now, there are six major classes of epoxy resins—bisphenol (A and F), novolac (phenolic and cresol), aliphatic (mono- and highly functional), glycidyl, and acrylic epoxy. Dozens of their subspecies are known, including light-cured and water-borne ones (their widespread introduction is hindered by high cost) [28].

An integral component of epoxy resin, as a two-component thermosetting polymer, is a hardener, of either the cold or hot type, which determines the further technical characteristics of the epoxy (ductility, strength, hardness, UV resistance, resistance to abrasion). Their percentage ratio is extremely important for the quality performance of the composition. The main part of the additives are the plasticizers: dibutyl phthalate, diethylene glycol (DEG-1), diphenyl phthalate, polyesters, styrene oxide, and thiokol, and the inclusion of silicon components in the mixture determines the resistance to heat.

The chemical modification of polymers is carried out by introducing small fragments of a different nature into the composition of macromolecules. Changing the chemical nature of oligomers and hardeners makes it possible to increase the length of the molecular chain of the oligomer and hardener to vary the structure of the internodal sections of the cured system, to modify the end groups of oligomer macromolecules, thereby changing the macroscopic properties of the epoxy polymer. The introduction of reactive additives that are capable of entering into a chemical reaction with the polymer makes it possible to

regulate the physical and mechanical properties of epoxides, such as heat resistance, aging resistance, etc., in a wide range [29].

It is known from the literature that dispersed fillers cause a change in almost all properties of liquid and cured epoxy compositions: they increase the viscosity of the binder, and reduce its mobility and viability [30–32], as well as affect the crack resistance, mechanical properties, degradation temperature, wear resistance, thermal conductivity, water resistance, and adhesion [33–35]. However, the introduction of dispersed fillers into the epoxy binder is accompanied by a deterioration in the water resistance of the material, which limits or makes it impossible to use it in contact with water [36]. Given that cured epoxy resin has a micro-heterogeneous structure [37,38] and its destruction upon contact with water begins with amorphous disordered areas, it is assumed that the introduction of polar fillers into the binder would contribute to the structuring of the cured resin and reduce water absorption; the introduction of non-polar fillers will lead to a disordering of the material and an increase in water absorption [39].

In the study and regulation of the dielectric properties of epoxy oligomers, using various thinners, fillers, curing accelerators, and plasticizers, special attention is paid to the molecular structure of the resulting composites.

The composition (epoxy–bakelite or epoxy–phenolic) has very high dielectric, and especially mechanical, properties, water resistance, and heat resistance. These epoxy compositions are widely used for the production of electrical insulating varnishes and adhesives. Polysulfide resins (thiokols) are also used to cure epoxy resins. The resulting compositions have high elasticity and impact strength, and good dielectric properties are applied to the production of elastic filling compounds. Epoxy–polyester compositions with the introduction of fillers are widely used for the manufacture of casting compounds for the cast insulation of windings of electrical machines, apparatus, and transformers [40]. Plasticizers, solvents, and non-reactive rubbers degrade the properties of epoxy compositions [41]. As active diluents and flexibilizers of ES, aliphatic compounds are widely used as epoxy-containing modifiers based on glycidyl ethers [42].

Due to their low viscosity, they are called active ES thinners, since they are able to replace solvents in the composition of epoxy compositions and copolymerize with ES without releasing by-products. There is a “chemical” modification of the epoxy composition due to the incorporation of flexible fragments into a rigid polymer network and an increase in the molecular weight of the segment [25,43,44]. Epoxy binders have the advantage of low shrinkage and high strength properties. However, scientific and technological progress constantly increases operational requirements, so polymers must be modified. The most promising are composite materials with nanosized fillers—nanocomposites [45–47].

The development of new composite materials has expanded the production and use of epoxy resins by several orders of magnitude. Depending on the use, the composition and the amount of filler (solvents, hardeners, stabilizers, plasticizers, and modifiers) are taken into account; thus, the dielectric and physicomachanical properties of cured epoxy resins can vary widely. Depending on the number of epoxy groups, uncured epoxy resins are in a liquid or solid state. They are popular and cover a wide range of applications (from 70 to 90%), such as epoxy–diane resins (diphenylol propane) based on bisphenol A.

The curing agent polyaminoamide is utilized for curing liquid, low-molecular-weight epoxy resins and their compounds. The weight ratio of epoxy resin to curing agent can be adjusted to achieve specific properties in the final cured material. A higher content of the curing agent (above 70% by weight) results in a more elastic and impact-resistant cured resin. However, this comes at the expense of reduced hardness and resistance to high temperatures (attributed to a lower glass transition temperature). This curing agent is suitable for applications requiring cold-cure epoxy resin, where the curing process occurs at room temperature. It is important to note that, according to the product’s safety data sheet, this substance is caustic, may cause skin irritation, and has the potential for sensitization [48].

When epoxy resins are exposed to compounds containing a mobile hydrogen atom, they are able to cure with the formation of three-dimensional infusible and insoluble products with high physical and technical properties. Thus, it is not the epoxy resins themselves that are thermosetting, but their mixtures with hardeners and catalysts. Various substances are used as hardeners for epoxy resins: diamines (hexamethylenediamine, metaphenylenediamine, polyethylenepolyamine), carboxylic acids, or their anhydrides (maleic, phthalic).

Epoxy resins mixed with the above hardeners form thermoset compositions with valuable properties:

- High adhesion to the surface of the material on which they harden;
- High dielectric properties;
- High mechanical strength;
- Good chemical resistance and water resistance;
- Hardening does not emit volatile products and are characterized by low shrinkage (2–2.5%) [40].

Recently, the traditionally used non-reactive modifiers (plasticizers, solvents, and rubbers), which, along with an increase in the elasticity of epoxy materials, lead to a decrease in network density and are able to migrate from the material during operation and increase shrinkage, are being replaced by modifiers that can be embedded in the epoxy matrix. In this case, preference is given to those modifiers that do not lead to the formation of by-products of the reaction and do not increase the number of volatiles released. Such modifiers include, in particular, mono- and polyfunctional low-molecular-weight and oligomeric epoxy compounds, as well as mono- and polyfunctional cyclocarbonates [49].

The study of the phenomenon of heat transfer is very important in the manufacturing of composite materials for protective screens. We consider multilayer plates as radiation shields, which compete with single-layer plates made from the same complex composite materials. Samples in the form of thin plates of epoxy resin grade ED-20 with a filler of soot, graphite, and aluminum powder were studied. Analyzing the results, we can conclude that the introduction of graphite and aluminum powder can significantly increase the effective thermal conductivity of the tested samples. The values of thermal conductivity with carbon black are ambiguous, and to determine the reason for this behavior, an X-ray diffraction study of both the carbon black and graphite that were used is necessary [50].

1.4. Dielectric Analysis

Dielectric analysis (DEA) is a method used to monitor the curing process of polymer materials. It involves the measurement of electrical properties, such as dielectric permittivity (or capacitance) and dielectric loss (or conductivity), as a function of time, temperature, or frequency during the curing process. DEA is particularly useful for materials like thermosetting resins, which undergo a chemical transformation during the curing process. It provides a non-destructive and real-time method to monitor and control the curing process, ensuring that the final material possesses the desired properties [51–54].

In the context of the dielectric analysis (DEA) method, the ionic viscosity parameter and the actual viscosity of a system are related through the dielectric properties of the material being analyzed. Specifically, the ionic viscosity parameter is related to the ion mobility of the material, which in turn can affect its dielectric properties. The actual viscosity of a material refers to its resistance to flow or deformation. It is a measure of the material's mechanical behavior. The ionic viscosity parameter is, on the other hand, related to ion mobility and electrical behavior; the actual viscosity is related to the material's mechanical response. In some cases, there may be a correlation between the ionic viscosity parameter and the actual viscosity, especially if the movement of ions significantly impacts the flow behavior of the material [53–55].

There are several important parameters of the curing process; among them are the gelation time and curing degree. In brief, the curing degree represents the extent of polymerization or cross-linking that has occurred, while the gelation time is the point in

time at which a material starts to transition from a liquid or gel to a solid. Both parameters are significant in various industries where the precise control of material properties is essential [56,57].

The curing process of a thermoset involves a complex series of chemical reactions. Primarily, both gelation and vitrification play pivotal roles [58]. This process commences with the creation and extension of linear chains, which then begin to branch and subsequently cross-link, resulting in the formation of three-dimensional networks in most cases. As the curing progresses, there is an escalation in molecular weight, culminating in various chains forming an extensive network with an infinite molecular weight. This abrupt and irreversible transition from a viscous liquid to a resilient gel is referred to as the “gel point”, which can be defined as the moment when the average molecular weight approaches infinity.

It is worth mentioning that it is also possible to monitor the curing process of a composite material using a multi-channel dielectric analysis (DEA) and potentially correlate it with the thickness of the composite. The thickness of a composite material can influence the curing process. Thicker sections may cure differently than thinner ones due to variations in heat distribution, mass, and heat dissipation. Monitoring multiple channels allows for a more comprehensive understanding of how thickness impacts the curing process. Variations in thickness can lead to non-uniform curing. A multi-channel DEA can detect inhomogeneities in the curing process, providing valuable insights into how different parts of the composite are curing [59,60].

2. Experimental Data on Modified ERs and Their Properties

2.1. Dielectric Strength Distribution in Modified ER

When modified with various substances, the properties of the polymer matrix (intermolecular interactions) change, affecting the kinetics and mechanisms of molecular processes, which significantly affect the technological and electrical properties of epoxy compounds.

The works [61,62] describe the principle of creating a chemical structure oriented at the molecular level, which makes it possible to create oriented structures along which a heat flux propagates. Based on the chemical structure of bisphenol epoxy resin, it is noted that the thermal conductivity of such oriented materials can reach $10 \text{ W}/(\text{m K})$. Oriented structures can also be obtained via the mechanical pressing of elongated fillers, simulating the formation of heat-conducting bridges. In [63], it was shown that when 50 wt% Al_2O_3 powder of three different sizes was introduced into the mixture of an epoxy compound (Shell Chemical (Houston, TX, USA)) without chemical modifications of the filler surface, as well as a combination of micro- and nano-sized fillers without changing the total percentage of the filler, the λ values of the epoxy compound increased when moving from the nano to the micro-sized filler. When half of the Al_2O_3 particles with a size of $100 \mu\text{m}$ in the epoxy compound are replaced by particles with a size of 25 nm , there is a significant decrease in the effective thermal conductivity. This may be due to a decrease in the number of large particles of the highly thermally conductive filler necessary to create a heat-conducting cluster [64].

Figure 2 illustrates the correlation between the DC breakdown strength and nano- SiO_2 concentration. Initially, the electric breakdown strength of nano- SiO_2 -enhanced RIP (resin-impregnated insulation paper) experiences an ascent with rising content, reaching its zenith at 2 wt%. Subsequently, it diminishes for 3 and 4 wt%. In comparison to unmodified RIP, the maximum DC breakdown strength saw an increment of 10.6% [65].

Figure 3 displays the temperature-dependent spectral characteristics of the complex permittivity at a frequency of 50 Hz, featuring different levels of liquid rubber content. In Figure 3a, we observe the relative permittivity (ϵ'), while in Figure 3b, the dielectric loss factor (ϵ'') is illustrated. Notably, the incorporation of liquid rubber leads to a significant increase in ϵ' within the composites.

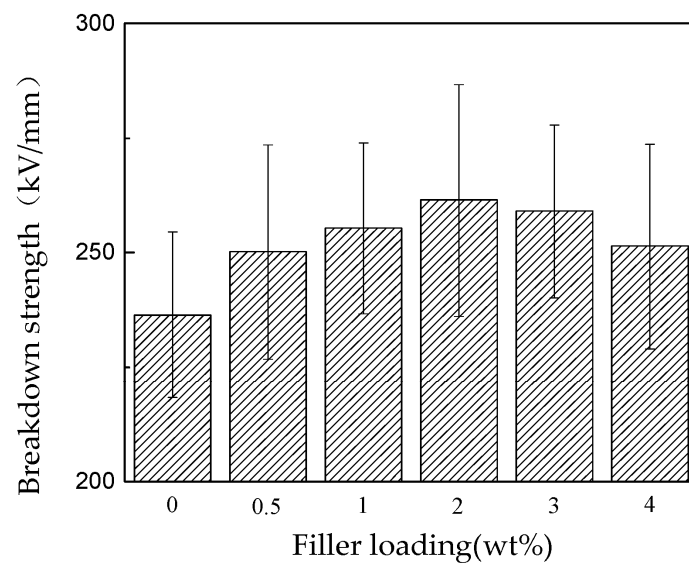


Figure 2. Histogram depicting the breakdown strength of RIP with varying nanoparticle constituents [65].

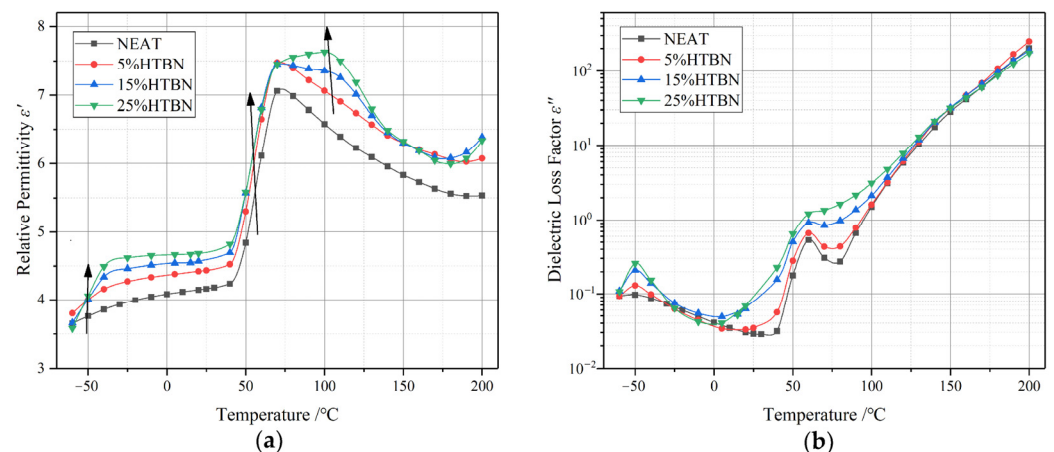


Figure 3. Temperature-dependent spectral properties of epoxy resin with varying proportions of hydroxyl-terminated liquid nitrile rubber (HTBN) at a frequency of 50 Hz: (a) relative permittivity; (b) dielectric loss factor [66].

Moreover, if we follow the arrow in Figure 1a, we notice variations in the dielectric relaxations across distinct temperature ranges: low (from -60 °C to -10 °C), medium (from 0 °C to 90 °C), and high temperatures (from 90 °C to 200 °C). In the low-temperature range, the ϵ'' initially rises and then declines with the increasing temperature. A notable relaxation peak emerges at -50 °C, representing the secondary transition of the epoxy resin. It is worth noting that composites that have been toughened with liquid rubber exhibit a considerably higher magnitude in the relaxation peak when compared to pure epoxy resin. The positions of the relaxation peak remain consistent across different filler contents, suggesting a superposition effect originating from the orientation of HTBN molecules (HTBN α relaxation) and the secondary transition within the epoxy resin.

There is a patent that describes a method for obtaining an electrically insulating material with excellent insulating properties [64]. The electrically insulating material contains epoxy resin; hardener; elastomeric particles; inorganic particles; and other additive materials. The authors proposed a solution to the problem of reducing the strength and electrical-insulating properties of high-voltage insulation due to the thermal expansion of the epoxy resin and the formation of cracks. The solution lies in the use of dielectric microparticles. The patent discloses a method of mixing together ultrafine particles, a

hardener, and a curing accelerator of thermosetting resins. The described method ensures the achievement of excellent electrically insulating, thermally conductive, and mechanical properties of the resulting material. In addition, the proposed inorganic filler may be Al_2O_3 , TiO_2 , AlN , BN , or a combination thereof. Preference is given to particles with an average size of 500 μm or less.

The patent [67] describes a process for producing an epoxy composite material with a low filler content, high thermal conductivity, and a triple nano/microstructure.

Carbon–polymer composites are widely used in the creation of new structural materials for conductive, heat-absorbing, and shielding coatings. In recent years, special attention has been paid to the study of polymer composite materials based on electrically conductive nanosized fillers, such as carbon nanotubes (CNTs) and nanofibers (CNFs) [68,69].

In [70], the reported dielectric constants for epoxy resins containing varying concentrations of carbon fibers demonstrated an uptick as the carbon fiber content increased. This outcome can be rationalized by the heightened polarity of all the blends resulting from the increased concentration of carbon fibers. This, in turn, leads to an augmentation in the orientation polarization, along with the presence of interfacial polarization. The rise in permittivity as the frequency decreases indicates that the system exhibits interfacial polarization at lower frequencies.

In [71], the results of determining the thermal conductivity and heat capacity of the epoxy material directly in the process of its curing, i.e., with a change in the phase state, are given. An epoxy composition based on epoxy resin and a modified aliphatic polyamine was used as the object of research. The thermophysical properties were determined for different degrees of conversion at room and elevated temperatures. Depending on the degree of conversion, the value of volumetric shrinkage and the values of residual stresses were also evaluated. It was established that during the curing process (i.e., when the degree of conversion changes), the heat capacity decreased by 32% and the thermal conductivity increased by more than 3 times.

During the curing of the epoxy oligomer, its phase state changes and the material initially passes from a liquid to a gel-like state and then to a solid [72–74]. The conditions for the transition from a liquid state to a gel state are determined by the values of temperature and the time of gelation [75–77].

2.2. Thermal Conductivity

The study [78] examined the temperature-dependent thermal conductivity of diene resin ED20, both in its pure form and when cured with an aromatic amine (in a 2:1 ratio). Additionally, the investigation included the same polymer with added fillers—aluminum oxide Al_2O_3 and iridium orthosilicate IrSiO_4 (constituting 72.1% of the composition), both in the presence and absence of a modifier, tetrabutoxytitanium (TBT) (see Figure 4).

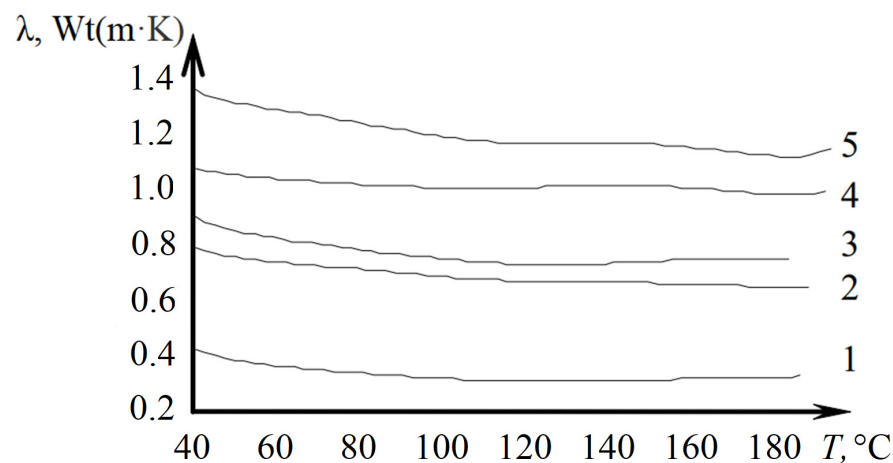


Figure 4. Dependences of thermal conductivity on temperature for materials 1—ED20; 2—ED20 + IrSiO_4 + TBT; 3—ED + IrSiO_4 ; 4—ED + Al_2O_3 + TBT; 5—ED20 + Al_2O_3 [78].

The incorporation of fillers or modifiers into the polymer has a discernible impact on thermal conductivity. The numerical value λ of the composite material is influenced not only by the quantity of the added component but also by its interaction with the polymer phase.

The results demonstrate that the inclusion of aluminum oxide Al_2O_3 significantly augments the thermal conductivity of the composite material, exhibiting a threefold increase across the entire temperature range (40–190 °C) while maintaining a consistent curve profile. Similarly, the use of iridium orthosilicate IrSiO_4 as a filler doubles the thermal conductivity of the cured epoxy composition within the specified temperature range (40–180 °C). On the other hand, the introduction of tetrabutoxytitanium as a modifier in the composite material composition does not notably alter the temperature-dependent behavior of thermal conductivity.

According to [79], the slight augmentation in the effective thermal conductivity of polymer nanocomposites (PNCs) reinforced with highly conductive nanofillers can be attributed to various factors. Firstly, the presence of carbon nanofillers often leads to agglomeration in bundles within the polymer matrix, driven by the Van der Waals interactions between them. This clustering of fillers may potentially hinder the overall thermal performance of the composite. Secondly, the Kapitza resistance (R_k) could represent a significant hindrance to heat transfer within PNCs.

2.3. Specific Conductivity

The authors of [80] experimentally studied the electrical conductivity of epoxy matrices modified with carbon nanotubes with a continuous current flow during their polymerization at a constant voltage. The research carried out in their work is connected with the study of possible technologies for accelerating the curing of composite materials for the manufacturing of large-sized structures in space conditions. The results obtained can also be used to develop promising technologies for the manufacturing of composite materials with desired electrophysical and mechanical properties by exposing the materials to electric fields of the appropriate configuration during their polymerization.

The investigation of [81], in which a study on the change in current at a constant voltage (28 V) over time from the moment the hardener was added was performed, is shown in Figure 5a, from which it follows that, for the selected cell sizes, the characteristic time of current settling is 100–120 min. Figure 5b shows the specific conductivity (σ) of the epoxy matrix at various mass concentrations (n) of CNTs.

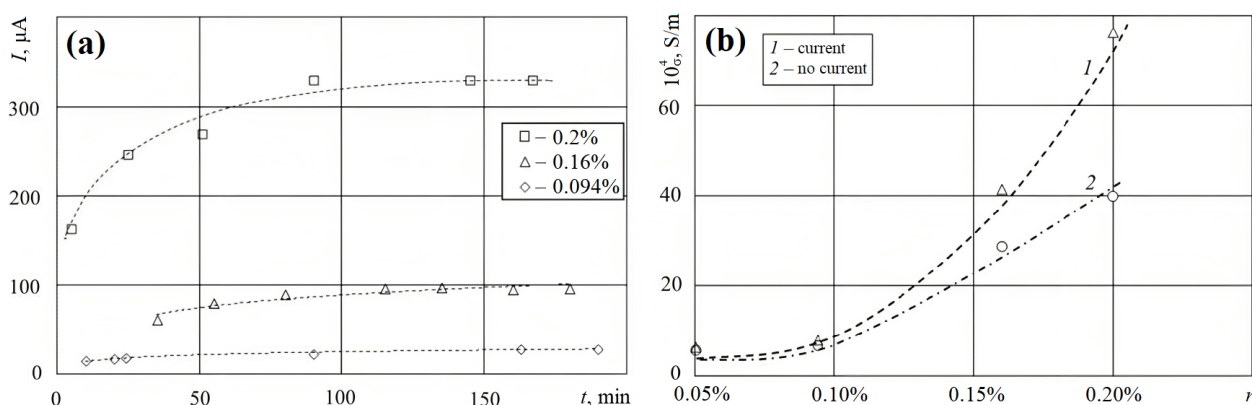


Figure 5. (a) Change in current at a constant voltage after adding a hardener ($t = 0$) for different concentrations of CNTs; (b) specific conductivity (σ) of the epoxy matrix at various mass concentrations (n) of CNTs; 1—samples through which current was passed during polymerization; 2—current was not passed [80].

The incorporation of nano-fillers has been widely suggested as a means to improve the dielectric properties of high voltage polymeric insulation, although there are conflicting reports in the literature. According to [81], the potential of silica nanoparticles to prolong

the time to failure, particularly by resisting the growth of electrical trees in epoxy resin, was investigated. It was evident that treating the nanoparticles with silane before compounding significantly retarded the tree growth and subsequently extended the time to failure. The growth of trees in needle-plane samples was experimentally assessed in a laboratory, employing loadings of 1, 3, and 5 wt% of nano-fillers. In all instances, the average times to failure showed an increase, but the application of silane treatment to the nanoparticles prior to compounding yielded markedly superior outcomes. Moreover, a distinct initiation period before tree growth was observed in the cases with higher loading levels and silane treatment. For the silane-treated material filled with 5 wt%, the average time to failure was 28 times greater than that of the unfilled resin.

2.4. Dependence of Dielectric Constant on Frequency

This study, based on [82], reveals that as the frequency and temperature rise, there is a decrease in breakdown strength. Furthermore, frequency has a significant influence on the reduction in breakdown strength. The application of high voltages introduces complex multi-frequency stresses to the insulation material. The decline in dielectric breakdown strength due to frequency is primarily attributed to heightened partial discharge (PD) activities and dielectric heating, factors that should be taken into account in insulation design. The decrease in the root mean square (RMS) electric fields and the rise in dielectric loss are potential contributors to the diminished breakdown strength of epoxy resin.

The purpose of this work [83] was the study of the permittivity (ϵ) and the tangent of the dielectric losses ($\tan \delta$) of epoxy polymers and electrets based on them. Materials based on the ED-20 epoxy resin, using the oligomeric reactive epoxyurethane modifier PEF-3A, were chosen as the objects of study. To cure the composition, amine-type hardeners PEPA and L-20 were used in a stoichiometric ratio. Figure 6, below, demonstrates the dependencies of the dielectric constant and dielectric loss tangent on frequency for various samples.

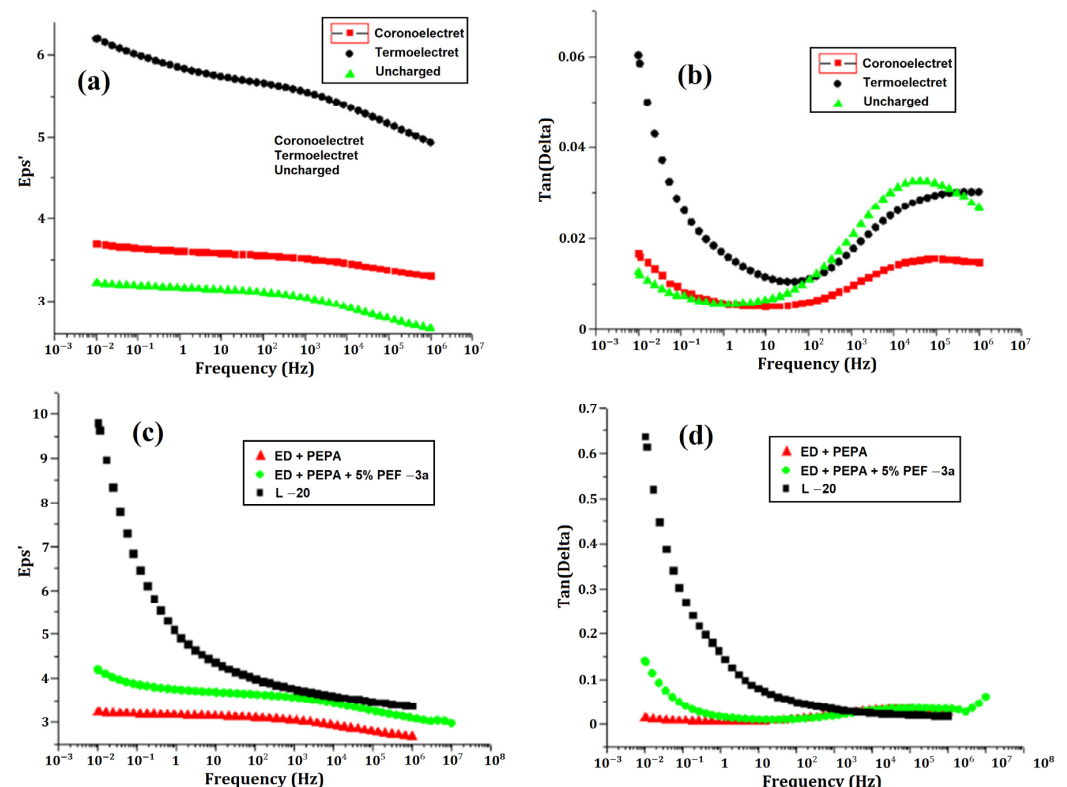


Figure 6. Dependence of dielectric constant (a,c) and the dielectric loss tangent (b,d) on frequency for various samples: uncharged sample (1), corona (2), and thermoelectric (3) based on ED-20 epoxy resin cured with PEPA in a stoichiometric ratio, and thermoelectrics based on epoxy resin ED-20, cured with PEPA (1), L-20 (2), and containing 5% wt. PEF-3A, when curing PEPA (3) [83].

To create polymer composites that reduce the impact of electromagnetic fields on electronic components of computer technology and biological objects, it is necessary to obtain materials with specified values of dielectric permittivity, a dielectric loss tangent, and electrical conductivity, which are determined by the operating frequency range of the nanocomposites.

Epoxy binders have the advantage of low shrinkage and high strength characteristics. However, scientific and technological progress constantly increases operational requirements, so polymers must be modified. The most promising are composite materials with nanosized fillers—nanocomposites [45–47,84].

2.5. Transmittance of Modified ERs

The research of [85] aimed to assess how the application of fluorination treatment influenced the dispersive stability of montmorillonite (MMT) and multi-walled carbon nanotubes (MWCNTs), as illustrated in Figure 7. In both instances, the transmittance intensity exhibited a reduction following the fluorination treatment, signifying a higher dispersion of particles within the epoxy blend solution. Specifically, the transmittance intensity decreased by approximately 29% for the MMT and 22% for the MWCNTs. This enhancement in dispersion could be linked to the introduction of functional groups onto the surfaces of MMT and MWCNT additives through the fluorination process.

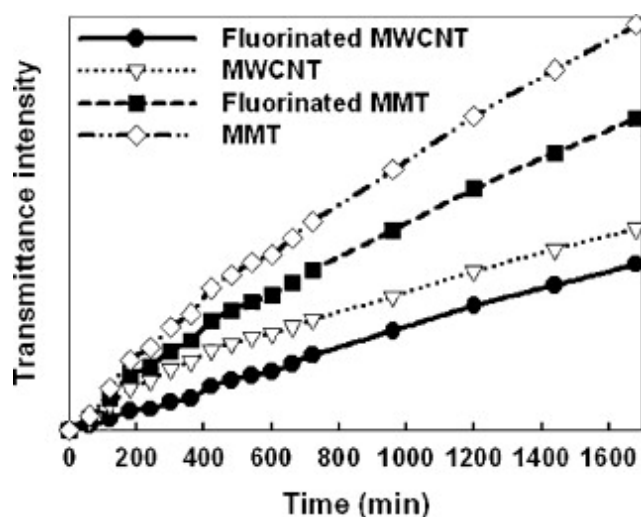


Figure 7. The impact of fluorination on the dispersion of MMT and MWCNTs within epoxy resin. (Figure from [85], permission granted by “Elsevier”).

The characteristics of the composite depend on the particle size of the filler. Large filler particles (315–500 microns) are isolated by a dielectric layer, so they have poor contact with each other. The maximum value of the dielectric constant is observed with the introduction of particles of a minimum size of 63–80 μm [86].

2.6. Electrical Conductivity of Modified ERs

In [87], the authors investigated the electrical conductivity at direct currents, as well as the dielectric characteristics, of epoxy nanocomposites filled with 37 single-walled carbon nanotubes (SWCNTs), MWCNTs, carbon black (CBH), and graphite (EG) at a frequency of 129 Hz (Figure 8) [84].

Composites containing SWCNTs exhibit their lowest electrical conductivity when operating in the region above the percolation threshold. The rationale behind this observation lies in the fact that SWCNTs, being the smallest in size, consequently offer the highest number of contact regions [86].

In a different study documented in [88], the research delved into the influence of multi-walled nanotube orientation methods on the electrical conductivity of epoxy nanocompos-

ites. The filler was subjected to orientation under both direct current (DC) and alternating current (AC) fields, each with a strength of 100 V/cm (as depicted in Figure 9). The results indicate that exposing the composite to an alternating current field during the curing process leads to a remarkable increase in its electrical conductivity, surpassing that of composites subjected to a direct current, even at equivalent filler concentrations. Hence, it can be inferred that nanotubes demonstrate more efficient orientation when subjected to an alternating field [86].

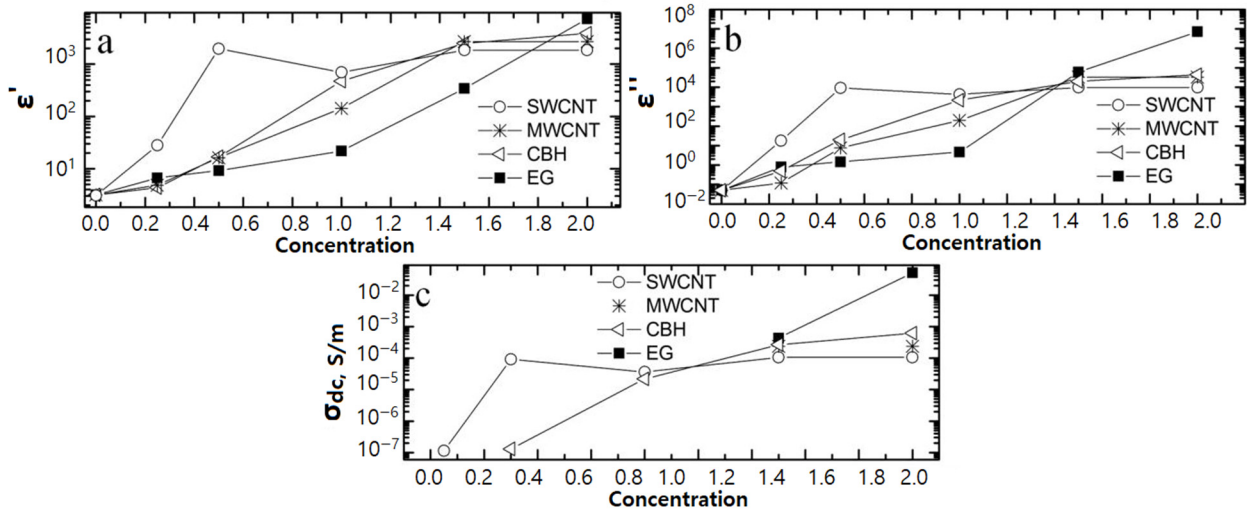


Figure 8. Dependence of ϵ' , ϵ'' , and σ of epoxy nanocomposites on the concentration of fillers. (a) ϵ' ; (b) ϵ'' ; (c) σ_{dc} . (Figure from [87], permission granted by “AIP Publishing”).

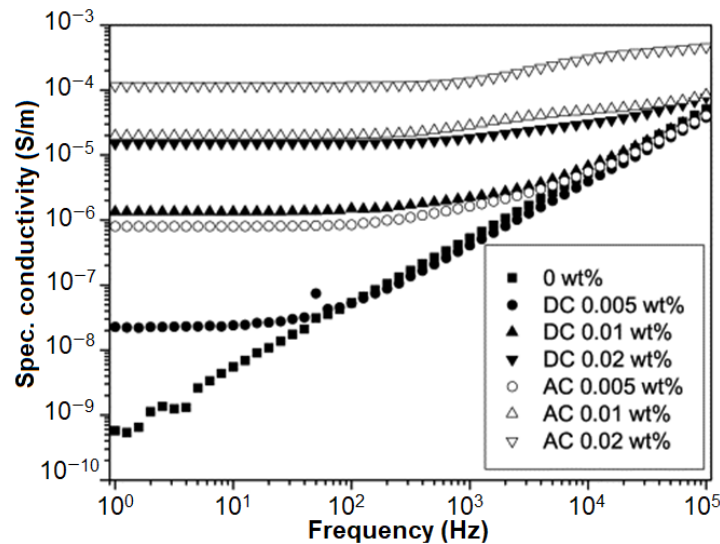


Figure 9. Frequency dependence of the specific conductivity of the epoxy nanocomposite on the concentration of the filler and the method of orientation in the field of direct (DC) and alternating (AC) currents. (Figure from [88], permission granted by “Elsevier”).

The incorporation of carbon fillers into the polymer matrix opens up avenues for obtaining materials with diverse properties. Parameters such as the particle shape, aspect ratio, and the evenness of their dispersion within the polymer matrix play pivotal roles in determining both the percolation threshold and the electrical conductivity of the resultant composites. Hence, carbon particles hold significant promise as fillers for crafting composite materials with tailored permittivity values, influenced by the operational frequency range of these nanocomposites [88].

The research of [89] explored the physical and mechanical attributes of epoxy nanocomposites featuring a 0.2 wt% concentration of SWCNTs sourced from OCSIAL, Novosibirsk, Russia.

The study of [90] delved into the curing process of heat-resistant epoxy compositions, enhancing them with functionalized nanotubes CNT-1, CNT-2 (GraNaT, Moscow, Russia), and CNT-3 (BAYER), each possessing specific surface areas of 0.08 m²/g, 0.05 m²/g, and 0.025 m²/g, respectively.

The authors of [91] investigated the impact of low concentrations of functionalized CNTs on the mechanical properties of epoxy nanocomposites. This endeavor yielded a heightened polymer strength and increased limiting deformation upon the incorporation of nanoparticles into a rigid epoxy matrix. Remarkably, the effect that was achieved with low concentrations of functionalized CNTs was akin to the outcomes observed with significantly higher concentrations of pure CNTs. The substantial specific surface area of the filler enables the reduction of the required concentration to attain the desired outcomes [86].

2.7. Bending Strength of Modified ERs

The flexural properties of composites composed of multi-walled carbon nanotubes (MWCNTs) and epoxy resin were found to be closely linked to two key factors: the dispersion of the MWCNTs within the matrix and the interactions occurring at the interface between the MWCNTs and the resin matrix [92]. Figure 10a illustrates typical stress-displacement curves for flexural tests conducted on DGEBA/DDM (diglycidyl ether of bisphenol A/diaminodiphenyl methane) reinforced with three different types of MWCNTs: MWCNT-NH₂, MWCNT-BuGE (n-butyl glycidylether), and MWCNT-BeGE (benzyl glycidylether). The average flexural strength and modulus are summarized in Figure 10b,c.

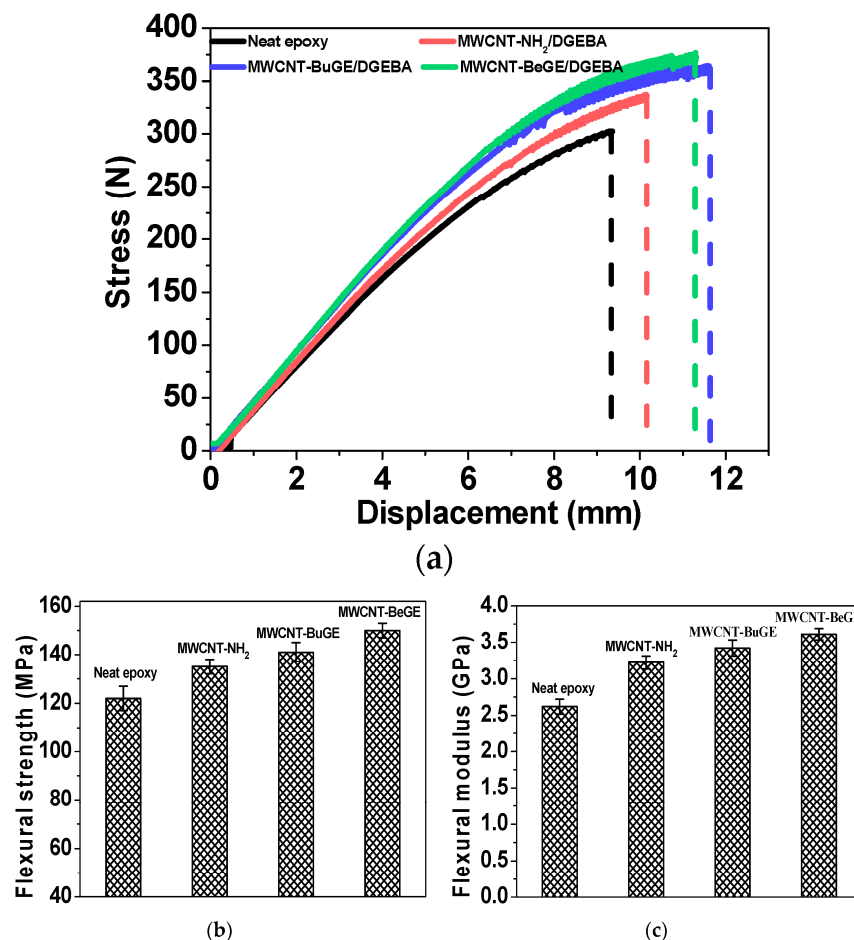


Figure 10. (a) Standard curves depicting flexural stress–displacement relationships, (b) the associated flexural strength, and (c) the flexural modulus for various nanocomposites [92].

The flexural strength and modulus of the pristine resin were measured at 122 MPa and 2.6 GPa, respectively. In comparison, the MWCNT-NH₂ reinforced nanocomposites exhibited improved flexural properties, with a strength reaching 135 MPa and a modulus of 3.2 GPa, representing an increase of 11.0% and 23.1% compared to the neat resin.

Conversely, the MWCNT/epoxy nanocomposites treated with surface sizing demonstrated superior flexural characteristics. This enhancement is attributed to the improved dispersion and increased wettability achieved by using epoxy-sizing MWCNTs, as opposed to MWCNT-NH₂. The flexural strength and modulus of the MWCNT-BeGE/epoxy nanocomposites could reach 150 MPa and 3.6 GPa, respectively, marking a significant improvement of 22.9% and 37.8% compared to the neat epoxy. Furthermore, when compared with the MWCNT-BuGE/epoxy nanocomposites featuring the same MWCNT content, the MWCNT-BeGE/epoxy nanocomposites displayed a 7.3% increase in strength and a 7.7% increase in modulus, demonstrating that the presence of benzene rings in the surface sizing offered a more effective local load-transfer mechanism between the MWCNTs and the epoxy matrix.

3. Discussion

Epoxy polymers are one of the most commonly used polymeric materials in the production of composites. This is due to the properties of epoxy materials, such as high strength, rigidity, chemical resistance, low weight, and a low residual stress in epoxy products due to the low degree of the shrinkage of materials during curing [93,94]. Epoxy polymer materials are insulators. The specific resistance of such materials is $>10^9$ ohm·m [95].

However, for application in some areas, composites based on polymeric materials must have electrical conductivity. One of the important areas for the application of polymer composite materials is the creation of coatings that prevent the accumulation of electrostatic charge (antistatic coatings). In accordance with the international standard IEC 61340-5-1 [96], coatings are divided into conductive (with a resistance $R < 10^6$ ohm·m), antistatic (dissipating static charge and characterized by resistance from 10^6 ohm·m to 10^9 ohm·m) and insulating (with a resistance of $>10^9$ ohm·m). Another important field in the application of polymer composites is for protection against electromagnetic radiation [97]. To improve the efficiency of shielding electromagnetic radiation, it is necessary to achieve a high conductivity in the protective material. To increase the electrical conductivity of polymer composites, additives of amorphous carbon, carbon fibers, and graphite are used. However, in order to achieve the required coating resistance, it is necessary to introduce a large amount of such additives (>10 wt.%) [98].

The use of nanosized additives makes it possible to achieve the required conductivity of the polymer composite with much lower amounts of the introduced additive. For these purposes, carbon nanotubes are used: multi-walled [99], single-walled [100], and graphene [101]. In [102,103], it is noted that the introduction of small amounts of carbon nanotubes into the composite leads not only to a change in its electrical properties, but also improves the mechanical characteristics of the composite. In addition, carbon-based additives are characterized by a good compatibility with the polymer matrix, light weight, and acceptable electrical parameters [104].

The introduction of graphene particles into the epoxy matrix has little effect on the electrical conductivity and mechanical properties of the composites. The addition of graphene particles to composites containing carbon nanotubes improves their electromagnetic shielding efficiency without significantly affecting their strength [105].

In the study of [106], it was found that composites based on epoxy resin with graphene (10 wt.%) and liquid fillers in situ (base oil SN150 or perfluoropolyether at 10 wt.%) provide low friction and high wear resistance in the form of thin coatings on a steel substrate.

The objective of the study described in reference [105] was to fabricate conductive composites based on epoxy resin that are uniformly filled with multi-walled carbon nanotubes (MWCNTs), graphene particles (GNPs), and MWCNT/GNP mixtures in varying proportions. The research aimed to investigate their electrical and mechanical properties, as

well as their effectiveness in shielding electromagnetic radiation within the radio frequency range. The findings revealed that incorporating 2 wt.% of carbon nanotubes into the epoxy matrix increased the electrical conductivity of the composite to 4 S/m. The percolation threshold for such a composite was determined to be 0.013 wt.% MWCNTs. As the electrical conductivity of the composite increased, its ability to shield electromagnetic radiation in the radio frequency range also improved proportionally, reaching 14 dB at 9.25 GHz with the introduction of 2 wt.% MWCNTs. The introduction of graphene particles into the epoxy matrix containing carbon nanotubes had a negligible impact on their conductivity and mechanical properties. When graphene particles were introduced into composites alongside carbon nanotubes, the shielding effectiveness against electromagnetic radiation increased without significantly compromising the composite's ultimate strength.

In the study [107] a range of functionalized carbon nanotubes (CNTs) was synthesized and their behavior in a colloidal state when combined with epoxy resin and the TETA (triethylenetetramine) hardener was investigated. The discussion centered on the impact of the interfacial interactions between the surface of CNTs and the polymer matrix. The type of functionalization and their unique interactions with polymer chains had notable effects on the physical, thermal, and electrical properties of the composites. For instance, at a 0.5 wt% CNT loading, enhancements in tensile strength were observed as follows: raw CNTs (7.2%), carboxylated CNTs (11.2%), octadecyl amide-functionalized CNTs (11.4%), and hydroxylated CNTs (14.2%). The functionalization of CNTs led to an improvement in the glass transition temperature (T_g) of the epoxy composites, with CNTs-OH demonstrating the highest enhancement (34%) in T_g . Furthermore, the incorporation of CNTs into the polymer matrix resulted in a significant reduction in electrical resistance. The varying re-aggregation behavior of CNTs in the presence of both the polymer and TETA indicated specific interactions between the CNTs and the polymer matrix system. It is worth noting that making a direct comparison with other data is challenging due to the wide range of variables, including the type of epoxy resin, hardener, and CNTs, as well as the degree of functionalization and the processing techniques employed across different studies.

As one of the ways to increase the strength of epoxy resins, the addition of carbon nanomaterials (graphenes and carbon nanotubes) is considered [108,109]. CNTs have significant advantages in this area over traditional dispersive fillers (metal wire, glass fiber, carbon fibers, etc.) due to their ultra-small dimensions (a few to tens of nanometers) and, as a result, being able to fill the micropores of the matrix, as well as due to the possibility of forming chemical bonds with the functional groups of the molecules of the matrix phase [110]. The main task with the introduction of carbon nanotubes as a hardening additive is the separation of tube agglomerates that are formed during synthesis into separate components; therefore, it is necessary to pre-treat CNTs, for example, via oxidative functionalization [111,112].

Scientists from Rice University [113] have developed a remarkable epoxy-graphene composite material that boasts unparalleled compressive strength and remarkably high conductivity. Traditionally, epoxy serves as an insulating material, necessitating the addition of other metals to confer electrical conductivity. However, the researchers at Rice University embarked on a novel approach: they infused the graphene framework with resin. This innovative method yielded a material that was characterized by a compressive strength that breaks records, exceeding that of a pure epoxy bar by a factor of seven. Additionally, the electrical conductivity of this material surged to 41 cm, as reported by Science Daily. It is noteworthy that, prior to this, engineers at the Massachusetts Institute of Technology (MIT) unveiled a self-regenerating material capable of autonomously mending the cracks that form on its surface.

4. Conclusions

The complex of the unique physicochemical and physicochemical properties of epoxy resin allows products based on them to cover a wide range of applications in various fields of electrical and radio engineering. Scientific and technical research that focuses on

the development of the most specialized coatings (epoxy fills) that are resistant to highly aggressive environments, improving the properties of epoxy resin as a dielectric (electrical conductivity and insulation strength), and satisfying certain operating conditions is steadily growing.

In conclusion, the resonance of epoxies as vital materials across industries is unmistakable. Their adaptability, versatility, and responsiveness to chemical and electrical factors render them as more than mere compounds—they are dynamic components that shape our technological landscape. By embracing their multifunctionality, researchers and practitioners stand poised to unlock the potential of epoxies in domains ranging from electronics to aerospace, ushering in a future where these remarkable materials continue to be at the forefront of innovation and progress.

Author Contributions: Conceptualization: R.D.; methodology, R.D.; software, N.P. and T.P.; validation, R.D., T.P. and N.P.; investigation, R.D. and T.P.; resources, P.S. and V.H.; data curation, N.P.; writing—original draft preparation, R.D.; writing—review and editing, R.D.; visualization, R.D., N.P. and T.P.; supervision, R.D.; project administration, V.H.; funding acquisition, P.S. and V.H. All authors have read and agreed to the published version of the manuscript.

Funding: This research was funded by the Internal Grant Agency of Brno University of Technology, grant No. FEKT-S-23-8228.

Conflicts of Interest: The authors declare no conflict of interest.

References

1. Ahmadi, Z. Epoxy in nanotechnology: A short review. *Prog. Org. Coatings* **2019**, *132*, 445–448. [[CrossRef](#)]
2. Xiang, Q.; Xiao, F. Applications of epoxy materials in pavement engineering. *Constr. Build. Mater.* **2020**, *235*, 117529. [[CrossRef](#)]
3. Osman, A.; Elhakeem, A.; Kaytbay, S.; Ahmed, A. *A Comprehensive Review on the Thermal, Electrical, and Mechanical Properties of Graphene-Based Multi-Functional Epoxy Composites*; Springer International Publishing: New York, NY, USA, 2022; Volume 5, ISBN 0123456789.
4. Tian, Z.-S.; Wang, Y.-Q.; Hou, X.-L. Review of chemical recycling and reuse of carbon fiber reinforced epoxy resin composites. *New Carbon Mater.* **2022**, *37*, 1021–1041. [[CrossRef](#)]
5. Mathews, L.D.; Capricho, J.C.; Peerzada, M.; Salim, N.V.; Parameswaranpillai, J.; Hameed, N. Recent progress and multifunctional applications of fire-retardant epoxy resins. *Mater. Today Commun.* **2022**, *33*, 104702. [[CrossRef](#)]
6. Pappa, C.; Feghali, E.; Vanbroekhoven, K.; Triantafyllidis, K.S. Recent advances in epoxy resins and composites derived from lignin and related bio-oils. *Curr. Opin. Green Sustain. Chem.* **2022**, *38*, 100687. [[CrossRef](#)]
7. Jin, F.-L.; Li, X.; Park, S.-J. Synthesis and application of epoxy resins: A review. *J. Ind. Eng. Chem.* **2015**, *29*, 1–11. [[CrossRef](#)]
8. Wei, H.; Xia, J.; Zhou, W.; Zhou, L.; Hussain, G.; Li, Q.; Ostrikov, K.K. Adhesion and cohesion of epoxy-based industrial composite coatings. *Compos. Part B Eng.* **2020**, *193*, 108035. [[CrossRef](#)]
9. Mashkovich, V.P.; Kudryavtseva, A.V. *Protection from Ionizing Radiation: A Handbook*, 4th ed.; Elektroatomizdat: Moscow, Russia, 1995; 496p.
10. Tominaga, Y.; Zhang, C.; Sato, K.; Imai, Y. Improvement of interfacial adhesion between oxide ceramic nanoparticles and epoxy resin by wet-jet milling. *Ceram. Int.* **2023**, *49*, 31658–31665. [[CrossRef](#)]
11. Dong, M.; Zhou, S.; Yang, H.; Xue, X. Gamma ray attenuation behaviors and mechanism of boron rich slag/epoxy resin shielding composites. *Nucl. Eng. Technol.* **2023**, *55*, 2613–2620. [[CrossRef](#)]
12. Zhao, S.; Chen, C.; Ueshima, M.; Haga, M.; Suganuma, K. Influence of interfacial interaction on the reliability of the bond between encapsulation epoxy and copper substrate. In Proceedings of the 2023 International Conference on Electronics Packaging (ICEP), Kumamoto, Japan, 19–22 April 2023; pp. 91–92. [[CrossRef](#)]
13. Li, X.; Deng, J.; Huang, Q.; Zhang, G.; Chen, K.; Wang, Y. Experimental investigation on immersion liquid cooled battery thermal management system with phase change epoxy sealant. *Chem. Eng. Sci.* **2022**, *264*, 118089. [[CrossRef](#)]
14. Verma, C.; Olasunkanmi, L.O.; Akpan, E.D.; Quraishi, M.; Dagdag, O.; El Gouri, M.; Sherif, E.-S.M.; Ebenso, E.E. Epoxy resins as anticorrosive polymeric materials: A review. *React. Funct. Polym.* **2020**, *156*, 104741. [[CrossRef](#)]
15. Song, K.; Pan, Y.-T.; Zhang, J.; Song, P.; He, J.; Wang, D.-Y.; Yang, R. Metal–Organic Frameworks–Based Flame-Retardant System for Epoxy Resin: A Review and Prospect. *Chem. Eng. J.* **2023**, *468*, 143653. [[CrossRef](#)]
16. Zhi, M.; Yang, X.; Fan, R.; Yue, S.; Zheng, L.; Liu, Q.; He, Y. A comprehensive review of reactive flame-retardant epoxy resin: Fundamentals, recent developments, and perspectives. *Polym. Degrad. Stab.* **2022**, *201*, 109976. [[CrossRef](#)]
17. Mousavi, S.R.; Estaji, S.; Kiaei, H.; Mansourian-Tabaei, M.; Nouranian, S.; Jafari, S.H.; Ruckdäschel, H.; Arjmand, M.; Khonakdar, H.A. A review of electrical and thermal conductivities of epoxy resin systems reinforced with carbon nanotubes and graphene-based nanoparticles. *Polym. Test.* **2022**, *112*, 107645. [[CrossRef](#)]

18. Lu, D.; Wong, C.P. *Materials for Advanced Packaging*; Springer: Berlin/Heidelberg, Germany, 2009; pp. 1–723. ISBN 978-0-387-78218-8. [CrossRef]
19. Teh, P.L.; Mariatti, M.; Akil, H.M.; Seetharamu, K.N.; Wagiman, A.N.R.; Beh, K.S. High Filled Epoxy Composites for Electronic Packaging Application. In Proceedings of the 2006 Thirty-First IEEE/CPMT International Electronics Manufacturing Technology Symposium, Petaling Jaya, Malaysia, 8–10 November 2006; pp. 275–281. [CrossRef]
20. Shundo, A.; Yamamoto, S.; Tanaka, K. Network Formation and Physical Properties of Epoxy Resins for Future Practical Applications. *JACS Au* **2022**, *2*, 1522–1542. [CrossRef] [PubMed]
21. Estridge, C.E. The effects of competitive primary and secondary amine reactivity on the structural evolution and properties of an epoxy thermoset resin during cure: A molecular dynamics study. *Polymer* **2018**, *141*, 12–20. [CrossRef]
22. Rozenberg, B.A. *Advance in Polymer Sciences*; Springer: Berlin/Heidelberg, Germany, 1986.
23. Kinjo, N.; Ogata, M.; Nishi, K.; Kaneda, A. Epoxy Molding Compounds as Encapsulation Materials for Microelectronic Devices. In *Speciality Polymers/Polymer Physics*; Springer Nature: Berlin, Germany, 2022; pp. 1–48. [CrossRef]
24. Hsissou, R. Review on epoxy polymers and its composites as a potential anticorrosive coatings for carbon steel in 3.5% NaCl solution: Computational approaches. *J. Mol. Liq.* **2021**, *336*, 116307. [CrossRef]
25. Osipchik, V.S.; Smotrova, S.A.; Tomilchik, Y.A. Study of the properties of modified epoxy-containing oligomers. *Plast. Masses* **2011**, *2*, 4–7.
26. Galikhanov, M.; Mochalova, E.; Gabdrakhmanov, I.; Galikhanov, E.; Lounev, I.; Gusev, Y. Study of Electret State in Epoxyamine Polymers by Dielectric Spectroscopy. *J. Electron. Mater.* **2019**, *48*, 4473–4477. [CrossRef]
27. Blagonravova, A.A. *Lacquer Epoxy Resins*; Blagonravova, A.A., Nepomniachtchi, A.I., Eds.; Chemistry: Moscow, Russia, 1970; 248p.
28. Electronic Source. Available online: <https://www.nkj.ru/archive/articles/32969/?ysclid=lhke7yzvk8640784726> (accessed on 30 August 2023).
29. Voronkov, A.G.; Yartsev, V.P. *Epoxy Polymer Solutions for the Repair and Protection of Building Products and Structures: Tutorial*; Tambov Publishing House: Tambov, Russia, 2006; 92p, ISBN 5-8265-0519-2.
30. Wu, H.; Rogalski, M.; Kessler, M.R. Zirconium Tungstate/Epoxy Nanocomposites: Effect of Nanoparticle Morphology and Negative Thermal Expansivity. *ACS Appl. Mater. Interfaces* **2013**, *5*, 9478–9487. [CrossRef]
31. Guo, L.; Zhang, Z.; Kang, R.; Chen, Y.; Hou, X.; Wu, Y.; Wang, M.; Wang, B.; Cui, J.; Jiang, N.; et al. Enhanced thermal conductivity of epoxy composites filled with tetrapod-shaped ZnO. *RSC Adv.* **2018**, *8*, 12337–12343. [CrossRef] [PubMed]
32. Shi, Z.; Li, X.-F.; Bai, H.; Xu, W.-W.; Yang, S.-Y.; Lu, Y.; Han, J.-J.; Wang, C.-P.; Liu, X.-J.; Li, W.-B. Influence of microstructural features on thermal expansion coefficient in graphene/epoxy composites. *Heliyon* **2016**, *2*, e00094. [CrossRef] [PubMed]
33. Kislyakov, P.A.; Nizina, T.A. Nanomodified epoxy composites for building purposes. *Perspekt. Mater.* **2010**, *9*, 113–116.
34. Tarrío-Saavedra, J.; López-Beceiro, J.; Naya, S.; Artiaga, R. Effect of silica content on thermal stability of fumed silica/epoxy composites. *Polym. Degrad. Stab.* **2008**, *93*, 2133–2137. [CrossRef]
35. Radoman, T.S.; Džunuzović, J.V.; Jeremić, K.B.; Grgur, B.N.; Miličević, D.S.; Popović, I.G.; Džunuzović, E.S. Improvement of epoxy resin properties by incorporation of TiO₂ nanoparticles surface modified with gallic acid esters. *Mater. Des.* **2014**, *62*, 158–167. [CrossRef]
36. Stoikovich, N.; Smilkovich, S.; Tsurkina, S.K.; Laketch, A. *Influence of Moisture on Adhesive Joints. Science and Innovations in Construction (to the 45th Anniversary of the Department of Construction and Municipal Economy): Sat. Report International Scientific-practical. Conf., Belgorod, April 21, 2017*; Belgorod State Technological University. V.G. Shukhova: Belgorod, Russia, 2017; pp. 40–49.
37. Plakunova, E.V.; Tatarintseva, E.A.; Mostovoy, A.S.; Panova, L.G. Structure and properties of epoxy thermosets. *Perspekt. Mater.* **2013**, *3*, 57–62.
38. Galeev, R.R.; Maisuradze, N.V.; Abdrakhmanova, L.A. Structure of polymer composites on the basis of epoxy resin and organic and inorganic dispersed industrial wastes. *Mater. Sci. Forum* **2016**, *871*, 216–222. [CrossRef]
39. Kotlyarova, I.A.; Stepina, I.V.; Ilyushkin, D.A.; Tsvetkov, I.S. Assessment of influence of disperse filler polarity on structure and water absorption of epoxy compositions. *Vestnik MGSU* **2019**, *6*, 690–699. [CrossRef]
40. Ma, J.; Yang, Y.; Wang, Q.; Deng, Y.; Yap, M.; Chern, W.K.; Oh, J.T.; Chen, Z. Degradation and Lifetime Prediction of Epoxy Composite Insulation Materials under High Relative Humidity. *Polymers* **2023**, *15*, 2666. [CrossRef]
41. Antipova, E.A.; Korotkova, N.P.; Lebedev, V.S. Modern polyurethane, epoxy, PU-acrylate and epoxyacrylate binders for industrial paintwork materials produced by LLC NPP Makromer. *Paint. Varn. Mater. Their Appl.* **2012**, *9*, 14–21.
42. Modeev, S.A.; Ladinin, M.E.; Kurbatov, V.G. Influence of active diluents on the properties of unfilled epoxy compositions. In Proceedings of the Sixty-sixth All-Russian Scientific and Technical Conference of Students, Undergraduates and Postgraduates of Higher Educational Institutions with International Participation, Yaroslavl, Russia, 23 April 2013.
43. Potapochkina, I.I.; Korotkova, N.P.; Loginova, S.E.; Lebedev, V.S. Epoxy and polyurethane adhesive materials of elad, aquapol, and acrolat brands and their components. *Glues Seal. Mater.* **2011**, *4*, 45–49. [CrossRef]
44. Javanyan, E.A. Influence of diluents on the physical and mechanical properties of 128 epoxy binders and composites based on them. *High-Mol. Compd.* **1994**, *36A*, 1349–1352.
45. Gojny, F.; Wichmann, M.; Köpke, U.; Fiedler, B.; Schulte, K. Carbon nanotube-reinforced epoxy-composites: Enhanced stiffness and fracture toughness at low nanotube content. *Compos. Sci. Technol.* **2004**, *64*, 2363–2371. [CrossRef]

46. Song, Y.S.; Youn, J.R. Influence of dispersion states of carbon nanotubes on physical properties of epoxy nanocomposites. *Carbon* **2005**, *43*, 1378–1385. [[CrossRef](#)]
47. Lau, K.; Lam, C. Thermal and mechanical properties of single-walled carbon nanotube bundle-reinforced epoxy nanocomposites: The role of solvent for nanotube dispersion. *Compos. Sci. Technol.* **2005**, *65*, 719–725. [[CrossRef](#)]
48. Rudawska, A.; Sarna-Boś, K.; Rudawska, A.; Olewnik-Kruszkowska, E.; Frigione, M. Biological Effects and Toxicity of Compounds Based on Cured Epoxy Resins. *Polymers* **2022**, *14*, 4915. [[CrossRef](#)]
49. Zagidullin, A.I.; Efremova, A.A.; Garipov, R.M.; Deberdeev, R.Y. Influence of reactive modifiers on the properties of epoxy compositions. *Bull. KSTU* **2003**, *1*, 313–319.
50. Danilenko, E.G.; Chesnokov, E.Y.; Telegin, S.V. *Influence of Technological Additives on the Effective Thermal Conductivity of Epoxy Resin*; Siberian State University of Science and Technology named after Academician M.F. Reshetnev: Krasnoyarsk, Russia, 2019.
51. Williams, T.S.; Hammoud, A.; Kelly, M. Application of Dielectric Thermal Analysis to Screen Electrical Insulation Candidates for High-Voltage Electric Machines. *ACS Omega* **2020**, *5*, 20004–20013. [[CrossRef](#)]
52. Steinhaus, J.; Moeginger, B.; Großgarten, M.; Hausnerova, B. Evaluation of dielectric curing monitoring investigating light-curing dental filling composites. *Mater. Eng.* **2011**, *18*, 30–35.
53. Senturia, S.D.; Sheppard, N.F., Jr. Dielectric Analysis of Thermoset Cure. In *Epoxy Resins and Composites IV*; Springer: Berlin/Heidelberg, Germany, 2005; pp. 1–47.
54. Philippi, F.; Rauber, D.; Eliassen, K.L.; Bouscharain, N.; Niss, K.; Kay, C.W.M.; Welton, T. Pressing matter: Why are ionic liquids so viscous? *Chem. Sci.* **2022**, *13*, 2735–2743. [[CrossRef](#)]
55. Shin, J.H.; Nutt, S. In situ resin age assessment using dielectric analysis and resin cure map for efficient vacuum infusion. *Adv. Manuf. Polym. Compos. Sci.* **2020**, *6*, 212–225. [[CrossRef](#)]
56. Núñez-Regueira, L.; Gracia-Fernández, C.; Gómez-Barreiro, S. Use of rheology, dielectric analysis and differential scanning calorimetry for gel time determination of a thermoset. *Polymer* **2005**, *46*, 5979–5985. [[CrossRef](#)]
57. Cadenato, A.; Salla, J.M.; Ramis, X.; Morancho, J.M.; Marroyo, L.M.; Martin, J.L. Determination of gel and vitrification times of thermoset curing process by means of TMA, DMTA and DSC techniques. *J. Therm. Anal. Calorim.* **1997**, *49*, 269–279. [[CrossRef](#)]
58. Bao, C.; Wang, Y.; Mushtaq, R.T.; Zhang, K.; Li, X.; Chen, X. Preparation, characterization, and curing kinetics of elevated and cryogenic temperature-resistant epoxy resin composites. *Polym. Test.* **2022**, *116*, 107783. [[CrossRef](#)]
59. Kaya, B.; Kaiser, J.M.; Becker, K.F.; Braun, T.; Lang, K.D. Evaluation of the Dielectric Cure Monitoring of Epoxy Molding Compound in Transfer Molding Process for Electronic Packages. In Proceedings of the 2015 European Microelectronics Packaging Conference (EMPC), Friedrichshafen, Germany, 14–16 September 2015; pp. 1–6.
60. Protsenko, A.E.; Telesh, V.V. Inhibition and Catalysis as a Method to Improve the Mechanical Properties of a Fiberglass-Reinforced Plastic. *Polym. Mech.* **2015**, *51*, 555–560. [[CrossRef](#)]
61. Park, J.-J.; Shin, S.-S.; Yoon, C.-Y.; Lee, J.-Y.; Park, J.-E. Electrical and Mechanical Properties of Epoxy/Micro-sized Alumina Composite and the Effect of Nano-sized Alumina on Those Properties. *Trans. Electr. Electron. Mater.* **2015**, *16*, 260–263. [[CrossRef](#)]
62. Ito, M. Development of High Thermal Conductive Laminates. In Proceedings of the 2005 International Symposium on Electrical Insulating Materials (ISEIM 2005), Kitakyushu, Japan, 5–9 June 2005; pp. 10–15.
63. Fan, L.; Su, B.; Qu, J.; Wong, C.P. Effects of nano-sized particles on electrical and thermal conductivities of polymer composites. In Proceedings of the 9th International Symposium on Advanced Packaging Materials: Processes, Properties and Interfaces (IEEE Cat. No.04TH8742), 2004 Proceedings, Atlanta, GA, USA, 24–26 March 2004; pp. 193–199.
64. Mannanov, E.R. On dielectric materials with high thermal conductivity for electrical insulation systems of high-voltage electrical machines: A review of domestic and foreign literature. *Mater. Science. Power Eng.* **2021**, *27*, 42. [[CrossRef](#)]
65. Chen, Q.; Yang, H.; Wang, X.; Liu, H.; Zhou, K.; Ning, X. Dielectric Properties of Epoxy Resin Impregnated Nano-SiO₂ Modified Insulating Paper. *Polymers* **2019**, *11*, 393. [[CrossRef](#)]
66. Chen, C.; Sun, Q.; Wang, C.; Bu, Y.; Zhang, J.; Peng, Z. Dielectric Relaxation Characteristics of Epoxy Resin Modified with Hydroxyl-Terminated Nitrile Rubber. *Molecules* **2020**, *25*, 4128. [[CrossRef](#)]
67. Yu, H.; Huo, R.; Wu, C.; Wu, X.; Wang, G.; Jiang, P. Influence of Interface Structure on Dielectric Properties of Epoxy/Alumina Nanocomposites. Patent CN103525005B, 4 May 2016.
68. Tibbetts, G.G.; Lake, M.L.; Strong, K.L.; Rice, B.P. A review of the fabrication and properties of vapor-grown carbon nanofiber/polymer composites. *Comp. Sci. Technol.* **2007**, *67*, 1709–1718. [[CrossRef](#)]
69. Cooper, C.A.; Ravich, D.; Lips, D.; Mayer, J.; Wagner, H.D. Distribution and alignment of carbon nanotubes and nanofibrils in a polymer matrix. *Compos. Sci. Technol.* **2002**, *62*, 1105–1112. [[CrossRef](#)]
70. Elimat, Z.M.; Hamideen, M.S.; Schulte, K.I.; Wittich, H.; de la Vega, A.; Wichmann, M.; Buschhorn, S. Dielectric properties of epoxy/short carbon fiber composites. *J. Mater. Sci.* **2010**, *45*, 5196–5203. [[CrossRef](#)]
71. Chen, Y.; Marakhovskiy, P.S.; Malysheva, G.V. Determination of thermophysical properties of epoxy materials during their curing. *Proc. VIAM* **2018**, *9*, 119–123. [[CrossRef](#)]
72. Bazhenov, S.L.; Berlin, A.A.; Kulkov, A.A.; Oshmyan, V.G. *Polymer Composite Materials; Intelligence: Dolgoprudny, Russia, 2010; 352p.*
73. Baurova, N.I.; Zorin, V.A. *The Use of Polymer Composite Materials in the Production and Repair of Machines: Textbook. Allowance; Izd-vo MADI: Moscow, Russia, 2016; 264p.*

74. Mishkin, S.I.; Raskutin, A.E.; Evdokimov, A.A.; Gulyaev, I.N. Technologies and main stages of construction of the first in Russia arch bridge from composite materials. *Proc. VIAM Electron. Sci. Tech. Mag.* **2017**, *6*, 5. [CrossRef]
75. Marakhovskiy, P.S.; Barinov, D.Y.; Pavlovskiy, K.A.; Aleksashin, V.M. Curing of multilayer polymeric composite materials. Part 1. Mathematical modeling of heat transfer during the formation of a thick carbon fiber plate. In *All Materials. Encyclopedic Reference Book*; Federal State Unitary Enterprise “All-Russian Research Institute of Aviation Materials”: Moscow, Russia, 2018; Volume 2, pp. 16–22.
76. Barinov, D.Y.; Marakhovskiy, P.S.; Kutsevich, K.E.; Chutskova, E.Y. Mathematical modeling of temperature fields taking into account the kinetics of solidification of a thick fiberglass plate. *Perspekt. Mater.* **2017**, *5*, 19–28.
77. Zuev, A.V.; Loshchinin, Y.V.; Barinov, D.Y.; Marakhovskiy, P.S. Computational and experimental studies of thermophysical properties. *Aviat. Mater. Technol.* **2017**, *5*, 575–595. [CrossRef]
78. Katsuba, D.S.; Vasilyev, S.O.; Saveliyev, D.N.; Mainikova, N.F. Research of temperature dependences of thermal conductivity of composite materials based on diene resin ED20. *Adv. Chem. Chem. Technol.* **2012**, *3*, 132.
79. Nejad, S.M.; Srivastava, R.; Bellussi, F.M.; Thielemann, H.C.; Asinari, P.; Fasano, M. Nanoscale thermal properties of carbon nanotubes/epoxy composites by atomistic simulations. *Int. J. Therm. Sci.* **2021**, *159*, 106588. [CrossRef]
80. Semenov, V.A.; Rusakov, S.V.; Gilev, V.G. About electrical conductivity of the epoxy matrix with carbon nanotubes. *PNRPU Mech. Bull.* **2019**, *3*, 88–93. [CrossRef]
81. Chen, S.; Rowland, S.; Carr, J.; Storm, M.; Choy, K.-L.; Clancy, A.J. The importance of particle dispersion in electrical treeing and breakdown in nano-filled epoxy resin. *Int. J. Electr. Power Energy Syst.* **2021**, *129*, 106838. [CrossRef]
82. Wang, W.; Wang, X.; He, J.; Liu, Y.; Li, S.; Nie, Y. Electric stress and dielectric breakdown characteristics under high-frequency voltages with multi-harmonics in a solid-state transformer. *Int. J. Electr. Power Energy Syst.* **2021**, *129*, 106861. [CrossRef]
83. Limarenko, N.A.; Mochalova, E.N.; Galikhanov, M.F.; Deberdeev, R.Y. Study of the dielectric properties of electrets based on epoxy polymers. *Bull. Kazan Technol. Univ.* **2013**, *2*, 178–180.
84. Gojny, F.H.; Wichmann, M.H.G. Influence of different carbon nanotubes on the mechanical properties of epoxy matrix composites—A comparative study. *Compos. Sci. Technol.* **2005**, *65*, 2300–2313. [CrossRef]
85. Im, J.S.; Lee, S.K.; In, S.J.; Lee, Y.-S. Improved flame retardant properties of epoxy resin by fluorinated MMT/MWCNT additives. *J. Anal. Appl. Pyrolysis* **2010**, *89*, 225–232. [CrossRef]
86. Klyuev, I.Y. Electrophysical Properties of Composites Based on Epoxy Resin Modified with Nanosized Carbon Fillers. OD 9 20-5/1157. Moscow, 2020, 23 sElectronic Resource. Available online: <https://viewer.rsl.ru/ru/rsl01010251638?page=1&rotate=0&theme=white> (accessed on 30 August 2023).
87. Kuzhir, P.; Paddubskaya, A.; Plyushch, A.; Volynets, N.; Maksimenko, S.; Macutkevicius, J.; Kranauskaite, I.; Banys, J.; Ivanov, E.; Kotsilkova, R.; et al. Epoxy composites filled with high surface area-carbon fillers: Optimization of electromagnetic shielding, electrical, mechanical, and thermal properties. *J. Appl. Phys.* **2013**, *114*, 164304. [CrossRef]
88. Martin, C.; Sandler, J.; Windle, A.; Schwarz, M.-K.; Bauhofer, W.; Schulte, K.; Shaffer, M. Electric field-induced aligned multi-wall carbon nanotube networks in epoxy composites. *Polymer* **2005**, *46*, 877–886. [CrossRef]
89. Afanaseva, E.S.; Babkin, A.V. Mechanical properties of epoxy binders modified with single-walled nanotubes for reinforced composite materials. *Vestn. VGU* **2016**, *12*, 10–18.
90. Marakhovskiy, P.S.; Kondrashov, S.V. On the modification of heat-resistant epoxy binders with carbon nanotubes. *Vestnik MTGU im. Bauman* **2015**, *2*, 118–127.
91. Akatenkov, R.V. Influence of small amounts of functionalized nanotubes on the physical and mechanical properties and structure of epoxy compositions. *Deform. Destr. Mater.* **2011**, *11*, 35–39.
92. Zhang, Q.; Zhao, X.; Sui, G.; Yang, X. Surface Sizing Treated MWCNTs and Its Effect on the Wettability, Interfacial Interaction and Flexural Properties of MWCNT/Epoxy Nanocomposites. *Nanomaterials* **2018**, *8*, 680. [CrossRef]
93. Banerjee, P.; Bhattacharjee, Y. Lightweight Epoxy-Based Composites for EMI Shielding Applications. *Electron. Mater.* **2020**, *49*, 1702–1720. [CrossRef]
94. Sprenger, S. Epoxy resin composites with surface-modified silicon dioxide nanoparticles: A review. *J. Appl. Polym. Sci.* **2013**, *130*, 1421–1428. [CrossRef]
95. Yuen, S.M.; Ma, C.C.; Wu, H.H.; Kuan, H.C.; Chen, W.J.; Liao, S.H.; Hsu, C.W.; Wu, H.L. Preparation and thermal, electrical and morphological properties of multiwalled carbon nanotube and epoxy composites. *J. Appl. Polym. Sci.* **2007**, *103*, 1272–1278. [CrossRef]
96. IEC 61340-5-1:2016; Electrostatics—Part 5-1: Protection of electronic devices from electrostatic phenomena—General requirements. IEC: Geneva, Switzerland, 2016.
97. Liang, J.; Wang, Y.; Huang, Y.; Ma, Y.; Liu, Z.; Cai, J.; Zhang, C.; Gao, H.; Chen, Y. Electromagnetic interference shielding of graphene/epoxy composites. *Carbon* **2009**, *47*, 922–925. [CrossRef]
98. Reis, J.M.L.; Martins, S.A.; da Costa Mattos, H.S. Combination of temperature and electrical conductivity on semiconductor graphite/epoxy composites. *J. Braz. Soc. Mech. Sci. Eng.* **2020**, *42*, 1–5. [CrossRef]
99. Lisunova, M.O.; Mamunya, Y.P.; Lebovka, N.I.; Melezhyk, A.V. Percolation behavior of ultrahigh molecular weight polyethylene/multi-walled carbon nanotubes composites. *Eur. Polym. J.* **2007**, *43*, 949–958. [CrossRef]
100. Moaisal, A.; Li, Q.; Kinloch, I.; Windle, A. Thermal and electrical conductivity of single- and multi-walled carbon nanotube-epoxy composites. *Compos. Sci. Technol.* **2006**, *66*, 1285–1288. [CrossRef]

101. Wang, F.; Drzal, L.T.; Qin, Y.; Huang, Z. Processing and characterization of high content multilayer grapheme/epoxy composites with high electrical conductivity. *Polym. Compos.* **2016**, *37*, 2897–2906. [[CrossRef](#)]
102. Allaoui, A.; Bai, S.; Cheng, H.M.; Bai, J.B. Mechanical and electrical properties of a MWNT/epoxy composite. *Compos. Sci. Technol.* **2002**, *62*, 1993–1998. [[CrossRef](#)]
103. Montazeri, A.; Khavandi, A.; Javadpour, J.; Tcharkhtchi, A. Viscoelastic properties of MWNT/epoxy composites using two different using cycles. *Mater. Des.* **2010**, *31*, 3383–3388. [[CrossRef](#)]
104. Zhang, W.; Dehghani-Sanij, A.A.; Blackburn, R.S. Carbon based conductive polymer composites. *J. Mater. Sci.* **2007**, *42*, 3408–3418. [[CrossRef](#)]
105. Ovodok, E.A.; Ivanovskaya, M.I.; Poznyak, S.K.; Maltanova, A.M.; Gaevskaya, T.V.; Kurilo, V.S. Epoxy Composites Filled with Carbon Nanotubes and Graphene. *Sviridovsky Readings: Sat. Art./Editorial Board: O. A. Ivashkevich (prev.) [and Others].*—Minsk: Krasiko-Print, 2021, Issue. 17, pp. 65–74. Available online: <https://elib.bsu.by/handle/123456789/273068> (accessed on 30 August 2023).
106. Kumar, V.; Sinha, S.K.; Agarwal, A.K. Tribological studies of epoxy composites with solid and liquid fillers. *Tribol. Internat.* **2017**, *105*, 27. [[CrossRef](#)]
107. Roy, S.; Petrova, R.S.; Mitra, S. Effect of carbon nanotube (CNT) functionalization in epoxy-CNT composites. *Nanotechnol. Rev.* **2018**, *7*, 475–485. [[CrossRef](#)] [[PubMed](#)]
108. Kharitonov, A.P.; Simbirtseva, G.V.; Tkachev, A.G. Reinforcement of epoxy resin composites with fluorinated carbon nanotubes. *Compos. Sci. Technol.* **2014**, *107*, 162–168. [[CrossRef](#)]
109. Nikolaev, A.F.; Kryzhanovsky, V.K.; Burlov, V.V. *Technology of Polymeric Materials*; Kryzhanovsky, V.K., Ed.; Profession: St. Petersburg, Russia, 2008; 544p.
110. Tomishko, M.M.; Alekseev, A.M.; Tomishko, A.G. Carbon nanotubes—The basis of materials of the future. *Nanotechnics* **2004**, *1*, 10–15.
111. Ovejero, G.; Sotelo, J.L.; Romero, M.D.; Rodríguez, A.; Ocaña, M.A.; Rodríguez, G.; García, J. Multiwalled Carbon Nanotubes for Liquid-Phase Oxidation. Functionalization, Characterization, and Catalytic Activity. *Ind. Eng. Chem. Res.* **2006**, *45*, 2206–2212. [[CrossRef](#)]
112. Peng, X.; Wong, S.S. Functional covalent chemistry of carbon nanotube surfaces. *Adv. Mater.* **2009**, *21*, 625–642. [[CrossRef](#)]
113. Han, X.; Wang, T.; Owuor, P.S.; Hwang, S.H.; Wang, C.; Sha, J.; Shen, L.; Yoon, J.; Wang, W.; Salvatierra, R.V.; et al. Ultra-Stiff Graphene Foams as Three-Dimensional Conductive Fillers for Epoxy Resin. *ACS Nano* **2018**, *12*, 11219–11228. [[CrossRef](#)]

Disclaimer/Publisher’s Note: The statements, opinions and data contained in all publications are solely those of the individual author(s) and contributor(s) and not of MDPI and/or the editor(s). MDPI and/or the editor(s) disclaim responsibility for any injury to people or property resulting from any ideas, methods, instructions or products referred to in the content.

Chapter 3. PVDF Properties and Applications Potential

3.1 Motivation of the article

PVDF has emerged as a crucial material in the realm of advanced polymer science due to its unique combination of properties and versatile applications. The motivation behind this review article stems from the growing interest in PVDF's potential across various fields, including electronics, energy, and materials science. By examining PVDF trademarks, applications, and properties, this review aims to provide a comprehensive resource for both new and experienced researchers. Delving into specific topics such as relaxation transitions, piezoelectric behavior, β -phase formation, and the effects of chemical and radiation carbonization, the review highlights the critical aspects that influence PVDF's performance. Understanding the role of phase state in piezoelectricity for isotropic PVDF films is particularly important for optimizing its functionality in practical applications. This review not only synthesizes current knowledge but also explores future prospects and outlooks, encouraging further innovations and advancements in the utilization of PVDF. By offering a thorough analysis of these topics, the review aims to inspire continued research and development, driving the evolution of next-generation polymeric materials.

3.2 Conclusion on the article

In conclusion, this review has highlighted the extensive applications and unique properties of PVDF, underscoring its significant role in the market of functional materials. The paper explored a broad spectrum of PVDF's attributes, including non-toxicity, fire-resistance, ease of processing, heat resistance, resistance to aging and chemicals, and low surface roughness. These characteristics make PVDF a versatile material suitable for diverse industries such as chemical and nuclear power engineering, aviation and aerospace, electronics, architecture, automotive, biomedical, and pharmaceuticals. The experimental sections focused on the formation of the piezoelectric β -phase and the method of radiation carbonization. The β -phase of PVDF is particularly noteworthy for its ability to convert mechanical movements into electrical responses, enhancing its application in sensors and actuators. The radiation carbonization method is crucial for modifying PVDF properties by removing hydrogen fluoride, thus extending the polymer chain length and tailoring end properties. This review demonstrates the immense potential of PVDF materials, including its copolymers and derivatives, for various advanced applications. The breadth of fundamental and applied research on PVDF attests to its growing importance and promising future.

3.3 Applicant's contribution

As the first author the applicant is responsible for the majority of the manuscript.





3.4 Article 3

The paper "*A Brief Overview on Epoxies in Electronics: Properties, Applications, and Modifications*" was published in November 2022 in "*Polymers*" journal (IF: 5.0; Q1).

*The paper is highly cited and gathered 63 citations to date (02.06.2024).

Review

Brief Review of PVDF Properties and Applications Potential

Rashid Dallaev ¹, Tatiana Pisarenko ¹, Dinara Sobola ^{1,2}, Farid Orudzhev ^{3,4}, Shikhgasan Ramazanov ⁴
and Tomáš Trčka ^{1,*}

¹ Department of Physics, Faculty of Electrical Engineering and Communication, Brno University of Technology, Technická 2848/8, 61600 Brno, Czech Republic

² Central European Institute of Technology, Purkyňova 656/123, 61200 Brno, Czech Republic

³ Immanuel Kant Baltic Federal University, 236041 Kaliningrad, Russia

⁴ Amirkhanov Institute of Physics, Dagestan Federal Research Center, Russian Academy of Sciences, 367003 Makhachkala, Russia

* Correspondence: trcka@vut.cz

Abstract: Currently, there is an ever-growing interest in carbon materials with increased deformation-strength, thermophysical parameters. Due to their unique physical and chemical properties, such materials have a wide range of applications in various industries. Many prospects for the use of polymer composite materials based on polyvinylidene fluoride (PVDF) for scientific and technical purposes explain the plethora of studies on their characteristics “structure-property”, processing, application and ecology which keep appearing. Building a broader conceptual picture of new generation polymeric materials is feasible with the use of innovative technologies; thus, achieving a high level of multidisciplinary and integration of polymer science; its fundamental problems are formed, the solution of which determines a significant contribution to the natural-scientific picture of the modern world. This review provides explanation of PVDF advanced properties and potential applications of this polymer material in its various forms. More specifically, this paper will go over PVDF trademarks presently available on the market, provide thorough overview of the current and potential applications. Last but not least, this article will also delve into the processing and chemical properties of PVDF such as radiation carbonization, β -phase formation, etc.

Keywords: polyvinylidene fluoride; sensor; flexible electronics; piezoelectricity; structural properties



Citation: Dallaev, R.; Pisarenko, T.; Sobola, D.; Orudzhev, F.; Ramazanov, S.; Trčka, T. Brief Review of PVDF Properties and Applications Potential. *Polymers* **2022**, *14*, 4793. <https://doi.org/10.3390/polym14224793>

Academic Editor: Victor Tcherdyntsev

Received: 12 September 2022

Accepted: 31 October 2022

Published: 8 November 2022

Publisher's Note: MDPI stays neutral with regard to jurisdictional claims in published maps and institutional affiliations.



Copyright: © 2022 by the authors. Licensee MDPI, Basel, Switzerland. This article is an open access article distributed under the terms and conditions of the Creative Commons Attribution (CC BY) license (<https://creativecommons.org/licenses/by/4.0/>).

1. Introduction

Polyvinylidene fluoride $-(\text{CH}_2\text{-CF}_2)_n-$ has a set of valuable properties [1,2]: a relatively high melting point, high mechanical strength even at high temperatures, chemical and radiation resistance, resistance to hydrolysis and ultraviolet radiation, good wear resistance, physiological inertness, very low thermal conductivity, and exceptional resistance to ignition. The β -phase of PVDF has ferroelectric and piezoelectric properties which is why it is especially interesting. Therefore, PVDF is widely used in electronics, acoustics, radio engineering, medicine, pharmaceuticals, production of components for the petrochemical, chemical, metallurgical, food, paper, textile and nuclear industries, as a structural and packaging material, in the manufacture of solar cells and piezoelectric elements. Scientific interest in PVDF is due to the possibility of synthesis on its surface by carbonization of various forms of carbon: structures with sp^2 —and sp -hybridization of valence electrons [3,4]. Radiation carbonization will be also discussed in this review as it is important aspect of PVDF processing. The surface of polymers such as PVDF can degrade under electron bombardment or X-ray radiation and which leads to the decrease of the fluorine concentration. This process is known as radiative carbonization, and it is one of the possible methods for obtaining carbene chains on the polymer surface of sufficient length [5]. Furthermore, radiation carbonization can lead to the appearance of new properties (chemical and physical) in the polymer which enhances its application potential. Additionally, the

carbon–carbon which form upon the removal of HF can connect with each other thereby forming chain-like structures such as: polycumulenes (double carbon-carbon bonds) or polyene (alternating triple carbon-carbon bonds). [6] Carbon substances consisting of such one-dimensional structures are referred to as carbinoids and can be used in optoelectronics or in the solid-state for emission electronics, not to mention other chemical and physical applications. There is also a possibility that the carbonized layer of PVDF will have superior conductivity compared to its polymer base [7–10].

PVDF is a highly reactive white crystalline thermoplastic fluoropolymer, unlike other fluoropolymers, it has a low density of 1.78 g/cm³. PVDF exists in various conformational states, its macromolecules can be in the state: disordered amorphous and ordered crystalline. Being a semi-crystalline thermoplastic, PVDF exhibits chemical, thermal and mechanical properties in a wide temperature range. Molecular weight of PVDF is above 100,000 g/mol, melting point is of 171–180 °C, the crystallization temperature is of 141–151 °C, and a glass transition temperature is of –40 °C. It is soluble in dimethylsulfonic acid, dimethylacetamide, dimethylformamide and insoluble in ketones and esters. It has high mechanical strength, wear and weather resistance, resistance to ultraviolet and ionizing radiation, the action of mineral acids, with the exception of fuming sulfuric, alkalis, halogens and hydrocarbons. It is easily dyed in bright colors [1–4].

It is important to provide a summary of the literature on PVDF that has been published so far. Table 1 contains a list of various published review papers related to PVDF. Most of them focus on the applications of the polymer for specific purposes. This particular review besides containing complementary information also provides a more general assessment of PVDF properties, its application potential and processing methods.

Table 1. A list of published review papers on PVDF and short descriptions of their contents.

Title of the Paper	Content Description
(1) Advances and prospects of PVDF based polymer electrolytes [11].	A review summarizing recent advances on gel polymer electrolytes and all solid polymer electrolytes on the basis of PVDF.
(2) Lithium-ion battery separators based on electrospun PVDF: A review [12].	A review emphasizing the potential of electrospun PVDF in batteries, and how it improves their performance.
(3) Insights and perspectives on graphene-PVDF based nanocomposite materials for harvesting mechanical energy [13].	A review describing how graphene and its derivatives can enhance PVDF capabilities in piezoelectric energy harvesting.
(4) PVDF based ionogels: applications towards electrochemical devices and membrane separation processes [14].	A review going over advantages of PVDF as a matrix material for ionogels based on polymers.
(5) Poly(vinylidene fluoride) (PVDF) membranes for fluid separation [15].	A review focuses on (but not limited to) the usage of PVDF membranes for water distillation.
(6) Flexible PVDF based piezoelectric nanogenerators [16].	A review summarizing latest information on PVDF used in nanogenerators.
(7) Progress in the production and modification of PVDF membranes [17].	A review highlighting various surface modifications in order to improve fouling resistance of PVDF membranes.
(8) A Brief Introduction and Current State of Polyvinylidene Fluoride as an Energy Harvester [18].	A review underlining the advantages of PVDF for the use as a nanogenerator
(9) Polyvinylidene fluoride: A multifunctional polymer in supercapacitor applications [19].	A review focusing on the potential of PVDF as well as its nanocomposites and copolymers in the supercapacitor industry
(10) Design strategy of poly(vinylidene fluoride) membranes for water treatment [20].	A review dedicated to understanding the science and engineering behind the membranes' preparations based on PVDF.

The uniform distribution of fluorine and hydrogen atoms along the PVDF polymer chain facilitates the possibility of HF (hydrogen fluoride) removal both in the polymer chain itself with the formation of conjugated double bonds and an increase in thermal stability,

and between adjacent polymer chains with the formation of cross-linked structures. During the pyrolysis of PVDF, C–C bonds can also be broken with the appearance of short-chain fragments of the polymer and free radicals as a result of disproportionation, which makes possible the chain process of degradation of a part of the polymer to a monomer [21]. PVDF is mechanically strong and flexible.

PVDF has been the dominant polymeric binder in the mass production of lithium-ion batteries (LIB) for decades [22,23]. PVDF belongs to the class of fluorinated polymers and is therefore characterized by a high melting point, chemical resistance to solvents and high electrochemical stability (up to 5 V). This polymer has a good binding capacity and, at the same time, swells to a limited extent in the electrolyte, facilitating the transfer of lithium ions to the surface of the active material [22,24]. Partially crystalline PVDF has several polymorphic modifications; however, it predominantly crystallizes with the formation of the α -phase, the formation rate of which is maximum. The degree of crystallinity of PVDF depends on the crystallization conditions and can reach 50–70% [25]. The high degree of crystallinity determines the minimum degree and low swelling rate of PVDF in the organic electrolyte, ensuring long-term and stable LIB operation. At the same time, the amorphous region in PVDF is a good matrix for the electrolyte, due to which lithium ions can pass through a thin layer of a swollen polymer binder [25].

It has a combination of valuable properties: a relatively high melting point, high mechanical strength, resistance to moderately aggressive media, good biocompatibility. One of the modifications (β -phase) of PVDF has ferroelectric and piezoelectric properties. The polymer is widely used for anti-corrosion coatings, manufacturing of acoustic devices, as a structural and packaging material. The unique combination of physicochemical characteristics allowed this polymer to be included in the so-called NASA list of materials promising for use in space [26].

The priority in obtaining high molecular weight PVDF, which is a technically useful product, belongs to 'Du Pont' company. The method patented by her is a water-suspension process under the action of such initiators as benzoyl peroxide, ammonium persulfate or molecular oxygen. Particular attention is paid to electroactive polymers capable of efficiently converting mechanical action into an electrical charge. A more promising representative is polyvinylidene fluoride (PVDF), which is used as sensors and transducers of acoustic signals. Unlike other polymers of fluorine-substituted ethylene, the electrical properties of PVDF do not allow them to be used as high-frequency insulation; however, the high values of the dielectric constant, the presence of ferroelectric and pyroelectric properties [27] make it promising to use the polymer and compositions based on it in acoustic and pyroelectric converters [28].

Polyvinylidene fluoride PVDF appeared on the world market in the early 1960s and was originally used for the manufacture of packaging films and protective coatings. The piezoelectric effect in PVDF films was first discovered by Japanese researchers in 1969 [29].

PVDF forms at least four distinct crystalline phases. The two most important are α , formed under normal crystallization conditions, and β , formed as a result of pressure crystallization or mechanical deformation of polymer films. The first is a thermodynamically stable structure and consists of chains with a trans-gauche conformation. In the latter case, the chains have a flat zigzag structure with fluorine on one side and hydrogen on the other. This polar structure is responsible for the piezoelectric and pyroelectric properties of PVDF [30].

The Japanese scientist Kawai noticed a strong piezoelectric effect in PVDF films, and also found that some plastics, such as polyvinyl fluoride (PVF) and polyvinylidene fluoride [31], have strong piezoelectric properties. It also turned out that these materials are also pyroelectrics. In 1975 Pioneer, Ltd. released the first loudspeakers and headphones based on PVDF [32]. In this case, the piezoelectric coefficient of thin films poled (placed in a strong electric field to create a total dipole moment) reached 6–7 PC/N: 10 times greater than that of any other polymer [29].

The main characteristics make this material very attractive for producing large-area PVDF films. The use of PVDF as coatings is made possible due to its thermal stability, resistance to creep at elevated temperatures and deformation under load, high degree of crystallinity, low permeability to gases and liquids, good resistance to mechanical damage—abrasion and cutting, corrosive effects, atmospheric—and fungus resistance, good dielectric properties. A distinctive feature of this PVDF fluoropolymer from other widely used ones is its ferroelectric properties (spontaneous polarization in the crystal).

PVDF is a semi-crystalline polymer with a degree of crystallization of 50%. PVDF films strongly absorb IR rays in the wavelength range of 7–20 μm . On the basis of PVDF films, sensors for the people movement are realized, as well as pyroelectric sensors for more complex devices, such as video cameras for night surveillance and laser copiers. Not so long ago, an IR matrix based on a PVDF film was presented, which makes it possible to identify fingerprints, using the pyroelectric effect inherent in polymers [33].

The widespread use of polyvinylidene fluoride is due to its consistent performance in certain high focus applications in products with particularly high requirements for ultraviolet radiation, microbiological damage, abrasion, scratch resistance, combined with relatively low cost.

The material is used in many electronic components, especially as a sheath material in cables used in voice and video transmission devices, as well as in alarm systems. PVDF does not burn well and emits little smoke, which is the main factor that allows it to be used in these areas.

New PVDF copolymers developed in recent years have found a wide range of applications in piezoelectric polymer sensors. Such copolymers are used at higher temperatures (135 $^{\circ}\text{C}$), and new forms of sensors can be obtained from them: cylindrical and hemispherical. They can be used to produce sensors whose thickness exceeds the limits for devices based on PVDF films: for example, silicon sensors with an ultra-thick (200 \AA) coating and sonars with a cylinder whose wall thickness exceeds 1200 microns. Piezoelectric cables are also made from copolymers. Copolymer films can be used and stored at temperatures not exceeding 135 $^{\circ}\text{C}$, and PVDF films are recommended for use at temperatures up to 100 $^{\circ}\text{C}$.

The insolubility and electrical properties of the material are explained by the presence of different polarities of alternating CH_2 and CF_2 groups located along the polymer chain.

PVDF dissolves at room temperature in polar organic solvents and forms homogeneous mixtures with some carbonyl-containing polymers. It has good chemical and oxidative stability but is much more sensitive to organic and inorganic bases [30]. Due to the good combination of properties and processability, PVDF has become the second most used fluoropolymer (after PTFE).

Melt processable fluoropolymers are a class of high-performance engineering plastics used in many niche industries through traditional processes such as injection molding and extrusion. PVDF is the only melt-processable fluoropolymer that is produced from a single repeating structure (VF₂). In most of these areas, PVDF is processed by extrusion and injection molding, where polymer specifications are designed for these processes so that molecular weight can control melt viscosity.

The good processability of PVDF from the melt facilitates the production of products from it by compression molding (bulk containers) and injection molding (sheets, coatings, plates and rods, films). Most often, PVDF is produced in the form of tubular products (tubes and fittings, pumps, valves), and ultrapure water is transported through PVDF pipelines. Manufacture of housings for quick couplings, locking sleeves, adapters, for a specific application and with the appropriate characteristics, are made from various polymeric materials: polyimide, polypropylene, synthetic materials (for example, PVDF). PVDF is used in the equipment of chemical, semiconductor industries (actuators, sensors and loudspeakers, plates and insulators for premium-class wire); as a binder in the production of cathodes and anodes for lithium-ion batteries (supercapacitors, battery separator in lithium-ion polymer systems); in the medical and defense industries, as well as in new

areas for the manufacture of components for air and sea vessels and the interior of office equipment, ultrafiltration membranes and membranes for fuel cells.

2. PVDF Trademarks

Today, PVDF is marketed under many different brands: PVDF is sold under a variety of brand names including KF (Kureha, Düsseldorf, Germany), Hylar (Solvay, Brussels, Belgium), Kynar (Arkema, Budapest, Hungary) and Solef (Solvay, Brussels, Belgium).

Arkema is the world's largest producer of PVDF. Its manufacturing facilities are located in the US, France and China. Arkema produces both homopolymer and copolymer grades under the Kynar[®] and Kynar Flex[®] brands. Kynar[®] brand polyvinylidene fluoride (PVDF) began in 1965 for chemical handling applications and electrical wire insulation and sheath materials, and by now Kynar[®] PVDF has become one of the materials of choice for many applications requiring high performance. Kynar Flex[®] PVDF was commercialized in the 1980s as a material similar in performance to Kynar[®], but with more versatility to meet the demands of new applications.

The new Kynar High Melt Strength (HMS) PVDF grades are molecular chain branched polymer resins that have high melt strength and resistance to sag during extrusion, making them candidates for future use in blow molding, thermoforming and film extrusion with bloat. This material provides an excellent balance of melt strength and elongation, high sag resistance at low viscosity, and high die swell. These improved properties are obtained by introducing a branch to form a long side chain.

Solvay Solexis now offers a growing selection of PVDF grades that are associated with new applications such as oil and gas, automotive, construction, electronics, chimney liners, lithium batteries, fuel cells, food and pharmaceuticals. In addition to Solef[®] and Hylar[®] PVDF resins, Solvay Solexis offers a wide range of other fluoropolymers that are also easily processed by injection, extrusion and all conventional processing methods:

- Halar[®] ECTFE (ethylene-chlorotrifluoroethylene copolymer),
- Hyflon[®] PFA (a copolymer of tetrafluoroethylene and perfluoroalkyl vinyl ether).
- Among the most important properties and advantages of PVDF Solef[®] are the following:
- Excellent chemical resistance. The use of Solef[®] resins, polymers of vinylidene fluoride, provides excellent corrosion and abrasion resistance when working with harsh chemicals.
- Excellent thermal stability.
- Fire resistance. Solef[®] PVDF resins are rated UL-94 V-O.
- Purity Solef[®] PVDF Resin is an extremely pure polymer free of stabilizers, plasticizers, lubricants and flame retardants.
- Increased abrasion resistance.

There are at least three varieties of PVDF on the market, differing from each other in the quantitative content of polyvinylidene fluoride and acrylic polymer: 50/50%, 70/30% and 80/20%. All of these varieties can be called PVDF. However, licensed PVDF is produced only under the well-known Kynar500 or Hylar5000 licenses and contains at least 70% polyvinylidene fluoride.

Georg Fischer's PVDF pipes, fittings and valves are a high-performance piping system with good impact resistance in all climatic conditions. Excellent chemical resistance, abrasion resistance up to the highest temperatures. Georg Fischer manufactures PVDF pipes, fittings and valves under the brand name SYGEF[®]. Georg Fischer's standard PVDF products are labeled SYGEF, additionally cleaned and packaged in a special way, products for the transport of very pure water (UPW) are labeled SYGEF PLUS.

- Nominal pressure up to 16 bar.
- Temperature ranges from $-20\text{ }^{\circ}\text{C}$ to $+140\text{ }^{\circ}\text{C}$.
- SYGEF[®] Standard—A one-piece and reliable solution for the transport of water and chemicals, also at high temperatures.

SYGEF[®] Plus—Double Packed High Purity (HP) piping system is widely applied in hot ultrapure water (HUPW) and microelectronics industries. Manufactured, cleaned and packaged in clean conditions up to ISO class (100), SYGEF Plus delivers superior leaching performance combined with high reliability and long product life.

3. Overview of Applications and Properties

3.1. Properties

One of the most important tasks of modern thermophysics and molecular physics is to establish the relationship between thermophysical properties (TPP), in particular thermal conductivity, of polymeric materials with their structure at various levels of its organization and the nature of thermal motion. Knowledge of this relationship makes it possible to deeply and comprehensively analyze the mechanism of heat transfer in polymer composite (PC) materials, which will help accelerate the solution of the problem of obtaining polymer materials with predetermined TPP. In particular, due to its relative technological simplicity, efficiency, and economy, the physical method of introducing various fillers into the polymer has received wide recognition [34].

The defining advantages of PVDF, which allow it to take one of the leading positions in the world market in a number of industries, are:

(1) Heat resistance to temperature fluctuations from -40 to $+140$ °C. Among fluorine-containing polymers, polyvinylidene fluoride (PVDF) is one of the most durable. It has good ductility, impact strength, and flexibility. The properties of PVDF are described in sufficient detail in [27,28,35–37]. The structure of PVDF macromolecule chains has been studied by many researchers who have used various techniques for this purpose [28,37,38].

(2) Purity of the composition is due to the components of the main substance that satisfies the necessary performance characteristics: it does not contain UV and heat stabilizers, various lubricants, softeners and other additives [39].

(3) Eco-friendliness—completely non-toxic and fully recyclable. It does not emit toxic, chemically harmful fumes into the environment even when melted [40].

(4) Protection against microorganisms—the polymer has very low adhesion to microorganisms (growth of fungi, algae and microbial films). Validity of its use for the storage of medical and food liquids; filters (filtration housings), track membranes, membrane packages, separation equipment and separation elements are expediently used: microfiltration for wastewater treatment and processing; seawater desalination; separation of liquids for cleaning oil, natural gas [41].

(5) Fire-resistance PVDF is a barely flammable material. Melts slowly without emitting much smoke.

(6) Easy processing allows the production of products of various shapes: by extrusion, injection molding, compression molding and machining. When heated, PVDF loses its rigidity and becomes ductile, which makes it possible to process end products from this material. It is easy to perform various connections and assembly of structures (butt and socket welding, flange and threaded connections). Furthermore, the PVDF can be modified by various additives to tailor its chemical and physical properties [42].

(7) Reliability, optimal wear resistance, the required mechanical strength of parts during installation and in industrial installations are provided by materials from polyvinylidene fluoride. Products are resistant to mechanical damage, surface abrasion, ozone, moisture and corrosion [43].

(8) Durability of products—have high resistance to aging and can last more than 50 years without loss of physical and mechanical properties [44].

PVDF shows little to no deterioration in mechanical properties after many years of outdoor use, which is why it is often used for coating the exterior surfaces of buildings. PVDF also stands out for its mechanical properties among conventional crystalline polymers: it ranks second after polyoxymethylene in terms of tensile strength, flexural stress and compressive stress, stiffness and hardness, has the highest impact strength, high coefficient

of curing (80–90% tsri thickness 100 microns) in the visible region of the electromagnetic spectrum [36].

(9) Low surface roughness—high flow rate (very smooth inner wall surface).

(10) Chemical resistance—the main indicator of resistance to most organic and inorganic chemically aggressive liquids (acids and bases, alcohols and petrochemical solvents) even at elevated temperatures.

3.2. Applications

- In the chemical/petrochemical industry—non-flammable, can be used in fire and explosion hazardous industries; filtration of aggressive media from particles of microimpurities; does not react with other compounds. Compatible with thermoplastic materials and has excellent inert resistance to concentrated inorganic acids even at high temperatures (the main material for storing concentrated nitric acid), aliphatic solvents, ionic and salt solutions, which is essential for the safety of roofing and wall cladding during long-term operation (up to forty years), excluding the effects of acetone, highly concentrated alkali and other solvents (strong bases, caustics, esters, amines, ketones).

In terms of resistance to UV rays and rays at 100 Mrad, PVDF is an exception [20] PVDF has very good weather resistance and high flexibility. Therefore, it can be used to make coatings that transmit sunlight, PVDF also has good chemical resistance; even at high temperatures (363 K), PVDF is not affected by inorganic acids, corrosive materials (halogens, oxidizing agents), weak bases and salts, aliphatic, aromatic and chlorinated solvents [34].

- In nuclear power engineering—handling of nuclear waste. PVDF is used as pipes, sheets and linings in high temperature, hot acidic, radiation environments due to PVDF's resistance characteristics and upper temperature thresholds. As piping, PVDF is rated for temperatures up to 248°F (120 °C). Examples of uses for PVDF include nuclear reactor waste management, chemical synthesis and production (conventional sulfuric acid), airboxes, and boiler service pipes. When heated above 350 °C, polyvinylidene fluoride begins to decompose with the release of toxic substances containing fluorine, so it is important during the operation of the material not to expose it to critical temperatures, including fire [45].
- Aviation industry—seals, linings, gaskets and other products that provide flexibility and resistance to corrosion [46].
- Aerospace industry—in wiring coatings as a thermal barrier. It is also available as a cross-linked, closed-cell foam, which is increasingly being used in the aviation and aerospace industries, and as an exotic 3D printer filament [29].

Interestingly, PVDF is even used in the manufacture of some devices for the space industry—for example, some devices are made using this polymer, which are installed in a space probe that measures the density of cosmic dust outside the solar system.

- In electronics/radio engineering—PVDF electronic components are used as a dielectric, insulation of electrical wires (light weight, flexibility, high coefficient of resistance to heat transfer). The unique piezoelectric properties allow the material to respond to and influence electrical and/or magnetic fields. PVDF is in demand in the production of complex electrodes for lithium-ion batteries because it does not react with electrolytes and lithium [47].

PVDF film is used in radio-electronic devices to protect highly sensitive devices; for the manufacture of printed circuit boards; insulation of wires/cable sheaths; for obtaining electrets and pyroelements; in touch switches and microprocessors; solar collectors, etc. [48].

The piezoelectric properties of PVDF are used in the manufacture of tactile sensor arrays, low-cost strain gauges, and lightweight sound transducers. Piezoelectric PVDF panels are used in the Venetia Burney Student Dust Counter, a New Horizons space probe science instrument that measures dust density in the outer solar system.

- In electrical engineering—the resistance of PVDF insulation to cutting allows it to be used in wires for panels of computing devices, for aviation instrumentation and other types of electronic equipment. As a winding and insulating material, as a protective coating for special overhead cables, electrical equipment (motor windings).

Sensing elements based on piezoceramic materials have been used in the creation of hydroacoustic antennas since the 1940s to the present due to their high sensitivity and electrical capacitance. It is advisable to create electroacoustic transducers based on PVDF films, which, in addition to improving the weight and size characteristics, will reduce the susceptibility of antennas to hydrodynamic interference without the use of additional rigid structural elements, will allow designing antennas using flexible receiving elements of a large area [49].

PVDF membranes can be used as separators in lithium-ion batteries because they have good chemical and heat resistance. Such membranes have good mechanical strength, sufficient pore size and interruption characteristics. The material can also be used to obtain piezoelectric sensors and laser beam profile sensors in modern applications [15–18].

- In construction—as erosion-resistant, protective anti-corrosion and weather-resistant coatings (films and enamels). Applicable to the material—all types of welding non-contact infrared and seamless, except for chemical (adhesive bonding). PVDF material is commonly used in the manufacture of various parts and equipment for pumping stations and pipelines suitable for pumping ultrapure water and chemicals (acids, gases, organics). The PVDF polymer coating is good for responsible outdoor use (during the construction of industrial facilities; chemical production facilities; cladding of the facades of buildings located in the industrial zone, where the walls must be frequently washed not only with water, but also with disinfectant solutions), reliably withstands heating up to 120 degrees, and frost—up to 60 [50].

Filled PVDF film—veneer material in construction; the coating is applied to gas ducts, chemical cabinets and boxes, facade fixtures, composite panels, roofs. Sandwich panels coated with PVDF can be used for buildings with specific operating conditions in areas with an aggressive climate (high resistance to sunlight, frost resistance, high salt vapors (cowsheds, pigsties, poultry houses) [51,52].

- In architectural structures—which are subject to increased aesthetic requirements for walls and architectural and decorative details for the decoration of facades (to maintain strength, color and gloss longer) and as an anti-vandal coating (unauthorized inscriptions).

The main application of PVDF is architectural coating (Iezzi 1997). PVDF dispersions are applied to metals such as steel or aluminum to provide a decorative and weather resistant coating for commercial and residential buildings. It is used for electrical insulation, despite its higher permittivity, and in the chemical industry [30].

- In the automotive industry—PVDF-based laminating multilayer films are used for decorating external surfaces. Multilayer films based on PVDF are versatile materials that allow you to create both transparent coatings and coatings of various colors, metallic colors, mother-of-pearl, imitate the texture of wood, leather, and apply geometric patterns. Parts that can be produced with these PVDF-based films include taillight surrounds, side mirror housings, front grilles, bumpers, door handles, body side moldings, and more. Decoration during molding allows obtaining surfaces with better color and gloss retention parameters and exceptional resistance to chemical pollution [53].
- In pharmaceutical industry—PVDF materials provide special cleanliness and sterility of rooms—premises, and due to excellent deformation characteristics and heat resistance, they allow autoclaving; serve as packaging for medical instruments; Surgical sutures made of PVDF are resistant to chemicals (do not cause an allergic reaction) and have extremely high tensile strength [54].

- In biomedicine (biomedical research). Polyvinylidene fluoride proved to be an absolutely ideal and stable material (minimal tissue reaction, no capillarity and wicking, perfect antithrombogenic effect) for use in gynecology (obstetrics); general surgery (orthopedics, cardiovascular, plastic and reconstructive) [55].

At present, polypropylene mesh endoprosthesis are widely used in domestic herniology. However, given the significant experience in the use of these materials, it can be said with confidence that these endoprosthesis are not ideal for hernioplasty [56,57]. Most of the known polypropylene endoprosthesis after implantation in the abdominal wall tissue cause an inflammatory reaction leading to the formation of a rough scar [58], which contributes to the wrinkling of the endoprosthesis [58] and disruption of the biomechanical parameters of the abdominal wall.

A promising way to prevent these complications is the use of polymers in hernioplasty that differ from polypropylene in chemical and physico-mechanical properties. One such polymer is polyvinylidene fluoride (PVDF), which is widely used in reconstructive surgery [59–62]. Studies show that PVDF, like polypropylene, has bioresistance, strength and resistance to infection, surpassing the latter in elasticity.

Another feature of the PVDF polymer is the possibility of coating its surface with a linear-chain carbon-carbonyl [63]. It is now known that carbonyl applied to polymeric materials can significantly increase the biocompatible properties of surgical suture materials [64].

The purpose of the study [64] is to experimentally substantiate the possibility of using mesh endoprosthesis based on PVDF-K to improve the immediate and long-term results of hernioplasty. The experiments consisted in comparing the biocompatibility of Esfil polymeric endoprosthesis widely used in herniology from polypropylene monofilaments and new experimental PVDF-K endoprosthesis. All studied materials had the same fiber structure and thickness. To study biocompatibility, these materials were implanted in the tissues of the anterior abdominal wall of animals in the on-lay position and fixed with the same name suture material (polypropylene and PVDF-K monofilaments, respectively), size 3/0. Comparative analysis of qualitative and quantitative changes in the tissues of the anterior abdominal wall in series with implantation of Esfil material and PVDF-K material confirms the best biocompatible properties of the carbonyl-coated PVDF-based endoprosthesis. Early relief of inflammatory changes, early maturation of granulation tissue, lack of encapsulation of endoprosthesis elements in the presence of a single histotypical structure of the emerging scar, and relatively rapid stabilization of the tissue response to the implant can be the overall result of adequate physical and mechanical properties of the PVDF polymer and pronounced biocompatible properties of the coating from carbonyl. All this gives the right to assert that the use of mesh endoprosthesis based on PVDF-K will improve the immediate and long-term results of hernioplasty.

PVDF is a non-absorbable monofilament synthetic surgical suture: well suited for cardiovascular surgery where resistance to cardiac movement is required, both in cases of prosthetic valves and vascular anastomoses. PVDF is recommended for applying removable cosmetic intradermal sutures, is approved for fixing various implants (hernioprosthesis, vascular prosthesis), is widely used in mammoplasty operations when applying a circular Benelli suture around the halo, and is used in plastic surgery and microsurgery.

PVDF, an inert material, has long been used as a suture material. It has a high degree of biocompatibility, similar to that of polypropylene or polyester. Due to the low incidence of inflammatory and fibrotic foreign body reactions and low shrinkage after implantation, PVDF has been shown in some studies to be a useful alternative to conventional materials such as polypropylene and polyester [65].

PVDF membranes can be used in other biomedical applications as part of a membrane filter device, often in the form of a syringe filter or wheel filter. The various properties of this material such as heat resistance, resistance to chemical corrosion and low protein binding make this material valuable in the biomedical sciences for drug preparation as a sterilizing filter and as a sample preparation filter for analytical methods such as high-performance

liquid chromatography (HPLC), where small amounts of particulate matter can damage sensitive and expensive equipment.

- In microelectronics and photonics, it has now been demonstrated that ultrathin PVDF films can be obtained using spin coating [66]. The production of ultra-thin, pinhole-free, smooth PVDF films paves the way for integrating ferroelectric and piezoelectric properties into microelectronic devices. Moreover, thin and smooth PVDF is a worthy candidate for photonic applications [67] due to its chemical and environmental stability. The surface roughness and smoothness presented here is sufficient to prevent optical losses in planar PVDF waveguides. In addition, PVDF can be used to incorporate complex functional materials providing electro-optical effects.

Fashion designer and professor Ying Gao's latest designs, titled "Can't" and "Won't", are two spectacular dresses made from "super organza" material, cotton and polyvinylidene fluoride. The latter is a piezoactive fluoropolymer capable of changing dimensions and/or bending under the influence of electricity. The highlight of the project is the "eye-tracking" system integrated into clothing, which is well known to smartphone users. Thus, clothes can be "activated" by the interested look of a nearby person.

- In the food industry—used in repeated contact with food, as it complies with FDA requirements and is non-toxic at temperatures below the decomposition temperature [29]. Production of containers for drinks; low thermal conductivity, eliminates the need for additional thermal insulation.
- Other applications. The aforementioned list of properties is not exhaustive. PVDF and materials on its basis also find applications in such areas as: textile industry, in the metallurgical industry, in the pulp and paper industry, etc. Furthermore, the characteristics of the polymer allow it to be used in the production of sorption columns. Such a product is suitable for the extraction of rare earth and precious metals: gold, uranium, copper, vanadium and others. The unit has low thermal conductivity and low weight. It has a high efficiency, due to the wide throughput and smooth surface—sorbates and metal products will not accumulate inside. Additionally, PVDF is also used to obtain porous tips (balls) in the production of ballpoint pens [11–18].

4. Experimental Data on PVDF

This chapter contains a brief overview of studies conducted in order to study PVDF's processability as well as its interesting properties characteristics.

4.1. Relaxation Transitions

Four main relaxation transitions in the PVDF phase were determined by dynamic mechanical spectroscopy [38]. In Figure 1, the temperature dependences of the dynamic Young's modulus (E) determined along and perpendicular to the direction of crystallization of the sample obtained by isothermal crystallization [34] are given.

γ -relaxation, which begins at low temperatures, corresponds to the amorphous phase and limited movement of chains, and specific ones—to rotations of chains in the amorphous region, γ -relaxation is associated with glass transition, it corresponds to the micro-Brownian motion of segments [34,37,38] of the amorphous region. α -relaxation is associated with the movement of molecules, which changes the dipole direction only along the chain axis, and not perpendicular to it [38]. It is possible that the relaxation behavior of PVDF varies not only at different temperatures, but also depends on the methods used to study these properties.

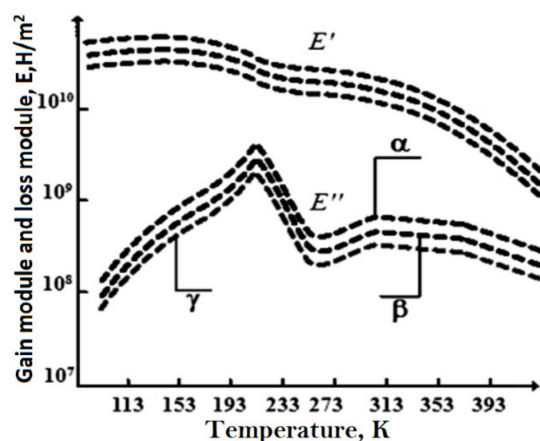


Figure 1. Temperature dependences of the dynamic mechanical characteristics of PVDF: storage modulus (E') and loss modulus (E'') of isothermally crystallized and directionally crystallized samples of the α -phase of PVDF: 1—parallel; 2—perpendicular; 3—isothermally crystallized sample (spectra are numbered from top to bottom) [34].

4.2. Piezoelectric Behavior

The most important piezoelectric coefficient of PVDF is d_{33} , also known as the compression mode. d_{31} is another common piezoelectric coefficient otherwise called transverse mode, which is associated with the application of mechanical stress at right angles to the polarization axis [18]. There are also shearing strain coefficients d_{24} , and d_{15} , which are oftentimes omitted due to their low magnitude [68]. PVDF are reported to have a very high d_{33} (~ 49.6 pm/V) [69] which can be measured by several methods: static, quasi-static and laser interferometer method [70]. These methods, however, have their disadvantages and limitations. Static and quasi static method produce too much of an electric charge by applying force to the samples which causes biaxial stress. Additionally, small thickness of the films entails complicated stress alignment [71]. Laser interferometer method on the other hand is quite sophisticated and requires excellent alignment of optical parts [72]. There is also a relatively new method proposed in [70]. The authors utilized a pneumatic pressure rig with a sole cavity for the measurement of PVDF piezoelectric coefficients. The method involves usage of highly pressurized nitrogen gas and the following monitoring of the induced charge variation. Thus, the d_{33} value was accurately measured without any associated stress effects.

Japanese scientists [67] from the Kagawa National Institute of Technology have developed a simple highly sensitive PVDF piezofilm sensor to monitor the respiratory status of public transport drivers, patients with artificial lung ventilation devices, as well as for screening tests of “apnea”—sudden cessation of breathing during dream. Figure 2 shows a PVDF piezoelectric film (DT2–028K/L, Tokyo Sensor Co. Ltd., Tokyo, Japan) used to develop a respiration sensor, which is 28 μm thick and has a surface area of 16 mm \times 73 mm. Both surfaces of the piezo film are covered with silver electrodes, which are physically protected and insulated with a plastic film. Piezoelectric film generates electrical signals proportional to mechanical stress or strain, making it suitable for breath sensors due to its high sensitivity. The piezo film generates very large signals, even with minimal movement. Breath sensors based on PVDF piezofilms have already been developed and put into practice.

In [73], the piezoelectricity was studied using optical imaging and piezoresponse force microscopy (PFM) based on a flexible piezoelectric poly(vinylidene fluoride) (PVDF) film and the surface morphology of PVDF was analyzed. The authors, using theoretical modeling, investigated the interference of signals between adjacent matrices. The results indicate a reduction in interference as the pressure decreases at a rate of 0.028 mV/kPa, which depends significantly on the size of the electrode and becomes negligible at a pressure level of less than 178 kPa. These studies indicate that the electromechanical properties of

the PVDF film sensor are characterized by both good piezoelectricity and excellent output characteristics and ultra-high signal-to-noise ratio.

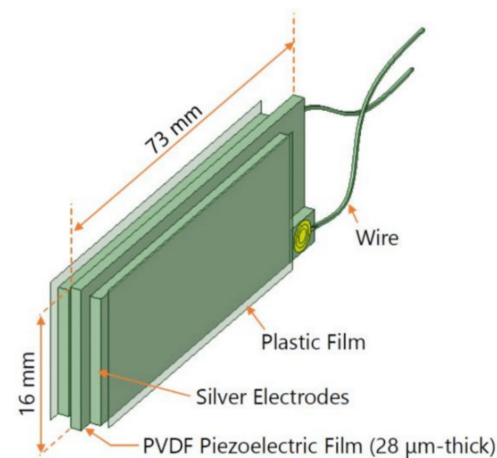


Figure 2. A schematic image of PVDF piezoelectric film (DT2-028K/L, Tokyo Sensor Co. Ltd.) which was utilized in the development of the respiration sensor [67].

The sensor matrix proposed by the authors has a sandwich structure based on a thin PVDF film with a thickness of $\sim 50 \mu\text{m}$ (Jinzhou Kexin Inc., Jinzhou, China). The PVDF films was coated on both sides by aluminum electrode arrays $20 \mu\text{m}$ thick. Figure 3a shows a schematic diagram of the sensor and Figure 3b shows the real physical picture of the device and demonstrates its flexibility. The sensor has 16 blocks of micro-capacitors; every 4 blocks have one connection wire to keep the number of electrode wires to a minimum.

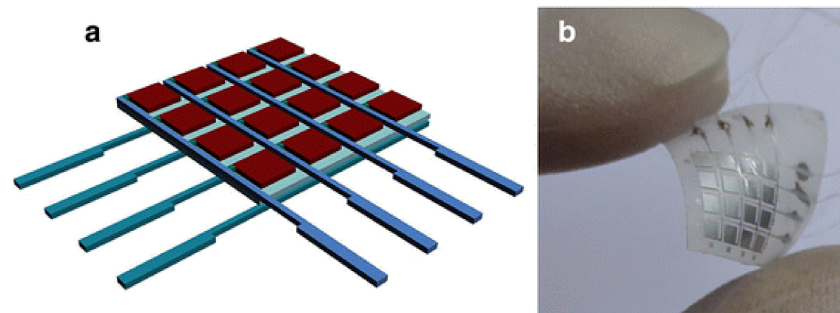


Figure 3. (a)—schematic diagram of the sensors matrix; (b)—physical picture of the end device [73].

Unlike piezoceramic transducers, sensors based on piezoelectric films have wider dynamic and frequency ranges. The wide frequency band (practically from 0 to 2 GHz) and low-quality factor can be explained by the softness inherent in polymers. Figure 4a shows the sensor surface morphology after Al etching, checked with an optical microscope. The rather bright and dark contrast suggests a clear interface between the PVDF and the etched aluminum electrodes.

Figure 4 shows the surface morphology and phase signal of the pressure sensor PVDF film. The surface of PVDF is stated to be smooth with a fabric structure. The phase image of the PFM measurement in Figure 4c shows a strong piezoelectric domain response which is in a good consistency with the surface structure observed in Figure 4b.

A sensor was utilized to measure the pressure state and its distribution caused by a finger of the human hand for a simple practical application. It is known that complex finger movement has some basic variations such as shiatsu, kneading, rubbing, etc. [74]. The three most commonly used movements, including shiatsu, kneading, and rubbing, were chosen to investigate the state of pressure and the finger surface area distribution. Figure 5 shows a diagram of the pressure distribution of the thumb, detected by the sensor, during three

finger movements, correspondingly. In Figure 4a, it is apparent that the pressure of 76 kPa was focused at the center of the thumb during the shiatsu movement, which differs quite strongly from the kneading and rubbing observed in Figure 5b,c, respectively. Figure 5b indicates that the pressure at the thumb front is higher than at other parts of the thumb during the kneading motion, whereas the pressure of the thumb is relatively uniform (about 68 kPa) when it comes to the rubbing motion, as shown in Figure 4c. The observed distribution of pressure in the finger bear some resemblance to the previous reports in clinical observations [75,76]. According to measurements, a load cell on the basis of flexible PVDF ferroelectric film demonstrated good sensitivity for characterizing complex finger movements. It is expected that the proposed sensor will be superior in terms of studying the human finger motion behavior, and it would also be useful for the development of a robot to replace human fingers in the future [74].

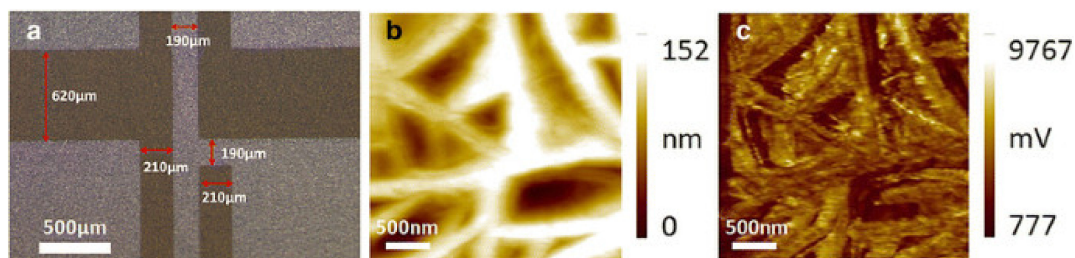


Figure 4. (a)—surface morphology of the proposed sensor after etching technology; (b)—Surface morphology and (c) PFM phase images of the PVDF sensor film [73].

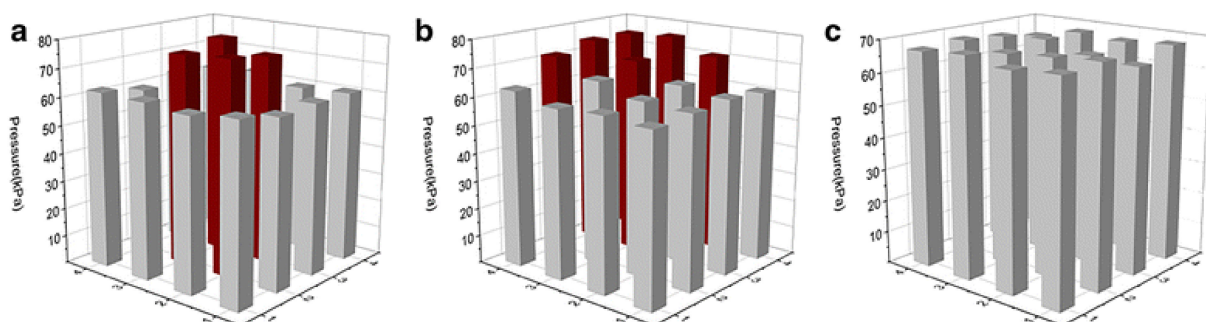


Figure 5. The state of pressure and distribution of movement of the thumb, characterized by the proposed sensor: (a) shiatsu, (b) kneading and (c) rubbing [73].

The author of [77] studied and obtained the properties of oriented and microporous PVDF films with piezoactive properties, as well as the development of composite materials based on microporous PVDF films with layers of an electrically conductive polymer (polypyrrole).

4.3. β -Phase Formation

According to the author of [77], one of the most productive methods for the formation of β -form crystallites in PVDF today is the orientational stretching of the film (extrusion). One of the most important parameters in orientational stretching is the process temperature; it was found [77] that the best performance is achieved at a stretching temperature of 50 °C (Figure 6).

After stretching, the film is annealed at 140 °C. At the stage of sample annealing, the crystal structure is improved (Figure 7).

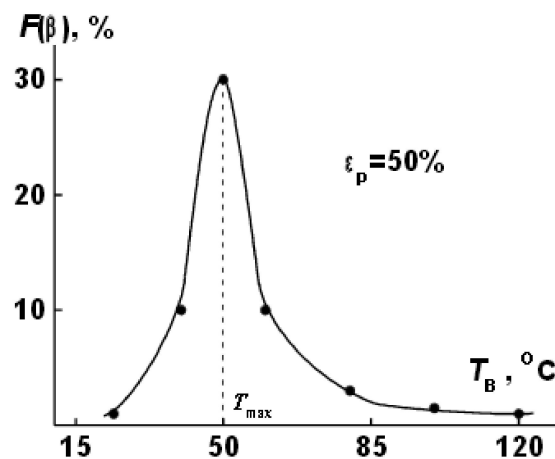


Figure 6. Dependence of the fraction of crystallites of the β -phase on the stretching temperature at a stretching ratio of 50% [77].

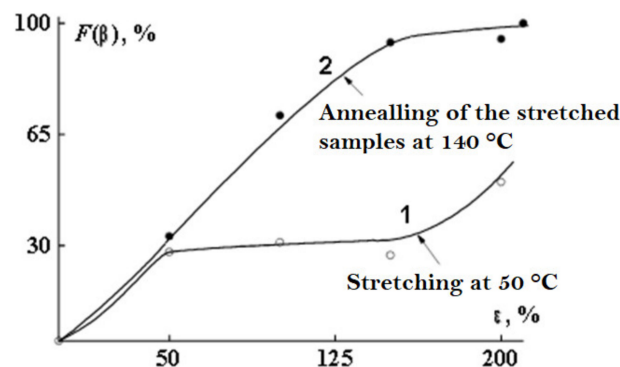


Figure 7. Dependence of the fraction of β -phase crystallites on the degree of stretching for PVDF films stretched at 50 °C (1) and for the same samples after annealing at 140 °C (2) [77].

As a result of annealing, the sample acquires rigid elastic properties and the ability of large reversible deformations with a high modulus of elasticity. It should be noted that, in a real sample, the formation of a porous structure is accompanied by the processes of orientation, rupture of passing chains, and destruction of crystallites. At the final stage—thermal fixation—there is a relaxation of internal stresses accumulated in the process of stretching. As a result, the formed structure becomes unstressed, and the dimensions of the cooled porous film do not change with time. It was found that isometric annealing of oriented polyvinylidene fluoride films leads to a significant increase in the content of p-shaped crystallites and an increase in the degree of crystallinity [77].

Special scientific interest in PVDF is caused by the possibility of synthesis on its surface by carbonization of various forms of carbon.

Based on PVDF, a thermionic cathode with a record low work function was obtained [78]. There are works on the synthesis of molecular magnets based on partially carbonized PVDF [79].

Chemical dehydrohalogenation of halogen-containing polymers (HCPs) is one of the most convenient and accessible methods for the synthesis of one-dimensional and quasi-one-dimensional carbon structures [80]. Among HCPs, PVDF is the most promising initial polymer for the production of articles from carbene due to its better solubility in the components of dehydrofluorinating mixtures [81]. A well-known method for smoothly changing the phase composition of PVDF composite films is their uniaxial mechanical stretching. An increase in the ratio of the final and -initial film sizes in the direction of stretching—the elongation factor—increases the content of the ferroelectric β -phase [82,83]

and also promotes amorphization of the polymer substance in partially crystalline films [84]. To identify the molecular composition of carbinoids, to study its changes depending on the conditions and duration of carbonization, IR spectroscopy has been successfully used for a long time [85].

The authors of [86] synthesized a model of the CH absorption band, which makes it possible to measure the frequency position and width of the peaks with a change in the concentration of the β -phase in the sample. At the same time, a correlation was found between the parameters of the absorption band of CH bonds in the IR spectra of uniaxially stretched PVDF samples and changes in the phase composition of the PVDF film (Figures 8 and 9. Designations \blacksquare and \diamond correspond to the positions of peaks 1, 2). The parameters of the curves were chosen so that their sum (dashed curve, Figure 10) best described the CH absorption region in the spectrum of the unstretched film (solid curve).

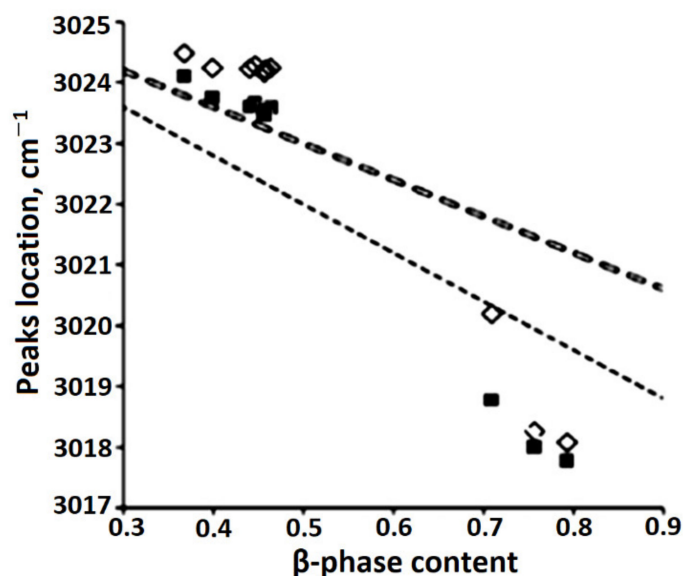


Figure 8. Dependence of the frequency position of peaks 1 and 2 on the concentration of the β -phase in the model and experimental IR spectra [26].

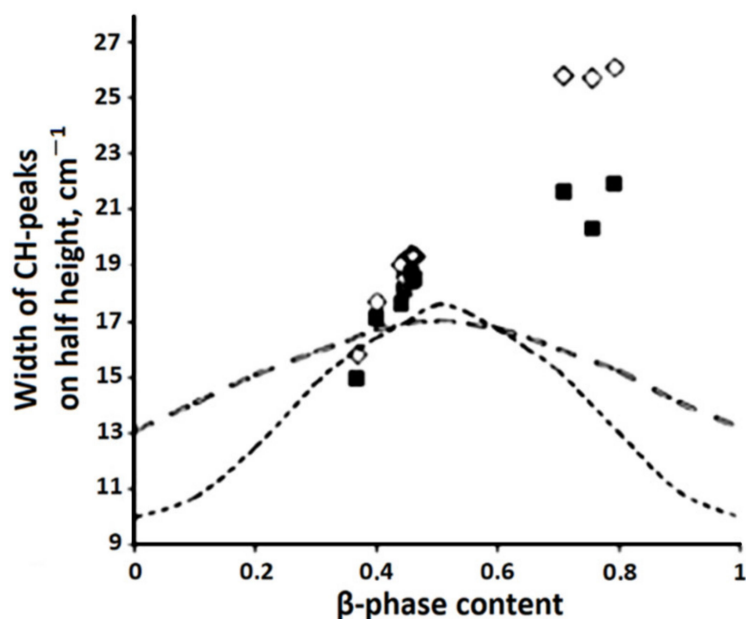


Figure 9. Change in the widths of CH peaks 1 and 2 depending on the concentration of the β phase in the model and experimental IR spectra. The designations are the same as in Figure 8 [26].

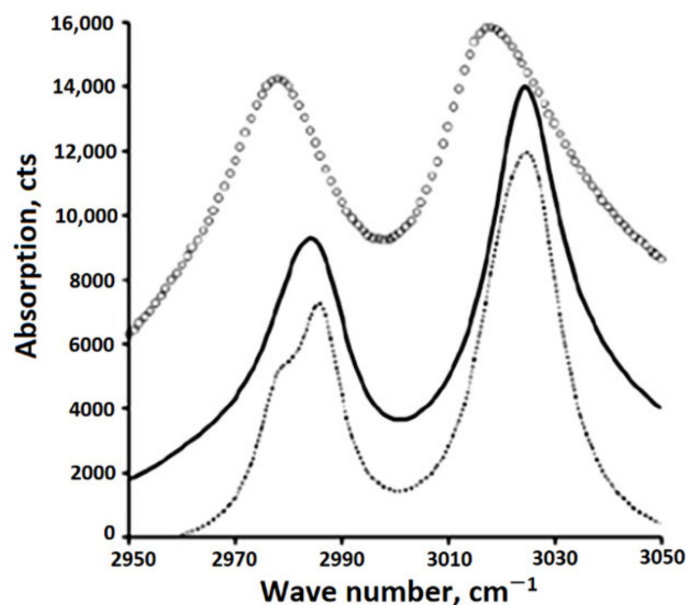


Figure 10. CH peaks of IR absorption of the experimental spectra of the maximally stretched (empty circles), initial (solid line) PVDF films and model simulation of a fragment of the spectrum of the initial film (dotted line). [26].

The model developed under the assumption of an additive contribution of crystalline phases to IR absorption is inconsistent with the experimental data. One of the reasons for the discrepancy between the model and experiment may be the still unexplored effect of the amorphous component on the shape of CH peaks [26].

One of the directions for the synthesis of chain carbon nanostructures is the carbonization of polymers whose chains have a carbon skeleton, for example, polyvinylidene fluoride (PVDF). PVDF itself has a number of useful properties due to which it is widely used in membrane technologies [29], electronics, medicine, acoustics, etc. [6,86]. Its molecules are carbon chains, to each atom of which two atoms of fluorine and hydrogen are alternately attached. There are three main types of chain conformation: α , β , and γ [6].

Two main methods of PVDF carbonization are known: radiation (irradiation with quanta and bombardment with microparticles of various energies) [82–89] and chemical [6,90–99].

The most productive method for the deep carbonization of PVDF, which makes it possible to modify a sufficiently large amount of polymer without creating special conditions, is chemical carbonization [81,84,96–99].

Research on the properties of chain carbon and development of methods to improve the synthesis of carbon-based nanomaterials is of fundamental interest.

In their work [100], using IR spectroscopy, the authors revealed changes in the molecular composition of polyvinylidene fluoride as a result of chemical dehydrofluorination and subsequent storage at normal and reduced air pressure (a sample of PVDF grade F-2ME with a thickness of 20 μm). During chemical dehydrofluorination of polyvinylidene fluoride, fluorine-substituted polyene fragments are formed, as well as conjugated double and triple carbon-carbon bonds. Attachment to the carbon chain of hydroxyl groups contained in water, components of the dehydrofluorinating mixture and atmospheric air prevents the formation of conjugated carbon-carbon bonds. Drying under reduced pressure of samples dehydrofluorinated in a liquid medium promotes the formation of more extended chain fragments in which carbon atoms are interconnected by multiple bonds. The observed increase in the IR absorption of triple carbon/carbon bonds in the region of 2050–2100 cm^{-1} most clearly demonstrates the appearance of carbene-like atomic ordering of the polyene type.

In works [101,102] on the study of the effect of heat treatment at 250 °C and above on the products of chemical carbonization of PVDF, it was possible to reveal the previously unknown effect of an abrupt multiple amplification of the EPR (electron paramagnetic resonance) signal with a change in its parameters—the width and position of the absorption line, which indicates the formation of a new paramagnetic carbon substance. Such controlled paramagnetic activity makes it possible to further expand the proposed area of practical application of the products of partial carbonization of PVDF. An amazing temperature dependence of the absorption EPR of chemically dehydrofluorinated samples was revealed, which indicates the presence of an activation contribution to the paramagnetic susceptibility [103].

Processing of films of PVDF grade F-2ME and products of their chemical carbonization by methods of synchronous thermal, gravimetric and mass spectrometric analysis revealed significant differences in the nature of fluorine desorption and changes in the masses of film samples of the original and partially chemically dehydrofluorinated PVDF during high-temperature (up to 600 and 800 °C) heat treatment in an inert atmosphere, leading to charring of the films and a very similar final state of their molecular structure [100,101]. During the chemical carbonization of the film, oxygen-containing groups are formed, which decompose at 430–650 °C. Chemical dehydrofluorination of PVDF leads to the formation of a carbon-enriched layer containing one-dimensional fragments on the PVDF surface. The addition of OH groups to the carbon skeleton prevents the formation of extended fragments dominated by multiple carbon-carbon bonds. In the early stages of dehydrofluorination (up to 3 h), the loss of methylene groups can be compensated by the addition of hydroxyl groups to the carbon skeleton. With an increase in the duration of dehydrofluorination, the number of multiple carbon-carbon bonds increases, as a result of which the possibility of such attachment is limited.

This leads to a slowdown in the rate of increase in the number of OH groups. Temperature treatment of a PVDF film chemically dehydrofluorinated for 15 h can significantly reduce the content of OH groups in it [32].

Previously [79,104,105], it was found that the aging of a partially chemically dehydrofluorinated PVDF film changes the EPR signal.

4.4. Chemical Carbonization

In [106], an efficient dehydrofluorinating mixture for PVDF was proposed. The mixture consists of a saturated (20 wt.%) solution of KOH in ethanol and acetone in a volume ratio of 1:9, respectively. The authors consider PVDF as the most promising starting material for the synthesis of carbene due to its better solubility, although the dehydrohalogenation reaction in it proceeds more slowly than in other halogen-containing polymers due to the highest halogen-carbon bond energy in the series C-F > C-Cl > C-Br [107]. XPS spectra of the corresponding samples are given in Figure 11.

It was noted in [108] that the treatment of PVDF films with aqueous solutions of alkalis in the presence of ammonium and phosphonium halides at 70–90 °C for 24 h led to the formation of only fluorine-substituted polyene structures. With a similar chemical treatment of PVDF powders for 5–24 h, an insignificant amount of triple carbon-carbon bonds were detected. If, however, a mixture of a saturated solution of KOH in ethanol with tetrahydrofuran is used for dehydrofluorination of PVDF, then IR spectroscopic analysis demonstrates the appearance of double and triple carbon-carbon bonds. Figure 12 demonstrates how the HF content changed with time during dehydrofluorination reaction.

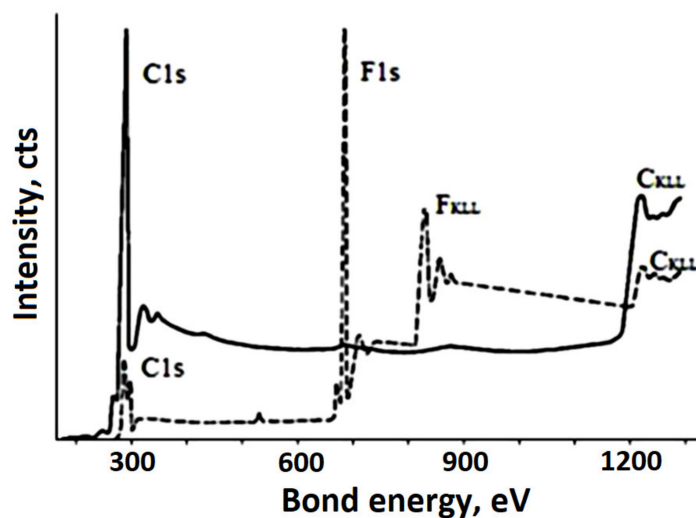


Figure 11. Panoramic photoelectron spectra of the original and dehydrofluorinated for 1 h at $-20\text{ }^{\circ}\text{C}$ PVDF film (dashed and solid lines, respectively) [106].

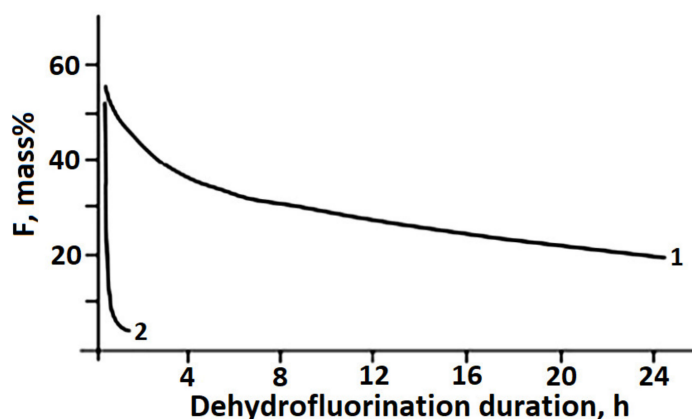


Figure 12. Dependence of the residual fluorine content in PVDF films on the DHF time during the reaction in an argon flow at (1) $22\text{ }^{\circ}\text{C}$ and (2) $68\text{ }^{\circ}\text{C}$ [108].

4.5. Radiation Carbonization

One of the methods for dehydrofluorination of PVDF to obtain chain carbon structures on its basis is radiation carbonization. For many polymers, the phenomenon of radiation degradation is observed when exposed to radiation and flows of particles of various nature. Studies of this phenomenon for polyvinylidene fluoride were carried out in [1–3]. It was shown in [2,3] that the radiation degradation of PVDF results in its carbonization due to dehydrofluorination. In radiation carbonization of polyvinylidene fluoride (PVDF), synthesized by exposure to $\text{AlK}\alpha$ photons and argon ions. The data obtained indicate a significant effect of the method of carbonizing treatment on the nature of the ordering of carbon atoms in the modified nanoscale layer of the polymer surface [109]. In this work, PVDF films of the Kynar brand (type 720, thickness $50\text{ }\mu\text{m}$) produced by Atofina (France) by blow extrusion were subjected to radiation carbonization. The measurements showed that both methods of exposure ($\text{Al K}\alpha$ photons and Ar^+ ions) cause defluorination of the surface of the studied films; however, the rate of defluorination in the second case is much higher.

In Figure 13 the first derivatives of the smoothed C KVV spectra of the initial PVDF (series of dots ■) and products of its deep dehydrofluorination with photons and ions (series of dots □) and (◇), respectively) are presented. All curves contain three dominant features A, B, and C, the energy positions and relative intensities of which differ markedly in the spectra of different samples. The results obtained demonstrate that the shape of the

electron emission spectra of the carbonized layer of the film is significantly different for the cases of Al K α irradiation with photons and Ar⁺ ions. In the near-surface nanolayers of films carbonized with ions, carbon structures with sp² hybridization of valence electrons predominate. When irradiated with soft X-ray photons, the dominant type of hybridization in the carbonized layer differs from sp². [109,110].

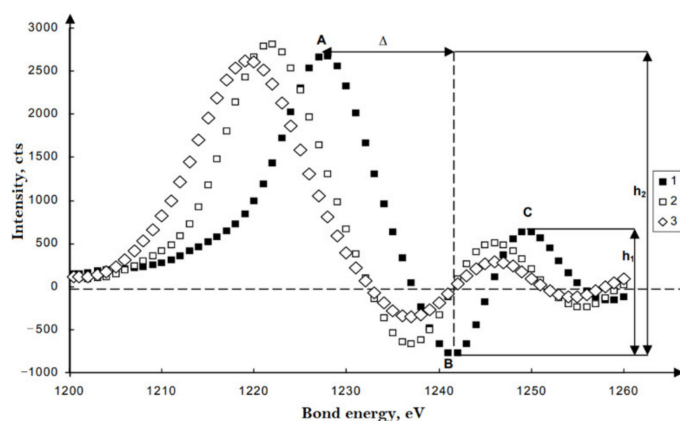


Figure 13. Derivatives of the Auger spectra of PVDF and its radiation carbonization products: h1 and h2 are, respectively, the intensities of singularities C and A with respect to the minimum of B; (Δ) is the Galuska criterion (the difference between the energy positions of the minimum B and maximum A) [109]. (■)—original PVDF; (□)—PVDF subjected to X-ray carbonization at maximum exposure; (◇)—PVDF carbonized with ions at the maximum dose.

The mechanism of piezoelectricity in ferroelectric PVDF and its copolymers should take into account the structural-dynamic heterogeneity of flexible-chain crystallizing polymers. The presence of at least two phases (crystalline and amorphous) in the bulk of the film ensures the existence of three components of the macroscopically manifested piezoactivity [111].

The author of [111] considered the specific role of the condensed state in crystallizing polymers for the macroscopic piezoactivity in PVDF. PVDF and copolymers based on vinylidene fluoride (VDF), as representatives of the class of flexible-chain crystallizing polymers, are of interest to fundamental science due to the discovery of ferroelectricity in them [112].

For applied research, these compounds are also of interest due to the presence of piezo- and pyroelectricity in them [113,114]. Crystallizing polymers, as a class of condensed states of matter, have a number of specific properties. Among them is the coexistence of crystalline and amorphous phases in the bulk of the polymer. For PVDF, these phases at room temperature differ significantly in elastic and electrical characteristics [115].

Such heterogeneity is the reason for the complex mechanism of piezoactivity. Analysis shows that it has three components: the piezoelectric effect from crystals with a noncentrosymmetric lattice, electrostriction, and size effect [116]. For practical applications as various sensors [112,113], films of PVDF and its copolymers are textured most often by uniaxial drawing. On Figure 1. It can be seen that in a uniaxially stretched PVDF film, a decrease in temperature to the glass transition temperature is accompanied by a more than twofold decrease in the e₃₁ piezoelectric constant. The dependence of the three parameters: ϵ , μ , k in the glass transition region for a single-stretched PVDF film is shown in Figures 14 and 15; it can be seen here that all three parameters decrease upon transition to the glassy state.

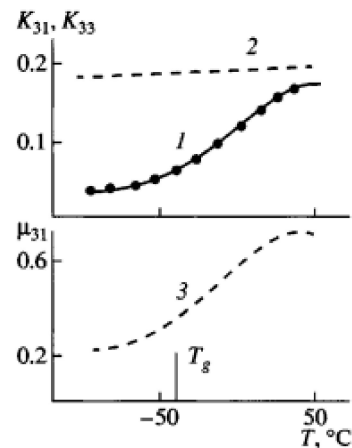


Figure 14. Temperature dependences of electromechanical coupling coefficients K_{31} (1) and K_{33} (2) [117] and Poisson's ratio μ_{31} (3) for an oriented PVDF film [118]. Reprinted/adapted with permission from Ref. [XX]. Reprinted/adapted with permission from Ref. [118]. 2022, Elsevier”.

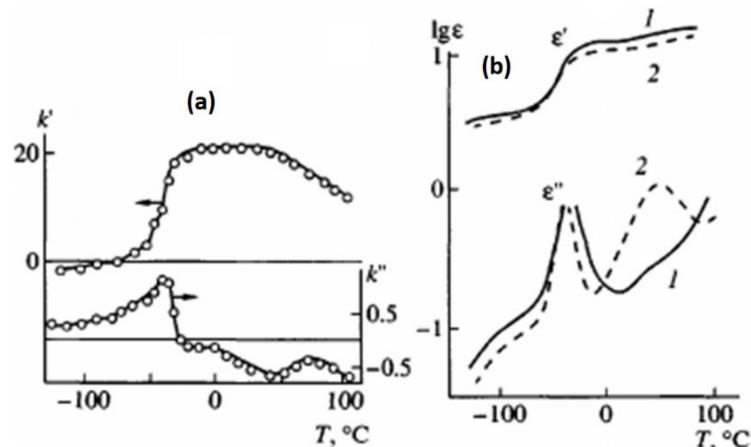


Figure 15. Temperature dependences of the components of the complex electrostriction constant (a) and permittivity (b) for oriented (1) and isotropic (2) PVDF films [119]. Reprinted/adapted with permission from Ref. [119]. 2022, AIP Publishing”.

4.5.1. The Role of the Phase State for Piezoelectricity in Isotropic PVDF Films

In a number of cases, for sensors based on the materials under consideration, a requirement arises for the isotropy of characteristics in the film plane. Obtaining such sensors based on homopolymer films seems to be a difficult task in practice. The problem is that, under normal conditions of crystallization from a melt, a nonpolar α -phase is formed in PVDF [115], which is not piezoactive. There is a fundamental possibility of converting it into a polar modification α_p or even into a ferroelectric α -phase due to polymorphic transformations in high-strength fields [115]. In practice, however, the fields required for this turn out to be higher than the breakdown ones, and the residual polarization cannot be obtained [120]. In this connection, the results of [121] are of interest, where the noted problem was solved by varying the crystallization conditions of isotropic PVDF films. It was noted that if crystallization from a melt proceeds at elevated pressure (more than 3 kbar), then the formation of a ferroelectric phase along with the nonpolar α modification is also possible [121]. By varying the pressure during crystallization, it was possible to obtain isotropic PVDF films with different ratios of α - and β -phases [111].

4.5.2. Effect of Chemical Modification of PVDF Chains on the Characteristics of the Observed Piezoelectricity

Another way to obtain isotropic films with ferroelectric crystals is the introduction of a comonomer of the tetrafluoroethylene (TFE) or trifluoroethylene (TrFE) type into the PVDF chain. It is known that these copolymers crystallize immediately in the polar β -phase even under normal conditions for preparing films from a melt [115].

One way to control the properties of films based on crystallizing polymers is their texturing. Therefore, the influence of such processes on the considered electromechanical properties is discussed below. With regard to this class of polymers, one of the most common methods of texturing is the uniaxial drawing of isotropic films. For PVDF, which is used for the manufacture of energy converters, such a procedure is necessary [111].

Thus, in [122,123], using the example of a number of PVDF films differing both in the synthesis conditions and in the thermal prehistory in the initial (isotropic) state, the influence of the drawing temperature T_d and its multiplicity λ on the piezoactivity.

As can be seen from Figure 16, as the temperature of the uniaxial drawing of PVDF decreases, both the fraction of the polar β -phase $F(\beta)$ and the product $F(\beta)$ by the degree of crystallinity ϕ of the oriented film increase. From Figure 3b it follows that the dependences of the piezoconstant e_{31} are linear functions of the product $\phi F(\beta)$. In [120], it is noted that on uniaxially oriented PVDF films, with an increase in the ferroelectric phase in them, an increase in the values of the polarization P_r was found.

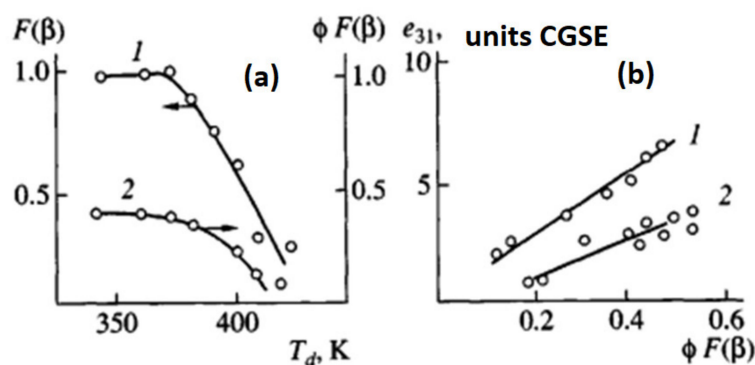


Figure 16. Change in the proportion of the β -phase $F(\beta)$ in its mixture with the α -phase in the PVDF film (1) and the product of the degree of crystallinity ϕ by $F(\beta)$ (2) as a function of T_d with the drawing ratio $\lambda = 4$ (a), as well as the dependence of the piezoconstant e_{31} on $\phi F(\beta)$ after uniaxial drawing of the film (1) and its subsequent isometric annealing (2) (b) [120].

To modify the properties of films of crystallizing polymers, their roller rolling is sometimes used. This method was also applied to PVDF films obtained by conventional uniaxial drawing [124].

In recent decades, there has been a search for various ways to improve the mechanical properties of polymer film materials. In particular, the technique of their formation from the dried gel has been developed. Its orientation can be carried out using solid phase co-extrusion. As applied to the polymers under consideration, this technique was used in [125,126].

The PVDF-based gel was prepared from a solution of PVDF in cyclohexanone prepared at 100 °C by cooling it; the solvent was removed from the gel by extraction with methanol. At an extrusion temperature of 160 °C, it was possible to obtain films with a stretching ratio of 8 [126] and even 10 [125]. Some physical characteristics of the obtained films are presented in Table 2.

Table 2. Characteristics of textured PVDF films obtained by solid-state gel extrusion (a) and uniaxial drawing with isometric annealing of a sample crystallized from the melt (b) [126].

Film	φ , %	f_c	Δn	$l_{100,200}$, nm	l_{001} , nm	L , nm	C_f , GPa	K_t
(a)	55	0.993	0.0346	8.6	6.4	13.2	8.3	0.24
(b)	33	0.986	0.0287	9.0	6.7	10.3	2.0	0.15

Note: $l_{110,200}$ —transverse size of crystallites, l_{001} —longitudinal size of crystallites, L —long period.

Two main differences between the films under consideration follow from it. The film obtained from the gel has a 4 times higher modulus along the stretch axis than the film obtained from the melt. In addition, a film prepared from a gel has a significantly higher coefficient of electromechanical coupling in the transverse direction K_t (K33).

The mechanism of macroscopic piezoactivity in ferroelectric films based on PVDF should take into account the structural and dynamic heterogeneity of crystallizing polymers. The main contribution to the observed piezocontacts for the transverse effect is made by the size effect and electrostriction, for which the regions of the disordered phase are responsible. The noted effects should be interrelated, and the mechanism of their manifestation requires taking into account the occurrence of molecular rearrangements in the mobile phase of the polymer under the action of mechanical or electric fields. Progress in understanding the mechanisms of macroscopic piezoactivity (and, as a consequence, in its regulation) is largely determined by the general state of the problem of the structure of flexible-chain crystallizing polymers in isotropic and textured form. Knowledge of the fine details of the microstructure and dynamics of the regions of the amorphous phase may help in the future to create a rigorous theory of the phenomena under consideration [111].

The paper shows the possibility of obtaining films from modified polyvinylidene fluoride (PVDF-2M) by laser sintering. The effect of laser radiation with a wavelength of 10.6 μm on the polymer structure and the quality of film sintering was studied [127]. Before laser processing, the polymer was pressed on a PgPr manual hydraulic press at a pressure of 50 kgf/cm^2 at room temperature: the dimensions of the pressed layer were 30 \times 60 mm^2 and the thickness was 0.8 mm. The polymer film up to 250 μm thick obtained as a result of laser treatment of the compact surface was mechanically separated from the green part. The authors of [127] found that the phase composition of the films practically does not change compared to the initial material, however, partial crystallization is observed when certain values of the power density and exposure time are reached.

In [128], the authors studied the influence of binder morphology (PVDF) on the cycling of a negative electrode based on a Sn/SnSb composite. It was found that in the case of dissolution of PVDF in a thermodynamically good solvent (NMP), the binder is evenly distributed inside the electrode, forming thin threads with a diameter of ≤ 30 nm between active material particles. At the same time, when a thermodynamically poor solvent (decane) is used, the macromolecules form spherical particles ~ 200 –300 nm in diameter, nonuniformly distributed inside the composite electrode. At the same time, the resistance to cycling was much higher for electrodes of the second type with an uneven distribution of the binder. The authors explained this effect by the unequal binding force and different swelling of PVdF particles of different morphology, as well as differences in the porosity of the electrodes and the probable “buffer” effect of polymer particles. The results obtained in this work clearly show to what extent the behavior of a composite electrode during cycling is determined by its morphology; this is especially important to take into account for lithium alloys, which significantly change their volume during cycling.

The use of PVDF for the manufacture of graphite electrodes creates certain problems [129]. First, it is reported that PVDF covers up to 40–70% of the graphite surface, slowing down the penetration of Li^+ ions into the depth of granules. Secondly, PVDF is predominantly adsorbed on the electrochemically active side faces of graphite particles (through which lithium intercalation/deintercalation occurs) and, due to its high viscosity, can aggregate into clusters, which additionally block the most reactive surface areas and reduce the charge

transfer rate. Thirdly, weak adhesive bonds of PVDF with graphite are destroyed due to the expansion of its particles during lithiation and cannot be completely restored after delithiation due to the low flexibility of the polymer chain; this leads to a breakdown of electrical contacts between particles.

The disadvantages of PVDF, one of the most chemically stable binders, can be largely compensated by introducing the second and third copolymerization components into the macromolecules or by creating a mixture of polymers based on PVDF.

A convenient approach to modifying PVDF is the use of a mixture of polymers, which allows combining the advantages of materials. Recently, polypropylene carbonate (PPC) or a block copolymer of polyethylene and polyethylene oxide (PE-PEO) was added to PVDF. It has been shown that the addition of PPC reduces the degree of crystallinity of PVDF, increasing the interfacial adhesion in the electrode mass based on LiCoO₂. PE-PEO macromolecules act as a surfactant for the conductive additive, which improves the distribution of the latter in the electrode mass. As a result, the specific capacitance and other characteristics of the obtained electrodes are better than when using individual PVDF. However, PPC and PE-PEO additions should not exceed 30 wt%, since this leads to a deterioration in the mechanical properties of the composite electrode.

The above examples show that the modification of polyvinylidene fluoride is a fairly effective way to improve the performance of electrodes. The introduction of functional groups into macromolecules makes it possible to change the nature of the interfacial interaction, varying it from van der Waals forces to hydrogen and even chemical bonding with the surface of the active material. At the same time, the modification does not completely eliminate the above disadvantages inherent in PVDF.

In this regard, a wide range of electrochemically stable non-fluorinated synthetic and natural polymers of various structures has been studied in recent years.

5. Future Prospects and Outlook

As was demonstrated in this review paper, there is a great abundance of possible applications for PVDF and materials on its basis. Taking into account the plethora of PVDF research papers currently available and their ever-increasing number, we believe it is safe to assume that research on these attractive polymers will continue to thrive. Further modifications and combinations of PVDF with other materials to meet certain needs or criteria can be expected as well as more in-depth analysis of their properties.

A significant proportion of the current studies seems to be dedicated to the use of PVDF in lithium-ion batteries (LIB), as a separator [12]. This popularity is understandable considering a number of PVDF properties which make this material extremely suitable for this application: non-reactive nature, thermal stability, good mechanical strength, easy processability. We expect that the emphasis on this direction of development will remain in the nearest future.

In our opinion, another noteworthy potential application of PVDF that was mentioned in this paper is in biomedicine and surgery. For instance, currently there is no ideal material for anterior abdominal wall plastic surgery which makes the search for optimal polymers for surgical reconstruction of the anterior abdominal wall a substantial task. One of the promising materials in this regard is polyvinylidene fluoride (PVDF) which is widely used for the manufacture of suture material [130]. The characteristics reviewed by the authors [59,130–132] showed that PVDF monofilaments, unlike polypropylene ones, do not contain stabilizers and plasticizers, do not undergo hydrolysis under the action of tissue fluids, this explains their greater biocompatibility and resistance to the action of factors of the internal environment of the body during implantation. In terms of textile parameters, endoprostheses made of PVDF are more elastic than those made of polypropylene. According to the biological inertness of PVDF, mesh endoprostheses are close to porous film endoprostheses made of polytetrafluoroethylene, but they are significantly superior in resistance to infection and reliability of integration in tissues. To further reduce the tissue reaction to the endoprosthesis, a coating of linear-chain carbon-

carbine (PVDF-K) was applied. In the process of forming a carbine coating on a PVDF endoprosthesis, there is a slight decrease in the strength characteristics of the material, but its elasticity practically does not change. The endoprosthesis PVDF has physical and chemical properties that ensure reliable prosthetics of abdominal wall tissues and is distinguished by good biological compatibility with human tissues. PVDF mesh implants are a promising alternative to the most common polypropylene endoprostheses in modern herniology [59,130–132]. In this regard, the investigation and improvement of PVDF to meet the needs of biomedical and surgical applications is a sensible direction for the future research.

6. Conclusions

This review was dedicated to PVDF applications, their trademarks, current position on the market of functional materials as well as to the study of the unique properties and processability. The list of properties that were discussed include (but not limited to): non-toxicity, fire-resistance, easy processing, heat resistance, resistance to aging, chemical resistance, low surface roughness, etc. These attractive characteristics naturally lead to a great variety of possible applications, such as: chemical, nuclear power engineering, aviation and aerospace, electronics and radio engineering, in architecture and automotive industries, in biomedical and pharmaceutical industries.

Among the most important aspects of the experimental section are: formation of the piezoelectric β -phase and radiation carbonization. β -phase of PVDF is of particular interest as it facilitates conversion of mechanical movements into electrical responses and vice versa. Radiation carbonization method is really important as it provides a tool to remove hydrogen fluoride (HF) in order to increase the chain length or alter the end properties.

We conclude this review by saying that, hopefully, the information provided in this review article is evidence enough to the great prospects of PVDF materials (as well as its copolymers and materials on its basis), and to the importance of continuation of research in this area. As was demonstrated, a great number of industries stand to benefit from the development and improvement of this material. A large amount of fundamental and applied research on the subject is a testament to that. Review papers, on the other hand, are also important as they systematize the information and facilitate consumption.

Author Contributions: Conceptualization, R.D. and D.S.; methodology, R.D.; software, S.R.; validation, R.D., T.P. and F.O.; formal analysis, T.T.; investigation, R.D.; resources, T.T.; data curation, T.P.; writing—original draft preparation, R.D.; writing—review and editing, D.S.; visualization, T.P., F.O. and S.R.; supervision, R.D.; project administration, D.S.; funding acquisition, T.T. All authors have read and agreed to the published version of the manuscript.

Funding: Research described in the paper was financially supported by the Internal Grant Agency of Brno University of Technology, grant No. FEKT-S-20-6352. This study was supported by Russian Science Foundation (Grant #22-73-10091). Part of the work was carried out with the support of CEITEC Nano Research Infrastructure supported by MEYS CR (LM2018110).

Institutional Review Board Statement: Not applicable.

Informed Consent Statement: Not applicable.

Data Availability Statement: The data presented in this study are available on request from the corresponding author.

Conflicts of Interest: The authors declare no conflict of interest.

Abbreviations

The paper contains the following abbreviations:

PVDF	Polyvinylidene fluoride
LIB	lithium-ion batteries
NASA	the national aeronautics and space administration
PVF	polyvinyl fluoride

PTFE	Polytetrafluoroethylene
IR	infra-red
HMS	high melt strength
HP	high purity
TPP	thermophysical properties
PC	polymer composite
UV	ultraviolet
HPLC	high performance liquid chromatography
FDA	Food and Drug Administration
HCP	halogen-containing polymers
EPR	electron paramagnetic resonance
TFE	tetrafluoroethylene
TrFE	trifluoroethylene
NPM	N-Methyl-2-pyrrolidone
PPC	polypropylene carbonate
PE-PEO	polyethylene and polyethylene oxide

References

1. Morilova, V.M. Study of the Carbonization of Polyvinylidene Fluoride by Emission and Absorption Spectroscopy. Master's Thesis, Chelyabinsk State University, Chelyabinsk, Russia, 2014.
2. Baskin, Z.L.; Shabalin, D.A.; Vyrzheikin, E.S.; Dedov, S.A. Range, properties and application of fluoropolymers of the Kirovo-Chepetsk Chemical Plant. *Russ. Chem. J.* **2008**, *3*, 13–23.
3. Voinkova, I.V.; Ginchitskii, N.N.; Gribov, I.V.; Klebanov, I.I.; Kuznetsov, V.L.; Moskvina, N.A.; Pesin, L.A.; Evsyukov, S.E. A Model of Radiation-Induced Degradation of the Poly(Vinylidene Fluoride) Surface During XPS Measurements. *Polym. Degrad. Stab.* **2005**, *89*, 471–477.
4. Joh, H.-I.; Ha, H.Y. Properties and Formation Mechanisms of Branched Carbon Nanotubes from Polyvinylidene Fluoride Fibers. *Carbon* **2013**, *63*, 567–571. [[CrossRef](#)]
5. Voinkova, I.V.; Pesin, L.A.; Volegov, A.A.; Evsyukov, S.E.; Gribov, I.V.; Kuznetsov, V.L.; Moskvina, N.A. Depth distribution of the fluorine concentration during radiative carbonization of PVDF. *J. Surf. Investig.* **2007**, *1*, 450–453. [[CrossRef](#)]
6. Heimann, R.B.; Evsyukov, S.E.; Kavan, L. (Eds.) *Carbyne and Carbynoid Structures Dordrecht*; Kluwer Academic Publishers: Amsterdam, The Netherlands, 1999; 446p.
7. Calcagno, L.; Musumeci, P.; Percolla, R.; Foti, G. Calorimetric measurements of MeV ion irradiated polyvinylidene fluoride. *Nucl. Inst. Methods Phys. Res. B* **1994**, *91*, 461–464. [[CrossRef](#)]
8. Oshima, A.; Ikeda, S.; Seguchi, T.; Tabata, Y. Temperature effect on radiation induced reactions in ethylene and tetrafluoroethylene copolymer (ETFE). *Radiat. Phys. Chem.* **1997**, *50*, 519–522. [[CrossRef](#)]
9. Zhudi, Z.; Jin, C.; Xinfang, C. Crystallite damage studies on irradiated poly(vinylidene fluoride). *Radiat. Phys. Chem.* **1994**, *43*, 523–526. [[CrossRef](#)]
10. Knápek, A.; Dallaev, R.; Burda, D.; Sobola, D.; Allaham, M.M.; Horáček, M.; Kaspar, P.; Matějka, M.; Mousa, M.S. Field Emission Properties of Polymer Graphite Tips Prepared by Membrane Electrochemical Etching. *Nanomaterials* **2020**, *10*, 1294. [[CrossRef](#)]
11. Wu, Y.; Li, Y.; Wang, Y.; Liu, Q.; Chen, Q.; Chen, M. Advances and prospects of PVDF based polymer electrolytes. *J. Energy Chem.* **2022**, *64*, 62–84. [[CrossRef](#)]
12. Bicy, K.; Gueye, A.B.; Rouxel, D.; Kalarikkal, N.; Thomas, S. Lithium-ion battery separators based on electrospun PVDF: A review. In *Surfaces and Interfaces*; Elsevier B.V.: Amsterdam, The Netherlands, 2022; Volume 31. [[CrossRef](#)]
13. Pusty, M.; Shirage, P.M. Insights and perspectives on graphene-PVDF based nanocomposite materials for harvesting mechanical energy. *J. Alloys Compd.* **2022**, *904*, 164060. [[CrossRef](#)]
14. Sahrash, R.; Siddiqa, A.; Razzaq, H.; Iqbal, T.; Qaisar, S. PVDF based ionogels: Applications towards electrochemical devices and membrane separation processes. *Heliyon* **2018**, *4*, e00847. [[CrossRef](#)] [[PubMed](#)]
15. Ji, J.; Liu, F.; Hashim, N.A.; Abed, M.M.; Li, K. Poly(vinylidene fluoride) (PVDF) membranes for fluid separation. *React. Funct. Polym.* **2015**, *86*, 134–153. [[CrossRef](#)]
16. Lu, L.; Ding, W.; Liu, J.; Yang, B. Flexible PVDF based piezoelectric nanogenerators. *Nano Energy* **2020**, *78*, 105251. [[CrossRef](#)]
17. Liu, F.; Hashim, N.A.; Liu, Y.; Abed, M.M.; Li, K. Progress in the production and modification of PVDF membranes. *J. Membr. Sci.* **2011**, *375*, 1–27. [[CrossRef](#)]
18. Papež, N.; Pisarenko, T.; Ščasnovič, E.; Sobola, D.; Tălu, Ș.; Dallaev, R.; Částková, K.; Sedlák, P. A Brief Introduction and Current State of Polyvinylidene Fluoride as an Energy Harvester. *Coatings* **2022**, *12*, 1429. [[CrossRef](#)]
19. Rajeevan, S.; John, S.; George, S.C. Polyvinylidene fluoride: A multifunctional polymer in supercapacitor applications. *J. Power Sources* **2021**, *504*, 230037. [[CrossRef](#)]
20. Zou, D.; Lee, Y.M. Design strategy of poly(vinylidene fluoride) membranes for water treatment. *Prog. Polym. Sci.* **2022**, *128*, 101535. [[CrossRef](#)]
21. Kuznetsov, E.V. *Workshop on Chemistry and Physics of Polymers*; Technosphere: Moscow, Russia, 1977; 256p.

22. Chen, H.; Ling, M.; Hencz, L.; Ling, H.Y.; Li, G.; Lin, Z.; Liu, G.; Zhang, S. Exploring Chemical, Mechanical, and Electrical Functionalities of Binders for Advanced Energy-Storage Devices. *Chem. Rev.* **2018**, *118*, 8936–8982. [[CrossRef](#)]
23. Lestriez, B. Functions of Polymers in Composite Electrodes of Lithium Ion Batteries. *Comptes Rendus Chim.* **2010**, *13*, 1341–1350.
24. Chou, S.L.; Pan, Y.; Wang, J.Z.; Liu, H.K.; Dou, S.X. Small Things Make a Big Difference: Binder Effects on the Performance of Li and Na Batteries. *Phys. Chem. Chem. Phys.* **2014**, *16*, 20347–20359. [[CrossRef](#)]
25. Nagai, A. Applications of PvdFRelated Materials for LithiumIon Batteries. In *Lithium-Ion Batteries: Science and Technologies*; Yoshio, M., Brodd, R.J., Kozawa, A., Eds.; Springer: New York, NY, USA, 2009; pp. 155–162.
26. Morilova, V.M.; Koryakova, O.V.; Evsyukov, S.E.; Pesin, L.A. Influence of Uniaxial Stretching of Polyvinylidene Fluoride Films on the Shape and Position of CH Peaks in IR Spectra. Herald of ChelGU. 2011. Available online: <https://cyberleninka.ru/article/n/vliyanie-odnoosnogo-rastyazheniya-plyonok-polivinilidenftorida-na-formu-i-polozhenie-sn-pikov-v-ik-spektrah> (accessed on 7 November 2022).
27. Tansel, T. Effect of electric field assisted crystallisation of PVDF-TrFE and their functional properties. *Sens. Actuators A Phys.* **2021**, *332*, 113059. [[CrossRef](#)]
28. Rakhmankulov, A.A.; Davlatov, F.F. Research on the effect of dispersed graphite grade GMZ on the thermophysical properties and structure of polyvinylidene fluoride. *Int. Sci. Tech. J.* **2019**, *87*, 11–15.
29. Kawai, H. The Piezoelectricity of Poly(Vinylidene Fluoride). *Jpn. J. Appl. Phys.* **1969**, *8*, 975–976. [[CrossRef](#)]
30. Chu, C.C. *Biotextiles as Medical Implants*; Chapter 11: Materials for Absorbable and Nonabsorbable Surgical Sutures; Woodhead Publishing Series in Textiles; Woodhead Publishing: Cambridge, UK, 2013; pp. 275–334.
31. Seiler, K.; Simon, W. Principles and mechanisms of ion-selective optodes. *Sens. Actuators B Chem.* **1992**, *6*, 295–298. [[CrossRef](#)]
32. Tang, T.K.; Liu, S.S. *Principles and Materials for Manufacturing Electrochemical Sensors in Chemical Sensor Technology*; Kodansha Ltd.: Tokyo, Japan, 1991; Volume 3.
33. Zhivulin, V.E. Synthesis and properties of paramagnetic layers on the surface of polyvinylidene fluoride. Master’s Thesis, South Ural State Humanitarian Pedagogical University, Chelyabinsk, Russia, 2016; pp. 1–127.
34. Rakhmankulov, A.A.; Khaidarov, T.Z. Peculiarities of thermal motion in polyvinylidene fluoride. *Sci. Educ. Cult.* **2020**, *10*, 4–6.
35. Rakhmankulov, A.A. Influence of dispersed fillers on the structure and thermal conductivity of unmodified and modified polyvinylidene fluoride. Master’s Thesis, Kyiv, Ukraine, 1986; pp. 1–205.
36. Kakutani, M. Dielectric Absorption of Oriented Polivinildenftuoride. *J. Polym. Sci. Part A-2 Polym. Phys.* **1970**, *8*, 1177–1183. [[CrossRef](#)]
37. Harris, G.R.; Preston, R.C.; DeReggi, A.S. Impact of piezoelectric PVDF on measurements, standards and regulations for medical ultrasound exposure. *IEEE Trans. Ultrason. Ferroelectr. Freq. Control.* **2000**, *47*, 1321–1335. [[CrossRef](#)]
38. Lovlnger, A.J. Crystallization of the P Base of Polivinilidenftuoride from the Melt. *Polymer* **1981**, *22*, 412–413. [[CrossRef](#)]
39. Kaspar, P.; Sobola, D.; Částková, K.; Dallaev, R.; Šťastná, E.; Sedlák, P.; Knápek, A.; Trčka, T.; Holcman, V. Case study of polyvinylidene fluoride doping by carbon nanotubes. *Materials* **2021**, *14*, 1428. [[CrossRef](#)]
40. Kaspar, P.; Sobola, D.; Částková, K.; Knápek, A.; Burda, D.; Orudzhev, F.; Dallaev, R.; Tofel, P.; Trčka, T.; Grmela, L.; et al. Characterization of polyvinylidene fluoride (PvdF) electrospun fibers doped by carbon flakes. *Polymers* **2020**, *12*, 2766. [[CrossRef](#)]
41. Sobola, D.; Kaspar, P.; Částková, K.; Dallaev, R.; Papež, N.; Sedlák, P.; Trčka, T.; Orudzhev, F.; Kaštyl, J.; Weiser, A.; et al. PVDF fibers modification by nitrate salts doping. *Polymers* **2021**, *13*, 2439. [[CrossRef](#)] [[PubMed](#)]
42. Sedlak, P.; Sobola, D.; Gajdos, A.; Dallaev, R.; Nebojsa, A.; Kubersky, P. Surface analyses of PVDF/NMP/[EMIM][TFSI] solid polymer electrolyte. *Polymers* **2021**, *13*, 2678. [[CrossRef](#)] [[PubMed](#)]
43. Smejkalová, T.; Třálu, Š.; Dallaev, R.; Částková, K.; Sobola, D.; Nazarov, A. SEM imaging and XPS characterization of doped PVDF fibers. *E3S Web Conf.* **2021**, *270*, 01011. [[CrossRef](#)]
44. Kerbow, D.L. *Modern Fluoropolymers*; Scheirs, J., Ed.; John Wiley & Sons: Chichester, UK, 1997; p. 301.
45. Cheng, Y.; Li, D. Numerical analysis of piezoelectric signal of PVDF membrane flapping wing in flight. *IOP Conf. Ser. Mater. Sci. Eng.* **2020**, *774*, 012090. [[CrossRef](#)]
46. Holmes-Siedle, A.G.; Wilson, P.D.; Verrall, A.P. PVdF: An electronically-active polymer for industry. *Mater. Des.* **1983**, *4*, 910–918. [[CrossRef](#)]
47. Liu, R.; Yuan, B.; Zhong, S.; Liu, J.; Dong, L.; Ji, Y.; Dong, Y.; Yang, C.; He, W. Poly(vinylidene fluoride) separators for next-generation lithium based batteries. *Nano Select* **2021**, *2*, 2308–2345. [[CrossRef](#)]
48. Shabanov, V.A.; Konnov, E.I. Sensing elements based on PVDF films for creating hydroacoustic transducers. In Proceedings of the 2nd Youth Scientific Conference “Actual problems of piezoelectric instrument making”, Rostov-on-Don, Russia, 6–10 September 2015; pp. 49–58.
49. Liu, T.; Zhou, X.; Sun, Y.; Bai, R. Anticorrosion performance of pvdF membranes modified by blending ptfE nanoemulsion and prepared through usual non-solvent-induced phase inversion method. *Membranes* **2021**, *11*, 420. [[CrossRef](#)]
50. Ghazali, N.; Basirun, W.J.; Nor, A.M.; Johan, M.R. Super-amphiphobic coating system incorporating functionalized nano-Al₂O₃ in polyvinylidene fluoride (PVDF) with enhanced corrosion resistance. *Coatings* **2020**, *10*, 387. [[CrossRef](#)]
51. Hussein, A.A.; Dawood, N.M.; Al-Kawaz, A.E. Corrosion protection of 316L stainless steel by (PVDF/HA) composite coating using a spinning coating technique. *Bull. Pol. Acad. Sci. Tech. Sci.* **2021**, *69*, e136810. [[CrossRef](#)]
52. Chakradhar, R.P.; Prasad, G.; Bera, P.; Anandan, C. Stable superhydrophobic coatings using PVDF-MWCNT nanocomposite. *Appl. Surf. Sci.* **2014**, *301*, 208–215. [[CrossRef](#)]

53. Burkhart, M.; Wermelinger, J.; Setz, W.; Müller, D. Suitability of polyvinylidene fluoride (PVDF) piping in pharmaceutical ultrapure water applications. *PDA J. Pharm. Sci. Technol.* **1996**, *50*, 246–251. [[PubMed](#)]
54. Yessari, M.; Fangachi, N.; Rguiti, M.; Hajjaji, A. Design and numerical simulation of a piezoelectric harvester using PVDF polymer for keyboard application. *Mater. Today Proc.* **2022**, *66*, 365–372. [[CrossRef](#)]
55. Klinge, U.; Klosterhalfen, B.; Birkenhauer, V.; Junge, K.; Conze, J.; Schumpelick, V. Impact of polymer pore size on the interface scar formation in a rat model. *J. Surg. Res.* **2002**, *103*, 208–214. [[CrossRef](#)] [[PubMed](#)]
56. Klosterhalfen, B.; Klinge, U.; Schumpelick, V. Functional and morphological evaluation of different polypropylene-mesh modifications for abdominal wall repair. *Biomaterials* **1998**, *19*, 2235–2246. [[CrossRef](#)]
57. Klinge, U.; Klosterhalfen, B.; Müller, M.; Öttinger, A.P.; Schumpelick, V. Shrinking of polypropylene mesh in vivo: An experimental study in dogs. *Eur. J. Surg.* **1998**, *164*, 965–969. [[CrossRef](#)]
58. Sukovatykh, B.S.; Netyaga, A.A.; Zhukovsky, V.A.; Valuyskaya, N.M.; Korovicheva, S.Y. The up to date polymer materials in plastic surgery of postoperative and recurrent ventral hernias. Modern methods of surgical treatment of ventral abdominal hernias and eventrations. Kursk scientific and practical bulletin “Man and his health”, 2006, No.1. Available online: <https://cyberleninka.ru/article/n/setchatye-implantaty-iz-polivinilidentforida-v-lechenii-gryzh-bryushnoy-stenki/viewer> (accessed on 7 November 2022).
59. Sedov, V.M.; Tarbaev, S.D.; Rostovskoy, A.A.; Gorelov, A.A. Surgical treatment of postoperative ventral hernias using polypropylene and PVDF mesh implants. In Proceedings of the 5th International Conference Modern Approaches to the Development and Clinical Use of Effective Dressings, Suture Materials and Polymeric Implants, Moscow, Russia, 24–25 January 2006; pp. 200–208.
60. Jansen, P.L.; Klinge, U.; Anurov, M.; Titkova, S.; Mertens, P.R.; Jansen, M. Surgical mesh as a scaffold for tissue regeneration in the esophagus. *Eur. Surg. Res.* **2004**, *36*, 104–111.
61. Junge, K.; Rosch, R.; Klinge, U.; Krones, C.; Klosterhalfen, B.; Mertens, P.R.; Lynen, P.; Kunz, D.; Preiß, A.; Peltroche-Llacsahuanga, H.; et al. Gentamicin supplementation of polyvinylidene fluoride mesh materials for infection prophylaxis. *Biomaterials* **2005**, *26*, 787–793. [[CrossRef](#)]
62. Klinge, U.; Klosterhalfen, B.; Öttinger, A.P.; Junge, K.; Schumpelick, V. PVDF as a new polymer for the construction of surgical meshes. *Biomaterials* **2002**, *23*, 3487. [[CrossRef](#)]
63. Lazarenko, V.A. The choice of suture material for vascular plasty. *Int. Congr. Surg. Petrozavodsk* **2002**, *1*, 369–370.
64. Bezhin, A.I.; Dolzhikov, A.A.; Zhukovsky, V.A.; Netyaga, A.A.; Plotnikov, R.V. Experimental substantiation of the use of new polyvinylidene fluoride endoprotheses with carbine coating for hernioplasty. *Bull. New Med. Technol.* **2007**, *1*, 99.
65. Lee, M.; Catsouras, I.; Asadi, K.; Blom, P.W.M.; de Leeuw, D.D. Low voltage extrinsic switching of ferroelectric δ -PVDF ultra-thin films. *Phys. Lett.* **2013**, *103*, 072903.
66. Ma, H.; Jen, A.Y.; Dalton, L.R. Polymer-based optical waveguides: Materials, processing, and devices. *Adv. Mater.* **2002**, *14*, 1339–1365.
67. Iwamoto, N.; Johnston, R.W.; Yokoi, K.; Nakano, K.; Fujita, K.; Misaki, S.; Sugimoto, M.; Johnston, R.W.; Kanazawa, K.; Misaki, Y. Respiration and Heartbeat Signal Measurement with A Highly Sensitive PVDF Piezoelectric Film Sensor. In Proceedings of the Second International Conference on Electronics and Software Science (ICESS2016), Takamatsu, Japan, 14–16 November 2016.
68. Hu, X.; You, M.; Yi, N.; Zhang, X.; Xiang, Y. Enhanced Piezoelectric Coefficient of PVDF-TrFE Films via In Situ Polarization. *Front. Energy Res.* **2021**, *9*, 621540. [[CrossRef](#)]
69. Kalimuldina, G.; Turdakyn, N.; Abay, I.; Medeubayev, A.; Nurpeissova, A.; Adair, D.; Bakenov, Z. A Review of Piezoelectric PVDF Film by Electrospinning and Its Applications. *Sensors* **2020**, *20*, 5214. [[CrossRef](#)] [[PubMed](#)]
70. Chen, W.W.; An, Z.L.; He, L.B.; Deng, Z. Piezoelectric coefficients measurement for PVDF films with pneumatic pressure rig in a sole cavity. In Proceedings of the 2015 Symposium on Piezoelectricity, Acoustic Waves and Device Applications, SPAWDA, Jinan, China, 30 October–2 November 2015; pp. 111–114. [[CrossRef](#)]
71. Xu, F.; Chu, F.; Trolier-McKinstry, S. Longitudinal piezoelectric coefficient measurement for bulk ceramics and thin films using pneumatic pressure rig. *J. Appl. Phys.* **1999**, *86*, 588–594.
72. Kholkin, A.L.; Wüthrich, C.; Taylor, D.V.; Setter, N. Interferometric measurements of electric field-induced displacements in piezoelectric thin films. *Rev. Sci. Instrum.* **1996**, *67*, 1935–1941. [[CrossRef](#)]
73. Lu, K.; Huang, W.; Guo, J.; Gong, T.; Wei, X.; Lu, B.-W.; Liu, S.-Y.; Yu, B. Supersensitive strain gauge based on flexible poly(vinylidene fluoride) piezoelectric film. *Nanoscale Resolut.* **2018**, *13*, 83. [[CrossRef](#)]
74. Furlan, A.D.; Brosso, L.; Imamura, M.; Irvin, E. Massage for low back pain: A systematic review within the Cochrane Collaboration Back Review Group. *Spine* **2002**, *27*, 1896–1910. [[CrossRef](#)]
75. Shirafuji, S.; Hosoda, K. Slip detection and prevention using sensors with different properties embedded in elastic artificial leather based on previous experience. In Proceedings of the International Conference on Advanced Robotics, New Taipei, Taiwan, 6–8 June 2014.
76. Liao, H.; Ava, L.; Nicola, R. The Evidence for Shiatsu: A Systematic Review of Shiatsu and Acupressure. *BMC Complementary Altern. Med.* **2011**, *11*, 88.
77. Dmitriev, I.Y. Electroactive polymer systems based on porous films of polyvinylidene fluoride: Dissertation of a candidate of physical and mathematical sciences. Master’s Thesis, Ioffe Institute, St. Petersburg, Russia, 2007; pp. 1–154.
78. Korobova, Y.G.; Babaev, V.G.; Khvostov, V.V.; Guseva, M.B. Emission characteristics of fibers based on linear chain carbon. *Vestn. Mosc. Univ. Ser. 3 Phys. Astron.* **2008**, *1*, 33–39.

79. Mavrinskaya, N.A.; Pesin, L.A.; Baumgarten, M.; Mavrinskiy, A.V.; Baitinger, E.M.; Evsyukov, S.E. ESR studies of chemically dehydrofluorinated poly(vinylidene fluoride). *Magn. Reson. Solids. E J* **2008**, *10*, 31–38.
80. Evsyukov, S.E.; Kudryavtsev, Y.P.; Korshak, Y.V. Chemical dehydrohalogenation of halogenated polymers. *Russ. Chem. Rev.* **1991**, *60*, 373–390. [[CrossRef](#)]
81. Kudryavtsev, Y.P.; Evsyukov, S.E.; Guseva, M.B. Karbin—The Third Allotropic Form of Carbon. *Nanotechnologies: Dev. Appl. XXI Century* **2010**, *1*, 37–52.
82. Sencadas, V.; Moreira, V.M.; Lanceros-Mendéz, S.; Pouzada, A.S.; Gregório, R., Jr. α - to $-\beta$ Transformation On PvdF Films Obtained By Uniaxial Stretch. *Mater. Sci. Forum* **2006**, *514/516*, 872–876. [[CrossRef](#)]
83. Makarevich, N.I.; Sushko, N.I. IR spectra and crystalline modifications of IR-polyvinylidene fluoride. *Zh. Butt. Spectrosc.* **1965**, *11*, 917–920.
84. Semochkin, P.S.; Andreychuk, V.P.; Pesin, L.A.; Evsyukov, S.E.; Koryakova, O.V.; Belenkov, E.A.; Shakhova, I.V. Effect of Uniaxial Tension on Phase Transformations of Polyvinylidene Fluoride Films. *Bull. South Ural. State University. Ser. Mathematics. Mechanics. Phys.* **2009**, *12/10*, 80–84.
85. Vointseva, I.I.; Gil'man, L.M.; Kudryavtsev, Y.P.; Evsyukov, S.E.; Pesin, L.A.; Gribov, I.V.; Moskvina, N.A.; Khvostov, V.V. Chemical Dehydrochlorination of Polytrichlorobutadienes. A New Route to Carbines. *Europ. Polym. J.* **1996**, *32*, 61–68.
86. Kochervinsky, V.V. Structure and properties of block polyvinylidene fluoride and systems based on it. *Adv. Chem.* **1996**, *65*, 936–987.
87. Duca, M.D.; PLoSceanu, C.L.; Pop, T. Effect of X-rays on Poly (Vinylidene Fluoride) in X-ray Photoelectron Spectroscopy. *J. Appl. Polym. Sci.* **1998**, *67*, 2125–2129.
88. Pesin, L.A.; Gribov, I.V.; Kuznetsov, V.L.; Evsyukov, S.E.; Moskvina, N.A.; Margamov, I.G. In Situ Observation of the Modification of Carbon Hybridization in Poly (Vinylidene Fluoride) during Xps/Xaes Measurements. *Chem. Phys. Lett.* **2003**, *372*, 825–830. [[CrossRef](#)]
89. Brzhezinskaya, M.M.; Morilova, V.M.; Baitinger, E.M.; Evsyukov, S.E.; Pesin, L.A. Study of Poly (Vinylidene Fluoride) Radiative Modification Using Core Level Spectroscopy. *Polym. Degrad. Stab.* **2014**, *99*, 176–179. [[CrossRef](#)]
90. Sidelnikova, A.L.; Andreichuk, V.P.; Pesin, L.A.; Evsyukov, S.E.; Gribov, I.V.; Moskvina, N.A.; Kuznetsov, V.L. Kinetics of Radiation-Induced Degradation of Cf2- And Cf-Groups in Poly (Vinylidene Fluoride): Model Refinement. *Polym. Degrad. Stab.* **2014**, *110*, 308–311. [[CrossRef](#)]
91. le Moël, A.; Duraud, J.P.; Balanzat, E. Modifications of Polyvinylidene Fluoride (PvdF) Under High Energy Heavy Ion, X-ray and Electron Irradiation Studied by X-ray Photoelectron Spectroscopy. *Nucl. Instrum. Methods Phys. Res. B* **1986**, *18*, 59–63. [[CrossRef](#)]
92. Le Moël, A.; Duraud, J.P.; Lemaire, I.; Balanzat, E. 1.; Ramillon, J.M.; Darnez, C. Electronic and Structural Modifications of Polyvinylidene Fluoride under High Energy Oxygen Ion Irradiation. *Nucl. Instrum. Methods Phys. Res. B* **1987**, *19/20*, 891–894.
93. le Moël, A.; Duraud, J.P.; Lecomte, C.; Valin, M.T.; Henriot, M.; le Gressus, C.; Darnez, C.; Balanzat, E.; Demanet, C.M. Modifications Induced in Polyvinylidene Fluoride by Energetic Ions. *Nucl. Instrum. Methods Phys. Res. B* **1988**, *32*, 115–119.
94. Adem, E.H.; Bean, S.J.; Demanet, C.M.; le Moel, A.; Duraud, J.P. Xps As A Tool For The Investigation of Polymers Irradiated By Energetic Ions. *Nucl. Instrum. Methods Phys. Res. B* **1988**, *32*, 182–185. [[CrossRef](#)]
95. Pesin, L.A.; Morilova, V.M.; Zherebtsov, D.A.; Evsyukov, S.E. Kinetics of PvdF Film Degradation under Electron Bombardment. *Polym. Degrad. Stab.* **2013**, *98*, 666–670. [[CrossRef](#)]
96. Zhang, S.; Shen, J.; Qiu, X.; Wend, D.; Zhu, W. ESR and Vibrational Spectroscopy Study on Poly (Vinylidene Fluoride) Membranes with Alkaline Treatment. *J. Power Sources* **2006**, *153*, 234–238. [[CrossRef](#)]
97. Volegov, A.A.; Pesin, L.A.; Margamov, I.G.; Evsyukov, S.E.; Koryakova, O.V.; Kochedykov, V.A. Evaluation of the depth and rate of penetration of a dehydrofluorinating mixture into polyvinylidene fluoride using IR spectroscopy. *Proc. Chelyabinsk Sci. Cent.* **2006**, *4*, 26–31.
98. Ross, G.J.; Watts, J.F.; Hill, M.P.; Morrissey, P. Surface Modification of Poly (Vinylidene Fluoride) by Alkaline Treatment 1. the Degradation Mechanism. *Polymer* **2000**, *41*, 1685–1696.
99. Ross, G.J.; Watts, J.F.; Hill, M.P.; Morrissey, P. Surface Modification of Poly (Vinylidene Fluoride) by Alkaline Treatment. Part 2. Process Modification by the Use of Phase Transfer Catalysts. *Polymer* **2001**, *42*, 403–413. [[CrossRef](#)]
100. Zhivulin, V.E.; Zherebtsov, D.A.; Pesin, L.A. Molecular structure of chemically carbonized films of polyvinylidene fluoride (according to IR spectroscopy). *Bull. Tomsk. Polytech. Univ. Eng. Georesources* **2018**, *329*, 80–87.
101. Zhivulin, V.E.; Pesin, L.A.; Morilova, V.M.; Koryakova, O.V. Influence of heat treatment on the magnetic activity of the products of chemical carbonization of polyvinylidene fluoride. *Bull. Juurgu Ser. Math. Mech. Phys.* **2014**, *6*, 56–62.
102. Zhivulin, V.E.; Pesin, L.A.; Mezhenina, O.A.; Kovalev, I.N.; Zlobina, N.A.; Gavrilov, M.A.; Morilova, V.M.; Koryakova, O.V. Influence of the duration of isothermal holding on the magnetic and structural properties of the products of chemical carbonization of polyvinylidene fluoride. *Proc. Tomsk. Polytech. Univ. Math. Mech. Phys.* **2014**, *325*, 149–157.
103. Zhivulin, V.E.; Pesin, L.A.; Ivanov, D.V. Peculiarities of temperature dependence of EPR absorption of chemically carbonized derivatives of polyvinylidene fluoride. *Solid State Phys.* **2016**, *58*, 87–91. [[CrossRef](#)]
104. Mavrinskaya, N.A.; Pesin, L.A.; Baumgarten, M.; Baitinger, E.M.; Mavrinsky, A.V.; Evsyukov, S.E. Optical properties and EPR absorption of chemically dehydrofluorinated polyvinylidene fluoride. *123 Bull. Juurgu Ser. Math. Phys. Chem.* **2008**, *7*, 80–88.

105. Mavrinskaya, N.A.; Mavrinsky, A.V.; Baumgarten, M.; Baitinger, E.M.; Evsyukov, S.E.; Pesin, L.A. Influence of conditions and duration of storage on the intensity of the EPR signal of chemically dehydrofluorinated derivatives of polyvinylidene fluoride. *Bull. Juurgu Ser. Math. Phys. Chem.* **2008**, *22*, 89–91.
106. Kudryavtsev, Y.P.; Evsyukov, S.E.; Babaev, V.G. Effective dehydrofluorinating system for polyvinylidene fluoride. *Proc. Acad. Sci. Chem. Ser.* **1992**, *5*, 1223–1225.
107. Gordon, A.; Ford, R. *A Companion to Chemistry*; Mir: Moscow, Russia, 1976; 134p.
108. Korshak, V.V.; Kudryavtsev, Y.P.; Korshak, Y.V.; Evsyukov, S.E.; Litovchenko, G.D. Dehydrofluorination of polyvinylidene fluoride in the presence of tetrahydrofuran. *Rep. Acad. Sci. USSR* **1987**, *294*, 127–130.
109. Pesin, L.A.; Chebotarev, S.S.; Kuvshinov, A.M.; Bespal, I.I.; Gribov, I.V.; Moskvina, N.A.; Kuznetsov, V.L.; Evsyukov, S.E.; Vyazovtsev, A.V.; Kravets, N.S. Peculiarities of electron emission spectra of products of radiation carbonization of polyvinylidene fluoride. *Surf. X-Ray Synchrotron Neutron Res.* **2010**, *3*, 37–44.
110. Voinkova, L.A.; Pesin, A.A.; Volegov, A.A.; Evsyukov, S. Depth distribution of fluorine concentration during radiation carbonization of PVDF. *Surf. X-Ray Synchrotron Neutron Stud.* **2007**, *8*, 1–5.
111. Kochervinsky, V.V. Structural aspects of piezoelectricity in crystallizing ferroelectric polymers on the example of homopolymer and copolymers of vinylidene fluoride. *VMS Ser. B* **2003**, *11*, 1922–1964.
112. Kochervinskii, V.V. Ferroelectricity of polymers based on vinylidene fluoride. *Russ. Chem. Rev.* **1999**, *68*, 821–857. [[CrossRef](#)]
113. Kochervinskii, V.V. The properties and applications of fluorine-containing polymer films with piezo- and pyro-activity. *Russ. Chem. Rev.* **1994**, *63*, 367–371. [[CrossRef](#)]
114. Wang, T.T.; Herbert, J.M. (Eds.) *The Application of Ferroelectric Polymers*; Blackie: Glasgow, UK; London, UK; Chapman and Hall: New York, NY, USA, 1988.
115. Kochervinskii, V.V. The structure and properties of block poly(vinylidene fluoride) and systems based on it. *Russ. Chem. Rev.* **1996**, *65*, 865–913. [[CrossRef](#)]
116. Kochervinsky, V.V. Piezoelectricity in crystallizing ferroelectric polymers by the example of polyvinylidene fluoride and its copolymers. *Crystallography* **2003**, *48*, 699–726.
117. Ohigashi, H. Electromechanical properties of polarized polyvinylidene fluoride films as studied by the piezoelectric resonance method. *J. Appl. Phys.* **1976**, *47*, 949–955. [[CrossRef](#)]
118. Sussner, H. Physical interpretation of the anisotropy and temperature dependence of the piezoelectric constant of polyvinylidene fluoride. *Phys. Lett. A* **1976**, *58*, 426. [[CrossRef](#)]
119. Furukawa, T.; Aiba, J.; Fukada, E. Piezoelectric relaxation in polyvinylidene fluoride. *J. Appl. Phys.* **1979**, *50*, 3615–3621. [[CrossRef](#)]
120. Kochervinsky, V.V.; Sokolov, V.G.; Zubkov, V.M. Influence of the molecular structure on the characteristics of the electrical hysteresis of polyvinylidene fluoride and its copolymers. *High Mol. Weight. Compd. A* **1991**, 530–537. Available online: <https://cyberleninka.ru/article/n/vliyanie-molekulyarnoy-struktury-na-harakteristiki-elektricheskogo-gistereziya-polivinilidenftorida-i-ego-sopolimerov> (accessed on 7 November 2022).
121. Scheinbeim, J.J.; Chung, K.T.; Rae, C.D.; Newman, B.A. The dependence of the piezoelectric response of poly (vinylidene fluoride) on phase-I volume fraction. *J. Appl. Phys.* **1979**, *50*, 6101.
122. Nix, E.L.; Holt, L.; Mcgrath, J.C.; Ward, I.M. Highly drawn poly (vinylidene fluoride) with enhanced mechanical and electrical properties. *Ferroelectrics* **1981**, *32*, 103–114. [[CrossRef](#)]
123. Tasaka, S.; Niki, J.; Ojio, T.; Miyata, S. Structure and Piezoelectricity of Poly (vinylidene fluoride) Films Obtained by Solid-State Extrusion. *Polym. J.* **1984**, *16*, 41–48.
124. Wang, T.T. Piezoelectricity in β -phase poly (vinylidene fluoride) having a “single-crystal” orientation. *J. Appl. Phys.* **1979**, *50*, 6091–6094.
125. Nagai, M.; Uehara, H.; Kanamoto, T. Drawing of poly (vinylidene fluoride): Effects of initial morphology and technique on the structure and properties of drawn products. *Kobunshi Ronbunshu* **1996**, *53*, 555–562. [[CrossRef](#)]
126. Nagai, M.; Nakamura, K.; Uehara, H.; Kanamoto, T.; Takahashi, Y.; Furukawa, T. Enhanced electrical properties of highly oriented poly (vinylidene fluoride) films prepared by solid-state coextrusion. *J. Polym. Sci. Polym. Phys.* **1999**, *37*, 2549–2556. [[CrossRef](#)]
127. Ibragimova, A.I.; Zhuravleva, I.I.; Kuznetsov, S.I.; Panin, A.S.; Tarasova, E.Y. Structure and phase composition of polyvinylidene fluoride films obtained by laser synthesis. *Bull. Lebedev Phys. Inst.* **2019**, *46*, 118–121. [[CrossRef](#)]
128. Wachtler, M.; Wagner, M.R.; Schmied, M.; Winter, M.; Besenhard, J.O. The Effect of the Binder Morphology on the Cycling Stability of LiAlloy Composite Electrodes. *J. Electroanal. Chem.* **2001**, *510*, 12–19. [[CrossRef](#)]
129. Yoo, M.; Frank, C.W.; Mori, S.; Yamaguchi, S. Interaction of Poly(Vinylidene Fluoride) with Graphite Particles. 2. Effect of Solvent Evaporation Kinetics and Chemical Properties of PvdF on the Surface Morphology of a Composite Film and Its Relation to Electrochemical Performance. *Chem. Mater.* **2004**, *16*, 1945–1953. [[CrossRef](#)]
130. Sedov, V.M.; Gostevskoy, A.A.; Tarbaev, S.D.; Gorelov, A.S.; Chulkhov, A.B.; Nutfullina, G.M.; Zhukovsky, V.A. Polyvinylidene fluoride mesh implants in the treatment of hernias abdominal wall. *Surg. Her.* **2008**, *2*, 17–21.
131. Egiev, V.N.; Voskresensky, P.K.; Emelyanov, S.I. *Tension-Free Hernioplasty*; Medpraktika-M.: Moscow, Russia, 2002; pp. 1–147.
132. Eremeev, V.P.; Rekhachev, V.P.; Kivermna, Z.I. Treatment of postoperative ventral hernia. *Surg. Her.* **1984**, *6*, 17–21.

Chapter 4. Current State of PVDF as an Energy Harvester

4.1 Motivation of the article

This review aims to synthesize current trends and developments in the use of PVDF, from its initial solution mixing to its final applications as flexible nanofibers or solid layers. By exploring the precise parameters necessary for fabrication, this paper provides a comprehensive guide for both novices and experts in the field. It addresses the fundamental aspects of PVDF processing, including solvent selection and ratio determination, and highlights the subsequent effects on the material's piezoelectric properties. Moreover, this review delves into the common degradation phenomena of PVDF, offering valuable insights into its durability and long-term performance. Understanding these aspects is crucial for advancing the use of PVDF in energy harvesting, active filtration, and sensing applications. By presenting a detailed overview of PVDF's properties, fabrication methods, and applications, this review seeks to serve as a foundational resource for researchers and practitioners. It aims to not only guide those new to PVDF production but also to provide a current and comprehensive perspective for those looking to deepen their expertise. The ultimate goal is to foster innovation and enhance the practical implementation of PVDF in various technological domains.

4.2 Conclusion on the article

Electrospinning stands out as the primary method for fabricating nanofibrous structures. Despite PVDF's flexibility, these structures often face challenges in charge generation and permittivity, which can be mitigated through tuning and doping. Standard characterization methods include SEM for imaging and XRD, FTIR, or Raman spectroscopy for studying the β -phase. Electrical properties are commonly assessed using the piezoelectric coefficient d_{33} and permittivity measurements. However, many studies overlook the crucial aspect of degradation. Questions about the stability, stress tolerance, and overall durability of PVDF materials remain. This is particularly important for applications involving mechanical stress, such as PENG (piezoelectric nanogenerators) and TENG (triboelectric nanogenerators). Although PVDF is durable, its specific use in experiments necessitates accelerated aging tests to ensure long-term viability beyond experimental conditions. Looking ahead, the development and commercialization of PVDF nanogenerators are expected to grow exponentially, expanding their applications and impact in various fields.

4.3 Applicant's contribution

The applicant is responsible for conceptualization and partial writing of the manuscript.

4.4 Article 4

The paper "*A Brief Introduction and Current State of Polyvinylidene Fluoride as an Energy Harvester*" was published in September 2022 in "*Coatings*" journal (IF: 3.4; Q2) and to date (02.06.2024) has 9 citations.

Review

A Brief Introduction and Current State of Polyvinylidene Fluoride as an Energy Harvester

Nikola Papež¹ , Tatiana Pisarenko¹ , Erik Ščasnovič² , Dinara Sobola^{1,3,†} , Ștefan Țălu^{4,*} , Rashid Dallaev¹ , Klára Částková^{2,5,‡}  and Petr Sedlák¹ 

¹ Department of Physics, Faculty of Electrical Engineering and Communication, Brno University of Technology, Technická 2848/8, 61600 Brno, the Czech Republic

² Central European Institute of Technology, Purkyňova 656/123, 61200 Brno, the Czech Republic

³ Institute of Physics of Materials, the Czech Academy of Sciences, Žitkova 22, 61662 Brno, the Czech Republic

⁴ Directorate of Research, Development and Innovation Management (DMCDI), Technical University of Cluj-Napoca, Constantin Daicoviciu Street, No. 15, 400020 Cluj-Napoca, Romania

⁵ Department of Ceramics and Polymers, Faculty of Mechanical Engineering, Brno University of Technology, Technická 2896/2, 61600 Brno, the Czech Republic

* Correspondence: stefan_ta@yahoo.com or stefan.talu@auto.utcluj.ro; Tel.: +40-264-401-200; Fax: +40-264-592-055

† Current address: Affiliation 3.

‡ Current address: Affiliation 2.

Abstract: This review summarizes the current trends and developments in the field of polyvinylidene fluoride (PVDF) for use mainly as a nanogenerator. The text covers PVDF from the first steps of solution mixing, through production, to material utilization, demonstration of results, and future perspective. Specific solvents and ratios must be selected when choosing and mixing the solution. It is necessary to set exact parameters during the fabrication and define whether the material will be flexible nanofibers or a solid layer. Based on these selections, the subsequent use of PVDF and its piezoelectric properties are determined. The most common degradation phenomena and how PVDF behaves are described in the paper. This review is therefore intended to provide a basic overview not only for those who plan to start producing PVDF as energy nanogenerators, active filters, or sensors but also for those who are already knowledgeable in the production of this material and want to expand their existing expertise and current overview of the subject.

Keywords: degradation; electrospinning; fabrication; nanofibers; nanogenerator; piezoelectricity; polymer; PVDF; solutions



Citation: Papež, N.; Pisarenko, T.; Ščasnovič, E.; Sobola, D.; Țălu, Ș.; Dallaev, R.; Částková, K.; Sedlák, P. A Brief Introduction and Current State of Polyvinylidene Fluoride as an Energy Harvester. *Coatings* **2022**, *12*, 1429. <https://doi.org/10.3390/coatings12101429>

Academic Editor: Wei Xu

Received: 6 September 2022

Accepted: 22 September 2022

Published: 29 September 2022

Publisher's Note: MDPI stays neutral with regard to jurisdictional claims in published maps and institutional affiliations.



Copyright: © 2022 by the authors. Licensee MDPI, Basel, Switzerland. This article is an open access article distributed under the terms and conditions of the Creative Commons Attribution (CC BY) license (<https://creativecommons.org/licenses/by/4.0/>).

1. Introduction

Nowadays, there are countless synthetically produced polymers with different properties and functions. Organic polyvinylidene fluoride (PVDF) can be classified as one of the most interesting. The reason that has made it so popular is due to its vast range of applications precisely because of its properties [1]. This semicrystalline fluoropolymer has a considerable chemical resistance, high mechanical strength, extensive operating temperature range (the glass transition temperature is $-35\text{ }^{\circ}\text{C}$ and the melting point is $177\text{ }^{\circ}\text{C}$). Moreover, it is biocompatible and highly hydrophobic. It can be argued that similar properties can be achieved with other types of polymers, which is certainly true. For example, polytetrafluoroethylene (PTFE) is regarded as an ideal alternative, but quite expensive [2]. As another similar, fluorinated ethylene propylene (FEP) can be considered, which is suitable for generators in an outdoor environment [3–5]. However, PVDF has one other unique property, and that is the ability to generate a charge, not only using the triboelectric effect but also using piezoelectricity, which is a great advantage over other polymers. Thus, PVDF can rightly be called a nanogenerator. Scientists in many fields are exploring the combination of all these properties and the ability to generate a charge [6–11]. This paper selects a few of the most widely used and interesting ones. In general, these

energy harvesters have taken the name of piezoelectric nanogenerators (PENGs) or triboelectric nanogenerators (TENGs). Although there are many other and not less interesting representatives of both PENGs or TENGs [12], PVDF can also act as a hybrid in both cases [10], and this capability makes it quite distinctive.

First of all, it is necessary to describe PVDF in terms of its chemical structure. The chemical formula is $(C_2H_2F_2)_n$. Its basic building blocks are therefore carbon, hydrogen, and fluorine. These three elements can form several crystalline chain conformations [13]. Conformations are defined by polar and nonpolar phases. Four phases are most commonly found in the literature: α -, β -, γ -, and δ -. Less commonly mentioned is a fifth ϵ -phase [14]. Phases α and ϵ belong to the nonpolar ones. Molecules with antiparallel packing of the dipoles are nonpolar bonds and have no dipole moment [14]. Conversely, polar molecules do not have a full covalent bond, so an imbalance in the electron charge of the molecule is present. The imbalance in the distribution of electrons generates dipoles. The dipoles will try to align themselves when an electric field is provided. The polarity of a molecule affects the attraction between molecular chains. Furthermore, nonpolar polymers are less permeable to water than polar polymers [15]. Thus, it is clear that the polar phases are the most interesting to observe in the case of charge generation. The most associated with charge generation is the β -phase [14]. Furthermore, not neglected is the polar γ -phase, where its polarization effect is weaker. This is because the gauche bond exists in every fourth repeat unit [16]. The often mentioned nonpolar α -phase is usually obtained from the melt by crystallization. The phase conformations of PVDF polymer are illustrated in Figure 1, where their different structures can be clearly seen.

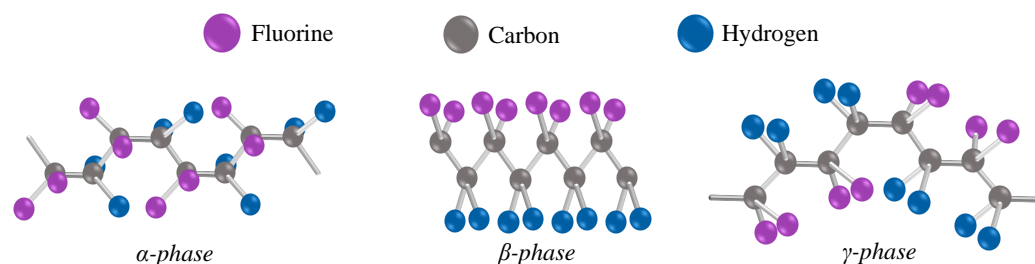


Figure 1. The chain conformation of the most observed phases in PVDF [17]. Because the fluorine atoms in the β -phase are situated on the same side of the molecular chains, which are arranged parallel to one another in a specific direction, with the same dipole orientation and enhanced polarity, the β -phase exhibits spontaneous polarization strength as well as pyro- and piezoelectric properties [18].

Popular methods for phase characteristics are Fourier transform infrared spectroscopy (FTIR), Raman Spectroscopy, X-ray diffraction (XRD), and differential scanning calorimetry (DSC). These methods are discussed later in Section 2.5.

The main effort during production is to increase the β -phase as much as possible. The simplest option is to change the fabrication parameters. The second option is to dope the material with so-called fillers. These also serve, for example, to increase permittivity or hydrophobicity, depending on the application of the material. All of the above issues and more are also discussed in the following sections.

As PVDF is a well-known and used material, it has been the subject of many reviews. Special types of applications or manufacturing are described. A selection of other and recommended papers on a related topic is mentioned in Table 1.

In this paper, the manufacturing and analysis of PVDF polymer is described in a comprehensive Section 2, where the main aspects that should be followed in the production of this material are highlighted. However, once production has been successfully mastered, there are risks that can cause degradation, which Section 3 discusses. As PVDF nanogenerators are currently widespread in many fields, Section 4 maps their current applications. On the contrary, Section 5 pushes the state of the art and goes further, describing new, emerging, and future trends. Finally, all findings presented so far are summarized in the conclusion in Section 6.

Table 1. Selected publications on a similar topic. The chosen studies are mainly complementary to the current paper.

Review Title	Short Description
<ul style="list-style-type: none"> A comprehensive review on fundamental properties and applications of poly(vinylidene fluoride) (PVDF) [19] 	Properties of PVDF and not only its applications as a nanogenerator.
<ul style="list-style-type: none"> Application and modification of poly(vinylidene fluoride) (PVDF) membranes—A review [20] 	PVDF mainly as membranes, their modification and comparison.
<ul style="list-style-type: none"> A brief review on piezoelectric PVDF nanofibers prepared by electrospinning [21] 	A short review focused on electrospinning.
<ul style="list-style-type: none"> Solution blow spinning of polyvinylidene fluoride based fibers for energy harvesting applications: a review [22] 	Alternatives for electrospinning.
<ul style="list-style-type: none"> Progress in piezoelectric nanogenerators based on PVDF composite films [23] 	Special and emerging types of fillers.
<ul style="list-style-type: none"> Electrospun PVDF nanofibers for piezoelectric applications: a review of the influence of electrospinning parameters on the β phase and crystallinity enhancement [24] 	Tuning the β -phase and crystallinity of nanofibers fabricated by electrospinning.
<ul style="list-style-type: none"> Progress in the production and modification of PVDF membranes [25] 	Rich review on membranes, many comparisons.
<ul style="list-style-type: none"> Recent advances in the preparation of PVDF-based piezoelectric materials [26] 	Fabrication, preparation, and β -phase formation of PVDF and its copolymers.

2. Materials and Methods

How to prepare the right solution (Section 2.1), how to choose (Section 2.2) and how to make (Section 2.3) fibers or layers from this solution, how to enhance the obtained material (Section 2.4), and how and what to measure (Section 2.5) are covered in this section. Various recommendations, known problems, or even possible interesting facts that many scientists over the last years have discovered can be found here.

2.1. Solution Preparation

For the formation of the material, the preparation of the solution precedes. The PVDF must be processed into a liquid form using a solvent, and if necessary, a specific filler must be added in the process. As PVDF has a relatively high toxic resistance, it is not easy to dissolve, and only small amounts of polar solvents need to be used. The standard solvents used are dimethyl sulfoxide (DMSO), dimethyl formamide (DMF), dimethyl acetamide (DMAc), or *N*-methyl pyrrolidone (NMP). These solvents are often combined with acetone (Ac) with various ratios. The addition of smaller amounts of acetone contributes to the volatilization of the solvent and an increase in the β -phase [24]. Acetone causes a faster evaporation of the solvent. There are also several papers experimenting with different solvent ratios [27] but DMSO/Ac with a 7:3 ratio is quite commonly used [6,28–30]. The amount of acetone is also reported with the ratio of 6:4 for DMF/Ac, DMSO/Ac, and NMP/Ac [31]. Different ratios have also been shown to affect the morphology of nanofibers [32]. Furthermore, the choice depends on the PVDF concentration. This is given in the range of 10 to 25 wt% [24,31,33]; the choice will of course affect the viscosity of the solution. Subsequently, essential parameters such as chain conformations are also affected. The optimum selection for a high β -phase is 20 wt% PVDF, then with a higher concentration the β -phase decreases. Lastly, molecular weight is also important. It also influences the viscosity of the resulting solution. Molecular weights of 70.000, 180.000, 275.000, 534.000, and 777.000 g/mol have already been used. The most currently used value for electrospinning is 275.000 g/mol [33–39]. After selecting the appropriate type of PVDF

and solvent, these substances are mixed. A standard stirrer at 40 to 80 °C is used, and the mixing time should be at least 4 h. However, many authors choose 24 h with known solvents such as DMSO, NMP, or DMF [40].

Nevertheless, it is essential to keep in mind that the parameters chosen in this way may affect the β -phase and other chain conformations. However, what matters most is the subsequent method of production and the capabilities of the apparatus. In particular, using nanofiber fabrication by the electrospinning method can lead to needle clogging during its use. When preparing the solution, it is advisable to take into account the way in which the resulting piezoelectric polymer will be processed.

Other lesser-known solvents for PVDF are as follows: acetyl triethyl citrate (ATEC), γ -butyrolactone (GBL), cyclohexanone (CHO), cyclopentanone (CPO), dibutyl phthalate (DBP), dibutyl sebacate (DBS), diethyl carbonate (DEC), diethyl phthalate (DEP), dihydrolevoglucosenone (Cyrene), 1,4-dioxane, 3-heptanone, hexamethyl phosphoramide (HMPA), 3-hexanone, methyl ethyl ketone (MEK), 3-octanone, Rhodiasolv PolarCleansa, 3-pentanone, propylene carbonate (PC), tetrahydrofuran (THF), tetramethylurea (TMU), triacetin, triethyl citrate (TEC), triethyl phosphate (TEP), trimethyl phosphate (TMP), and *N,N'*-tetrabutylsuccinidamide (TBSA) [41–43].

2.2. Fibers or Solid Layers?

Where and how the material will be used also determines whether the PVDF will be in the form of nanofibers or solid layers. Both have advantages and disadvantages, and scientists are experimenting with them [18]. For obvious reasons, a significantly stronger piezo effect, and not only that, can be expected with solid layers—films. Here, one must consider the reduced flexibility or the impossibility of using the material as a filter (often also for the utilization of photocatalysis [44]), which is not the case with nanofibers. However, the characterization of nanofibers is much more challenging than for solid layers. Indeed, the fiber mat is an inhomogeneous material where the individual fibers are chaotically distributed. While the arrangement of the fibers can be controlled (e.g., by the rotation of the collector cylinder during electrospinning), it is not such that it can be accurately quantified and has not yet been described mathematically. The fiber mat is filled with air, which affects every measurement. The interpretation of the results is then much more complex, for example, in any spectroscopic measurement due to the uneven structure or in electrical measurements, such as permittivity, where the air inside the fiber mat is partly measured. Therefore, these are negative properties that must be taken into account when choosing nanofibers.

2.3. Material Fabrication

Electroactive PVDF can be formed in two variants—fibers or layers. As outlined in previous sections, the choice of the form of this material depends mainly on the area of use. Thus, if there are high requirements for flexibility, breathability, or even elasticity, it is better to define the form of the fibers. In this case, such a nanogenerator finds perfect use in the field of tissue engineering [45], smart textiles [46], or as an active filter [47]. Otherwise, layers or rather thinner films can be used, for example, as a pressure sensor [48,49].

Currently, the most widely used methods for producing PVDF nanogenerators, sensors, membranes, and other electrical-signal-generating products include spin-coating—for thin films [23,50], and electrospinning—for fibers. Electrospinning in the field of nanogenerators is relatively predominant [24,51–54]. Other lesser-known methods include electrospraying—a layer in the form of nanoparticles [55,56], or the Langmuir–Blodgett method—a layer formed by chemical deposition [57,58]. Using the method of electrospinning is quite extensive and is divided into many subcategories of how electrospinning can be performed. Notwithstanding, the basic principle is the same—in a high voltage system, a liquid solution in the form of a fiber is drawn by an electric force between the emitter and the collector. Due to the electric field, the so-called Taylor cone forms on the emitter, which acts as the liquid source. At the tip of this cone, the fiber is pulled towards whipping the collector (Figure 2). The result is a nanofiber structure.

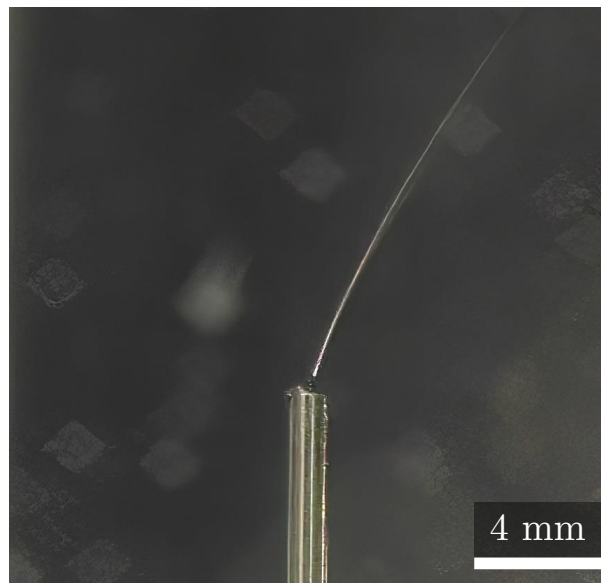


Figure 2. Drawing of a fiber from a forming Taylor cone at the tip of the emitter, in this case, a needle. The fiber is attracted towards the collector, which is no longer captured in this image. The material is 20% PVDF. The heated solution is still liquid in the emitter but during the whipping of the collector and fiber formation the solvent dries, and the PVDF solidifies [17].

The most well-known electrospinning method is when the needle is placed as the emitter, through which the solution flows towards the collector, which is in the form of a rotating cylinder (Figure 3). Researchers like this method mainly because they can very carefully control every parameter of production of literally every fiber on the resulting fiber mat. The thickness of the fibers and their shape, tension, or evaporation time can be controlled, for example, the distance between the emitter and collector, the high voltage value between them, cylinder rotation speed, needle diameter, solution flow rate, or air temperature or atmosphere in a chamber where the fiber is formed. The following Table 2 lists the most common problems that can occur with single-needle electrospinning on the rotating collector [30,59,60].

Table 2. The most common electrospinning problems in which PVDF nanofiber imperfections occur [30,59,60].

Problem	Cause
Fiber bonding	Short emitter–collector distance
Formation of droplets in fibers	High dosing rate (emitter flow)
	High emitter–collector voltage
Nonformation of droplets in fibers	High viscosity
Chaotically oriented fibers, thick fibers	Low emitter–collector voltage
	Low collector cylinder speed
	Higher molecular weight
Spinning outside the cylinder	Low emitter–collector voltage
	High collector cylinder speed
Low fiber tension	Solution without ions/salts (small number of charges)

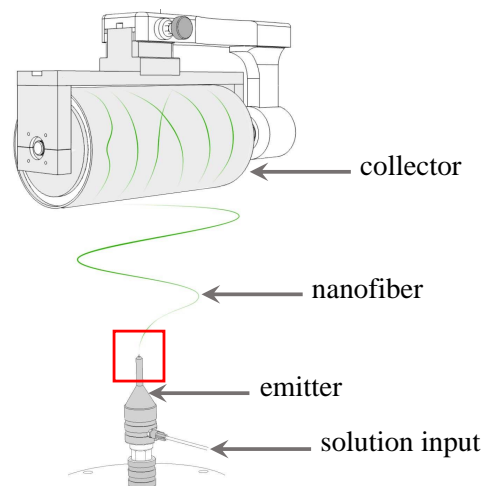


Figure 3. Illustration of the method of electrospinning in the form of a single needle acting as an emitter and a rotating cylinder acting as a collector, on which the nanofiber is gradually wound, and as a result it then creates a kind of fabric that can be used as the basis of a simple nanogenerator [17]. The red square highlights the emitter—the needle with the solution changing to a fiber, which was also described in Figure 2.

In this way, the specific parameters of the fiber can be achieved relatively accurately, and the β -phase of the resulting fiber can be successfully tuned [24]. The labeling as “nanofibers” can rightly be used for the size of such fibers, as their thickness can range from microns to tens of nanometers [61]. In some cases, it is even possible to create structures in the order of nanometer units. Černohorský et al. in Figure 4 demonstrated that these structures resembling a cobweb were formed in the combination of PVDF and nylon-6 (PA6) [61].

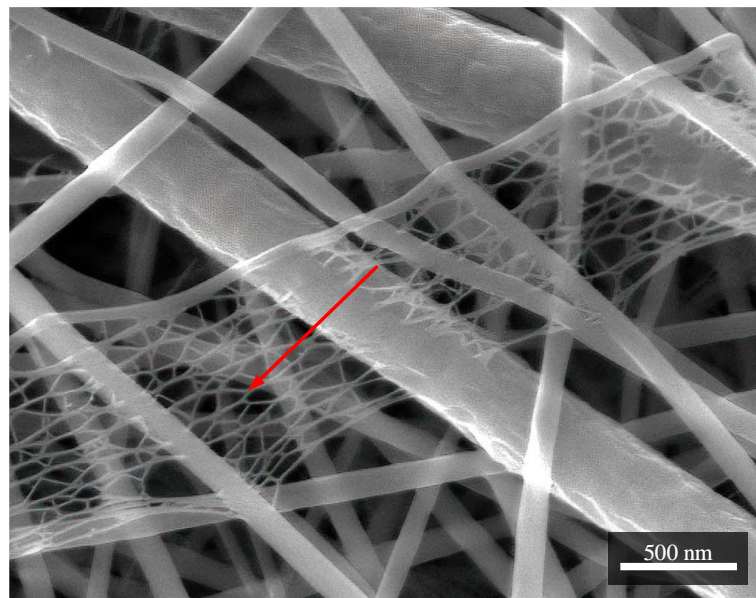


Figure 4. A structure of porous character resembling a cobweb. This structure was observed in combination with nylon-6 (PA6) [61]. The structures of smaller nanofibers within tens of nanometers are indicated by the arrow.

However, this precise production control based on a single drawn fiber is, of course, redeemed by the production time when the fiber is wound on the cylinder. This can be solved relatively easily by replacing one needle with two or more but at the cost of less control over the process. Furthermore, as already mentioned, electrospinning exists in many variants. Thus, for example, a coaxial needle can be used instead of a single needle,

where two types of solutions flow through the needle and where the fiber core can thus be of a different type than its shell. This type of nanofibers is also called core-shell nanofibers. It is also a relatively popular method [62–64]. Instead of the coaxial needle, two different needles with different solutions or several more needles can be used. The so-called metal rod can also be used instead of needles. However, compared to Figure 3, the emitter serves as the metal rod from which liquid is released, placed from the top, and the collector from the bottom. If the electrospray method is considered, it is necessary to use the appropriate part (instead of the needle) as the emitter. The type of collector can also be changed, where a static plate can be used instead of the rotating cylinder on which the fiber would be applied. Nevertheless, the rotating cylinder can also serve as the emitter when it is partially immersed in the solution and constantly wets into it during rotation and thus “brings” the solution to the collector, where the material is again drawn in the form of fibers. No higher control can be expected here when drawing the fibers. It is also worth noting that a solution is not always used in electrospinning. With the required aperture, direct melting of the material can also occur at the cost of a much higher viscosity [65].

2.4. Tuning and Improving the Properties

Although PVDF can be considered a very successful and popular material, perhaps also because of this, scientists are constantly trying to improve its properties. There are a large number of articles in the databases not only about how to improve its β -phase, which is usually the primary goal but also about how to improve other properties, such as hydrophobicity, tensile strength, etc., [66–72].

The first option is to adjust the production parameters [73]. For example, several research groups have shown that the β -phase for the fibrous PVDF structure can rise by increasing the speed of the collector cylinder. Higher collector cylinder speeds can also cause different material flexibility. In this case, the arrangement of the fibers in the overall fiber mat is different. At low speeds of around 300 rpm, the fibers are much more chaotically distributed. At high speeds, such as 2000 rpm, the fibers are again much more aligned, i.e., made tensile and thus with smaller diameters. That is why electrospinning with the needle and the rotating cylinder is so much used [17,30,51,61,74].

The second option is doping, mixing, and adding additional material. The result is a new composite. It could be, for example, the previously mentioned nylon (PA6), which can be spun in parallel with PVDF, and which can be used to control hydrophobicity, stress, and the magnitude of the triboelectric effect etc. [6,51]. The core-shell is often used, i.e., a combination of two solutions using a coaxial needle [64,75–77]. The variation of solutions to PVDF is relatively large, so it cannot yet be said with certainty that one composite predominates more than another.

Another option is to use fillers, which are various powders mixed with a solution. However, it is necessary to pay much more attention to the affinity of the material and thus check its mutual compatibility [78–80]. For example, there are efforts to improve ferroelectric and magnetic properties with BiFeO_3 [81–84], or also with the relatively popular BaTiO_3 to increase the β -phase [78,85–91]. Other authors use ZnO to improve output voltage and improve crystalline structure [92,93]. There is also a rich use of PZT ceramics to increase piezoelectric properties [94], which can also be used as a smart air filter [95]. Almost all of these methods use electrospinning. Of course, this selection does not cover (nor is it intended to) the very broad combination of materials that are used with PVDF. However, the possibilities mentioned are ones of the most common.

2.5. Characterization and Electrical Measurement Methods

This part of the section describes the most widespread methods of characterization, material composition, and electrical properties of PVDF, especially nanofibers. The most investigated parameter of this material is usually its phase conformation, which is associated with the piezoelectric effect. The large part of the work is then focused mainly on studying the β -phase. All these results are based on the used spinning methods, specific production parameters, fillers, but also on the specific type of (commercial) PVDF [14,96–101]. For

spectroscopic methods studying fibers, the characterization of fibers can be considered relatively complex. The reason is simple, namely, the inhomogeneous structure of the sample surface, so it can be assumed that these methods will be more accurate for solid PVDF layers [17,74,102].

For ease of reference, Table 3 below summarizes the most commonly used methods for PVDF analysis with a brief description of each technique.

Table 3. The most used methods for the study of PVDF nanogenerators.

Measurement Method	Short Description
Scanning electron microscopy (Section 2.5.1)	Structure, shape, thickness, cross section
Fourier transform infrared spectroscopy (Section 2.5.2)	Determination of the phase conformations
Raman spectroscopy (Section 2.5.3)	Similar to FTIR, sample fingerprint analysis
X-ray photoelectron spectroscopy (Section 2.5.4)	Elemental composition
X-ray diffraction (Section 2.5.5)	Structure of a crystal, phase conformations
Atomic/piezoresponse force microscopy (Section 2.5.6)	Fiber diameter, piezoresponse
Permittivity and dielectric properties (Section 2.5.7)	Dielectric constant ϵ_r
Piezoelectric coefficient (Section 2.5.8)	Piezoelectric coefficient d
Wettability (Section 2.5.9)	Contact angle
Surface area analysis (Section 2.5.10)	Gas adsorption
Thermogravimetric analysis (Section 2.5.11)	Weight percentage composition, thermal properties
Differential scanning calorimetry (Section 2.5.12)	Crystallinity
Mechanical properties (Section 2.5.13)	Tensile stress, Young's modulus, and tensile strain

2.5.1. Scanning Electron Microscopy (SEM)

It is used mainly for studying the structure of nanofibers. There are several reasons for its use. One of the main reasons is to examine the condition of the fiber—its shape, thickness, and defects [32,68]. It is also possible to perform statistical calculations [32,88,102–104] and observe the attachment of various fillers. In the case of experiments with production parameters that affect the physical properties of fibers, SEM is a necessary method. This method may also include an FIB (Figure 5) [17] for examining the fiber cross section or an EDS for an elemental analysis [105].

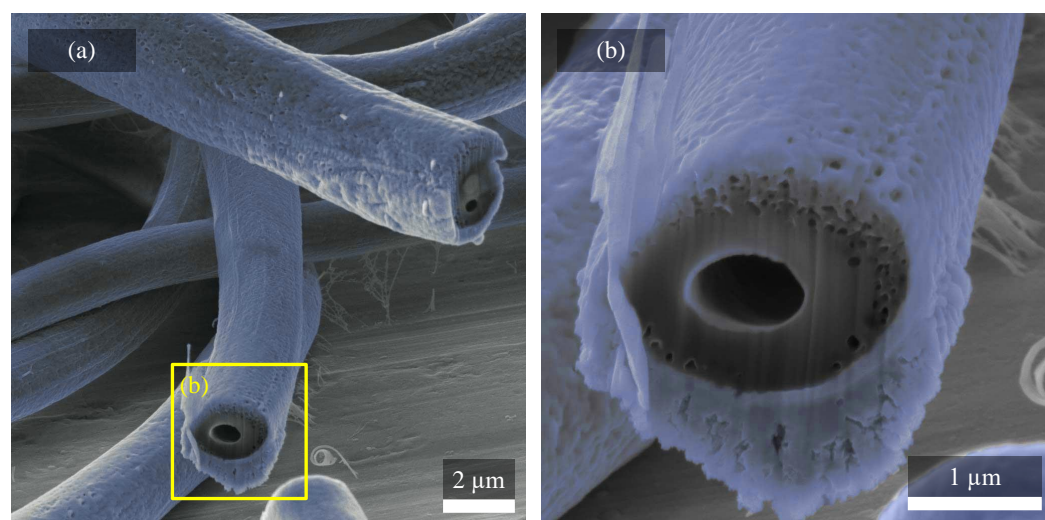


Figure 5. Example of PVDF nanofibers that have been cut using FIB. Several interesting aspects can be seen in (a). In the fiber cut at the upper part, it can be seen that its structure is not perfectly oval. Both cut fibers appear hollow in some parts, or it may also be an air bubble. On closer examination in (b), it can be seen that particularly in the surface region, the fibers are quite porous. Since PVDF is the polymer, it has been coated to prevent charging of fibers, as indicated by the color highlighting [17].

2.5.2. Fourier Transform Infrared Spectroscopy (FTIR)

A relatively popular and frequently used method just after SEM characterization is FTIR, where its use for PVDF investigation is in the order of hundreds of papers [106]. It is used to accurately determine the phase conformations in the sample. The exact proportion of the β -phase can thus be calculated quite accurately [17]. The determination of PVDF phases is not identical among all authors, but there are also exclusive peaks or even dual peaks (mainly β - γ) (Table 4). In some cases, the attenuated total reflection system ATR with FTIR is also used to determine the functional groups and bonds (for example, with hydrogen) [107]. The group CH_2 bending vibration occurs at 1402 cm^{-1} , the CF_2 bending vibration at 508 cm^{-1} and 473 cm^{-1} , and the stretching band at 1180 cm^{-1} [108–110]. There is also a shift of about 2 cm^{-1} in some articles [106].

Table 4. List of the most commonly identified values for α -, β -, and γ -phases in FTIR absorption spectrum. The last line also lists the values of the so-called dual peaks, as they are denoted by some authors [97,106,111].

Spectral Area	Value
α -phase peak	410, 489, 532, 614, 763, 795, 854, 975, 1149, 1209, 1383, and 1423 cm^{-1}
β -phase peak	445, 473, and 1275 cm^{-1}
γ -phase peak	431, 482, 811, and 1234 cm^{-1}
Dual β - γ peak *	510, 840, and 881 cm^{-1}

* Some authors consider these dual peaks to be purely β -phase, others purely γ -phase, the largest divergence can be considered at 840 cm^{-1} .

2.5.3. Raman Spectroscopy

Raman spectroscopy is also used for a precise phase and sample fingerprint analysis, like FTIR, and thus considered to be a complementary or alternative method due to its similar characteristics. The reasons for the use of both methods may also be as a result of the aforementioned inhomogeneity of the nanofiber sample surface, where the outcomes from the characterizations may correlate each other. Although we want to display the same phase, it can differ between FTIR and Raman spectroscopy, as Raman spectroscopy can show different rotations, bending, and stretching of molecules. It also depends on the light source used for Raman spectroscopy and device sensitivity on the lower wavelengths. The fraction crystallinity of each phase can be calculated from Raman as well as from the FTIR [112]. Furthermore, here again, several less intense peaks can be found in the spectrum, which have been adequately described [74,102,113,114]. Typical wavenumbers for the crystalline phases from Raman spectroscopy are: the α -phase occurring at 794 and 874 cm^{-1} , the β -phase or the β - γ combination found at 839 cm^{-1} , and the γ -phase found at 812 cm^{-1} [115]. Since, the polymer is investigated by Raman spectroscopy, it is not recommended to set the laser power higher than in mW units.

2.5.4. X-ray Photoelectron Spectroscopy (XPS)

Because XPS tracks the elemental composition on the surface of a sample, it is not as commonly used as further spectroscopic and other methods for determining phase structure. However, it is relatively important for accurate monitoring material changes, for example, when using different solvents or fillers. The most commonly observed regions for PVDF are carbon C1s, fluorine F1s, their bonds, and possibly hydrogen H bonding [116]. For example, the peaks at 286 eV originated from the $-\text{CH}_2-$, and the one at 290 eV originated from the $-\text{CF}_2-$ components, the one at 288 eV originated from the $-\text{CH}-$, and the one at 293 eV corresponds to $-\text{CF}_3-$ groups. Some bonds cannot be easily detected without fitting. Hydrogen itself is undetectable by XPS.

2.5.5. X-ray Diffraction (XRD)

It is a crystallographic method used to analyze the phase structure of a sample. It is standardly expressed as intensity vs. 2θ . All PVDF phases here have specific values in units of degrees. The characteristic patterns of PVDF are mainly between 14 and 26° [117]. The β -phase has a characteristic value of 20.26° . Saha et al. states its value of 20.4° [118], Moazeni et al. reports a β -phase of $2\theta = 20.6^\circ$ (200/110) [117], Chethan et al. provides $2\theta = 20.8^\circ$ (110/200) [119]; the α -phase peaks occur at 17.7° , 18.3° , and 19.9° ; the γ -phase peaks are 18.5° , 19.2° , and 20° [14,120]. It is obvious that, for example, 20° for the γ -phase can be easily mistaken for the β -phase and vice versa.

2.5.6. Atomic Force Microscopy (AFM) and Piezoresponse Force Microscopy (PFM)

Using AFM, it is also possible to measure the piezoresponse of the sample, i.e., its ferro- and piezoelectric domain, specifically when using the PFM mode. In most cases, this is a very precise examination of only one fiber with a diameter of 100 nm to 3000 nm [18,24,121–123], where the authors prove the properties of a particular sample (Figure 6) [120,124].

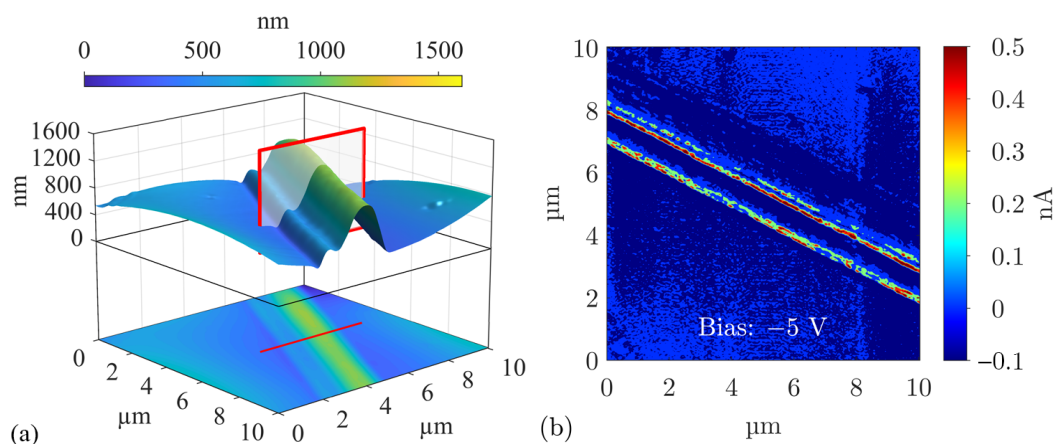


Figure 6. (a) Fiber similar in shape to the one that was acquired by SEM and mentioned in Figure 5a. The same fiber is also measured using the (b) PFM method, where the authors confirm the different orientation of the domains with a bias of -5 V [17].

2.5.7. Permittivity and Other Dielectric Properties

Permittivity is an important electrical property that affects charge generation. For polymers, permittivity is limited by a low intrinsic dielectric constant ϵ_{eff} . In nanofiber PVDF, it can be increased mainly by adding ceramic fillers or by forming a composite [90]. In this case, solid layers have a higher permittivity for obvious reasons (Section 2.2). When measuring a nanofibrous material, the sample is largely filled with air, which complicates the measurement, makes it harder to determine the specific thickness of the material (which must be known when measuring permittivity), and generally reduces the resulting value. It is not entirely surprising that the resulting real part of the permittivity is close to the value of the relative permittivity of the air. The dielectric constant ϵ_r or ϵ' of a normal undoped pure sample at 100 Hz is around 1.5 – 3 [61,125], and for most PVDF samples is not higher than 10 . If no characteristic is given, the values at 1 kHz should also be added. In addition, the loss coefficient $\tan \delta$ or the imaginary component ϵ'' is usually stated.

High dielectric properties are expected to result in increased energy storage density. Given the constant miniaturization, this capability of the material is also highly demanded and desirable. Table 5 shows selected research that aims to maximize energy storage density. It is apparent from the results that polymers with several layers achieve the highest values.

Table 5. Concise demonstration of several selected PVDF composites having high dielectric properties.

Utilized Composite	Achieved Energy Storage Density
6-fold P&F PVDF films [126]	39.80 J/cm ² at 880 kV/mm
BaTiO ₃ /PVDF layers [127]	20.70 J/cm ² at 690 kV/mm
BiFeO ₃ TiO ₂ -PVDF/PMMA [128]	19.30 J/cm ² at 549 kV/mm
BN/PVDF/BN [129]	19.26 J/cm ² at 465 kV/mm
Three-layer PVDF [130]	11.00 J/cm ² at 440 kV/mm
Pure PVDF [127]	9.30 J/cm ² at 500 kV/mm
3 wt% BZT-BCT NFs/PVDF [131]	7.86 J/cm ² at 310 kV/mm
0.1 wt% graphene/P(VDF-TrFE-CFE) [132]	7.00 J/cm ² at 300 kV/mm
BaTiO ₃ -CoFe ₂ O ₄ /PVDF [133]	5.60 J/cm ² at 263 kV/mm
1.25 wt% Ba(Zr,Ti)O ₃ /P(VDF-TrFE-CFE) [134]	2.80 J/cm ² at 75 kV/mm

2.5.8. Piezoelectric Coefficient

Although the high β -phase is a prerequisite for a high piezoelectric effect, some experiments are combined with the measurement of the piezoelectric coefficient [124]. The piezoelectric coefficient d , more precisely piezoelectric charge coefficient or piezoelectric strain coefficient, belongs to the group of piezoelectric constants, which also includes piezoelectric voltage coefficient g , piezoelectric stress coefficient e , and piezoelectric stiffness coefficient h .

The piezoelectric coefficient d_{ij} is defined by two subscripts i and j and is most often given in pC/N units. Subscripts i and j are expressed by numbers that represent the designation of the axes and the directions of deformation. Subscript i shows the direction of polarization, and subscript j shows the direction of the applied stress. The compression mode, as the d_{33} coefficient is otherwise called [135], is one of the most frequently observed piezoelectric characteristics in PVDF [136–140]. It indicates that mechanical deformation occurs in the same direction as the polarization. Another of the common piezoelectric coefficients is d_{31} or transverse mode, where mechanical stress is applied at right angles to the polarization axis. The following empirical relationship holds between d_{33} and d_{31} [141]:

$$d_{33} \approx -2.5 \cdot d_{31} \quad (1)$$

The results from the measurements vary widely depending on the application of the fibers/layers. Standard results are usually in tens of pC/N units. When using ceramics, values in the hundreds of pC/N can be achieved. In the case of other electrical characteristics, for example, the voltage response [142,143] or hysteresis loop [14] is widely measured.

2.5.9. Wettability

The hydrophobicity and hydrophilicity of PVDF are another of the relatively frequently investigated properties [144]. These properties may be important, for example, for active filters, membranes [66,67], or textiles [145,146]. It has been shown that with a higher collector cylinder speed during electrospinning, these properties can be controlled (Figure 7) [17]. Various collector speeds give the sample structure a different morphology, and as the collector speed increases, the fibers become more aligned. It is generally known that PVDF is a hydrophobic material, and researchers are trying to modify it to higher values up to superhydrophobic properties, with a contact angle $>150^\circ$ [68,147].

2.5.10. Brunauer–Emmett–Teller (BET) Surface Area Analysis

It is a standardized technique (ISO 9277) for determining surface areas that uses a measurement of a physisorption of a gas. Most often gas adsorption in units of area per mass of sample (m²/g) is mentioned, but it may also be given as area per volume (m²/cm³). It is performed using the adsorption of nitrogen (most often) at 77 K, argon at 87 K, krypton at 77 K, carbon dioxide at 0 °C or 25 °C, and water at 20 °C. The specific results for PVDF with fillers vary. Rosman et al. stated [148] that for pure PVDF nanofibers, the specific surface was revealed to be about 3.76 m²/g, and increased with the addition of ZnO up to 6.61 m²/g.

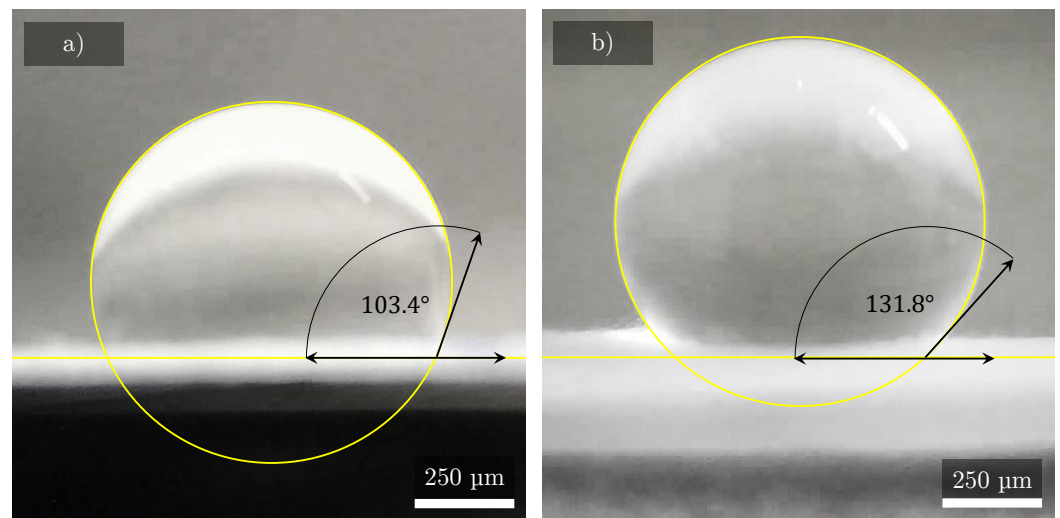


Figure 7. Captured images shows the hydrophobicity of the same type of PVDF without any fillers, produced by the method of electrospinning with different rotation of the collector cylinder. The figure shows the contact angle of a 3 μL distilled water droplet on the PVDF nanofiber mat. Sample (a) was made with the rotation of 300 rpm, and sample (b) with the rotation of 2000 rpm. The difference in contact angle is almost 30° [17].

Yardimci et al. in their work reported [149] that PAN/PVDF nanofibers with 5 wt% AgNO_3 was 22.09 m^2/g , with 10 wt% AgNO_3 was 11.58 m^2/g , and with 20 wt% AgNO_3 , it was 5.97 m^2/g . Thus, the opposite trend to that of Rosman et al. with a ZnO filler [148].

Cvek et al. [150] in their research using combined PVDF/PVDF-TrFE blends loaded with BaTiO_3 obtained a value of 17 m^2/g .

2.5.11. Thermogravimetric Analysis (TGA)

By so-called thermographs, PVDF is characterized by the weight percentage composition, thermal properties, and stability of the sample [151]. By default, it is compared with doped samples to determine the weight loss of the doped sample. For pure PVDF, degradation has been measured by most authors at a temperature around 430 °C [69,152–155].

2.5.12. Differential Scanning Calorimetry (DSC)

The crystallinity of PVDF is usually investigated with DSC. The heat which is associated with the fusion of the polymer is quantified [69]. The melting point T_m , heat of fusion ΔH_f , and of course crystalline phases X_C [124,156–158] are most often mentioned. In the case of the original PVDF, the crystallinity X_C value can be up to 80% [159], but this is a relatively high value and values of around 50% most often occur in scientific studies [17,30,89,111,151].

2.5.13. Mechanical Properties

Some works also test the mechanical properties of PVDF. Usually, tensile stress (MPa), Young's modulus (MPa), and tensile strain (%) are tested [103]. It is generally known that the PVDF structure contains pores that can affect mechanical properties [147]. PVDF can be reinforced, for example, in combination with nylon [61] or silver [69].

An important parameter for specifying the mechanical properties of fibers is the fiber volume fraction V_f [160], which according to standard ASTM D2584 is defined as

$$V_f = \frac{\rho_m \cdot w_f}{\rho_m \cdot w_f + \rho_f \cdot w_m}, \quad (2)$$

where ρ_m is the density of the matrix, w_f is the weight of the fibers, ρ_f is the density of the fibers, and w_m is the weight of the matrix. Nevertheless, the mentioned fiber volume can change, for example, due to the moisture, which swells the fibers and changes their weight.

This difference can entirely change the mechanical properties of the fiber. If the actual fiber weight (including moisture content) is denoted as w_{fc} , then

$$w_{fc} = w_f(1 - w_c), \quad (3)$$

where w_c is the weight of the water content. Similarly, the density of fibers ρ_f should be modified to the density of the fibers with moisture content ρ_{fc} :

$$\rho_{fc} = \frac{1 + MC}{\frac{1}{\rho_{f0}} + MC}, \quad (4)$$

where MC is the moisture content and ρ_{f0} is the density of the dry fibers. With this assumption, the modified equation of the fiber volume fraction (including moisture content) V_{fc} is

$$V_{fc} = \frac{\rho_m \cdot w_{fc}}{\rho_m \cdot w_{fc} + \rho_{fc} \cdot w_m}. \quad (5)$$

3. Material Reactions and Degradation

As already mentioned, PVDF is a nonreactive polymer and has a high toxic resistance. Its resistance to degradation can be considered higher compared to other polymers [161]. Changes occur mainly with higher temperatures and standardly may be combinations of two or more effects (mechanical properties, crystallinity, color, etc.) [162]. It is commonly able to resist basic solutions, chlorine solution, alcohols, several acids, halogens, and aliphatic or aromatic compounds [19]. PVDF weakens when various alkaline solutions are used [163,164]. Lactic acid $C_3H_6O_3$, nitric acid HNO_3 , sulfuric acid H_2SO_4 , and tetrahydrofuran C_4H_8O are mentioned as having little resistance to acids. Its color may change from pure white to yellow, and during the dehydrochlorination process (loss of hydro fluoride units from the polymer chain), it may darken to black [165]. Furthermore, less resistant are glucose and wine vinegar, which is essentially a concentrate of acetic acid. When exposed to higher temperatures, the damage caused by these substances increases.

Regarding thermal degradation, temperature can affect charge generation mainly because of the weakening of mechanical properties at very low temperatures, i.e., the glass transition temperature of $-35^\circ C$, when the material hardens and becomes more brittle. Below this critical value, the material may degenerate as it loses its elasticity and flexibility, which naturally limits the development of piezoelectric phenomena. This temperature is relatively low compared to commonly known polymers. For example, PTFE has $T_g = 115^\circ C$. On the other hand, at the melting temperature of $177^\circ C$, the crystallization process is affected. For PTFE, $T_m = 327^\circ C$. Exceeding any of these threshold temperatures can lead to a different phase transition of the material, which is addressed, for example, by the previously mentioned DSC [166]. Despite all the mentioned drawbacks, PVDF is very stable within these values and it is often called a thermoplastic polymer. The temperatures mentioned may vary slightly in units of degrees depending on the manufacturer of the commercial polymer type.

For PVDF, which has flexible fibers, the critical issue is mechanical strength which is, of course, very different from solid layers. In fact, a good tensile strength is required for a piezoelectric generator. If the nanofibers do not have additional support, they can be damaged more quickly. Microcracks and point defects can already occur with imperfect fabrication, which can be, for example, a contamination of the microparticles. However, it can still be argued that cracks may not be spread throughout the material in the case of single fibers as opposed to solid layers. The tensile strength, elongation at break, and Young's modulus of the PVDF fiber were measured by Hasim, Liu, and Li [167] in sodium hydroxide $NaOH$ solutions. The results in degradation changes were classified as significant. Here again, the increased temperature also accelerated the aging of the samples.

4. Utilization in Real Applications

Although PVDF can be used as a nanogenerator of energy, it is a relatively broad concept. Therefore, it is appropriate to mention several interesting works that are exper-

imentally devoted to specific applications. Hence, this section does not primarily serve to describe the various fillers and other composite combinations that can improve PVDF properties (which have already been mentioned in Section 2.4), but to describe the direct applications of PVDF itself.

A widespread and intended use of PVDF as a nanofabric is directly for the human body. There can be several uses. The simplest uses can be as a wearable shirt, generating charge when walking and moving [168], during inhaling and exhaling [169], or blood flow [170–172], or as gloves [173]. It can also serve as a shoe insole [49,174–176], or while typing on the keyboard [177]. For these applications, PVDF can operate just as a common sensor (safety monitoring, medical diagnostics), or as a nanogenerator depending on its performance [40,178]. In these cases, the connection to the IoT is also assumed [179]. In addition to such practical uses, PVDF can also be used purely as a green energy harvester, for example, for wind energy harvesting [3,5,180], or for energy harvesting from ocean waves and applications [181,182].

Among the less common but emerging uses may include the use of PVDF as scaffolds in tissue engineering due to its biocompatibility. For example, for osteoblasts (bone cells), where their electromechanical stimulation can accelerate cell spreading [183–185]. For solar cells, PVDF can serve as an enhancer of the crystallinity of currently very popular perovskites [186], when there are already attempts to create a hybrid inducing the piezophototronic effect [187]. Another unique use of the PVDF nanogenerator also appears to be energy harvesting from sound waves [188,189].

5. Future Perspectives

The implementation of clean PVDF fibers or layers themselves as an energy generator seems to be an inexpensive and easy way, but the current trend is to use PVDF mainly as a composite, doped with fillers, for this sector (discussed in Section 2.4). Most databases are oversaturated with papers on experiments with new PVDF composites and combinations as energy generators; and the knowledge on clean PVDF polymer material itself is rather repetitive.

Another interesting point is the continuing and ongoing growth of attention on the topic of wearables. This is understandable and desirable with respect to the forthcoming miniaturization and the fact that PVDF is a mechanically tough material that is flexible in both fiber and film form [168,190,191].

A relatively popular type of energy harvesting in recent years is PVDF as a thermoelectric generator (TEG) [192–196]. That means generating an electrical voltage due to an applied temperature gradient. The Seebeck effect on which TEGs are based of course is not a new concept, but in combination with PVDF, these experiments are emerging, and given their increasing number, their subsequent evolution can still be expected. Similarly, as the β -phase determines the piezoelectric coefficient, it has also been reported to be more thermodynamically favorable [197], and therefore PVDF also becomes a candidate for TEG [198]. It most often acts as a composite together with other materials [199–202], although generally as a film. Fibers such as TEG alone do not appear much in scientific papers yet, which can be concluded due to the expectation of low effectiveness. The use of TEG, especially in a flexible form, is also applied as mentioned above in wearable materials such as body heat harvesting [203–206]. Kumar, Singh, and Khare [207] even used this PVDF generator as a hybrid TEG/PENG, where a PVDF film was encapsulated with TEG.

The hybridization of PVDF and the use of a combination of different possible energy sources at the same time seems to be a very efficient and modern approach, not only for green energy harvesting [44,208]. However, their production is more complex. The most common is the combination of piezo- and triboelectric phenomena, which currently consist of, for example, the already mentioned perovskite structures and PVDF, and which can be considered as a prospective topic [209–212].

6. Conclusions

As a highlight of this review, it can be concluded that it guides the reader from the very beginning of the PVDF nanogenerator design to its final form based on current trends. The review was also written in such a way that its contents can be used by scientists who have not had much experience with PVDF before. On the other hand, for those who already have this knowledge, it may broaden their horizons in the case of new designs and solutions.

It can be summarized from the current research that the scope of PVDF nanofibers is extensive, and their combination potential is considerable. New ways of improving the fibers or layers and where to apply them are constantly evolving. According to the ScienceDirect database, the number of publications on PVDF nanogenerators has been increasing rapidly in recent years, and currently, their total number is already in the thousands. Their significant increase can be seen especially in areas such as material science and energy in the last five years. The most common topics are the aforesaid variations, mixtures, and tuning of nanofibers.

Electrospinning, which can be used to create nanofibrous structures, can be quite reliably identified as the leading fabrication method. However, despite the flexible advantage of PVDF, these structures lose out quite understandably in the areas of charge generation and permittivity. Nonetheless, this is often compensated by the mentioned tuning and doping.

The most popular characterization methods can be considered SEM for conventional imaging, together with studying the β -phase by XRD, FTIR, or Raman spectroscopy. These last three methods can be combined or may complement each other. For electrical properties investigations, the piezoelectric coefficient d_{33} , which appears in almost every electrical characterization, and the permittivity of the material are measured.

In spite of that, many papers do not discuss a reasonably important topic, and that is degradation. Therefore, it raises many questions for newly created materials. How long will these materials retain their stability? How much stress can they withstand, and what else is harmful to them? This is especially relevant in combination with perovskites. Since their primary use is as PENG, TENG, or combinations of these, increasing the mechanical stress is to be expected. Even though PVDF is in some aspects a durable polymer, it should not be relied upon entirely on this fact, given that its use is highly specific to each experiment. It is thus appropriate to use accelerated aging degradation tests to verify that the design can be utilized more than just on an experimental level.

Hence, in future years, there is expected to be a continuing trend of almost exponential growth in the development of this material, expanding the scope and commercialization of such nanogenerators for specific applications.

Author Contributions: Conceptualization, N.P., R.D. and D.S.; software, N.P.; validation, T.P. and E.Š.; formal analysis, Š.Ț. and K.Č.; resources, P.S. and K.Č.; writing—original draft preparation, N.P.; writing—review and editing, T.P., R.D. and N.P.; visualization, N.P.; project administration, Š.Ț.; funding acquisition, Š.Ț. and P.S. All authors have read and agreed to the published version of the manuscript.

Funding: Research described in the paper was financially supported by the Ministry of Education, Youth and Sports of the Czech Republic under the project CEITEC 2020 (LQ1601), by the Internal Grant Agency of Brno University of Technology, grant No. FEKT-S-20-6352, and by the Grant Agency of Czech Republic under project No. 19-17457S. Part of the work was carried out with the support of CEITEC Nano Research Infrastructure supported by MEYS CR (LM2018110).

Institutional Review Board Statement: Not applicable.

Informed Consent Statement: Not applicable.

Conflicts of Interest: The authors declare no conflicts of interest

Sample Availability: Data will be provided upon personal request to Nikola Papež. E-mail: papez@vut.cz.

Abbreviations

The following abbreviations are used in this manuscript:

AC	acetone
AFM	atomic force microscopy
ASTM	American Society for Testing and Materials
ATEC	acetyl triethyl citrate
ATR	attenuated total reflection
BET	Brunauer–Emmett–Teller
BN	boron nitride
CFE	chlorofluoroethylene
CHO	cyclohexanone
CPO	cyclopentanone
DBP	dibutyl phthalate
DBS	dibutyl sebacate
DEC	diethyl carbonate
DEP	diethyl phthalate
DMAc	dimethylacetamide
DMF	dimethyl formamide
DMSO	dimethylsulphoxide
DSC	differential scanning calorimetry
EDS	energy dispersive spectroscopy
FIB	focused ion beam
FEP	fluorinated ethylene propylene
FTIR	Fourier transform infrared spectroscopy
GBL	γ -butyrolactone
HMPA	hexamethyl phosphoramidate
IoT	internet of things
MEK	methyl ethyl ketone
NMP	<i>N</i> -methyl-2-pyrrolidone
PA6	nylon-6
PAN	polyacrylonitrile
PC	propylene carbonate
PFM	piezoresponse force microscopy
PZT	lead zirconate titanate
P&F	Press & Folding
UHD	ultrahigh definition
PENG	piezoelectric nanogenerator
PFM	piezoresponse force microscopy
PTFE	polytetrafluoroethylene
PMMA	poly(methyl methacrylate)
PVDF	polyvinylidene fluoride
PZT	lead zirconate titanate
SEM	scanning electron microscope
TBSA	<i>N,N'</i> -tetrabutylsuccindiamide
TEC	triethyl citrate
TEG	thermoelectric generator
TENG	triboelectric nanogenerator
TEP	triethyl phosphate
TGA	thermogravimetric analysis
THF	tetrahydrofuran
TMP	trimethyl phosphate
TMU	tetramethylurea
TrFE	trifluoroethylene
XPS	X-ray photoelectron spectroscopy
XRD	X-ray crystallography

References

1. Centa, U.G.; Mihelčič, M.; Bobnar, V.; Remškar, M.; Perše, L.S. The Effect of PVP on Thermal, Mechanical, and Dielectric Properties in PVDF-HFP/PVP Thin Film. *Coatings* **2022**, *12*, 1241. [[CrossRef](#)]
2. Zhang, S.; Shen, J.; Qiu, X.; Weng, D.; Zhu, W. ESR and vibrational spectroscopy study on poly(vinylidene fluoride) membranes with alkaline treatment. *J. Power Sources* **2006**, *153*, 234–238. [[CrossRef](#)]
3. Ren, Z.; Wang, Z.; Liu, Z.; Wang, L.; Guo, H.; Li, L.; Li, S.; Chen, X.; Tang, W.; Wang, Z.L. Energy Harvesting from Breeze Wind (0.7–6 m s⁻¹) Using Ultra-Stretchable Triboelectric Nanogenerator. *Adv. Energy Mater.* **2020**, *10*, 2001770. [[CrossRef](#)]
4. Ren, Z.; Ding, Y.; Nie, J.; Wang, F.; Xu, L.; Lin, S.; Chen, X.; Wang, Z.L. Environmental Energy Harvesting Adapting to Different Weather Conditions and Self-Powered Vapor Sensor Based on Humidity-Responsive Triboelectric Nanogenerators. *ACS Appl. Mater. Interfaces* **2019**, *11*, 6143–6153. [[CrossRef](#)]
5. Ren, Z.; Wang, Z.; Wang, F.; Li, S.; Wang, Z.L. Vibration behavior and excitation mechanism of ultra-stretchable triboelectric nanogenerator for wind energy harvesting. *Extrem. Mech. Lett.* **2021**, *45*, 101285. [[CrossRef](#)]
6. Tofel, P.; Částková, K.; Říha, D.; Sobola, D.; Papež, N.; Kaštyl, J.; Ťálu, Š.; Hadaš, Z. Triboelectric Response of Electrospun Stratified PVDF and PA Structures. *Nanomaterials* **2022**, *12*, 349. [[CrossRef](#)]
7. Singh, H.H.; Khare, N. Flexible ZnO-PVDF/PTFE based piezo-tribo hybrid nanogenerator. *Nano Energy* **2018**, *51*, 216–222. [[CrossRef](#)]
8. Mariello, M. Recent Advances on Hybrid Piezo-Triboelectric Bio-Nanogenerators: Materials, Architectures and Circuitry. *Nanoenergy Adv.* **2022**, *2*, 4. [[CrossRef](#)]
9. Wang, X.; Yang, B.; Liu, J.; Zhu, Y.; Yang, C.; He, Q. A flexible triboelectric-piezoelectric hybrid nanogenerator based on P(VDF-TrFE) nanofibers and PDMS/MWCNT for wearable devices. *Sci. Rep.* **2016**, *6*, 36409. [[CrossRef](#)]
10. Jung, W.S.; Kang, M.G.; Moon, H.G.; Baek, S.H.; Yoon, S.J.; Wang, Z.L.; Kim, S.W.; Kang, C.Y. High Output Piezo/Triboelectric Hybrid Generator. *Sci. Rep.* **2015**, *5*, 9309. [[CrossRef](#)]
11. Lapčinskis, L.; Mā Lnieks, K.; Linarts, A.; Blū Ms, J.; Šmits, K.N.; Järvekūlg, M.; Knite, M.R.; Šutka, A. Hybrid Tribo-Piezo-Electric Nanogenerator with Unprecedented Performance Based on Ferroelectric Composite Contacting Layers. *ACS Appl. Energy Mater.* **2019**, *2*, 4027–4032. [[CrossRef](#)]
12. Ren, Z.; Nie, J.; Shao, J.; Lai, Q.; Wang, L.; Chen, J.; Chen, X.; Lin Wang, Z.; Ren, Z.; Nie, J.; et al. Fully Elastic and Metal-Free Tactile Sensors for Detecting both Normal and Tangential Forces Based on Triboelectric Nanogenerators. *Adv. Funct. Mater.* **2018**, *28*, 1802989. [[CrossRef](#)]
13. Bohlén, M.; Bolton, K. Conformational studies of poly(vinylidene fluoride), poly(trifluoroethylene) and poly(vinylidene fluoride-co-trifluoroethylene) using density functional theory. *Phys. Chem. Chem. Phys.* **2014**, *16*, 12929–12939. [[CrossRef](#)] [[PubMed](#)]
14. Ruan, L.; Yao, X.; Chang, Y.; Zhou, L.; Qin, G.; Zhang, X. Properties and Applications of the β Phase Poly(vinylidene fluoride). *Polymers* **2018**, *10*, 228. [[CrossRef](#)]
15. McKeen, L. *Film Properties of Plastics and Elastomers*, 3rd ed.; William Andrew Publishing: Boston, MA, USA, 2012; p. 408. [[CrossRef](#)]
16. Song, R.; Yang, D.; He, L. Effect of surface modification of nanosilica on crystallization, thermal and mechanical properties of poly(vinylidene fluoride). *J. Mater. Sci.* **2007**, *42*, 8408–8417. [[CrossRef](#)]
17. Pisarenko, T.; Papež, N.; Sobola, D.; Ťálu, Š.; Částková, K.; Škarvada, P.; Macků, R.; Ščasnovič, E.; Kaštyl, J. Comprehensive Characterization of PVDF Nanofibers at Macro- and Nanolevel. *Polymers* **2022**, *14*, 593. [[CrossRef](#)]
18. Lin, Y.; Zhang, Y.; Zhang, F.; Zhang, M.; Li, D.; Deng, G.; Guan, L.; Dong, M. Studies on the electrostatic effects of stretched PVDF films and nanofibers. *Nanoscale Res. Lett.* **2021**, *16*, 79. [[CrossRef](#)]
19. Saxena, P.; Shukla, P. A comprehensive review on fundamental properties and applications of poly(vinylidene fluoride) (PVDF). *Adv. Compos. Hybrid Mater.* **2021**, *4*, 8–26. [[CrossRef](#)]
20. Kang, G.-d.; ming Cao, Y. Application and modification of poly(vinylidene fluoride) (PVDF) membranes—A review. *J. Membr. Sci.* **2014**, *463*, 145–165. [[CrossRef](#)]
21. Xin, Y.; Zhu, J.; Sun, H.; Xu, Y.; Liu, T.; Qian, C. A brief review on piezoelectric PVDF nanofibers prepared by electrospinning. *Ferroelectrics* **2018**, *526*, 140–151. [[CrossRef](#)]
22. Atif, R.; Khaliq, J.; Combrinck, M.; Hassanin, A.H.; Shehata, N.; Elnabawy, E.; Shyha, I. Solution Blow Spinning of Polyvinylidene Fluoride Based Fibers for Energy Harvesting Applications: A Review. *Polymers* **2020**, *12*, 1304. [[CrossRef](#)] [[PubMed](#)]
23. Wang, Y.; Zhu, L.; Du, C. Progress in Piezoelectric Nanogenerators Based on PVDF Composite Films. *Micromachines* **2021**, *12*, 1278. [[CrossRef](#)] [[PubMed](#)]
24. He, Z.; Rault, F.; Lewandowski, M.; Mohsenzadeh, E.; Salaün, F. Electrospun PVDF nanofibers for piezoelectric applications: A review of the influence of electrospinning parameters on the β phase and crystallinity enhancement. *Polymers* **2021**, *13*, 174. [[CrossRef](#)]
25. Liu, F.; Hashim, N.A.; Liu, Y.; Abed, M.R.; Li, K. Progress in the production and modification of PVDF membranes. *J. Membr. Sci.* **2011**, *375*, 1–27. [[CrossRef](#)]
26. Wu, L.; Jin, Z.; Liu, Y.; Ning, H.; Liu, X.; Alamusi.; Hu, N. Recent advances in the preparation of PVDF-based piezoelectric materials. *Nanotechnol. Rev.* **2022**, *11*, 1386–1407. [[CrossRef](#)]
27. Palazzetti, R.; Zucchelli, A. Electrospun nanofibers as reinforcement for composite laminates materials—A review. *Compos. Struct.* **2017**, *182*, 711–727. [[CrossRef](#)]

28. Fotouhi, M.; Saghafi, H.; Brugo, T.; Minak, G.; Fragassa, C.; Zucchelli, A.; Ahmadi, M. Effect of PVDF nanofibers on the fracture behavior of composite laminates for high-speed woodworking machines. *Proc. Inst. Mech. Eng. Part J. Mech. Eng. Sci.* **2016**, *231*, 31–43. [[CrossRef](#)]
29. Wu, Q.; Tiraferri, A.; Wu, H.; Xie, W.; Liu, B. Improving the Performance of PVDF/PVDF-g-PEGMA Ultrafiltration Membranes by Partial Solvent Substitution with Green Solvent Dimethyl Sulfoxide during Fabrication. *ACS Omega* **2019**, *4*, 19799–19807. [[CrossRef](#)]
30. Částková, K.; Kastyl, J.; Sobola, D.; Petruš, J.; Šťastná, E.; Říha, D.; Tofel, P. Structure–Properties Relationship of Electrospun PVDF Fibers. *Nanomaterials* **2020**, *10*, 1221. [[CrossRef](#)]
31. Gee, S.; Johnson, B.; Smith, A.L. Optimizing electrospinning parameters for piezoelectric PVDF nanofiber membranes. *J. Membr. Sci.* **2018**, *563*, 804–812. [[CrossRef](#)]
32. Ghafari, E.; Jiang, X.; Lu, N. Surface morphology and β -phase formation of single polyvinylidene fluoride (PVDF) composite nanofibers. *Adv. Compos. Hybrid Mater.* **2017**, *1*, 332–340. [[CrossRef](#)]
33. Shao, H.; Fang, J.; Wang, H.; Lin, T. Effect of electrospinning parameters and polymer concentrations on mechanical-to-electrical energy conversion of randomly-oriented electrospun poly(vinylidene fluoride) nanofiber mats. *RSC Adv.* **2015**, *5*, 14345–14350. [[CrossRef](#)]
34. Fu, R.; Chen, S.; Lin, Y.; He, Y.; Gu, Y. Preparation and piezoelectric investigation of electrospun polyvinylidene fluoride fibrous membrane. *J. Nanosci. Nanotechnol.* **2016**, *16*, 12337–12343. [[CrossRef](#)]
35. Magniez, K.; De Lavigne, C.; Fox, B.L. The effects of molecular weight and polymorphism on the fracture and thermo-mechanical properties of a carbon-fibre composite modified by electrospun poly(vinylidene fluoride) membranes. *Polymer* **2010**, *12*, 2585–2596. [[CrossRef](#)]
36. Zaarour, B.; Zhu, L.; Jin, X. Controlling the surface structure, mechanical properties, crystallinity, and piezoelectric properties of electrospun PVDF nanofibers by maneuvering molecular weight. *Soft Mater.* **2019**, *17*, 181–189. [[CrossRef](#)]
37. Lei, T.; Yu, L.; Zheng, G.; Wang, L.; Wu, D.; Sun, D. Electrospinning-induced preferred dipole orientation in PVDF fibers. *J. Mater. Sci.* **2015**, *50*, 4342–4347. [[CrossRef](#)]
38. Liu, Z.H.; Pan, C.T.; Lin, L.W.; Huang, J.C.; Ou, Z.Y. Direct-write PVDF nonwoven fiber fabric energy harvesters via the hollow cylindrical near-field electrospinning process. *Smart Mater. Struct.* **2013**, *23*, 025003. [[CrossRef](#)]
39. Wang, Y.R.; Zheng, J.M.; Ren, G.Y.; Zhang, P.H.; Xu, C. A flexible piezoelectric force sensor based on PVDF fabrics. *Smart Mater. Struct.* **2011**, *20*, 045009. [[CrossRef](#)]
40. Mokhtari, F.; Shamsirsaz, M.; Latifi, M.; Foroughi, J. Nanofibers-Based Piezoelectric Energy Harvester for Self-Powered Wearable Technologies. *Polymers* **2020**, *12*, 2697. [[CrossRef](#)]
41. Hansen, C.M. *Hansen Solubility Parameters: A User's Handbook*, 2nd ed.; CRC Press: Boca Raton, FL, USA, 2007; p. 544. [[CrossRef](#)]
42. Egemen, E.; Nirmalakhandan, N.; Trevizo, C. Predicting surface tension of liquid organic solvents. *Environ. Sci. Technol.* **2000**, *34*, 2596–2600. [[CrossRef](#)]
43. Marshall, J.E.; Zhenova, A.; Roberts, S.; Petchey, T.; Zhu, P.; Dancer, C.E.; McElroy, C.R.; Kendrick, E.; Goodship, V. On the Solubility and Stability of Polyvinylidene Fluoride. *Polymers* **2021**, *13*, 1354. [[CrossRef](#)] [[PubMed](#)]
44. Zhou, Y.; Zhang, S.; Xu, X.; Liu, W.; Zhang, S.; Li, G.; He, J. Dynamic piezo-thermoelectric generator for simultaneously harvesting mechanical and thermal energies. *Nano Energy* **2020**, *69*, 104397. [[CrossRef](#)]
45. Li, Y.; Liao, C.; Tjong, S.C. Electrospun Polyvinylidene Fluoride-Based Fibrous Scaffolds with Piezoelectric Characteristics for Bone and Neural Tissue Engineering. *Nanomaterials* **2019**, *9*, 952. [[CrossRef](#)] [[PubMed](#)]
46. Li, B.M.; Ju, B.; Zhou, Y.; Knowles, C.G.; Rosenberg, Z.; Flewellin, T.J.; Kose, F.; Jur, J.S. Airbrushed PVDF-TrFE Fibrous Sensors for E-Textiles. *ACS Appl. Electron. Mater.* **2021**, *3*, 5307–5326. [[CrossRef](#)]
47. Cho, E.; Kim, C.; Kook, J.K.; Jeong, Y.I.; Kim, J.H.; Kim, Y.A.; Endo, M.; Hwang, C.H. Fabrication of electrospun PVDF nanofiber membrane for Western blot with high sensitivity. *J. Membr. Sci.* **2012**, *389*, 349–354. [[CrossRef](#)]
48. Gupta, V.; Babu, A.; Ghosh, S.K.; Mallick, Z.; Mishra, H.K.; Saini, D.; Mandal, D. Revisiting δ -PVDF based piezoelectric nanogenerator for self-powered pressure mapping sensor. *Appl. Phys. Lett.* **2021**, *119*, 252902. [[CrossRef](#)]
49. Yu, L.; Zhou, P.; Wu, D.; Wang, L.; Lin, L.; Sun, D. Shoepad nanogenerator based on electrospun PVDF nanofibers. *Microsyst. Technol.* **2018**, *25*, 3151–3156. [[CrossRef](#)]
50. Sedlak, P.; Gajdos, A.; Macku, R.; Majzner, J.; Holcman, V.; Sedlakova, V.; Kubersky, P. The effect of thermal treatment on ac/dc conductivity and current fluctuations of PVDF/NMP/[EMIM][TFSI] solid polymer electrolyte. *Sci. Rep.* **2020**, *10*, 21140. [[CrossRef](#)]
51. Kalimuldina, G.; Turdakyn, N.; Abay, I.; Medeubayev, A.; Nurpeissova, A.; Adair, D.; Bakenov, Z. A Review of Piezoelectric PVDF Film by Electrospinning and Its Applications. *Sensors* **2020**, *20*, 5214. [[CrossRef](#)]
52. Sengupta, A.; Das, S.; Dasgupta, S.; Sengupta, P.; Datta, P. Flexible Nanogenerator from Electrospun PVDF-Polycarbazole Nanofiber Membranes for Human Motion Energy-Harvesting Device Applications. *ACS Biomater. Sci. Eng.* **2021**, *7*, 1673–1685. doi: 10.1021/acsbiomaterials.0c01730. [[CrossRef](#)]
53. Shi, L.; Jin, H.; Dong, S.; Huang, S.; Kuang, H.; Xu, H.; Chen, J.; Xuan, W.; Zhang, S.; Li, S.; et al. High-performance triboelectric nanogenerator based on electrospun PVDF-graphene nanosheet composite nanofibers for energy harvesting. *Nano Energy* **2021**, *80*, 105599. [[CrossRef](#)]
54. Li, C.; Wang, H.; Yan, X.; Chen, H.; Fu, Y.; Meng, Q. Enhancement Research on Piezoelectric Performance of Electrospun PVDF Fiber Membranes with Inorganic Reinforced Materials. *Coatings* **2021**, *11*, 1495. [[CrossRef](#)]

55. Costa, L.M.M.; Bretas, R.E.S.; Gregorio, R.; Costa, L.M.M.; Bretas, R.E.S.; Gregorio, R. Effect of Solution Concentration on the Electrospay/Electrospinning Transition and on the Crystalline Phase of PVDF. *Mater. Sci. Appl.* **2010**, *1*, 247–252. [[CrossRef](#)]
56. Correia, D.M.; Gonçalves, R.; Ribeiro, C.; Sencadas, V.; Botelho, G.; Ribelles, J.L.; Lanceros-Méndez, S. Electrospayed poly(vinylidene fluoride) microparticles for tissue engineering applications. *RSC Adv.* **2014**, *4*, 33013–33021. [[CrossRef](#)]
57. Kliem, H.; Tadros-Morgane, R. Extrinsic versus intrinsic ferroelectric switching: Experimental investigations using ultra-thin PVDF Langmuir–Blodgett films. *J. Phys. Appl. Phys.* **2005**, *38*, 1860. [[CrossRef](#)]
58. Chen, S.; Li, X.; Yao, K.; Tay, F.E.H.; Kumar, A.; Zeng, K. Self-polarized ferroelectric PVDF homopolymer ultra-thin films derived from Langmuir–Blodgett deposition. *Polymer* **2012**, *53*, 1404–1408. [[CrossRef](#)]
59. Cozza, E.S.; Monticelli, O.; Marsano, E.; Cebe, P. On the electrospinning of PVDF: Influence of the experimental conditions on the nanofiber properties. *Polym. Int.* **2013**, *62*, 41–48. [[CrossRef](#)]
60. Motamedi, A.S.; Mirzadeh, H.; Hajiesmaeilbaigi, F.; Bagheri-Khoulenjani, S.; Shokrgozar, M.A. Effect of electrospinning parameters on morphological properties of PVDF nanofibrous scaffolds. *Prog. Biomater.* **2017**, *6*, 113–123. [[CrossRef](#)]
61. Černohorský, P.; Pisarenko, T.; Papež, N.; Sobola, D.; Ťálu, Š.; Částková, K.; Kaštyl, J.; Macků, R.; Škarvada, P.; Sedlák, P. Structure Tuning and Electrical Properties of Mixed PVDF and Nylon Nanofibers. *Materials* **2021**, *14*, 6096. [[CrossRef](#)]
62. Yu, Z.; Chen, M.; Wang, Y.; Zheng, J.; Zhang, Y.; Zhou, H.; Li, D. Nanoporous PVDF Hollow Fiber Employed Piezo-Tribo Nanogenerator for Effective Acoustic Harvesting. *ACS Appl. Mater. Interfaces* **2021**, *13*, 26981–26988. [[CrossRef](#)]
63. Na, H.; Chen, P.; Wong, S.C.; Hague, S.; Li, Q. Fabrication of PVDF/PVA microtubules by coaxial electrospinning. *Polymer* **2012**, *53*, 2736–2743. [[CrossRef](#)]
64. Ponnamma, D.; Chamakh, M.M.; Alahzm, A.M.; Salim, N.; Hameed, N.; Almaadeed, M.A.A. Core-Shell Nanofibers of Polyvinylidene Fluoride-based Nanocomposites as Piezoelectric Nanogenerators. *Polymers* **2020**, *12*, 2344. [[CrossRef](#)]
65. Asai, H.; Kikuchi, M.; Shimada, N.; Nakane, K. Effect of melt and solution electrospinning on the formation and structure of poly(vinylidene fluoride) fibres. *RSC Adv.* **2017**, *7*, 17593–17598. [[CrossRef](#)]
66. Fontananova, E.; Bahattab, M.A.; Aljlil, S.A.; Alowairdy, M.; Rinaldi, G.; Vuono, D.; Nagy, J.B.; Drioli, E.; Di Profio, G. From hydrophobic to hydrophilic polyvinylidene fluoride (PVDF) membranes by gaining new insight into material's properties. *RSC Adv.* **2015**, *5*, 56219–56231. [[CrossRef](#)]
67. Hamad, M.E.; Al-Gharabli, S.; Kujawa, J. Tunable hydrophobicity and roughness on PVDF surface by grafting to mode—Approach to enhance membrane performance in membrane distillation process. *Sep. Purif. Technol.* **2022**, *291*, 120935. [[CrossRef](#)]
68. Sheikh, F.A.; Cantu, T.; Macossay, J.; Kim, H. Fabrication of Poly(vinylidene fluoride) (PVDF) Nanofibers Containing Nickel Nanoparticles as Future Energy Server Materials. *Sci. Adv. Mater.* **2011**, *3*, 216–222. [[CrossRef](#)]
69. Issa, A.; Al-Maadeed, M.; Luyt, A.; Ponnamma, D.; Hassan, M. Physico-Mechanical, Dielectric, and Piezoelectric Properties of PVDF Electrospun Mats Containing Silver Nanoparticles. *C J. Carbon Res.* **2017**, *3*, 30. [[CrossRef](#)]
70. Mokhtari, F.; Spinks, G.M.; Fay, C.; Cheng, Z.; Raad, R.; Xi, J.; Foroughi, J. Wearable Electronic Textiles from Nanostructured Piezoelectric Fibers. *Adv. Mater. Technol.* **2020**, *5*, 1900900. [[CrossRef](#)]
71. Ji, J.; Liu, F.; Hashim, N.A.; Abed, M.R.; Li, K. Poly(vinylidene fluoride) (PVDF) membranes for fluid separation. *React. Funct. Polym.* **2015**, *86*, 134–153. [[CrossRef](#)]
72. Shen, L.; Feng, S.; Li, J.; Chen, J.; Li, F.; Lin, H.; Yu, G. Surface modification of polyvinylidene fluoride (PVDF) membrane via radiation grafting: novel mechanisms underlying the interesting enhanced membrane performance. *Sci. Rep.* **2017**, *7*, 2721. [[CrossRef](#)]
73. He, Z.; Rault, F.; Vishwakarma, A.; Mohsenzadeh, E.; Salaün, F. High-Aligned PVDF Nanofibers with a High Electroactive Phase Prepared by Systematically Optimizing the Solution Property and Process Parameters of Electrospinning. *Coatings* **2022**, *12*, 1310. [[CrossRef](#)]
74. Sobola, D.; Kaspar, P.; Částková, K.; Dallaev, R.; Papež, N.; Sedlák, P.; Trčka, T.; Orudzhev, F.; Kaštyl, J.; Weiser, A.; et al. PVDF Fibers Modification by Nitrate Salts Doping. *Polymers* **2021**, *13*, 2439. [[CrossRef](#)] [[PubMed](#)]
75. Tubio, C.R.; Costa, P.; Nguyen, D.N.; Moon, W. Significant Electromechanical Characteristic Enhancement of Coaxial Electrospinning Core-Shell Fibers. *Polymers* **2022**, *14*, 1739. [[CrossRef](#)]
76. Sharma, T.; Naik, S.; Langevine, J.; Gill, B.; Zhang, J.X. Aligned PVDF-TrFE nanofibers with high-density PVDF nanofibers and PVDF core-shell structures for endovascular pressure sensing. *IEEE Trans. Biomed. Eng.* **2015**, *62*, 188–195. [[CrossRef](#)]
77. Wang, S.; Shi, K.; Chai, B.; Qiao, S.; Huang, Z.; Jiang, P.; Huang, X. Core-shell structured silk Fibroin/PVDF piezoelectric nanofibers for energy harvesting and self-powered sensing. *Nano Mater. Sci.* **2022**, *4*, 126–132. [[CrossRef](#)]
78. Horchidan, N.; Ciomaga, C.E.; Curecheriu, L.P.; Stoian, G.; Botea, M.; Florea, M.; Maraloiu, V.A.; Pintilie, L.; Tufescu, F.M.; Tiron, V.; et al. Increasing Permittivity and Mechanical Harvesting Response of PVDF-Based Flexible Composites by Using Ag Nanoparticles onto BaTiO₃ Nanofillers. *Nanomaterials* **2022**, *12*, 934. [[CrossRef](#)]
79. Mendes, S.F.; Costa, C.M.; Caparros, C.; Sencadas, V.; Lanceros-Méndez, S. Effect of filler size and concentration on the structure and properties of poly(vinylidene fluoride)/BaTiO₃ nanocomposites. *J. Mater. Sci.* **2012**, *47*, 1378–1388. [[CrossRef](#)]
80. Lee, Y.J.; Jeong, S.K.; Jo, N.J. PVDF-Based Nanocomposite Solid Polymer Electrolytes; the Effect of Affinity Between PVDF and Filler on Ionic Conductivity. *Compos. Interfaces* **2012**, *16*, 347–358. [[CrossRef](#)]
81. Li, Y.; Wang, Z.; Li, Y.; Yi, Z. Enhanced breakdown strength of PVDF textile composites by BiFeO₃ fibers in low loading. *J. Mater. Sci. Mater. Electron.* **2022**, *33*, 3215–3224. [[CrossRef](#)]
82. Ichangi, A.; Khan, L.; Queraltó, A.; Grosch, M.; Weißing, R.; Ünlü, F.; Chijioke, A.K.; Verma, A.; Fischer, T.; Surmenev, R.; et al. Electrospun BiFeO₃ Nanofibers for Vibrational Energy Harvesting Application. *Adv. Eng. Mater.* **2021**, *24*, 2101394. [[CrossRef](#)]

83. Hu, X.; Che, Y.; Zhang, Z.; Shen, Q.D.; Chu, B. BiFeO₃-BaTiO₃/P(VDF-TrFE) Multifunctional Polymer Nanocomposites. *ACS Appl. Electron. Mater.* **2021**, *3*, 743–751. [[CrossRef](#)]
84. Ramazanov, S.; Sobola, D.; Orudzhev, F.; Knápek, A.; Polčák, J.; Potoček, M.; Kaspar, P.; Dallaev, R. Surface Modification and Enhancement of Ferromagnetism in BiFeO₃ Nanofilms Deposited on HOPG. *Nanomaterials* **2020**, *10*, 1990. [[CrossRef](#)] [[PubMed](#)]
85. Kalani, S.; Kohandani, R.; Bagherzadeh, R. Flexible electrospun PVDF–BaTiO₃ hybrid structure pressure sensor with enhanced efficiency. *RSC Adv.* **2020**, *10*, 35090–35098. [[CrossRef](#)]
86. Kumar, M.; Kulkarni, N.D.; Kumari, P. Fabrication and characterization of PVDF/BaTiO₃ nanocomposite for energy harvesting application. *Mater. Today Proc.* **2022**, *56*, 1151–1155. [[CrossRef](#)]
87. Abdolmaleki, H.; Agarwala, S. PVDF–BaTiO₃ Nanocomposite Inkjet Inks with Enhanced β -Phase Crystallinity for Printed Electronics. *Polymers* **2020**, *12*, 2430. [[CrossRef](#)]
88. Ramesh, D.; D'Souza, N.A. One-step fabrication of biomimetic PVDF–BaTiO₃ nanofibrous composite using DoE. *Mater. Res. Express* **2018**, *5*, 085308. [[CrossRef](#)]
89. Sreejivungsa, K.; Phromviyo, N.; Swatsitang, E.; Thongbai, P. Characterizations and Significantly Enhanced Dielectric Properties of PVDF Polymer Nanocomposites by Incorporating Gold Nanoparticles Deposited on BaTiO₃ Nanoparticles. *Polymers* **2021**, *13*, 4144. [[CrossRef](#)]
90. Wang, J.; Hu, J.; Sun, Q.; Zhu, K.; Li, B.W.; Qiu, J. Dielectric and energy storage performances of PVDF-based composites with colossal permittivity Nd-doped BaTiO₃ nanoparticles as the filler. *AIP Adv.* **2017**, *7*, 125104. [[CrossRef](#)]
91. Hussein, A.D.; Sabry, R.S.; Abdul Azeez Dakhil, O.; Bagherzadeh, R. Effect of Adding BaTiO₃ to PVDF as Nano Generator. *J. Phys. Conf. Ser.* **2019**, *1294*, 022012. [[CrossRef](#)]
92. Ma, J.; Zhang, Q.; Lin, K.; Zhou, L.; Ni, Z. Piezoelectric and optoelectronic properties of electrospinning hybrid PVDF and ZnO nanofibers. *Mater. Res. Express* **2018**, *5*, 35057. [[CrossRef](#)]
93. Li, G.Y.; Zhang, H.D.; Guo, K.; Ma, X.S.; Long, Y.Z. Fabrication and piezoelectric-pyroelectric properties of electrospun PVDF/ZnO composite fibers. *Mater. Res. Express* **2020**, *7*, 095502. [[CrossRef](#)]
94. Yun, J.S.; Park, C.K.; Jeong, Y.H.; Cho, J.H.; Paik, J.H.; Yoon, S.H.; Hwang, K.R. The Fabrication and Characterization of Piezoelectric PZT/PVDF Electrospun Nanofiber Composites. *Nanomater. Nanotechnol.* **2016**, *6*, 20. [[CrossRef](#)]
95. He, W.; Guo, Y.; Zhao, Y.B.; Jiang, F.; Schmitt, J.; Yue, Y.; Liu, J.; Cao, J.; Wang, J. Self-supporting smart air filters based on PZT/PVDF electrospun nanofiber composite membrane. *Chem. Eng. J.* **2021**, *423*, 130247. [[CrossRef](#)]
96. Fortunato, M.; Cavallini, D.; De Bellis, G.; Marra, F.; Tamburrano, A.; Sarto, F.; Sarto, M.S. Phase Inversion in PVDF Films with Enhanced Piezoresponse Through Spin-Coating and Quenching. *Polymers* **2019**, *11*, 1096. [[CrossRef](#)] [[PubMed](#)]
97. Salimi, A.; Yousefi, A.A. Analysis Method: FTIR studies of β -phase crystal formation in stretched PVDF films. *Polym. Test.* **2003**, *22*, 699–704. [[CrossRef](#)]
98. Lim, J.Y.; Kim, S.; Seo, Y. Enhancement of β -phase in PVDF by electrospinning. *AIP Conf. Proc.* **2015**, *1664*, 070006. [[CrossRef](#)]
99. Kabir, E.; Khatun, M.; Nasrin, L.; Raihan, M.J.; Rahman, M. Pure β -phase formation in polyvinylidene fluoride (PVDF)-carbon nanotube composites. *J. Phys. Appl. Phys.* **2017**, *50*, 163002. [[CrossRef](#)]
100. Vasic, N.; Steinmetz, J.; Görke, M.; Sinapius, M.; Hühne, C.; Garnweitner, G. Phase Transitions of Polarised PVDF Films in a Standard Curing Process for Composites. *Polymers* **2021**, *13*, 3900. [[CrossRef](#)]
101. Meng, N.; Ren, X.; Santagiuliana, G.; Ventura, L.; Zhang, H.; Wu, J.; Yan, H.; Reece, M.J.; Bilotti, E. Ultrahigh β -phase content poly(vinylidene fluoride) with relaxor-like ferroelectricity for high energy density capacitors. *Nat. Commun.* **2019**, *10*, 4535. [[CrossRef](#)]
102. Sedlak, P.; Sobola, D.; Gajdos, A.; Dallaev, R.; Nebojsa, A.; Kubersky, P. Surface Analyses of PVDF/NMP/[EMIM][TFSI] Solid Polymer Electrolyte. *Polymers* **2021**, *13*, 2678. [[CrossRef](#)]
103. Naga Kumar, C.; Prabhakar, M.N.; il Song, J. Synthesis of vinyl ester resin-carrying PVDF green nanofibers for self-healing applications. *Sci. Rep.* **2021**, *11*, 908. [[CrossRef](#)] [[PubMed](#)]
104. Victor, F.S.; Kugarajah, V.; Bangaru, M.; Ranjan, S.; Dharmalingam, S. Electrospun nanofibers of polyvinylidene fluoride incorporated with titanium nanotubes for purifying air with bacterial contamination. *Environ. Sci. Pollut. Res.* **2021**, *28*, 37520–37533. [[CrossRef](#)] [[PubMed](#)]
105. Sheikh, F.A.; Zargar, M.A.; Tamboli, A.H.; Kim, H. A super hydrophilic modification of poly(vinylidene fluoride) (PVDF) nanofibers: By in situ hydrothermal approach. *Appl. Surf. Sci.* **2016**, *385*, 417–425. [[CrossRef](#)]
106. Ding, R.; Wong, M.C.; Hao, J. Recent advances in hybrid perovskite nanogenerators. *EcoMat* **2020**, *2*, e12057. [[CrossRef](#)]
107. Abdullah, I.Y.; Yahaya, M.; Jumali, M.H.H.; Shanshool, H.M. Effect of annealing process on the phase formation in Poly(vinylidene fluoride) thin films. *AIP Conf. Proc.* **2014**, *1614*, 147–151. [[CrossRef](#)]
108. Mohd Dahan, R.; Arshad, A.N.; Mohamed, N.A.; Engku Zawawi, E.Z.; Kamarun, D.; Wahid, M.H.; Sarip, M.N.; Rusop Mahmood, M. ATR-FTIR Analysis on Polymorphism of PVDF/MgO Nanocomposite Thin Films. *Adv. Mater. Res.* **2016**, *1134*, 39–43. [[CrossRef](#)]
109. Nakhowong, R. Fabrication of PVDF/PVP nanofiltration membrane containing chitosan/activated carbon/Ag nanoparticles by electrospinning and their antibacterial activity. *SNRU J. Sci. Technol.* **2020**, *12*, 137–145.
110. Bai, H.; Wang, X.; Zhou, Y.; Zhang, L. Preparation and characterization of poly(vinylidene fluoride) composite membranes blended with nano-crystalline cellulose. *Prog. Nat. Sci. Mater. Int.* **2012**, *22*, 250–257. [[CrossRef](#)]
111. Lanceros-Méndez, S.; Mano, J.F.; Costa, A.M.; Schmidt, V.H. FTIR and DSC studies of mechanically deformed β -PVDF films. *J. Macromol. Sci. Part B* **2007**, *40 B*, 517–527. [[CrossRef](#)]

112. Chapron, D.; Rault, F.; Talbourdet, A.; Lemort, G.; Cochrane, C.; Bourson, P.; Devaux, E.; Campagne, C. In-situ Raman monitoring of the poly(vinylidene fluoride) crystalline structure during a melt-spinning process. *J. Raman Spectrosc.* **2021**, *52*, 1073–1079. [[CrossRef](#)]
113. Kobayashi, M.; Tashiro, K.; Tadokoro, H. Molecular Vibrations of Three Crystal Forms of Poly(vinylidene fluoride). *Macromolecules* **1975**, *8*, 158–171. [[CrossRef](#)]
114. Chipara, D.; Kuncser, V.; Lozano, K.; Alcoutlabi, M.; Ibrahim, E.; Chipara, M. Spectroscopic investigations on PVDF-Fe₂O₃ nanocomposites. *J. Appl. Polym. Sci.* **2020**, *137*, 48907. [[CrossRef](#)]
115. Shepelin, N.A.; Glushenkov, A.M.; Lussini, V.C.; Fox, P.J.; Dicinowski, G.W.; Shapter, J.G.; Ellis, A.V. New developments in composites, copolymer technologies and processing techniques for flexible fluoropolymer piezoelectric generators for efficient energy harvesting. *Energy Environ. Sci.* **2019**, *12*, 1143–1176. [[CrossRef](#)]
116. Tabari, R.S.; Chen, Y.; Thummavichai, K.; Zhang, Y.; Saadi, Z.; Neves, A.I.; Xia, Y.; Zhu, Y. Piezoelectric Property of Electrospun PVDF Nanofibers as Linking Tips of Artificial-Hair-Cell Structures in Cochlea. *Nanomaterials* **2022**, *12*, 1466. [[CrossRef](#)]
117. Moazeni, N.; Latifi, M.; Merati, A.A.; Rouhani, S. Crystal polymorphism in polydiacetylene-embedded electrospun polyvinylidene fluoride nanofibers. *Soft Matter* **2017**, *13*, 8178–8187. [[CrossRef](#)]
118. Saha, S.; Yauvana, V.; Chakraborty, S.; Sanyal, D. Synthesis and Characterization of Polyvinylidene-fluoride (PVDF) Nanofiber for Application as Piezoelectric Force Sensor. *Mater. Today Proc.* **2019**, *18*, 1450–1458. [[CrossRef](#)]
119. Chethan, P.B.; Renukappa, N.M.; Sanjeev, G. Preparation and crystalline studies of PVDF hybrid composites. *AIP Conf. Proc.* **2018**, *1942*, 050066. [[CrossRef](#)]
120. Huang, F.; Wei, Q.; Wang, J.; Cai, Y.; Huang, Y. Effect of temperature on structure, morphology and crystallinity of PVDF nanofibers via electrospinning. *e-Polymers* **2008**, *8*, 1–8. [[CrossRef](#)]
121. Liu, X.; Kuang, X.; Xu, S.; Wang, X. High-sensitivity piezoresponse force microscopy studies of single polyvinylidene fluoride nanofibers. *Mater. Lett.* **2017**, *191*, 189–192. [[CrossRef](#)]
122. Pisarenko, T. Characterization of PVDF nanofibers created by the electrospinning method. In Proceedings of the 26th Conference STUDENT EEICT 2020, Brno, Czech Republic, 23 April 2020; Vítězslav, N., Ed.; Brno University of Technology, Faculty of Electrical Engineering and Communication: Brno, Czech Republic, 2020; pp. 287–291.
123. Țălu, Ș. *Micro and Nanoscale Characterization of Three Dimensional Surfaces: Basics and Applications*; Napoca Star Publishing House: Cluj-Napoca, Romania, 2015.
124. Szewczyk, P.K.; Gradys, A.; Kim, S.K.; Persano, L.; Marzec, M.; Krysztal, A.; Busolo, T.; Toncelli, A.; Pisignano, D.; Bernasik, A.; et al. Enhanced Piezoelectricity of Electrospun Polyvinylidene Fluoride Fibers for Energy Harvesting. *ACS Appl. Mater. Interfaces* **2020**, *12*, 13575–13583. [[CrossRef](#)] [[PubMed](#)]
125. Tohluébaji, N.; Putson, C.; Muensit, N.; Yuennan, J. Electrostrictive and structural properties of poly(Vinylidene fluoride-hexafluoropropylene) composite nanofibers filled with polyaniline (emeraldine base). *Polymers* **2021**, *13*, 3250. [[CrossRef](#)] [[PubMed](#)]
126. Ren, X.; Meng, N.; Zhang, H.; Wu, J.; Abrahams, I.; Yan, H.; Bilotti, E.; Reece, M.J. Giant energy storage density in PVDF with internal stress engineered polar nanostructures. *Nano Energy* **2020**, *72*, 104662. [[CrossRef](#)]
127. Wang, T.; Peng, R.C.; Peng, W.; Dong, G.; Zhou, C.; Yang, S.; Zhou, Z.; Liu, M.; Wang, T.; Peng, R.C.; et al. 2–2 Type PVDF-Based Composites Interlayered by Epitaxial (111)-Oriented BTO Films for High Energy Storage Density. *Adv. Funct. Mater.* **2022**, *32*, 2108496. [[CrossRef](#)]
128. Jing, L.; Li, W.; Gao, C.; Li, M.; Fei, W. Achieving High Energy Storage Performance in Polymer-Based Composites with Opposite Double Heterojunction Via Electric Field Tailoring. *SSRN Electron. J.* **2022**. [[CrossRef](#)]
129. Meng, G.; She, J.; Wang, C.; Wang, W.; Pan, C.; Cheng, Y. Sandwich-Structured h-BN/PVDF/h-BN Film With High Dielectric Strength and Energy Storage Density. *Front. Chem.* **2022**, *10*, 681. [[CrossRef](#)]
130. Cui, Y.; Ma, Y.; Zhang, Y.; Lin, X.; Zhang, S.; Si, T.; Zhang, C. Effect of multilayer structure on energy storage characteristics of PVDF ferroelectric polymer In Proceedings of the 2022 4th International Conference on Intelligent Control, Measurement and Signal Processing (ICMSP), Hangzhou, China, 8–10 July 2022; pp. 582–586. [[CrossRef](#)]
131. Chi, Q.; Ma, T.; Zhang, Y.; Cui, Y.; Zhang, C.; Lin, J.; Wang, X.; Lei, Q. Significantly enhanced energy storage density for poly(vinylidene fluoride) composites by induced PDA-coated 0.5Ba(Zr_{0.2}Ti_{0.8})O₃–0.5(Ba_{0.7}Ca_{0.3})TiO₃ nanofibers. *J. Mater. Chem. A* **2017**, *5*, 16757–16766. [[CrossRef](#)]
132. Ye, H.; Jiang, H.; Luo, Z.; Xu, L. Elastic interface in few-layer graphene/poly(vinylidene fluoride-trifluoroethylene-chlorofluoroethylene) nanocomposite with improved polarization. *J. Appl. Polym. Sci.* **2022**, *139*, 52030. [[CrossRef](#)]
133. Wang, Q.; Zhang, J.; Zhang, Z.; Hao, Y.; Bi, K. Enhanced dielectric properties and energy storage density of PVDF nanocomposites by co-loading of BaTiO₃ and CoFe₂O₄ nanoparticles. *Adv. Compos. Hybrid Mater.* **2020**, *3*, 58–65. [[CrossRef](#)]
134. Hambal, Y.; Shvartsman, V.V.; Michiels, I.; Zhang, Q.; Lupascu, D.C. High Energy Storage Density in Nanocomposites of P(VDF-TrFE-CFE) Terpolymer and BaZr_{0.2}Ti_{0.8}O₃ Nanoparticles. *Materials* **2022**, *15*, 3151. [[CrossRef](#)]
135. Kumar, A.; Roy, A. Structural and electromechanical characterization of lead magnesium niobate-lead titanate (PMN-0.3PT) piezoceramic for energy harvesting applications. *arXiv* **2022**, arXiv:2205.04313. <https://doi.org/10.48550/arxiv.2205.04313>.
136. Han, M.; Chan, Y.C.; Liu, W.; Zhang, S.; Zhang, H. Low frequency PVDF piezoelectric energy harvester with combined *d*₃₁ and *d*₃₃ operating modes. In Proceedings of the 8th Annual IEEE International Conference on Nano/Micro Engineered and Molecular Systems, IEEE NEMS 2013, Suzhou, China, 7–10 April 2013, pp. 440–443. [[CrossRef](#)]

137. Ahmad, K.A.; Rahman, M.F.; Hussain, Z.; Osman, M.K.; Sulaiman, S.N.; Abdullah, M.F.; Abdullah, N.; Manaf, A.A. Design and development of D33 mode piezoelectric acoustic transducer array using PVDF for underwater application. In Proceedings of the 7th IEEE International Conference on Control System, Computing and Engineering, ICCSCE 2017, Penang, Malaysia, 24–26 November 2017; pp. 1–5. [\[CrossRef\]](#)
138. Zhou, W.; Lin, Y.; Zou, K.; Zhou, C.; Gong, X.; Cao, Y.; Jiang, S. Enhancement of piezoelectricity in polymer PVDF based on molecular chain structure. *J. Mater. Sci. Mater. Electron.* **2021**, *32*, 28708–28717. [\[CrossRef\]](#)
139. Zhang, C.; Wei, W.; Sun, H.; Zhu, Q. Performance enhancements in poly(vinylidene fluoride)-based piezoelectric films prepared by the extrusion-casting process. *J. Mater. Sci. Mater. Electron.* **2021**, *32*, 21837–21847. [\[CrossRef\]](#)
140. Chen, W.W.; An, Z.L.; He, L.B.; Deng, Z. Piezoelectric coefficients measurement for PVDF films with pneumatic pressure rig in a sole cavity. In Proceedings of the 2015 Symposium on Piezoelectricity, Acoustic Waves and Device Applications, SPAWDA 2015, Jinan, China, 30 October–2 November 2015; pp. 111–114. [\[CrossRef\]](#)
141. Li, J.F. *Lead-Free Piezoelectric Materials*; Wiley: Hoboken, NJ, USA, 2021; p. 242.
142. Bai, Z.; Song, Y.; Peng, J.; Chen, D.; Zhou, Y.; Tao, Y.; Gu, S.; Xu, J.; Deng, Z.; Yin, X.; et al. Poly(Vinylidene Fluoride) Nanofiber Array Films with High Strength for Effective Impact Energy Harvesting. *Energy Technol.* **2021**, *9*, 2100345. [\[CrossRef\]](#)
143. Rajeev, S.P.; Karimuthil, S.C.; Bhanuprakash, L.; Varghese, S. Flexible nanoenergy harvester using piezo-tribo functional polymer and carbon fibre as electrodes. *Mater. Res. Express* **2018**, *5*, 075509. [\[CrossRef\]](#)
144. Yang, F.; Zhao, X.; Xue, T.; Yuan, S.; Huang, Y.; Fan, W.; Liu, T. Superhydrophobic polyvinylidene fluoride/polyimide nanofiber composite aerogels for thermal insulation under extremely humid and hot environment. *Sci. China Mater.* **2020**, *64*, 1267–1277. [\[CrossRef\]](#)
145. Li, K.; Hou, D.; Fu, C.; Wang, K.; Wang, J. Fabrication of PVDF nanofibrous hydrophobic composite membranes reinforced with fabric substrates via electrospinning for membrane distillation desalination. *J. Environ. Sci.* **2019**, *75*, 277–288. [\[CrossRef\]](#)
146. Kim, H.B.; Yun, C.; Park, C.H. Development of superhydrophobic textiles via polyvinylidene fluoride phase separation in one-step process. *Text. Res. J.* **2018**, *89*, 2595–2603. [\[CrossRef\]](#)
147. Li, M.; Li, J.; Zhou, M.; Xian, Y.; Shui, Y.; Wu, M.; Yao, Y. Super-hydrophilic electrospun PVDF/PVA-blended nanofiber membrane for microfiltration with ultrahigh water flux. *J. Appl. Polym. Sci.* **2020**, *137*, 48416. [\[CrossRef\]](#)
148. Rosman, N.; Norharyati Wan Salleh, W.; Asikin Awang, N.; Fauzi Ismail, A.; Jaafar, J.; Harun, Z. Wettability and Surface Area Characteristic of PVDF Nanofibrous Composite Film. *Mater. Today Proc.* **2019**, *19*, 1413–1419. [\[CrossRef\]](#)
149. Ince Yardimci, A.; Durmus, A.; Kayhan, M.; Tarhan, O. Antibacterial Activity of AgNO₃ Incorporated Polyacrylonitrile/Polyvinylidene Fluoride (PAN/PVDF) Electrospun Nanofibrous Membranes and Their Air Permeability Properties. *J. Macromol. Sci. Part B* **2022**, 1–14. [\[CrossRef\]](#)
150. Cvek, M.; Mrlík, M.; Osička, J.; Gorgol, D.; Tofel, P. PVDF/PVDF-TRFE blends loaded with BaTiO₃: from processing to performance testing. In Proceedings of the NANOCON Conference Proceedings—International Conference on Nanomaterials, Brno, Czech Republic, 20–22 October 2021; pp. 131–136. [\[CrossRef\]](#)
151. Mohamadi, S.; Sharifi-Sanjani, N. Crystallization of PVDF in graphene-filled electrospun PVDF/PMMA nanofibers processed at three different conditions. *Fibers Polym.* **2016**, *17*, 582–592. [\[CrossRef\]](#)
152. Ma, J.; Haque, R.I.; Larsen, R.M. Crystallization and mechanical properties of functionalized single-walled carbon nanotubes/polyvinylidene fluoride composites. *J. Reinf. Plast. Compos.* **2012**, *31*, 1417–1425. [\[CrossRef\]](#)
153. Kim, M.; Wu, Y.S.; Kan, E.C.; Fan, J. Breathable and Flexible Piezoelectric ZnO@PVDF Fibrous Nanogenerator for Wearable Applications. *Polymers* **2018**, *10*, 745. [\[CrossRef\]](#)
154. Martins, P.; Costa, C.M.; Benelmekki, M.; Lanceros-Mendez, S. Preparation of magnetoelectric composites by nucleation of the electroactive β -phase of poly(vinylidene fluoride) by NiZnFe₂O₄ nanoparticles. *Sens. Lett.* **2013**, *11*, 110–114. [\[CrossRef\]](#)
155. Sui, Y.; Wang, Z.; Gao, C. A new synthetical process of PVDF derivatives via atom transfer radical graft polymerizations and its application in fabrication of antifouling and antibacterial PVDF ultrafiltration membranes. *Desalin. Water Treat.* **2014**, *52*, 6377–6388. [\[CrossRef\]](#)
156. Satapathy, S.; Pawar, S.; Gupta, P.K.; Varma, B.R. Effect of annealing on phase transition in poly(vinylidene fluoride) films prepared using polar solvent. *Bull. Mater. Sci.* **2011**, *34*, 727–733. [\[CrossRef\]](#)
157. Azzaz, C.M.; C Mattoso, L.H.; Demarquette, N.R.; Zednik, R.J. Polyvinylidene fluoride nanofibers obtained by electrospinning and blowspinning: Electrospinning enhances the piezoelectric β -phase—Myth or reality? *J. Appl. Polym. Sci.* **2021**, *138*, 49959. [\[CrossRef\]](#)
158. Loizou, K.; Evangelou, A.; Marangos, O.; Koutsokeras, L.; Chrysafi, I.; Yiatros, S.; Constantinides, G.; Zaoutsos, S.; Drakonakis, V. Assessing the performance of electrospun nanofabrics as potential interlayer reinforcement materials for fiber-reinforced polymers. *Compos. Adv. Mater.* **2021**, *30*, 263498332110025. [\[CrossRef\]](#)
159. Nasir, M.; Matsumoto, H.; Danno, T.; Minagawa, M.; Irisawa, T.; Shioya, M.; Tanioka, A. Control of diameter, morphology, and structure of PVDF nanofiber fabricated by electro-spray deposition. *J. Polym. Sci. Part B Polym. Phys.* **2006**, *44*, 779–786. [\[CrossRef\]](#)
160. Messiry, M.E. Theoretical analysis of natural fiber volume fraction of reinforced composites. *Alex. Eng. J.* **2013**, *52*, 301–306. [\[CrossRef\]](#)
161. Wang, H.; Klosterhalfen, B.; Müllen, A.; Otto, T.; Dievernich, A.; Jockenhövel, S. Degradation resistance of PVDF mesh in vivo in comparison to PP mesh. *J. Mech. Behav. Biomed. Mater.* **2021**, *119*, 104490. [\[CrossRef\]](#) [\[PubMed\]](#)
162. de Jesus Silva, A.J.; Contreras, M.M.; Nascimento, C.R.; da Costa, M.F. Kinetics of thermal degradation and lifetime study of poly(vinylidene fluoride) (PVDF) subjected to bioethanol fuel accelerated aging. *Heliyon* **2020**, *6*, e04573. [\[CrossRef\]](#) [\[PubMed\]](#)

163. Hoa, S.V.; Ouellette, P. Stress corrosion cracking of poly(vinylidene fluoride) in sodium hydroxide. *Polym. Eng. Sci.* **1983**, *23*, 202–205. [[CrossRef](#)]
164. Zhao, X.; Song, L.; Fu, J.; Tang, P.; Liu, F. Experimental and DFT investigation of surface degradation of polyvinylidene fluoride membrane in alkaline solution. *Surf. Sci.* **2011**, *605*, 1005–1015. [[CrossRef](#)]
165. Shinohara, H. Fluorination of polyhydrofluoroethylenes. II. Formation of perfluoroalkyl carboxylic acids on the surface region of poly(vinylidene fluoride) film by oxyfluorination, fluorination, and hydrolysis. *J. Polym. Sci. Polym. Chem. Ed.* **1979**, *17*, 1543–1556. [[CrossRef](#)]
166. Ross, G.J.; Watts, J.F.; Hill, M.P.; Morrissey, P. Surface modification of poly(vinylidene fluoride) by alkaline treatment1. The degradation mechanism. *Polymer* **2000**, *41*, 1685–1696. [[CrossRef](#)]
167. Awanis Hashim, N.; Liu, Y.; Li, K. Stability of PVDF hollow fibre membranes in sodium hydroxide aqueous solution. *Chem. Eng. Sci.* **2011**, *66*, 1565–1575. [[CrossRef](#)]
168. Tao, X.; Zhou, Y.; Qi, K.; Guo, C.; Dai, Y.; He, J.; Dai, Z. Wearable textile triboelectric generator based on nanofiber core-spun yarn coupled with electret effect. *J. Colloid Interface Sci.* **2022**, *608*, 2339–2346. [[CrossRef](#)]
169. Mhetre, M.R.; Abhyankar, H.K. Human exhaled air energy harvesting with specific reference to PVDF film. *Eng. Sci. Technol. Int. J.* **2017**, *20*, 332–339. [[CrossRef](#)]
170. Wang, Y.J.; Sue, C.Y. Noninvasive Blood Pressure Measurement Using PVDF Fibers Fabricated by NFES and A Photoplethysmography Sensor. *J. Autom. Control. Eng.* **2017**, *7*, 34–38. [[CrossRef](#)]
171. Bifulco, P.; Gargiulo, G.D.; D'Angelo, G.; Liccardo, A.; Romano, M.; Clemente, F.; Cesarelli, M. Monitoring of respiration, seismocardiogram and heart sounds by a PVDF piezo film sensor. In Proceedings of the 20th IMEKO TC4 Symposium on Measurements of Electrical Quantities: Research on Electrical and Electronic Measurement for the Economic Upturn, Together with 18th TC4 International Workshop on ADC and DCA Modeling and Testing, IWADC 2014, Benevento, Italy, 15–17 September 2014; pp. 786–789.
172. Lee, W.K.; Chung, G.S.; Baek, H.J.; Park, K.S. Heart sounds measurement using PVDF film sensor and their comparison with RR intervals of ECG signals. In Proceedings of the IEEE-EMBS International Conference on Biomedical and Health Informatics: Global Grand Challenge of Health Informatics, BHI 2012, Hong Kong, China, 5–7 January 2012; pp. 864–866. [[CrossRef](#)]
173. Åkerfeldt, M.; Lund, A.; Walkenström, P. Textile sensing glove with piezoelectric PVDF fibers and printed electrodes of PEDOT:PSS. *Text. Res. J.* **2015**, *85*, 1789–1799. [[CrossRef](#)]
174. Xin, Y.; Li, X.; Tian, H.; Guo, C.; Sun, H.; Wang, S.; Wang, C. A shoe-equipped piezoelectric transducer system based on PVDF film. *Integr. Ferroelectr.* **2016**, *176*, 140–149. [[CrossRef](#)]
175. Klimiec, E.; Zaraska, W.; Piekarski, J.; Jasiewicz, B. PVDF Sensors—Research on Foot Pressure Distribution in Dynamic Conditions. *Adv. Sci. Technol.* **2013**, *79*, 94–99. [[CrossRef](#)]
176. Lee, D.W.; Jeong, D.G.; Kim, J.H.; Kim, H.S.; Murillo, G.; Lee, G.H.; Song, H.C.; Jung, J.H. Polarization-controlled PVDF-based hybrid nanogenerator for an effective vibrational energy harvesting from human foot. *Nano Energy* **2020**, *76*, 105066. [[CrossRef](#)]
177. Liu, S.; Chen, L.; Zhu, X.; Dai, L.; Xin, Y. Digital piano keyboard based on PVDF piezoelectric film. In Proceedings of the ICALIP 2010—2010 International Conference on Audio, Language and Image Processing, Shanghai, China, 23–25 November 2010; pp. 378–382. [[CrossRef](#)]
178. Szperlich, P. Piezoelectric A15B16C17 Compounds and Their Nanocomposites for Energy Harvesting and Sensors: A Review. *Materials* **2021**, *14*, 6973. [[CrossRef](#)] [[PubMed](#)]
179. Dai, Y.; Chen, J.; Tian, W.; Xu, L.; Gao, S. A PVDF/Au/PEN Multifunctional Flexible Human–Machine Interface for Multidimensional Sensing and Energy Harvesting for the Internet of Things. *IEEE Sens. J.* **2020**, *20*, 7556–7568. [[CrossRef](#)]
180. Wen, Q.; He, X.; Lu, Z.; Streiter, R.; Otto, T. A comprehensive review of miniaturized wind energy harvesters. *Nano Mater. Sci.* **2021**, *3*, 170–185. [[CrossRef](#)]
181. Viet, N.V.; Wu, N.; Wang, Q. A review on energy harvesting from ocean waves by piezoelectric technology. *J. Model. Mech. Mater.* **2017**, *1*. [[CrossRef](#)]
182. Jbaily, A.; Yeung, R.W. Piezoelectric devices for ocean energy: A brief survey. *J. Ocean. Eng. Mar. Energy* **2015**, *1*, 101–118. [[CrossRef](#)]
183. Gong, T.; Li, T.; Meng, L.; Chen, Y.; Wu, T.; Zhou, J.; Lu, G.; Wang, Z. Fabrication of piezoelectric Ca-P-Si-doped PVDF scaffold by phase-separation-hydration: Material characterization, in vitro biocompatibility and osteoblast redifferentiation. *Ceram. Int.* **2022**, *48*, 6461–6469. [[CrossRef](#)]
184. Dumitrescu, L.N.; Neacsu, P.; Necula, M.G.; Bonciu, A.; Marascu, V.; Cimpean, A.; Moldovan, A.; Rotaru, A.; Dinca, V.; Dinescu, M. Induced Hydrophilicity and In Vitro Preliminary Osteoblast Response of Polyvinylidene Fluoride (PVDF) Coatings Obtained via MAPLE Deposition and Subsequent Thermal Treatment. *Molecules* **2020**, *25*, 582. [[CrossRef](#)] [[PubMed](#)]
185. Kitsara, M.; Blanquer, A.; Murillo, G.; Humblot, V.; De Bragança Vieira, S.; Nogués, C.; Ibáñez, E.; Esteve, J.; Barrios, L. Permanently hydrophilic, piezoelectric PVDF nanofibrous scaffolds promoting unaided electromechanical stimulation on osteoblasts. *Nanoscale* **2019**, *11*, 8906–8917. [[CrossRef](#)]
186. Sun, C.; Guo, Y.; Fang, B.; Yang, J.; Qin, B.; Duan, H.; Chen, Y.; Li, H.; Liu, H. Enhanced Photovoltaic Performance of Perovskite Solar Cells Using Polymer P(VDF-TrFE) as a Processed Additive. *J. Phys. Chem. C* **2016**, *120*, 12980–12988. [[CrossRef](#)]
187. Nie, J.; Zhang, Y.; Dan, M.; Wang, J.; Li, L.; Zhang, Y. Piezophototronic Effect Enhanced Perovskite Solar Cell Based on P(VDF-TrFE). *Solar RRL* **2021**, *5*, 2100692. [[CrossRef](#)]

188. Park, S.; Kim, Y.; Jung, H.; Park, J.Y.; Lee, N.; Seo, Y. Energy harvesting efficiency of piezoelectric polymer film with graphene and metal electrodes. *Sci. Rep.* **2017**, *7*, 17290. [[CrossRef](#)] [[PubMed](#)]
189. Kargar, S.M.; Hao, G. An Atlas of Piezoelectric Energy Harvesters in Oceanic Applications. *Sensors* **2022**, *22*, 1949. [[CrossRef](#)]
190. Koç, M.; Paralı, L.; Şan, O. Fabrication and vibrational energy harvesting characterization of flexible piezoelectric nanogenerator (PEN) based on PVDF/PZT. *Polym. Test.* **2020**, *90*, 106695. [[CrossRef](#)]
191. Bae, J.; Song, J.; Jeong, W.; Nandanapalli, K.R.; Son, N.; Zulkifli, N.A.B.; Gwon, G.; Kim, M.; Yoo, S.; Lee, H.; et al. Multi-deformable piezoelectric energy nano-generator with high conversion efficiency for subtle body movements. *Nano Energy* **2022**, *97*, 107223. [[CrossRef](#)]
192. Zhang, Y.; Lu, R.; Zhang, S.; Tang, B. Intelligent light-driven flexible solar thermoelectric system. *Chem. Eng. J.* **2021**, *423*, 130260. [[CrossRef](#)]
193. Han, S.; Chen, S.; Jiao, F. Insulating polymers for flexible thermoelectric composites: A multi-perspective review. *Compos. Commun.* **2021**, *28*, 100914. [[CrossRef](#)]
194. Kumar, A.; Kumar, R.; Satapathy, D.K. Bi₂Se₃-PVDF composite: A flexible thermoelectric system. *Phys. B Condens. Matter* **2020**, *593*, 412275. [[CrossRef](#)]
195. Li, X.; Cai, K.; Gao, M.; Du, Y.; Shen, S. Recent advances in flexible thermoelectric films and devices. *Nano Energy* **2021**, *89*, 106309. [[CrossRef](#)]
196. Wang, J.; Xiao, F.; Zhao, H. Thermoelectric, piezoelectric and photovoltaic harvesting technologies for pavement engineering. *Renew. Sustain. Energy Rev.* **2021**, *151*, 111522. [[CrossRef](#)]
197. Dun, C.; Hewitt, C.A.; Huang, H.; Montgomery, D.S.; Xu, J.; Carroll, D.L. Flexible thermoelectric fabrics based on self-assembled tellurium nanorods with a large power factor. *Phys. Chem. Chem. Phys.* **2015**, *17*, 8591–8595. [[CrossRef](#)] [[PubMed](#)]
198. Paulraj, I.; Lourduhasamy, V.; Liu, C.J. Organic/Inorganic n-type PVDF/Cu_{0.6}Ni_{0.4} hybrid composites for thermoelectric application: A thermoelectric generator made of 8 pairs of p-leg ZnSb/Sb and n-leg β-PVDF/Cu_{0.6}Ni_{0.4}. *Chem. Eng. J.* **2022**, *446*, 137083. [[CrossRef](#)]
199. Hu, S.; Zeng, S.; Li, X.; Jiang, J.; Yang, W.; Chen, Y.; Li, M.; Zheng, J. Flexible and high performance of n-type thermoelectric PVDF composite film induced by nickel nanowires. *Mater. Des.* **2020**, *188*, 108496. [[CrossRef](#)]
200. Park, D.; Kim, M.; Kim, J. High-performance PANI-coated Ag₂Se nanowire and PVDF thermoelectric composite film for flexible energy harvesting. *J. Alloys Compd.* **2021**, *884*, 161098. [[CrossRef](#)]
201. Park, D.; Ju, H.; Kim, J. Enhanced thermoelectric properties of flexible N-type Ag₂Se nanowire/polyvinylidene fluoride composite films synthesized via solution mixing. *J. Ind. Eng. Chem.* **2021**, *93*, 333–338. [[CrossRef](#)]
202. Zhang, Y.; Rhee, K.Y.; Park, S.J. Facile design of a domestic thermoelectric generator by tailoring the thermoelectric performance of volume-controlled expanded graphite/PVDF composites. *Compos. Part B Eng.* **2019**, *176*, 107234. [[CrossRef](#)]
203. Chen, Y.; He, M.; Tang, J.; Bazan, G.C.; Liang, Z. Flexible Thermoelectric Generators with Ultrahigh Output Power Enabled by Magnetic Field-Aligned Metallic Nanowires. *Adv. Electron. Mater.* **2018**, *4*, 1800200. [[CrossRef](#)]
204. Kim, M.S.; Jo, S.E.; Ahn, H.R.; Kim, Y.J. Modeling of a honeycomb-shaped pyroelectric energy harvester for human body heat harvesting. *Smart Mater. Struct.* **2015**, *24*, 065032. [[CrossRef](#)]
205. Chen, W.Y.; Shi, X.L.; Zou, J.; Chen, Z.G. Wearable fiber-based thermoelectrics from materials to applications. *Nano Energy* **2021**, *81*, 105684. [[CrossRef](#)]
206. Na, Y.; Kim, S.; Mallem, S.P.R.; Yi, S.; Kim, K.T.; Park, K.I. Energy harvesting from human body heat using highly flexible thermoelectric generator based on Bi₂Te₃ particles and polymer composite. *J. Alloys Compd.* **2022**, *924*, 166575. [[CrossRef](#)]
207. Kumar, S.; Singh, H.H.; Khare, N. Flexible hybrid piezoelectric-thermoelectric generator for harnessing electrical energy from mechanical and thermal energy. *Energy Convers. Manag.* **2019**, *198*, 111783. [[CrossRef](#)]
208. Pan, J.; Li, Y.; Guo, G.; Zhao, X.; Yu, J.; Li, Z.; Xu, S.; Man, B.; Wei, D.; Zhang, C. Synergizing piezoelectric and plasmonic modulation of PVDF/MoS₂ cavity/Au for enhanced photocatalysis. *Appl. Surf. Sci.* **2022**, *577*, 151811. [[CrossRef](#)]
209. Banerjee, S.; Bairagi, S.; Ali, S.W. A lead-free flexible piezoelectric-triboelectric hybrid nanogenerator composed of uniquely designed PVDF/KNN-ZS nanofibrous web. *Energy* **2022**, *244*, 123102. [[CrossRef](#)]
210. Lee, Y.H.; Kim, D.H.; Kim, Y.; Shabbir, I.; Li, M.; Yoo, K.H.; Kim, T.W. Significant enhancement of the output voltage of piezoelectric/triboelectric hybrid nanogenerators based on MAPbBr₃ single crystals embedded into a porous PVDF matrix. *Nano Energy* **2022**, *102*, 107676. [[CrossRef](#)]
211. Mallick, Z.; Saini, D.; Sarkar, R.; Kundu, T.K.; Mandal, D. Piezo-phototronic effect in highly stable lead-free double perovskite Cs₂SnI₆-PVDF nanocomposite: Possibility for strain modulated optical sensor. *Nano Energy* **2022**, *100*, 107451. [[CrossRef](#)]
212. He, Y.; Wang, H.; Sha, Z.; Boyer, C.; Wang, C.H.; Zhang, J. Enhancing output performance of PVDF-HFP fiber-based nanogenerator by hybridizing silver nanowires and perovskite oxide nanocrystals. *Nano Energy* **2022**, *98*, 107343. [[CrossRef](#)]

PART II

Original experimental data on PVDF

Chapter 5. PVDF Fibers Modified by Carbon Nanotubes

5.1 Motivation of the article

The recent study show that CNTs in PVDF contribute to a significant enhancements in the material's β -phase, along with improved electrical and chemical properties, making these composites promising for energy storage applications. Given the widespread use of CNTs due to their large surface area, electron-rich nature, flexibility, and durability, their integration into PVDF is a logical progression. This combination has been shown to substantially boost the pyroelectric, ferroelectric, and piezoelectric properties of PVDF, suggesting potential applications in smart materials. However, existing studies primarily focus on PVDF in the form of thin films or bulkier states, leaving the binding mechanisms within these composites largely unexplored. This research addresses this gap by investigating the properties and evaluating the results of PVDF fibers integrated with CNTs, produced through electrospinning. The novelty of this study lies in its detailed examination of the interactions and binding mechanisms within this composite material, providing new insights and expanding the potential applications of PVDF-CNT composites.

5.2 Conclusion on the article

The integration CNTs into PVDF fibers represents a significant advancement in material science, particularly for applications requiring precise control over electrical and mechanical properties. This study, explored the unique chemical bonding that occurs during the electrospinning process, where CNTs form chemical bonds with PVDF, rather than being merely embedded within the polymer matrix. This bonding, confirmed by XPS and photoluminescence, alters the crystalline phase distribution of the PVDF, as shown through Raman spectroscopy, FTIR, and XRD analyses. These changes in phase composition, along with the presence of CNTs, influence the permittivity and conductivity of the fibers, suggesting that such materials can be tailored for specific applications. The main contribution of this research lies in its detailed examination of the CNT-PVDF interactions, providing new insights and opening up avenues for the development of advanced polymer composites with customized properties.

5.3 Applicant's contribution

The applicant is responsible for the entire XPS analysis (measurement, interpretation and visualisation) which is a sizable part of this paper.







5.4 Article 5

The paper "*Case Study of Polyvinylidene Fluoride Doping by Carbon Nanotubes*" was published in 2021 in "*Materials*" journal (IF: 3.8; Q2).

*The paper is highly cited and gathered 52 citations to date (02.06.2024).

Article

Case Study of Polyvinylidene Fluoride Doping by Carbon Nanotubes

Pavel Kaspar ^{1,*}, Dinara Sobola ^{1,2,3}, Klára Částková ^{2,4}, Rashid Dallaev ¹, Eva Šťastná ², Petr Sedlák ¹, Alexandr Knápek ⁵, Tomáš Trčka ¹ and Vladimír Holcman ¹

- ¹ Department of Physics, Faculty of Electrical Engineering and Communication, Brno University of Technology, Technická 2848/8, 616 00 Brno, Czech Republic; sobola@feec.vutbr.cz (D.S.); xdalla03@stud.feec.vutbr.cz (R.D.); sedlakp@feec.vutbr.cz (P.S.); trcka@feec.vutbr.cz (T.T.); holcman@feec.vutbr.cz (V.H.)
- ² Central European Institute of Technology BUT, Purkyňova 123, 612 00 Brno, Czech Republic; klara.castkova@ceitec.vutbr.cz (K.Č.); eva.jindrova@ceitec.vutbr.cz (E.Š.)
- ³ Department of Inorganic Chemistry and Chemical Ecology, Dagestan State University, Makhachkala, St. M. Gadjeva 43-a, 367015 Makhachkala, Russia
- ⁴ Department of Ceramics and Polymers, Faculty of Mechanical Engineering, Brno University of Technology, Technická 2, 616 69 Brno, Czech Republic
- ⁵ Institute of Scientific Instruments of the Czech Academy of Sciences, Královopolská 147, 612 64 Brno, Czech Republic; knapek@isibrno.cz
- * Correspondence: kasparp@feec.vutbr.cz

Abstract: Modern material science often makes use of polyvinylidene fluoride thin films because of various properties, like a high thermal and chemical stability, or a ferroelectric, pyroelectric and piezoelectric activity. Fibers of this polymer material are, on the other hand, much less explored due to various issues presented by the fibrous form. By introducing carbon nanotubes via electrospinning, it is possible to affect the chemical and electrical properties of the resulting composite. In the case of this paper, the focus was on the further improvement of interesting polyvinylidene fluoride properties by incorporating carbon nanotubes, such as changing the concentration of crystalline phases and the resulting increase of the dielectric constant and conductivity. These changes in properties have been explored by several methods that focused on a structural, chemical and electrical point of view. The resulting obtained data have been documented to create a basis for further research and to increase the overall understanding of the properties and usability of polyvinylidene fluoride fiber composites.

Keywords: polyvinylidene fluoride; carbon nanotubes; crystalline phases; dielectric constant



Citation: Kaspar, P.; Sobola, D.; Částková, K.; Dallaev, R.; Šťastná, E.; Sedlák, P.; Knápek, A.; Trčka, T.; Holcman, V. Case Study of Polyvinylidene Fluoride Doping by Carbon Nanotubes. *Materials* **2021**, *14*, 1428. <https://doi.org/10.3390/ma14061428>

Academic Editor: Klara Hernadi

Received: 2 February 2021

Accepted: 8 March 2021

Published: 15 March 2021

Publisher's Note: MDPI stays neutral with regard to jurisdictional claims in published maps and institutional affiliations.



Copyright: © 2021 by the authors. Licensee MDPI, Basel, Switzerland. This article is an open access article distributed under the terms and conditions of the Creative Commons Attribution (CC BY) license (<https://creativecommons.org/licenses/by/4.0/>).

1. Introduction

Polymer materials are an ever-expanding and always attractive topic for a number of scientific fields, such as material engineering, electro-technology or even biomedical purposes. In particular, fluoropolymers have gained prominence in recent years [1–5]. Their excellent biocompatibility and high resistance to chemical and physical stress make them useful and sought after, but at the same time cause their patterning to be difficult [6]. The most active and broadly successful of these fluoropolymers is polyvinylidene fluoride (PVDF). Even though PVDF requires a specific approach to patterns, for example sputtering, otherwise widely used methods for patterning other polymers cannot be used, and a sufficient and reliable patterning can today be achieved by a number of methods, most commonly spin-coating of PVDF solution in a polar solvent [7,8]. In the case of nanofiber production, electrospinning arose as the method with the best results and most control over the parameters of the resulting fiber, such as the diameter, inclusions and to some extent even crystalline phases [9,10]. For this reason, electrospinning was also used to create the materials described in this paper.

PVDF has a number of desirable properties for many applications. It is a polymer with a high degree of thermoplasticity and low reactivity, and because of that it is used

in many fields, from semiconductors via chemistry to biology. The creation of PVDF is achieved by the polymerization of vinylidene difluoride into a polymer chain (Figure 1).

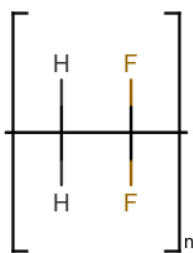


Figure 1. Poly(1,1-difluorethylene)-Vinylidene fluoride polymer.

PVDF can show different properties depending on the conformation of the polymer chain and production parameters. It is possible to achieve the poling of the molecular chain under tension by mechanical stretching, giving it ferroelectric, pyroelectric and piezoelectric properties [11–15]. In recent years, PVDF materials were subjected to doping by several interesting materials, namely BiFeO₃, TiO₂ and carbon nanofibers, modifying and enhancing its properties.

As with other polymeric structures, efforts to enrich PVDF with other materials have been explored as well. PVDF films and composite polymers have been blended with carbon nanotubes (CNTs) [16–18], and studies have found this process to enhance the β -phase, as well as all the electric and chemical properties that go with it, even making them a viable candidate for energy storage uses [19]. Since CNTs are widely used today, mainly for their large surface areas rich with electrons but also for their flexibility and durability, their incorporation into PVDF was a logical next step. Their presence in the polymer improved the pyroelectric, ferroelectric and piezoelectric properties in a major way [20–22]. The possible options of this material blend also qualify it as a candidate for smart materials [9]. While these inclusions have already been performed and evaluated on PVDF in some of the papers referenced above, the polymer was mostly in the form of a thin film or in a bulkier state. The binding mechanism, however, remains largely unexplored. The novelty of this paper, then, is the exploration of the properties and evaluation of the results of PVDF fibers bonded with carbon nanotubes in a composite material produced by electrospinning.

2. Materials and Methods

The PVDF material used in the measurements described in this paper was in the form of fibers ($M_w = 275,000$ g/mol) manufactured by electrospinning from 15 wt% PVDF solution (Sigma Aldrich, Munich, Germany) in a solution blend of dimethyl sulfoxide and acetone (Penta, Prague, Czech Republic) in a volume ratio of 7/3. The resulting material created under a constant voltage of 50 kV took the form of a 25 μm thick fiber mat. The process of electrospinning was performed on 4-spin equipment (Contipro, Dolní Dobrouč, Czech Republic) at a feeding rate of $20 \mu\text{L} \times \text{min}^{-1}$ through a thin needle with a diameter of 1.067 mm (17G). An aluminum foil-covered rotation collector (Contipro, Dolní Dobrouč, Czech Republic) was used to gather the resulting fibers at a speed of 2000 rpm for 30 min. The distance between the tip of the needle and the collector was kept constant at 20 cm. The resulting nonwoven mats were left to dry overnight at laboratory temperature. Fibers created by this process were 195.2 nm thick.

The nanotubes used in the experiments in this paper are NANOCYL NC7000 thin multiwall carbon nanotubes (CNTs, Sigma Aldrich, Munich, Germany) with an average diameter of 9.5 nm, average length of 1.5 μm and 90% carbon purity. 1 wt% of CNTs was dispersed in the 15 wt% PVDF solution using an ultrasound probe (Bandelin, Berlin, Germany) and were further electro-spun under the same process conditions mentioned for the neat PVDF solution, except for the feeding rate. That was optimally set at $80 \mu\text{L} \times \text{min}^{-1}$ due to the enhanced ability to withdraw a drop of CNTs/PVDF precursor during the electrospinning process.

Scanning electron microscopy images were obtained by using a high-resolution scanning electron microscope FEI Verios 460L (FEI, Brno, Czech Republic).

Raman spectra were taken by a WITec alpha300 R device (WITec, Ulm, Germany) at an excitation wavelength of 532 nm and power of the laser of 1 mW. The signal gained from this measurement was reconstructed from 50 accumulations under an integration time of 20 s.

Photoluminescence spectra were acquired on the same device as Raman spectroscopy, with a laser power of 4 mW at a 355 nm wavelength. Through a 40× objective, the results were accumulated 20 times over a 5 s integration.

The device used for the acquisition of XPS spectra was an AXIS Supra X-ray photoelectron spectrometer (Kratos Analytical, Manchester, UK). The resulting information were captured under an emission current of 15 mA and resolution of 20 for wide spectra and 80 for the element-specific spectra. The fitting of the spectra was done using CasaXPS software (Casa Software Ltd., Teignmouth, UK).

Data from FTIR (Bruker, Billerica, MA, USA) were acquired in transmission mode over 512 iterations with a resolution of 1 cm^{-1} .

An XRD analysis was performed with the X-ray powder diffractometer Rigaku Smart-Lab 3 kW (Rigaku Corporation, Tokyo, Japan) in the Bragg-Brentano configuration. Diffraction patterns were obtained between 10° and 50° (2 θ) with Cu K α radiation.

The dielectric properties were measured by a Novocontrol Alpha Analyzer device (Novocontrol Technologies, Montabaur, Germany) in the frequency range of 1 to 100,000 Hz. All of the measurements mentioned in this chapter were carried out at room temperature.

3. Results and Discussion

One of the more challenging issues is the dispersion of the carbon nanotubes within the PVDF solution before electrospinning and the distribution in the final product that it directly affects. For the illustration of surface changes, SEM images were taken of both the pure PVDF fibers and the PVDF fibers modified with CNTs (Figure 2). While the pure PVDF fibers have fairly clean and smooth surface (Figure 2a), a number of bumps and bulges has been detected in the combined material (Figure 2b). Not only are the CNTs incorporated inside the PVDF fibers, but we can see them protruding out in some places. The agglomeration in the center of the mixed material image (Figure 2b) also points to the possibility of the filler material forming clusters that are large enough to be clearly visible under scanning electron microscopy. The CNTs are, however, mostly incorporated into the fibers from the inside, and no separate formations of pure CNTs material without any attachment to the PVDF fibers have been detected.

Samples of PVDF with carbon nanotubes were subjected to Raman spectroscopy. Figure 3 shows the wide Raman spectrum of the materials. The individual spectra are horizontally shifted for clarity. Carbon nanotubes have a number of highly visible bands present in the spectrum. The most prominent are D-band at around 1341 cm^{-1} caused by graphene structure disorder and, at 1580 cm^{-1} , the G-band representing vibrations of the C–C bond [23]. Two smaller bands of note are located between 2500 and 2850 cm^{-1} , assigned to the 2D group [24], and there is a very minor band around 3200 cm^{-1} , representing a slightly displaced combined G + D' band [25]. The pure CNTs part of the spectra offers one more piece of information about the material. The ratio of D- and G-bands can be used to determine the concentration of CNTs with different numbers of walls.

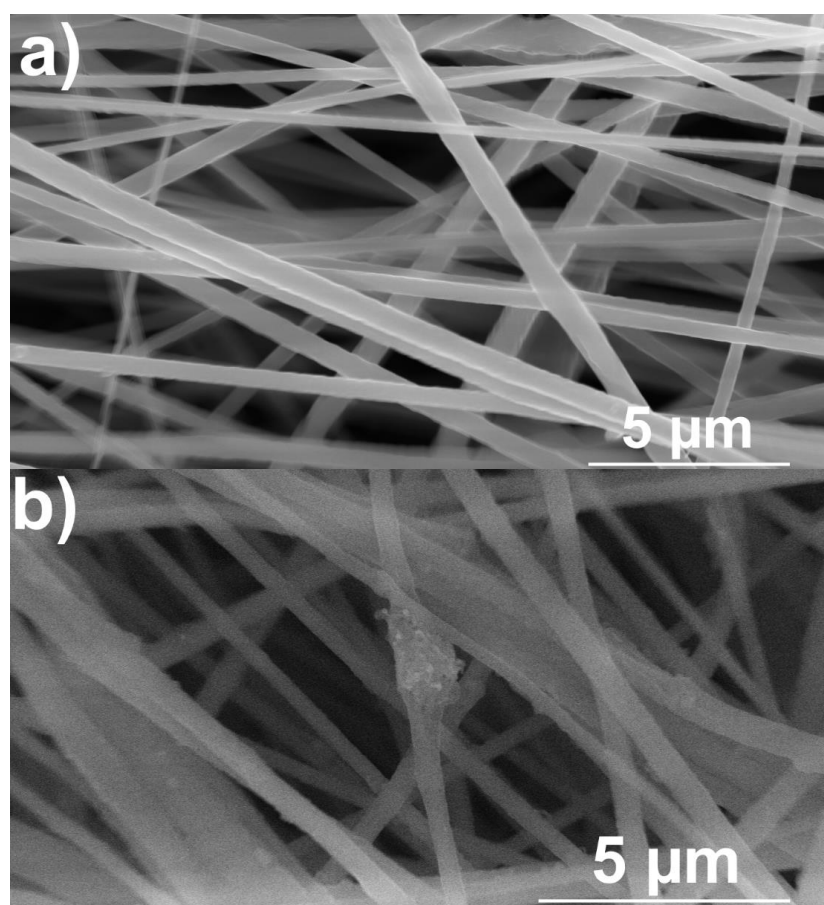


Figure 2. SEM images of pure PVDF fibers (a) and PVDF fibers with CNTs (b).

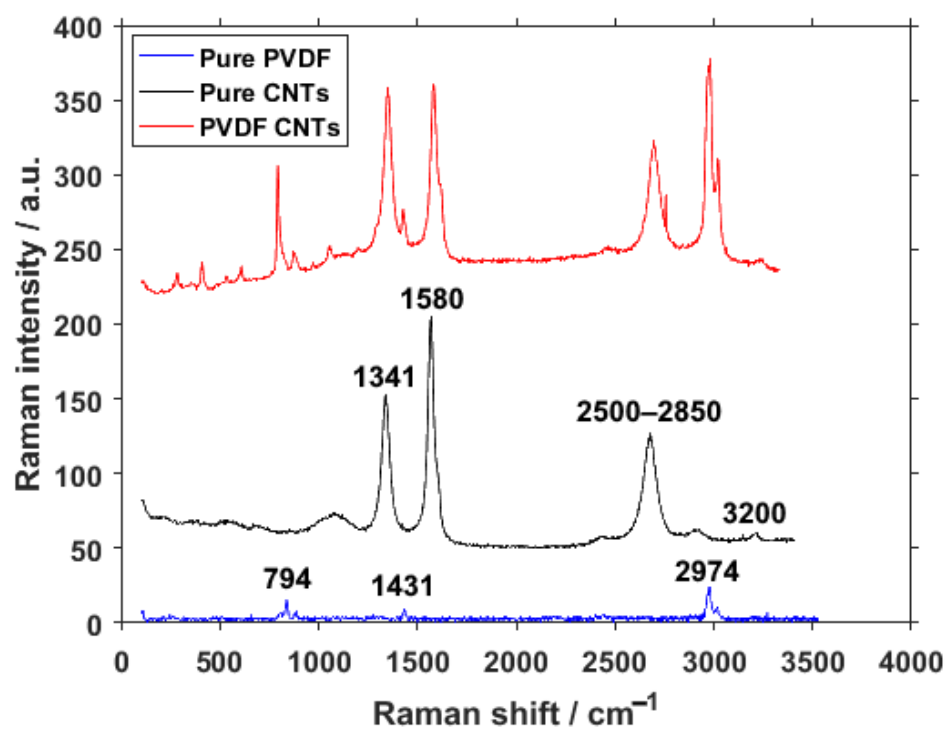


Figure 3. Raman spectra of pure PVDF fibers, pure CNTs and PVDF fibers with CNTs.

While the material is purchased and the documentation containing this information is available from the manufacturer [26], the spectrum lacks the presence of the radial breathing mode (RBM), which should be located between 150 and 200 cm^{-1} . This absence points to a very low to no presence of single-wall carbon nanotubes (SWCNTs) [27]. For pure PVDF, the signal is very low, but there are still three visible bands. The band at around 794 cm^{-1} is assigned to the rocking motion of CH_2 and is a typical band for α -phase rich PVDF. The band around 1431 cm^{-1} is caused by bending CH_2 vibrations [28,29], present in all three crystalline phases of PVDF but mainly in the β - and γ -phases. The band at 2974 cm^{-1} is usually attributed to CH_2 symmetric stretching [30], commonly associated with the β -phase.

In the spectrum of PVDF combined with CNTs, all the previously mentioned peaks are present and visible, but their intensities are put into relative perspective to each other. The change in ratio of the D/G bands can be ascribed to processes during the chemical bonding of the two materials, specifically the reduction of the crystallite size and an increased number of formed defects.

The resulting emission spectra from the photoluminescence measurement of pure PVDF and PVDF with integrated carbon nanotubes can be seen in Figure 4. The recorded spectrum of pure PVDF shows two very visible peaks around 500 and 590 nm. These peaks can be assigned to ${}^4\text{F}_{9/2} - {}^6\text{H}_{15/2}$ and ${}^4\text{F}_{9/2} - {}^6\text{H}_{13/2}$ transitions, respectively [31,32]. This response was expected under the excitation wavelength of 354 nm. With the addition of carbon nanotubes, however, the previous signals of the transition got converted into a single wide peak at around 530 nm. This change can be attributed to bonds forming in the material after the introduction of the carbon nanotube, and not to the CNTs itself, since the standard photoluminescence peaks belonging to carbon nanotubes are usually located in higher wavelengths [33,34].

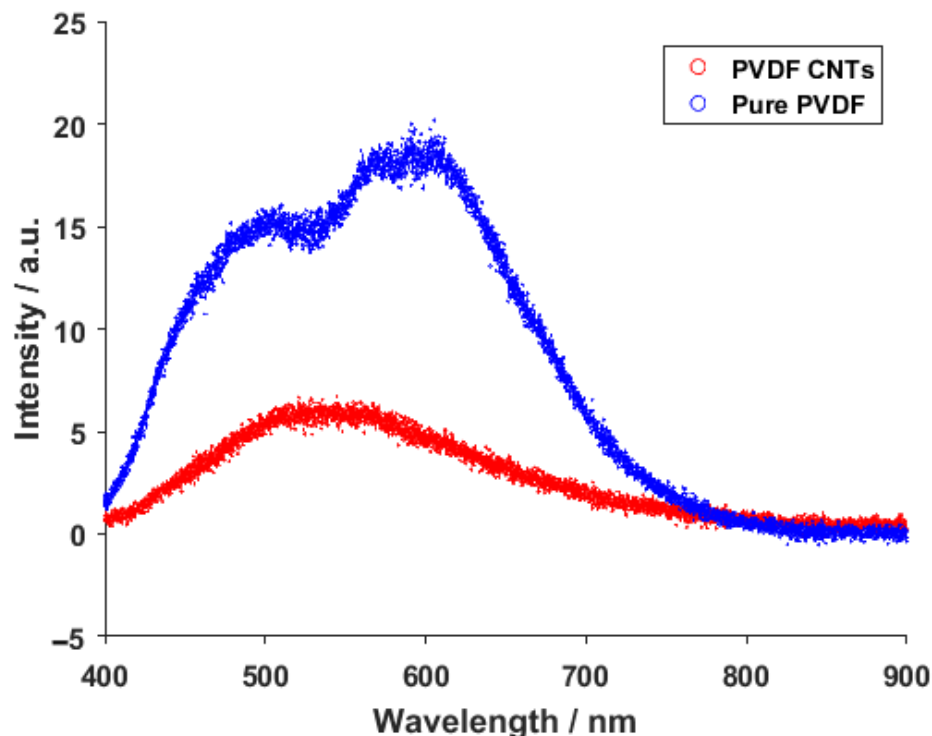


Figure 4. Photoluminescence spectra of pure PVDF fibers and PVDF fibers with CNTs.

The C1s XPS spectra of the analyzed material show a standard set of bands expected for carbon nanotubes [35] and PVDF [36]. The C–C band at 285 eV (Figure 5a) is one of the main pillars of any carbon XPS measurement and can be used as an identifier for the presence of graphite in almost any formation, like sheets, nanotubes or others. This peak is

overshadowed by the C–O/CH₂ band in the combined material (Figure 5c), as the material ratio of PVDF to CNTs is heavily in favor of PVDF. The combined C1s spectra also show a slight change in the ratio of the C–O/CH₂ band to the FC–OH band, in favor of the former, when compared to pure PVDF (Figure 5b). The ratio of CF₂ to the FC–OH bond increases in favor of CF₂ in the combined material as well, representing the bonding process of CNTs to PVDF.

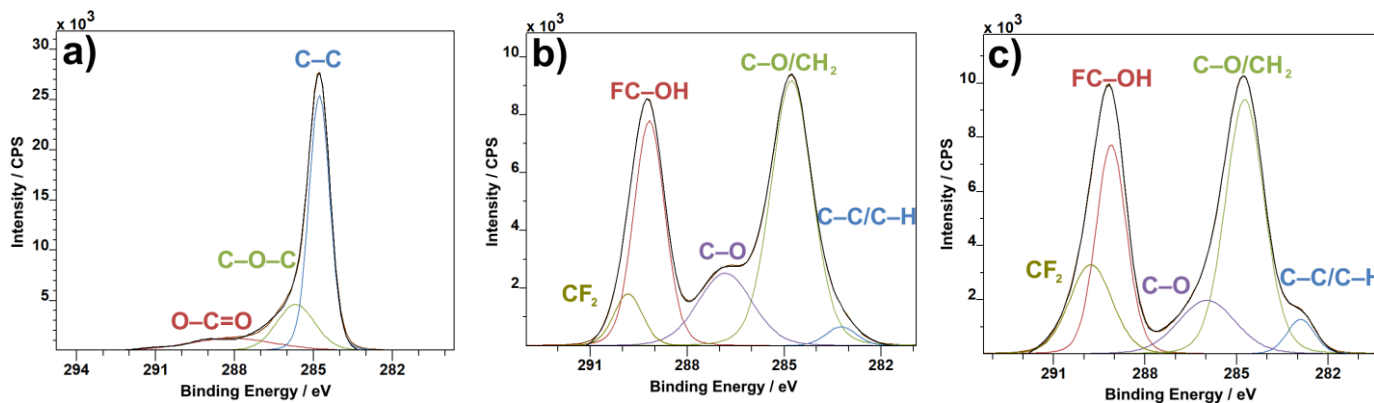


Figure 5. C1s XPS spectra of CNTs (a), PVDF (b) and PVDF with CNTs (c).

In the case of the O1s XPS spectra, the C–OH band from both CNTs (Figure 6a) and PVDF (Figure 6b) gets carried over to the combined material (Figure 6c), as expected. The most prominent band from pure CNTs, the C–O band, which is present in pure PVDF as well, is distinctly reduced in the combined material in favor of the C=O band, which increases in comparison to both pure CNT and pure PVDF. The O=C–O bond from the C1s spectra (Figure 5) and C=O from the O1s spectra (Figure 6) represent the ends of carbon nanotubes. When introduced to PVDF, the ends of CNTs bind to the polymer material, thus causing the C=O bond to decrease in concentration. This applies for the C–O bond as well, and, in turn, the C–OH bond, which is the bond of CNTs to PVDF, gains in prominence.

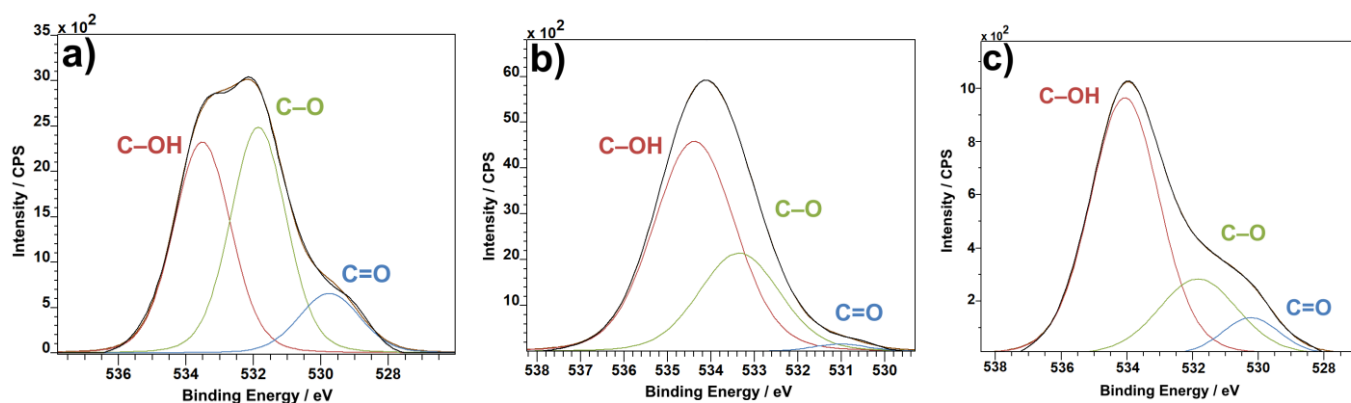


Figure 6. O1s XPS spectra: CNTs (a), PVDF (b) and PVDF with CNTs (c).

The F1s spectra show a change in the ratio of covalent and semi-ionic bonds. Although the change is not enormous, semi-ionic bonds are more prevalent in pure PVDF material (Figure 7a) than in the combination of PVDF with CNTs (Figure 7b). The change in bond concentration reflects the shift of crystalline phases. Where semi-ionic bonds are more oriented than covalent bonds, the same can be said about the β and γ phases being more oriented than the α phase. The F1 spectra could then be read not only as a change in bonds in favor of covalent, less oriented bonds, but at the same time as an increase in concentration of the less oriented α phase.

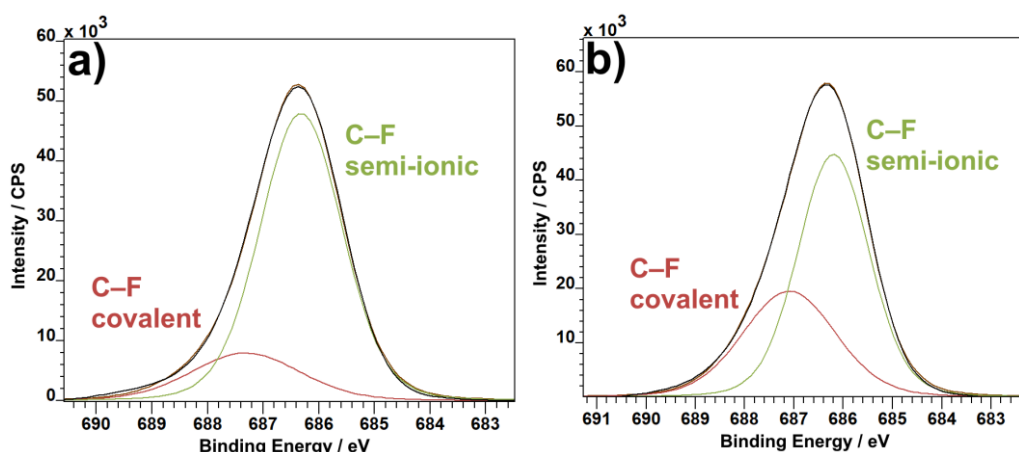


Figure 7. F1s XPS spectra: PVDF (a) and PVDF with CNTs (b).

The FTIR measurement was performed in order to obtain the percentages of different PVDF phases with and without the enrichment by CNTs. The graphical interpretation of the result can be seen in Figure 8. At first glance, there are almost no differences between the spectra. The only visible variation is the presence of a peak on PVDF with CNTs at 743 cm^{-1} , whereas this location is much flatter in pure PVDF. This location belongs to the α -phase of PVDF. Together with the peak at 840 cm^{-1} belonging to the β -phase, they can tell us the ratio of these two phases present in the material [37]. To fully understand what this ratio means, the relative concentration of phases was calculated from the results. The relative fraction of phases for pure PVDF was 13.45% for α , 82.52% for β and 4.03% for γ . This was changed with the addition of CNTs to 17.80% for the α -phase, 74.37% for β and 7.83% for γ . From these results, it could be seen that the inclusion of CNTs in PVDF fibers caused an increase mainly in the α -phase but also in the γ -phase of PVDF at the expense of the β -phase. This result supports the conclusions gained from XPS, namely the F1 spectra (Figure 7), which suggested a shift in concentration towards the α -phase based on the increase of covalent bond representation. Changes in the concentration suggest that the fibers bond with the PVDF structure and alter the polymer chain orientation, rather than just being lodged in between the individual fibers. It is also interesting to note that the previous measurements with carbon flakes incorporated into the PVDF fibers caused a decrease in α -phase concentration [38], as opposed to the CNTs presented in this paper.

The XRD measurement revealed three places of interest in the spectra of pure PVDF and CNTs-infused PVDF. The first important peak is located at 27° (Figure 9a) and can only be seen in the spectrum belonging to PVDF with CNTs. Since this peak belongs to carbon, its presence in the combined material and absence in the pure PVDF spectrum is to be expected. Previous measurements on this material with powdered carbon instead of CNTs showed this peak to be much more pronounced [38], so the conformation of carbon plays a role when determining the intensity of the carbon response from this method. The other two places of interest belong to the α -phase of PVDF and the combination of the α and β -phases at around 18° and 21° , respectively (Figure 9b) [39]. In the combined material, it seems as if the α -phase peak has almost disappeared, though it can still be seen. This is caused by the change in ratio of the first and second peak. For the pure PVDF material, the ratio of the 18° and 21° peaks is clearly different than in the combined material. Specifically, with the introduction of CNTs into PVDF the ratio shifts more toward the 18° peak, representing a higher concentration of the α -phase than in the pure material. This corresponds with the results from other measurements described in this paper.

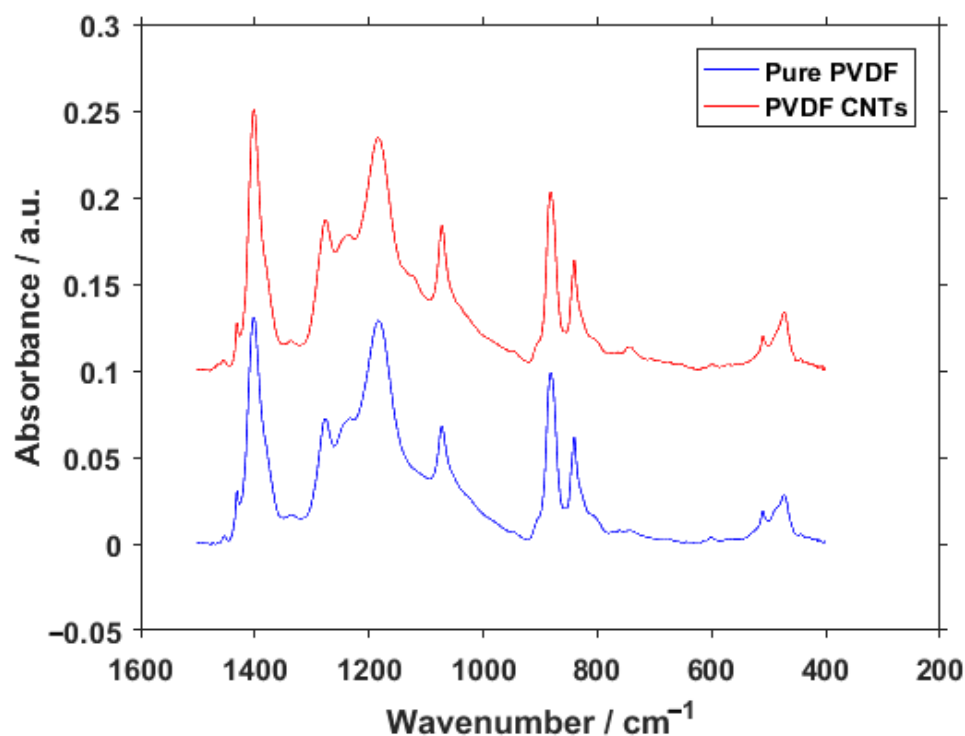


Figure 8. FTIR spectra of pure PVDF fibers and PVDF fibers with CNTs.

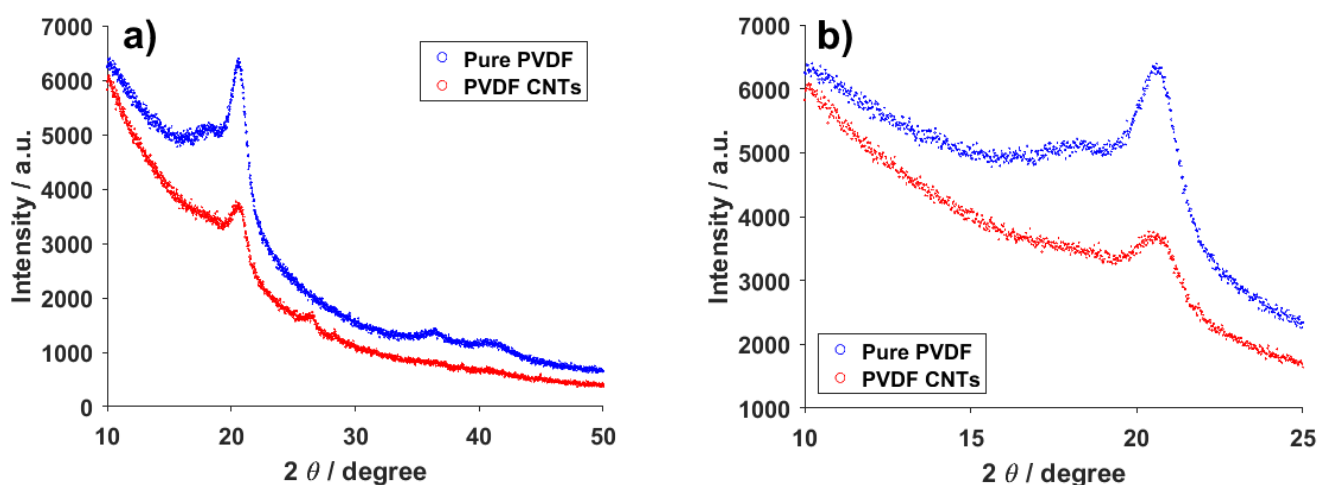


Figure 9. XRD (a) wide and (b) focus spectra of pure PVDF fibers and PVDF fibers with CNTs.

Carbon nanotubes are also often explored and exploited because of their electrical properties [40]. The addition of CNTs into PVDF was expected to have an effect on the overall electrical behavior of the material. From the dielectric measurements depicted in Figure 10 it appears that the effect of the carbon nanotubes presence cannot be simply disregarded. On lower frequencies, the dielectric constant (ϵ_r') is noticeably higher, even though the difference decreases rapidly with an increasing frequency. The imaginary part (ϵ_r''), a.k.a. dielectric loss, follows a similar trend for both the pure and doped PVDF material, but with different starting values at the lower frequencies and almost blending together on higher frequencies. More interesting information can be obtained from the conductivity part of Figure 10. As expected, the introduction of the carbon nanotubes increases the conductivity of the fibers, though the effect is mainly noticeable at lower frequencies, as was the case for the dielectric constant. In the case of the imaginary part of the conductivity (σ''), the values for the pure and doped PVDF are virtually indistinguishable. These trends

are all in line with the expectations and measurements made on PVDF films, where the electrical properties should not be too different [41,42].

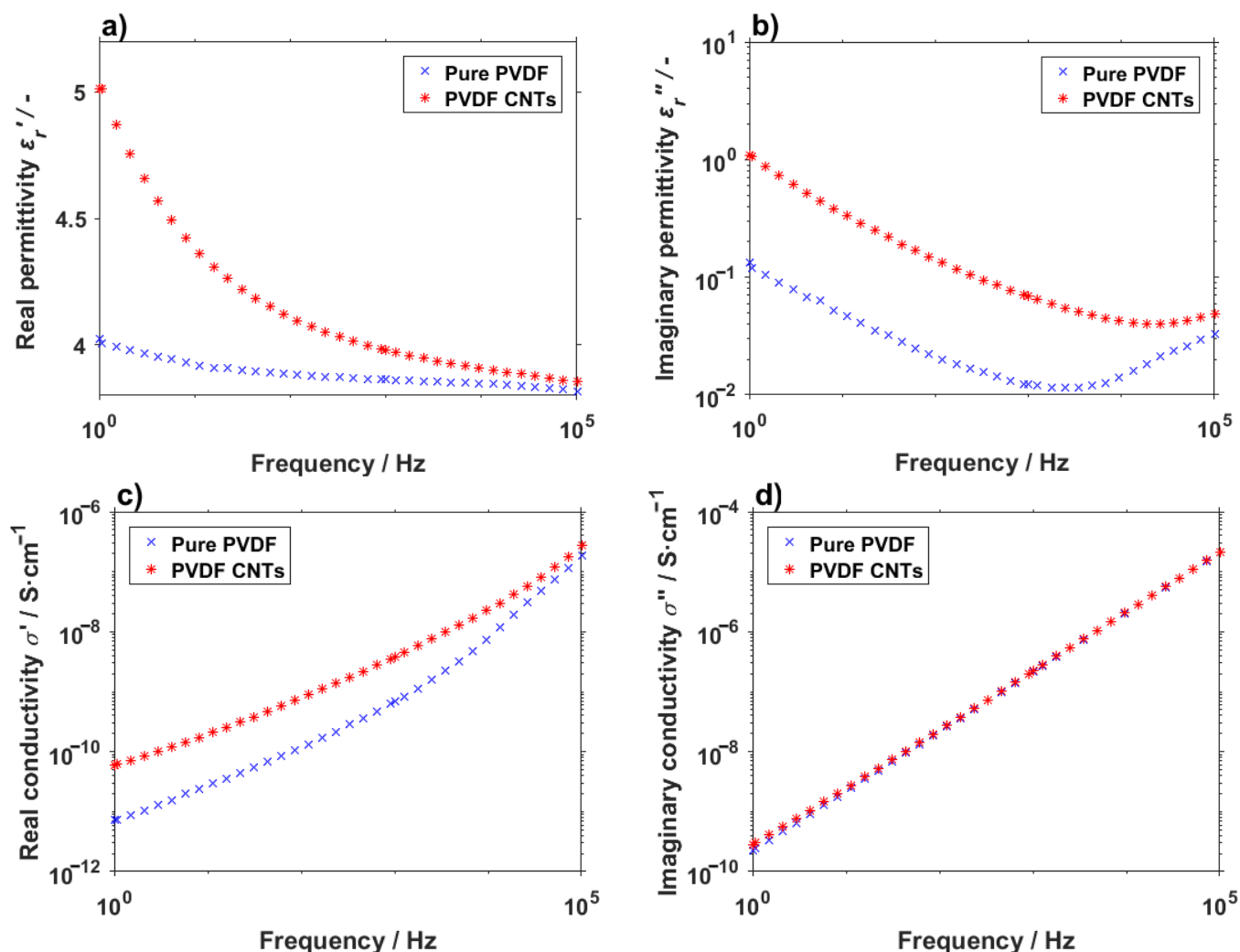


Figure 10. (a) Real and (b) imaginary permittivity and (c) real and (d) imaginary conductivity of pure PVDF fibers and PVDF with carbon nanotubes.

4. Conclusions

During the electrospinning process used to include carbon nanotubes into polyvinylidene fluoride fibers upon creation, the CNTs formed chemical bonds with PVDF and were not just mechanically inserted into a previously existing material. The resulting bonds were detectable by XPS and photoluminescence. Such an interaction affected the properties and structure of the polymer, most noticeably in the ratio of crystalline phases, as presented by Raman spectroscopy, FTIR and XRD. The concentration of the α -, β - and γ -phases, not to mention the presence of the nanotubes on their own, also had an effect on the permittivity and conductivity of the material and could allow the resulting fibers to be modified for specific use on demand. The specific acquired results are valid for the 1 wt% of CNTs in the 15 wt% solution used for electrospinning. The performed inclusion and analysis of CNTs into PVDF fibers has not been described before, and it offers an important look into the mechanisms of fiber-inclusion interactions, opening new possibilities for the utilization of polyvinylidene fluoride fibers with the inclusions of other materials.

Author Contributions: Conceptualization, P.K. and D.S.; methodology, D.S.; validation, K.Č. and P.S.; formal analysis, A.K., P.S. and K.Č.; investigation, D.S., R.D., P.K., E.Š. and T.T.; resources, E.Š.

and A.K.; data curation, D.S.; writing—original draft preparation, P.K.; writing—review and editing, P.K. and D.S.; visualization, R.D. and V.H.; supervision, V.H. All authors have read and agreed to the published version of the manuscript.

Funding: The research described in this paper was financially supported by the Ministry of Education, Youth and Sports of the Czech Republic under the project CEITEC 2020 [grant number LQ1601], by the Internal Grant Agency of Brno University of Technology [Grant No. FEKT-S-20-6352] and the Grant Agency of Czech Republic under project No. 19-17457S. A part of the work was carried out with the support of CEITEC Nano Research Infrastructure [grant ID LM2015041, MEYS CR, 2016–2019], CEITEC Brno University of Technology. We also acknowledge the Czech Academy of Sciences (RVO:68081731).

Institutional Review Board Statement: Not applicable.

Informed Consent Statement: Not applicable.

Data Availability Statement: The authors declare that, to the best of their knowledge, all data and material comply with field standards. Data are available by request.

Acknowledgments: In this section, you can acknowledge any support given which is not covered by the author contribution or funding sections. This may include administrative and technical support, or donations in kind (e.g., materials used for experiments).

Conflicts of Interest: The authors have no conflict of interest to declare that are relevant to the content of this article.

References

1. Jia, N.; He, Q.; Sun, J.; Xia, G.; Song, R. Crystallization behavior and electroactive properties of PVDF, P(VDF-TrFE) and their blend films. *Polym. Test.* **2017**, *57*, 302–306. [[CrossRef](#)]
2. Bian, X.; Shi, L.; Yang, X.; Lu, X. Effect of Nano-TiO₂ Particles on the Performance of PVDF, PVDF-g-(Maleic anhydride), and PVDF-g-Poly(acryl amide) Membranes. *Ind. Eng. Chem. Res.* **2011**, *50*, 12113–12123. [[CrossRef](#)]
3. Yang, J.; He, F.; Wu, H.; Liang, Y.; Wang, Y.; Sun, Z. Engineering Surface and Optical Properties of TiO₂-Coated Electrospun PVDF Nanofibers Via Controllable Self-Assembly. *Nanomaterials* **2018**, *8*, 741. [[CrossRef](#)]
4. Ma, Z.; Wang, G.; Rui, X.; Yang, F.; Wang, Y. Temperature compensation of a PVDF stress sensor and its application in the test of gun propellant charge compression stress. *Smart Mater. Struct.* **2019**, *28*, 025018. [[CrossRef](#)]
5. Sharma, M.; Madras, G.; Bose, S. Unusual Fragility and Cooperativity in Glass-Forming and Crystalline PVDF/PMMA Blends in the Presence of Multiwall Carbon Nanotubes. *Macromolecules* **2015**, *48*, 2740–2750. [[CrossRef](#)]
6. McKeen, L.W. Fluoropolymers. In *Fatigue and Tribological Properties of Plastics and Elastomers*; Rogers, M., Ed.; Elsevier BV: Amsterdam, The Netherlands, 2016; pp. 291–315.
7. Cardoso, V.F.; Minas, G.; Lanceros-Méndez, S. Multilayer spin-coating deposition of poly(vinylidene fluoride) films for controlling thickness and piezoelectric response. *Sens. Actuators A Phys.* **2013**, *192*, 76–80. [[CrossRef](#)]
8. Shaik, H.; Rachith, S.N.; Rudresh, K.J.; Sheik, A.S.; Raman, K.H.T.; Kondaiah, P.; Rao, G.M. Towards β -phase formation probability in spin coated PVDF thin films. *J. Polym. Res.* **2017**, *24*, 35. [[CrossRef](#)]
9. Wu, C.-M.; Chou, M.-H.; Zeng, W.-Y. Piezoelectric Response of Aligned Electrospun Polyvinylidene Fluoride/Carbon Nanotube Nanofibrous Membranes. *Nanomaterials* **2018**, *8*, 420. [[CrossRef](#)] [[PubMed](#)]
10. Castkova, K.; Kastyk, J.; Sobola, D.; Petrus, J.; Stasna, E.; Riha, D.; Tofel, P. Structure-Properties Relationship of Electrospun PVDF Fibers. *Nanomaterials* **2020**, *10*, 1221. [[CrossRef](#)] [[PubMed](#)]
11. Kawai, H. The Piezoelectricity of Poly (vinylidene Fluoride). *Jpn. J. Appl. Phys.* **1969**, *8*, 975–976. [[CrossRef](#)]
12. Fukada, E.; Takashita, S. Piezoelectric Effect in Polarized Poly (vinylidene Fluoride). *Jpn. J. Appl. Phys.* **1969**, *8*, 960. [[CrossRef](#)]
13. Nakamura, K.; Wada, Y. Piezoelectricity, pyroelectricity, and the electrostriction constant of poly(vinylidene fluoride). *J. Polym. Sci. Part A-2 Polym. Phys.* **1971**, *9*, 161–173. [[CrossRef](#)]
14. Tamura, M.; Ogasawara, K.; Ono, N.; Hagiwara, S. Piezoelectricity in uniaxially stretched poly(vinylidene fluoride). *J. Appl. Phys.* **1974**, *45*, 3768–3771. [[CrossRef](#)]
15. Oshiki, M.; Fukada, E. Inverse piezoelectric effect and electrostrictive effect in polarized poly(vinylidene fluoride) films. *J. Mater. Sci.* **1975**, *10*, 1–6. [[CrossRef](#)]
16. Levi, N.; Czerw, R.; Xing, S.; Iyer, P.; Carroll, D.L. Properties of Polyvinylidene Difluoride–Carbon Nanotube Blends. *Nano Lett.* **2004**, *4*, 1267–1271. [[CrossRef](#)]
17. Chatterjee, J.; Nash, N.; Cottinet, P.-J.; Wang, B. Synthesis and characterization of poly(vinylidene fluoride)/carbon nanotube composite piezoelectric powders. *J. Mater. Res.* **2012**, *27*, 2352–2359. [[CrossRef](#)]
18. Mousa, M.S. Comparison between Single-Walled CNT, Multi-Walled CNT, and Carbon Nanotube-Fiber Pyrograf III. *IOP Conf. Ser. Mater. Sci. Eng.* **2018**, *305*, 012025. [[CrossRef](#)]

19. Aqeel, S.M.; Huang, Z.; Walton, J.; Baker, C.; Falkner, D.; Liu, Z.; Wang, Z. Polyvinylidene fluoride (PVDF)/polyacrylonitrile (PAN)/carbon nanotube nanocomposites for energy storage and conversion. *Adv. Compos. Hybrid Mater.* **2017**, *1*, 185–192. [[CrossRef](#)]
20. Ahn, Y.; Lim, J.Y.; Hong, S.M.; Lee, J.; Ha, J.; Choi, H.J.; Seo, Y. Enhanced Piezoelectric Properties of Electrospun Poly(vinylidene fluoride)/Multiwalled Carbon Nanotube Composites Due to High β -Phase Formation in Poly(vinylidene fluoride). *J. Phys. Chem. C* **2013**, *117*, 11791–11799. [[CrossRef](#)]
21. Huang, S.; Yee, W.A.; Tjiu, W.C.; Liu, Y.; Kotaki, M.; Boey, Y.C.F.; Ma, J.; Liu, T.; Lu, X. Electrospinning of Polyvinylidene Difluoride with Carbon Nanotubes: Synergistic Effects of Extensional Force and Interfacial Interaction on Crystalline Structures. *Langmuir* **2008**, *24*, 13621–13626. [[CrossRef](#)] [[PubMed](#)]
22. Mago, G.; Kalyon, D.M.; Fisher, F.T. Membranes of Polyvinylidene Fluoride and PVDF Nanocomposites with Carbon Nanotubes via Immersion Precipitation. *J. Nanomater.* **2008**, *2008*, 1–8. [[CrossRef](#)]
23. Bokobza, L.; Bruneel, J.-L.; Couzi, M. Raman spectroscopy as a tool for the analysis of carbon-based materials (highly oriented pyrolytic graphite, multilayer graphene and multiwall carbon nanotubes) and of some of their elastomeric composites. *Vib. Spectrosc.* **2014**, *74*, 57–63. [[CrossRef](#)]
24. Peña-Álvarez, M.; Del Corro, E.; Langa, F.; Baonza, V.G.; Taravillo, M. Morphological changes in carbon nanohorns under stress: A combined Raman spectroscopy and TEM study. *RSC Adv.* **2016**, *6*, 49543–49550. [[CrossRef](#)]
25. Ferreira, E.H.M.; Moutinho, M.; Stavale, F.; Lucchese, M.M.; Capaz, R.B.; Achete, C.A.; Jorio, A. Evolution of the Raman spectra from single-, few-, and many-layer graphene with increasing disorder. *Phys. Rev. B* **2010**, *82*, 125429. [[CrossRef](#)]
26. NC7000TM—Technical Data Sheet. Available online: <https://www.nanocyl.com/download/tds-nc7000/> (accessed on 13 November 2020).
27. Singh, K.; Chaudhary, S.; Venugopal, R.; Gaurav, A. Bulk synthesis of multi-walled carbon nanotubes by AC arc discharge method. *Proc. Inst. Mech. Eng. Part N J. Nanomater. Nanoeng. Nanosyst.* **2017**, *231*, 141–151. [[CrossRef](#)]
28. Satapathy, S.; Pawar, S.; Gupta, P.K.; Varma, K.B.R. Effect of annealing on phase transition in poly(vinylidene fluoride) films prepared using polar solvent. *Bull. Mater. Sci.* **2011**, *34*, 727–733. [[CrossRef](#)]
29. Boccaccio, T.; Bottino, A.; Capannelli, G.; Piaggio, P. Characterization of PVDF membranes by vibrational spectroscopy. *J. Membr. Sci.* **2002**, *210*, 315–329. [[CrossRef](#)]
30. Constantino, C.J.L.; Job, A.E.; Simoes, R.D.; Giacometti, J.A.; Zucolotto, V.; Oliveira, O.N.; Gozzi, G.; Chinaglia, D.L. The Investigation of α / β Phase Transition in Poly(Vinylidene Fluoride) (PVDF). In Proceedings of the 2005 12th International Symposium on Electrets, IEEE, Salvador, Bahia, Brazil, 11–14 September 2005; pp. 178–181.
31. Wang, G.-L.; Tian, Y.-M.; Cao, D.-X.; Yu, Y.-S.; Sun, W.-B. One-dimensional Salen-type Chain-like Lanthanide(III) Coordination Polymers: Syntheses, Crystal Structures, and Fluorescence Properties. *Z. Für Anorg. Und Allg. Chem.* **2010**, *637*, 583–588. [[CrossRef](#)]
32. Li, Z.-F.; Cheng, X.-X.; Li, G.; Lu, H.-J.; Zhang, H.-F. Syntheses, structures, fluorescence and thermal properties of three lanthanide coordination polymers built by N-benzoyl-N'-(4-benzoxy)thiourea. *J. Lumin.* **2010**, *130*, 2192–2200. [[CrossRef](#)]
33. Hartschuh, A.; Pedrosa, H.N.; Novotny, L.; Krauss, T.D. Simultaneous Fluorescence and Raman Scattering from Single Carbon Nanotubes. *Science* **2003**, *301*, 1354–1356. [[CrossRef](#)]
34. Högele, A.; Galland, C.; Winger, M.; Imamoğlu, A. Photon Antibunching in the Photoluminescence Spectra of a Single Carbon Nanotube. *Phys. Rev. Lett.* **2008**, *100*, 217401. [[CrossRef](#)]
35. Okpalugo, T.; Papakonstantinou, P.; Murphy, H.; McLaughlin, J.; Brown, N. High resolution XPS characterization of chemical functionalised MWCNTs and SWCNTs. *Carbon* **2005**, *43*, 153–161. [[CrossRef](#)]
36. Duca, M.D.; Plosceanu, C.L.; Pop, T. Surface modifications of polyvinylidene fluoride (PVDF) under rf Ar plasma. *Polym. Degrad. Stab.* **1998**, *61*, 65–72. [[CrossRef](#)]
37. Constantino, C.J.L.; Job, A.E.; Simões, R.D.; Giacometti, J.A.; Zucolotto, V.; Oliveira, O.N.; Gozzi, G.; Chinaglia, D.L. Phase Transition in Poly(Vinylidene Fluoride) Investigated with Micro-Raman Spectroscopy. *Appl. Spectrosc.* **2005**, *59*, 275–279. [[CrossRef](#)]
38. Kaspar, P.; Sobola, D.; Částková, K.; Knápek, A.; Burda, D.; Orudzhev, F.; Dallaev, R.; Tofel, P.; Trčka, T.; Grmela, L.; et al. Characterization of Polyvinylidene Fluoride (PVDF) Electrospun Fibers Doped by Carbon Flakes. *Polymers* **2020**, *12*, 2766. [[CrossRef](#)] [[PubMed](#)]
39. Cai, X.; Lei, T.; Sun, D.; Lin, L. A critical analysis of the α , β and γ phases in poly(vinylidene fluoride) using FTIR. *RSC Adv.* **2017**, *7*, 15382–15389. [[CrossRef](#)]
40. Li, Q.W.; Li, Y.; Zhang, X.F.; Chikkannanavar, S.B.; Zhao, Y.H.; Dangelewicz, A.M.; Zheng, L.X.; Doorn, S.K.; Jia, Q.X.; Peterson, D.E.; et al. Structure-Dependent Electrical Properties of Carbon Nanotube Fibers. *Adv. Mater.* **2007**, *19*, 3358–3363. [[CrossRef](#)]
41. Puértolas, J.; García-García, J.; Pascual, F.; González-Domínguez, J.; Martínez, M.; Ansón-Casaos, A. Dielectric behavior and electrical conductivity of PVDF filled with functionalized single-walled carbon nanotubes. *Compos. Sci. Technol.* **2017**, *152*, 263–274. [[CrossRef](#)]
42. Sedlak, P.; Gajdos, A.; Macku, R.; Majzner, J.; Holcman, V.; Sedlakova, V.; Kubersky, P. The effect of thermal treatment on ac/dc conductivity and current fluctuations of PVDF/NMP/[EMIM][TFSI] solid polymer electrolyte. *Sci. Rep.* **2020**, *10*, 1–12. [[CrossRef](#)]

Chapter 6. PVDF Fibers Modified by Carbon Flakes

6.1 Motivation of the article

Creating nanocomposites with PVDF films has proven effective in boosting their functionality in challenging environments, particularly in sensor and actuator applications. Carbon materials are frequently combined with PVDF to further improve these properties, leading to the development of hybrid composite films and improved piezoelectric characteristics. While significant research has focused on PVDF films, this study shifts the attention to PVDF fibers and their combination with carbon materials. Previous studies have explored the enhancement of PVDF fibers with carbon nanofibers and the carbonization of PVDF fibers, along with the inclusion of graphene nanoparticles. However, these methods can be complex and costly. This paper introduces a novel approach by incorporating graphite flakes into PVDF fibers during their fabrication. Graphite flakes are an accessible and cost-effective material that, when integrated into the fiber structure, can modify and potentially enhance the properties of PVDF fibers. This research aims to provide a simpler and more economical method for improving PVDF fibers, broadening their applicability and performance in various advanced technological applications.

6.2 Conclusion on the article

It was discovered that carbon flakes within PVDF fibers, rather than applying a carbon film coating, significantly alters the properties of the PVDF material. SEM analysis confirmed the integration of flakes into the fiber structure. This inclusion notably changes the crystalline phase concentrations of α , β , and γ phases, as detected by Raman spectroscopy, FTIR, and XRD. Carbon flakes themselves do not introduce new peaks in Raman or FTIR spectra and appear only at one significant peak location in XRD. XPS revealed two key findings: a shift from semi-ionic to covalent bonding, likely due to the formation of covalent C–F bonds between fluorine atoms and graphite defects, and the elimination of adsorbed oxygen and water. This bond reformation likely prevents water and oxygen adsorption. Additionally, the presence of carbon altered the electric properties of PVDF, increasing the dielectric constant and reducing triboelectric properties with higher carbon content. These findings demonstrate that incorporating inexpensive and accessible carbon flakes into PVDF fibers not only modifies their structural and electrical properties but also opens up new possibilities for advanced applications of this modified material.

6.3 Applicant's contribution

The applicant is responsible for the entire XPS analysis (measurement, interpretation and visualisation).

6.4 Article 6

The paper "*Characterization of Polyvinylidene Fluoride (PVDF) Electrospun Fibers Doped by Carbon Flakes*" was published in November 2020 in "*Polymers*" journal (IF: 5.0; Q1).

*The paper is highly cited and gathered 74 citations to date (02.06.2024).

Article

Characterization of Polyvinylidene Fluoride (PVDF) Electrospun Fibers Doped by Carbon Flakes

Pavel Kaspar ¹, Dina Sobola ^{1,2,3}, Klára Částková ^{2,4}, Alexandr Knápek ^{5,*},
Daniel Burda ^{1,5}, Farid Orudzhev ³, Rashid Dallaev ¹, Pavel Tofel ^{1,2}, Tomáš Trčka ¹,
Lubomír Grmela ^{1,2} and Zdeněk Hadaš ⁶

¹ Department of Physics, Faculty of Electrical Engineering and Communication, Brno University of Technology, Technická 2848/8, 616 00 Brno, Czech Republic; kasparp@feec.vutbr.cz (P.K.); sobola@feec.vutbr.cz (D.S.); burda@isibrno.cz (D.B.); xdalla03@stud.feec.vutbr.cz (R.D.); tofel@feec.vutbr.cz (P.T.); trcka@feec.vutbr.cz (T.T.); grmela@vutbr.cz (L.G.)

² Central European Institute of Technology BUT, Purkyňova 123, 612 00 Brno, Czech Republic; klara.castkova@ceitec.vutbr.cz

³ Department of Inorganic Chemistry and Chemical Ecology, Dagestan State University, Makhachkala, St. M. Gadjeva 43-a, 367015 Dagestan Republic, Russia; farid-stkha@mail.ru

⁴ Department of Ceramics and Polymers, Faculty of Mechanical Engineering, Brno University of Technology, Technická 2, 616 69 Brno, Czech Republic

⁵ Institute of Scientific Instruments of the Czech Academy of Sciences, Královopolská 147, 612 64 Brno, Czech Republic

⁶ Faculty of Mechanical Engineering, Brno University of Technology, Technická 2896/2, 616 69 Brno, Czech Republic; hadas@fme.vutbr.cz

* Correspondence: knapek@isibrno.cz; Tel.: +420-541-514-258

Received: 30 October 2020; Accepted: 21 November 2020; Published: 24 November 2020



Abstract: Polyvinylidene fluoride (PVDF) is a modern polymer material used in a wide variety of ways. Thanks to its excellent resistance to chemical or thermal degradation and low reactivity, it finds use in biology, chemistry, and electronics as well. By enriching the polymer with an easily accessible and cheap variant of graphite, it is possible to affect the ratio of crystalline phases. A correlation between the ratios of crystalline phases and different properties, like dielectric constant as well as piezo- and triboelectric properties, has been found, but the relationship between them is highly complex. These changes have been observed by a number of methods from structural, chemical and electrical points of view. Results of these methods have been documented to create a basis for further research and experimentation on the usability of this combined material in more complex structures and devices.

Keywords: polyvinylidene fluoride; graphite; scanning electron microscopy; X-ray diffraction; Raman spectroscopy; Fourier-transform infrared spectroscopy; triboelectric effect

1. Introduction

Polymers are very topical materials useful in a great number of scientific fields. They are sought after for their excellent properties, namely high chemical stability and biocompatibility [1]. One of the more interesting materials that has gained a lot of popularity amongst scientists in the last couple of years, is polyvinylidene fluoride (PVDF). The great properties of this polymer, like low reactivity and high degree of thermoplasticity, as well as low cytotoxicity or chemical reactivity [2], have secured it a place in many areas, like semiconductors, biology, or chemistry. PVDF, though it can be difficult to manufacture and prepare, has a great potential for application in many areas of science and life. Preparation of PVDF requires a specialized approach, because preparation methods used for other

polymers are not capable of producing homogeneous and usable products [3,4]. To create a PVDF fiber, methods like spin coating or electrospinning, are used to manufacture fibers with stable and repeatable results. Electrospinning specifically has been used in the case of this paper, as it allows for control over fiber diameter, inclusions, and crystalline phase to a certain extent [5].

Polyvinylidene fluoride has seen almost immediate use and a great deal of modification, further improving on its properties. By creating nanocomposites of the PVDF films with other materials, it is possible to increase their performance in difficult environments and to preserve and enhance their functional abilities as sensors and actuators [6,7]. Among the most popular materials for combination with PVDF is carbon. There are many papers focusing on the creation of hybrid composite films from PVDF and carbon [8], to use with carbon quantum dots for creation of films [9], or to use carbon with PVDF to improve its piezoelectric properties [10,11]. The focus of this paper is, however, not on films, but rather on PVDF fibers, and their combination with carbon. Research has been conducted into enhancing PVDF in both fiber and film form with carbon nanofibers already, [12,13], and even on carbonization of the PVDF fiber itself [14]. Graphene nanoparticles are among the inclusions for PVDF as well [15]. In this paper, we have decided to focus on carbon as well, but to use a much simpler and cheaper method in comparison to nanoparticles. Graphite flakes, a highly accessible and cheap material, are introduced into the fibers during their creation, which incorporates them into the fiber structure and changes their properties as well. To properly understand all the changes this incorporation of graphite flakes causes in PVDF, the pure original materials and their combination have been subjected to several measurements, namely scanning electron microscopy (SEM) to capture the topography, Raman spectroscopy, X-ray diffraction measurement (XRD), X-ray photoelectron spectroscopy (XPS), and Fourier-transform infrared spectroscopy (FTIR) to describe the properties and their changes on chemical level, and permittivity measurement to observe the electrical properties. The overarching reason for these experiments is that there are several benefits to changing the concentration of phases. α phase has higher dielectric constant and can therefore be used, where high energy storage properties are required. When combined with a relatively high breakdown voltage of the polymer, controlling the dielectric constant can be of great interest. β phase, on the other hand, lowers the dielectric constant, but introduces piezoelectric activity into the material and modifies triboelectric properties, which can then be used for energy harvesting or storage related purposes [16]. The ability to dictate the concentration of crystalline phases and dielectric and piezoelectric properties linked to them is very important for the maximalization of potential usefulness of the material. The novelty of this work is in the use of low-cost carbon materials and description of structure and properties in dependence on the powder concentration. We show that the incorporation of carbon powder as a filler into PVDF, even without functionalization and surface activation of the powder, allows for the control of properties of the resulting composite. This work contributes to the study of the formation of complex polymer systems and its modifications.

2. Materials and Methods

The main material in question is PVDF ($M_w = 275.000$ g/mol, Sigma Aldrich, Munich, Germany), more specifically, PVDF fibers. These fibers were manufactured by the method of electrospinning from 15 wt% PVDF solution in dimethylsulfoxide-aceton blend in volume ratio of 7/3 under a constant voltage of 50 kV, creating a fiber mat with the thickness of around 25 μm . The PVDF, or graphite doped PVDF solutions, were electrospun using 4-spin electrospinning equipment (Contipro, Dolní Dobrouč, Czech Republic) at a feeding rate of 20 $\mu\text{l}\cdot\text{min}^{-1}$ through a needle with an inner diameter of 1.067 mm (17 G) on a rotation collector covered by aluminum foil at a speed of 2000 rpm for 30 min. The distance between the needle tip and the collector was 20 cm. The fibers were collected in the form of non-woven mats, which were dried at laboratory temperature overnight. The whole process yielded resulting fibers with the width of 195.2 nm. In the case of enriched fibers, the 1% wt of graphite flakes were added into the polymer solution and the electrospinning process was performed with the same properties as with the pure PVDF solution.

Graphite powder is of the D50 grade with size of the particles of 3.5 μm . The powder was purchased from GK Graphite and the parameters were taken from their documentation. This material is widely accessible and is the same grade used for manufacture of pencil lead.

Raman spectroscopy was performed using WITec alpha300 R device (WITec, Ulm, Germany). Excitation wavelength for the experiments was set at 532 nm. Power of the laser used for excitation of the samples was 0.5 mW for the graphite flakes and PVDF fibers with the flakes, whereas for PVDF fibers without the flakes the power had to be increased to 1 mW to obtain a viable signal to noise ratio. The resulting signal was reconstructed from 50 accumulations with the integration time of 20 s.

SEM images were captured by a high-resolution scanning electron microscope FEI Verios 460 L (FEI, Brno, Czech Republic). To allow the use of SEM and improve the quality of obtained images, samples of pure PVDF and those with graphite flakes were covered with a 15 nm thick carbon film to improve their conductivity. The coating was done by carbon thread evaporator Leica EM ACE600. Carbon was used because of its accessibility and to prevent artefacts in the image due to conglomeration of golden particles during coating. Voltage of the electron beam was kept at 5 kV during the whole process, whereas the current was adjusted according to circumstances to receive the best images possible. In addition to the “through-lens detector” (TLD), charge neutralization mode (CN) had to be used as well for some samples, where charging of the edges was an issue.

XPS spectra were taken by AXIS Supra X-ray photoelectron spectrometer (Kratos Analytical, Manchester, UK). Emission current used to capture the resulting information was set at 15 mA. During the process, resolution 20 was utilized to for the measurement of wide spectra, and 80 for the element spectra. Final fitting of the spectra was performed using CasaXPS software.

FTIR measurement was taken in transmission mode (Bruker, Billerica, MA, USA), with resolution of 1 cm^{-1} , over 512 iterations.

XRD analysis was done using X-ray powder diffractometer Rigaku SmartLab 3 kW (Rigaku Corporation, Tokyo, Japan) in Bragg-Brentano configuration was performed. Diffraction patterns were measured from 10° to 50° (2 θ) with Cu K α radiation.

Dielectric measurement was performed with Novocontrol Alpha Analyzer (Novocontrol Technologies, Montabaur, Germany) in the range between 1 Hz and 100,000 Hz in room temperature for the acquisition of basic information about dielectric properties, mainly permittivity of the material.

Triboelectric energy performance of the proposed materials was evaluated by electrometer 6517b (Keithley, Solon, Ohio, USA). The triboelectric generator was assembled in vertical contact-separation mode. Moving part consisting of Cu electrode was controlled by vibration test system TV 50,018 (Tira, Schalkau, Germany). Sample was clamped on a fixed Cu electrode. The area of the active part of the generator was 30 \times 30 mm. Mechanical force was measured by sensor 208C01 (PCB Piezotronics, Huckelhoven, Germany) and this sensor was situated on the side of fixed electrode. Displacement between electrodes was measured via interferometer ILD 1402-10 (Micro Epsilon, Ortenburg, Germany).

All of the methods described above, except for temperature dependent ones, were taken in room temperature.

3. Results and Discussion

To get a basic idea about the structural composition of the explored materials, SEM measurement was conducted on the three stages of the samples: pure PVDF, carbon flakes, and PVDF fibers with carbon flakes (Figure 1). Since the manufacturing process of PVDF fibers allows for the introduction of other materials into the source solution, the carbon flakes are incorporated into the structure of the fibers and thus become a part of it. Not only does this mean, that the flakes cannot be extracted from the composite by basic mechanical perturbations, like shaking or twisting of the fiber, but also that the structure of the polymer had to adapt and engulf the flakes. This can be best seen in detail in Figure 1b,d,f, depicting a focused detail of a single PVDF fiber, a carbon flake, and the resulting incorporated flake into the fiber, respectively.

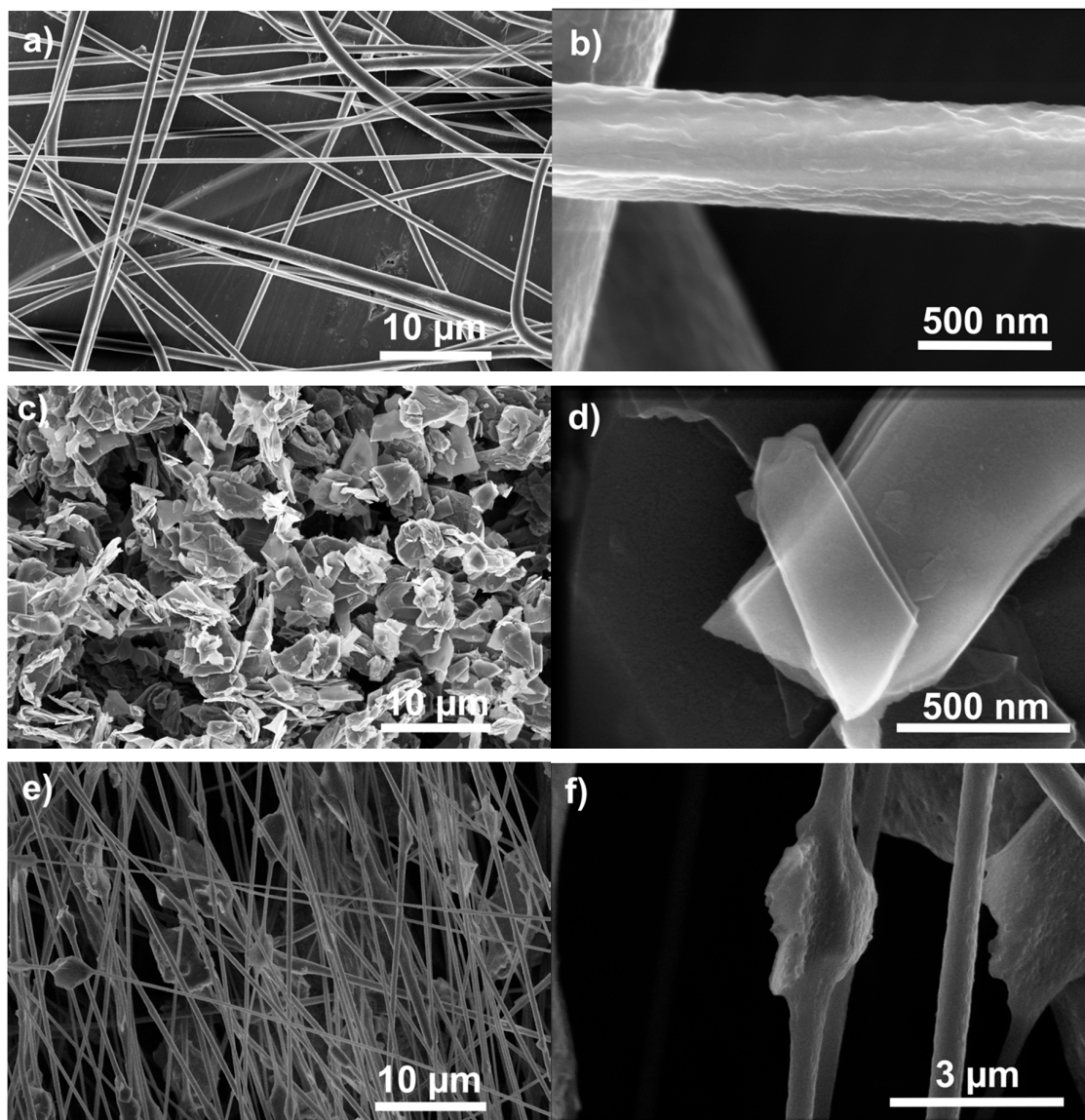


Figure 1. Pure PVDF Fibers, wide (a), and detail (b). Graphite flakes, wide (c) and detail (d) PVDF fibers with graphite flakes, wide (e) and detail (f).

The samples were subjected to XPS measurement. Figure 2a–c show the wide spectra of pure carbon flakes, pure PVDF and PVDF combined with carbon flakes, respectively. In the combined material (Figure 2c) the proportional content of carbon is slightly higher, which is to be expected from the addition of carbon flakes. In the pure carbon spectrum (Figure 2a), it is possible to spot a peak belonging to oxygen, likely caused by oxidization of the surface or residual adsorbed moisture.

From the XPS measurement it can be seen that the XPS spectrum of pure graphite flakes (Figure 3a) is very much like it can be expected [17,18]. The C–C peak at 285 eV is a staple of graphite, for nano size or bigger as well. This presence can be seen altering the dominant C–O/CH₂ peak of PVDF (Figure 3c), making it wider, and taking over from the C–O peak at 287 eV (Figure 3b). This is the most visible change in the XPS spectrum from the point of view of C1 peaks.

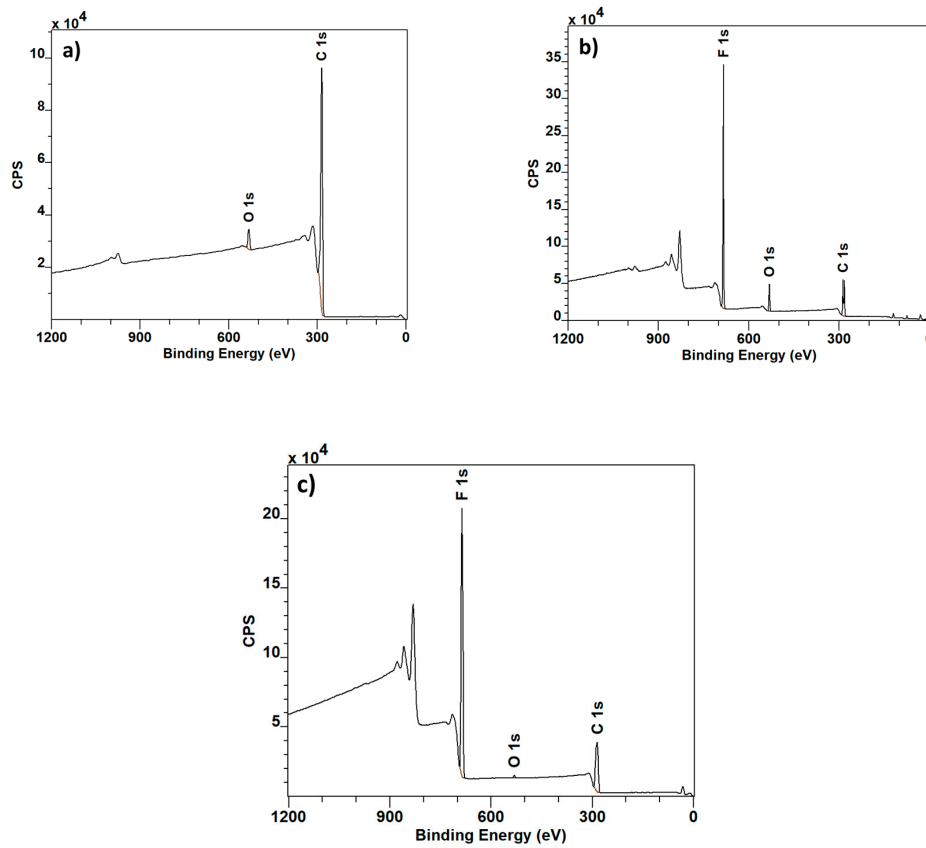


Figure 2. Wide XPS spectra: Graphite (a), PVDF (b) and PVDF with Graphite (c).

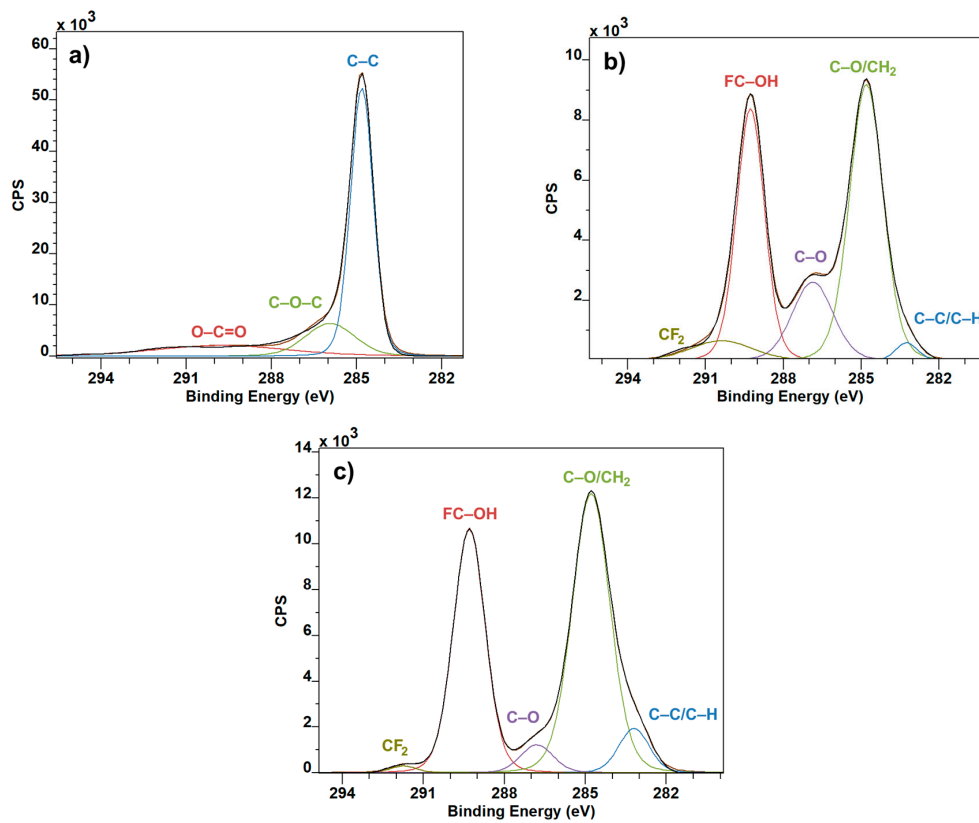


Figure 3. C1 XPS spectra: Graphite (a), PVDF (b) and PVDF with Graphite (c).

The greatest inconsistencies can be seen in the O1 spectra. The easily recognizable C=O bond at 529 eV is carried over from the pure graphite (Figure 4a) into the PVDF/graphite combination (Figure 4c). The magnitude of C–OH peaks was reduced in the combined material, and the C–O increased, when compared to the pure PVDF sample (Figure 4b) [19]. The somewhat unexpected part here is the presence of peaks in graphite at around 527 eV, and 535 eV in pure PVDF. These are rather uncommon, and after an extensive search they have been identified as adsorbed oxygen [20] and adsorbed water [21], respectively. Their presence is virtually eliminated in the combined material, supporting this opinion.

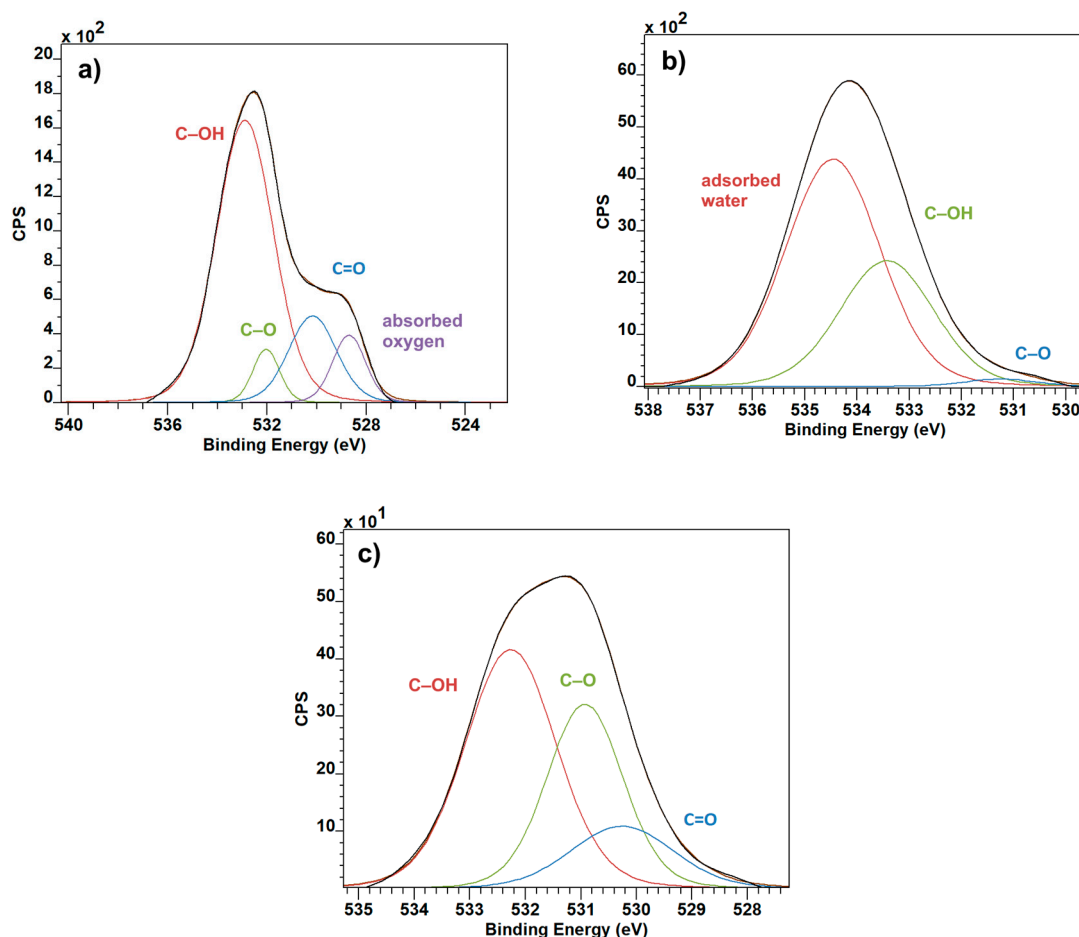


Figure 4. O1 XPS spectra: Graphite (a), PVDF (b) and PVDF with Graphite (c).

The F1 spectra show a change in the dynamic of covalent and semi-ionic bonds after the introduction of graphite. In pure PVDF (Figure 5a), the more prevalent of these two are the semi-ionic bonds, whereas in the combined material, the ratio shifts in the favor of covalent bonds (Figure 5b) [22].

Figure 6 shows the wide Raman spectra taken from pure carbon, pure PVDF, and combined material from locations of a fiber and of a flake. D-band at 1341 cm^{-1} is activated by the presence of disorder in graphite and is clearly visible in pure carbon and combined material taken at the place of a graphite flake. The most prominent peak in the spectrum is located at 1580 cm^{-1} in carbon and at graphite flake location of PVDF with carbon and belongs to a G band representing in-plane vibrations of C–C bond [23]. Smaller peaks from 2500 to 2850 belong to the 2D group [24], and the last peak belonging to carbon at 3260 cm^{-1} belongs to a G + D'-combined band [25]. Band located around 794 cm^{-1} is attributed to CH₂ rocking, associated with both α and β phases of PVDF, whereas the band at around 2974 cm^{-1} is assigned to CH₂ symmetric stretching, associated with β phase [26]. Both these bands are, as expected, present only in material containing PVDF.

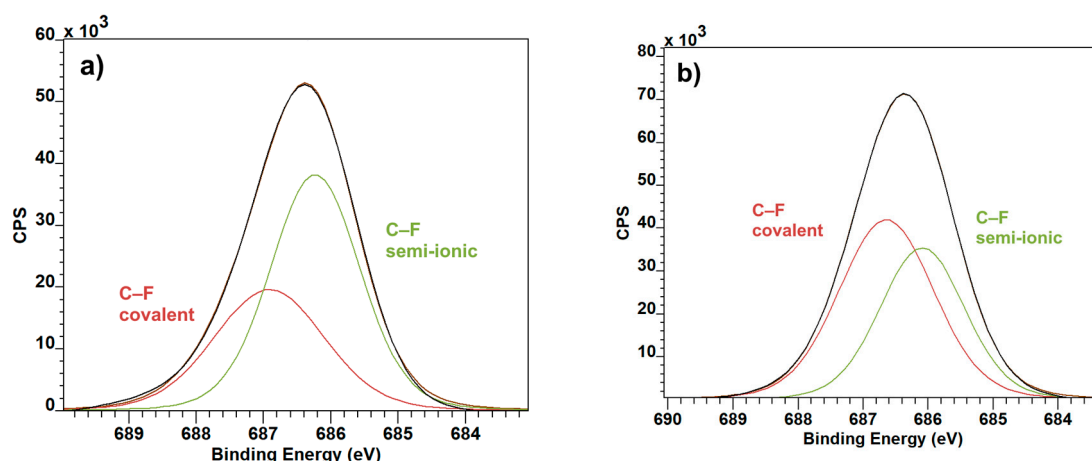


Figure 5. F1 XPS spectra: PVDF (a) and PVDF with Graphite (b).

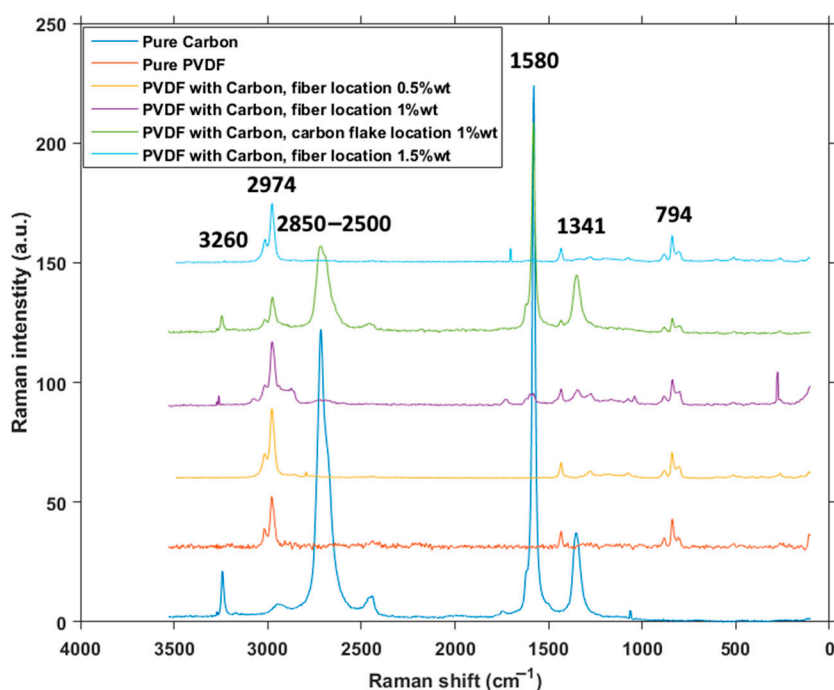


Figure 6. Raman wide spectra.

In the focused Raman spectrum (Figure 7) there are peaks commonly associated with vibration of CH₂ and CF₂, corresponding with α and β phases of PVDF [27]. The signal gained from pure carbon in this spectral range is virtually non-existent, which in itself is advantageous for this purpose, since it does not add any interference to the information about phases of PVDF. When the locations of phase peaks are compared to one another, the α phase peak in pure PVDF material is much more pronounced than in PVDF with carbon flakes. In the combined material, the ratio of α and β phases appears to change even more in the favor of β phase in comparison to pure PVDF. This would mean that the incorporation of carbon flakes into PVDF fibers created by electrospinning increases the concentration of β phase above the initial amount granted by the method itself.

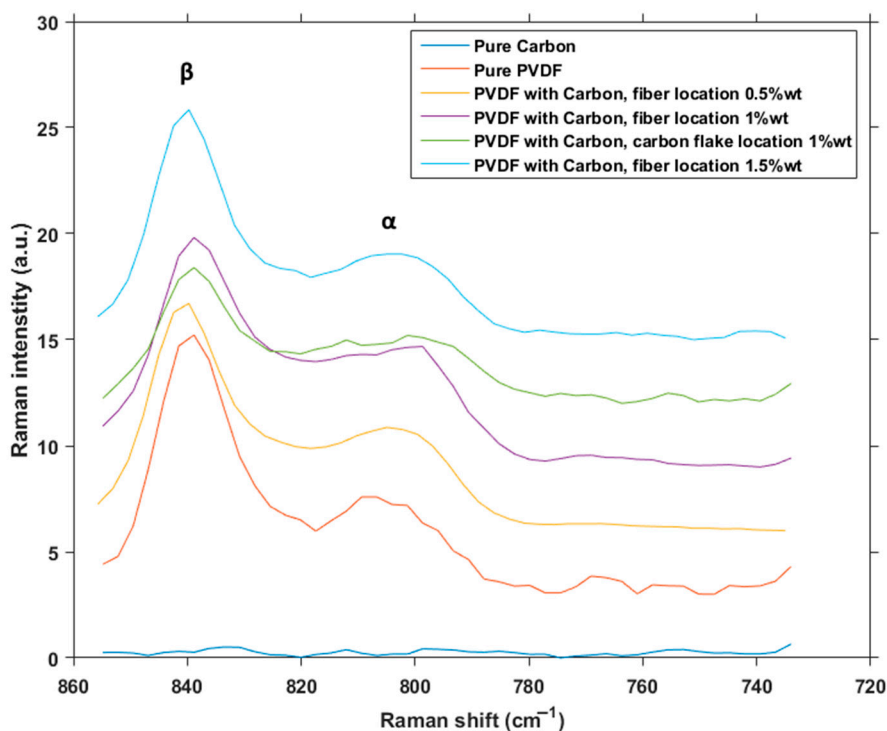


Figure 7. Raman spectra focused on locations of phases.

Samples of pure PVDF and PVDF with graphite flakes were subjected to FTIR measurement as well. Reason for this was mainly to compare the concentration of different phases. In Figure 8, it can be seen that, at the first glance, the absorption spectra are almost identical. Locations of virtually all of the peaks remain the same, and their sizes are comparable as well, with a couple of exceptions.

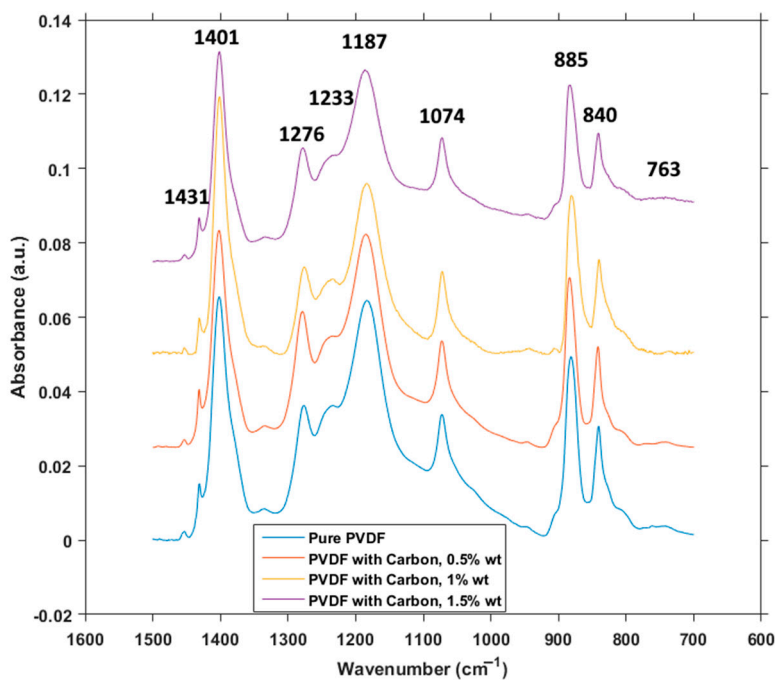


Figure 8. FTIR spectra.

There is a very small and flat peak at 763 cm^{-1} , assigned to α phase, but the differences in size correspond with the concentration of this phase in all of the samples. Peak at 840 cm^{-1} is significantly

larger as it represents β phase, as do the peaks at 1431 cm^{-1} and 1276 cm^{-1} , being characteristic for this crystalline phase. Peak at 1074 cm^{-1} represents mostly the β phase, but references to other phases can be found around this location as well, making the analysis more complicated. From the characteristic peaks there is also 1233 cm^{-1} , exclusive for the γ phase. 1187 cm^{-1} is assigned to the combination of β and γ , and the large peaks at 885 cm^{-1} and 1401 cm^{-1} represent the combination of all three phases [28]. Numerical values of concentrations of crystalline phases for each measured content of carbon powder can be seen in Table 1.

Table 1. Percentage concentration of phases and measured relative permittivity at 1 kHz of pure PVDF and varying content of carbon powder.

	Pure PVDF	PVDF with 0.5% wt Carbon Powder	PVDF with 1.0% wt Carbon Powder	PVDF with 1.5% wt Carbon Powder
α phase concentration [%]	13.454	4.3404	4.622	38.287
β phase concentration [%]	82.521	94.631	85.840	60.526
γ phase concentration [%]	4.025	1.029	9.538	1.187
Relative permittivity ϵ_r	3.986	1.970	7.998	4.714
Standard deviation of ϵ_r	0.201	0.087	1.028	0.935

The large similarity between presence and locations of the peaks would mean that, since the graphite flakes are not simply scattered on the top of the fibers, but are integrated inside of the material, as was shown in Figure 1e,f, the presence of the flakes influences the ratio of crystalline phases on the level of chemical structures. A small peak of α phase can be seen in Figure 8 for pure PVDF, but disappears almost completely in PVDF with carbon flakes, which corresponds with the relative ratio calculation from the absorbance measurements. The increase of γ phase, that is present in the calculations, is however overshadowed by the peak of β phase in Figure 8, as their absorbances share a very close proximity [29]. An effect on the concentration of β phase has been observed by other authors [30] with other materials, like cellulose and carbon nanotubes. In the case of graphite flakes, the large surface area of the graphite acts as a site for heterogeneous nucleation of PVDF during the electrospinning process, which allows the β phase, a crystalline phase more demanding on the conditions of electrospinning process and more prone to destabilization during formation, to crystallize without the increased stress on material caused by uneven and small surfaces [31].

XRD measurement was performed on samples of pure PVDF and PVDF with graphite flakes. The very first clearly visible thing from the resulting spectra (Figure 9a) is the dominance of carbon peak at around 27° , which overshadows every other peak by far. This is, however, to be expected, as the peak is present only in the material with the carbon flakes and as such serves more as a check for the presence of graphite. More interesting peaks are to be found at around 18° and 21° (Figure 9b), as they belong to α phase and β phase respectively [28]. As with the other measurement methods mentioned here, this result also supports the fact that the ratio of crystalline phases can change by a large amount the PVDF material enriched with carbon flakes in comparison to the pure PVDF.

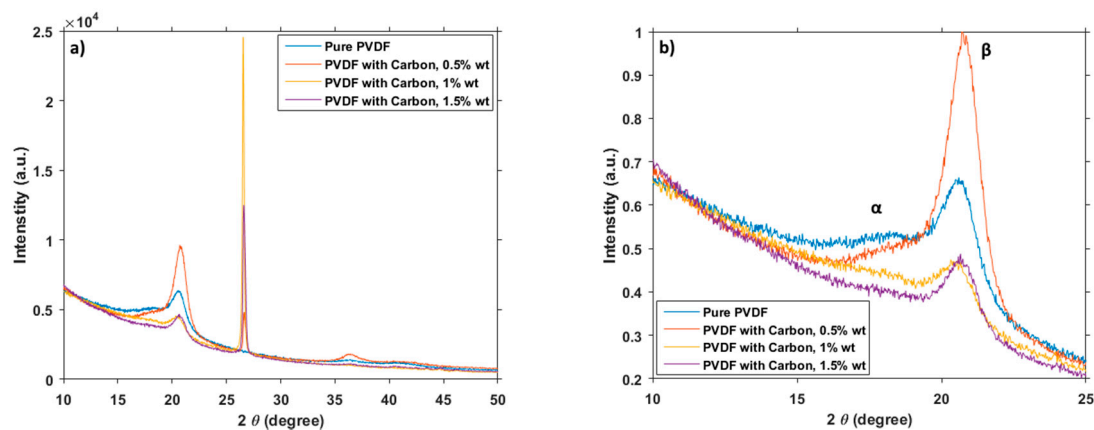


Figure 9. XRD wide spectra (a) and focused (b).

Dielectric properties of the samples were also measured to get a better idea about the overall behavior of electrical properties. In the case of PVDF polymer, dielectric properties are influenced by the crystalline phase of the material, its orientation and temperature [32–34]. Table 1 shows the relation between crystalline phases and measured relative permittivity at 1 kHz. The standard deviation of all the phase concentrations is 5%, corresponding with the claim from the manufacturer of the electrospinning device. From the numbers acquired it is clear, that the dependency between these values is not simple. Because the permittivity was measured under constant temperature, we can disregard its influence on the results in Table 1. We are, then, left with values that, at the first glance, do not have any correlation to one another. Relative permittivity is not directly dependent solely on one of the phases, but rather on all three combined. The greatest upset in the expected values is presented in the material with 1.0 wt% carbon powder content, and its abnormally high concentration of γ phase. This is one of the main influences on the large value of relative permittivity, though not the only one. All three crystalline phases together influence the resulting measured permittivity values in some manner. In addition to the crystallinity, there were also other, better documented influences on the dielectric constant, working against the influence of graphite flakes in the material, such as presence of defects or irregularities in the sample, which tend to cause a higher mobility of dipole moments and the growth of dielectric constant [35].

During the piezoelectricity measurements, however, we have found out, that, while the concentrations of the phases did indeed change, and while concentrations of phases have a well-documented effect on piezoelectric capabilities of PVDF film, we were unable to measure any reasonable piezoelectric response. This is likely because the fibers are not strictly oriented, and any possible piezoelectric effect it can have will cancel itself out with fibers going in all directions, even though in PVDF films the crystalline phases are directly linked to its piezoelectric behavior [36]. In addition, within the fiber, the molecular chains are not strictly oriented either, enhancing this problem further. For this reason, we have chosen to perform triboelectric measurements instead, as they were capable of yielding possible useful data.

Triboelectric generator was assembled in vertical contact-separation mode as was mentioned above in section materials and methods. Fixed electrode was made up of a PVDF sample clamped on the side. Active bottom electrode was controlled by a shaker to facilitate the pressure changes in the measurement. Both electrodes were electrically connected by resistor representing load resistance. AC voltage was measured on the load resistance and corresponding DC value was established by root mean square (RMS), as is done by many authors [37–40]. Output RMS voltage of the triboelectric generator was measured for different values of load. We have decided to measure the power from RMS voltage, without the use of any type of rectification from AC to DC. Then, the output power is not influenced by the type of rectification and the type of diodes, and raw power from material is captured. Maximal average power was evaluated for optimal value of load connected to triboelectric

nanogenerator. It is necessary to note that the output power of the generator is strongly influenced by mechanical frequency of operation and mechanical force of the touch of electrodes. We used constant operation conditions for our triboelectric generator, only the triboelectric fiber material inside was changed. In this way, it was possible to compare the triboelectric output capability of the materials and compare them. We used constant frequency of operation of 5 Hz, constant force of the touch of electrodes of 1 N and constant maximal gap between electrodes was 1.6 mm. Measurement setup and record of measurement in time can be seen in Figure 10. Force and Displacement represent input conditions for testing of the materials (upper chart in Figure 10). Force is measured in positive and negative direction. Force in negative direction appears when the upper (fixed) electrode is released, and then the own weight of the electrode is measured by the force meter. Red color shows position of the bottom electrode (active electrode). In Figure 10, we can see that the highest force $F = 1$ N appears when the electrodes are maximally pressed. Motion of the active electrode is blocked at this position as can be seen from the red line in the Figure 10 (upper chart). The lower chart in the Figure 10 shows electric behavior of the tested sample. The open circuit voltage, short circuit, and charge generated by the sample during operation can be seen in Figure 10.

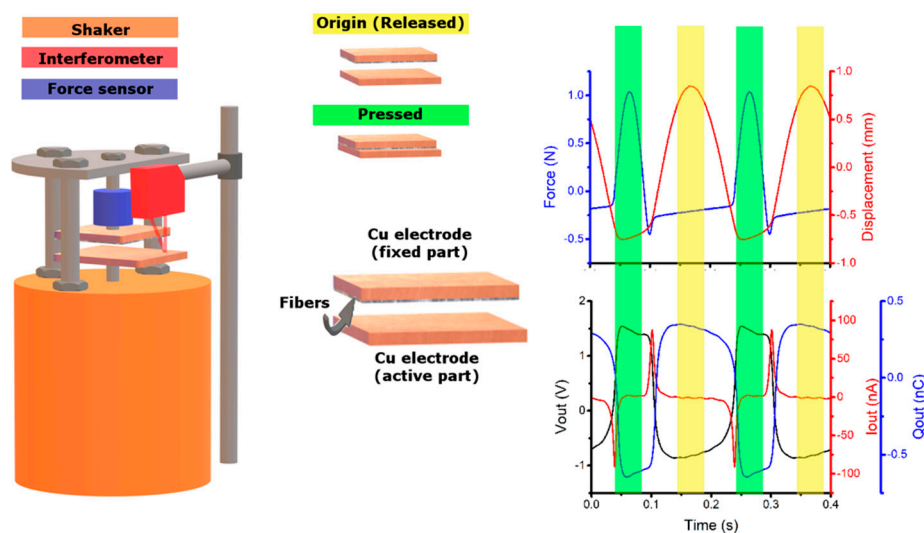


Figure 10. Triboelectric measurement setup. Time dependent chart on the right side shows Force and Displacement during measurement (upper chart—input conditions for the triboelectric nanogenerator) and open circuit voltage V_{out} , short circuit I_{out} and charge generated by the sample Q_{out} (lower chart—output electrical performance of the triboelectric nanogenerator).

Average power for different values of loads connected to the sample PVDF with 0.5% wt carbon powder is shown in Figure 11, for input conditions of 1 N pressing force, displacement between electrodes at 1.6 mm and frequency of 5 Hz. Optimal load is 70 M Ω for this sample and maximal power is 5.5 nW. This measurement was performed for comparison of our materials between each other from triboelectric point of view, how the content of carbon influences this property. We used low frequency of vibration 5 Hz and low force of touch of the electrodes with consideration to stiffness of the construction on the shaker.

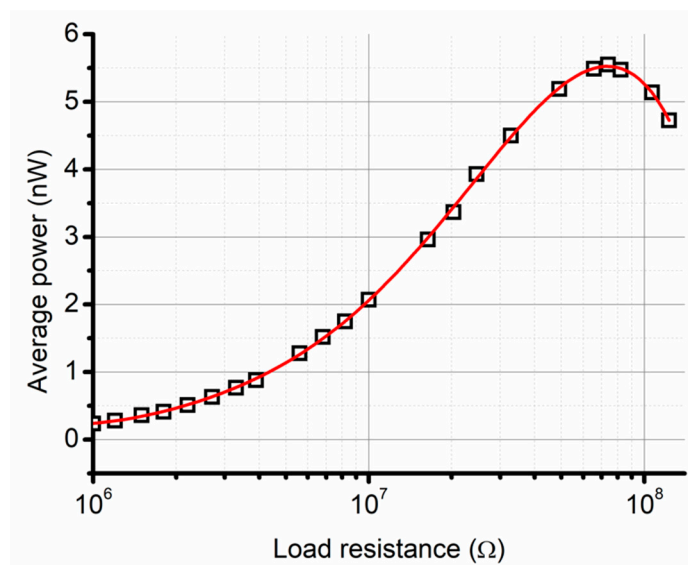


Figure 11. Average power as a function of load connected to the sample PVDF with 0.5% wt carbon powder.

From the measured values (Table 2), it is visible that the average power decreases with the increased concentration of carbon powder. This seems to be a fairly straightforward dependency, be it because of the increase of concentration of foreign material to PVDF in the form of carbon powder, or because of the decrease of β phase concentration with the increased percentage of carbon powder.

Table 2. Relative permittivity and maximum RMS power from triboelectric measurements of the pure PVDF fibers and those with carbon powder of different concentrations.

	Average Power [nW]	Standard Deviation of the Average Power [nW]
PVDF with 0.5% wt carbon powder	5.5	0.02
PVDF with 1.0% wt carbon powder	4.8	0.04
PVDF with 1.5% wt carbon powder	4.2	0.03

4. Conclusions

Polyvinylidene fluoride fibers enriched by incorporating carbon flakes inside of them during their weaving display a number of properties differing from pure PVDF material. Results obtained from an array of measurements are greatly affected by the fact that it is not a carbon film coating the fibers, but rather flakes inside of the fiber structure, as demonstrated by SEM. One of the most prominent changes, captured by Raman spectroscopy, FTIR, and XRD, is the change in crystalline phase concentration. Incorporating carbon flakes appears modify the concentrations of α , β and γ phases greatly. Carbon itself does not add any peaks in Raman spectroscopy and FTIR, and in XRD it is visible at one location only, even if the peak is quite big in comparison to others. XPS measurement managed to detect two important things. The first is the shift of ratio of semi-ionic bonds and covalent bonds, where, in pure PVDF material, semi-ionic bonds are more prevalent, but in the combined material, the ratio shifts in the favor of covalent bonds. This is likely due to fluorine atom bonding to a graphite structure defect, forming a covalent C–F bond. The second is the disappearance of adsorbed oxygen and water from the pure forms of carbon and PVDF, respectively. The reason for this is likely connected with the reforming of bonds in the materials when combined, losing the ability to adsorb water and oxygen in any measurable degree. The introduction of carbon had also an effect on the electric properties of PVDF, drastically changing the dielectric constant, and with an increased content of carbon powder lowering triboelectric properties. The results gathered and

described open a new window of opportunity for utilizing polyvinylidene fluoride modified by a cheap and accessible material.

Author Contributions: Conceptualization, P.K. and D.S.; methodology, A.K., T.T., Z.H., F.O., and R.D.; validation, P.T.; formal analysis, P.K.; investigation, K.Č., D.B., F.O., and R.D.; data curation, K.Č. and L.G.; writing—original draft preparation, P.K. and D.S.; visualization, D.S. and R.D.; supervision, L.G. All authors have read and agreed to the published version of the manuscript.

Funding: The research described in this paper was financially supported by the Ministry of Education, Youth and Sports of the Czech Republic under the project CEITEC 2020 [grant number LQ1601], by Internal Grant Agency of Brno University of Technology [Grant No. FEKT-S-20-6352] and Grant Agency of Czech Republic under project No. 19-17457S. A part of the work was carried out with the support of CEITEC Nano Research Infrastructure [grant ID LM2015041, MEYS CR, 2016–2019], CEITEC Brno University of Technology. We also acknowledge the Czech Academy of Sciences (RVO:68081731) and Technology Agency of Czech Republic (TN01000008).

Conflicts of Interest: The authors declare no conflict of interest. The funders had no role in the design of the study; in the collection, analyses, or interpretation of data; in the writing of the manuscript, or in the decision to publish the results.

References

1. McKeen, L.W. Fluoropolymers. In *Fatigue and Tribological Properties of Plastics and Elastomers*; Elsevier: Amsterdam, The Netherlands, 2016; pp. 291–315.
2. Kitsara, M.; Blanquer, A.; Murillo, G.; Humblot, V.; De Bragança Vieira, S.; Nogués, C.; Ibáñez, E.; Esteve, J.; Barrios, L. Permanently hydrophilic, piezoelectric PVDF nanofibrous scaffolds promoting unaided electromechanical stimulation on osteoblasts. *Nanoscale* **2019**, *11*, 8906–8917. [[CrossRef](#)] [[PubMed](#)]
3. Shaik, H.; Rachith, S.N.; Rudresh, K.J.; Sheik, A.S.; Thulasi Raman, K.H.; Kondaiah, P.; Mohan Rao, G. Towards β -phase formation probability in spin coated PVDF thin films. *J. Polym. Res.* **2017**, *24*, 35. [[CrossRef](#)]
4. Cardoso, V.F.; Minas, G.; Lanceros-Méndez, S. Multilayer spin-coating deposition of poly(vinylidene fluoride) films for controlling thickness and piezoelectric response. *Sens. Actuators A Phys.* **2013**, *192*, 76–80. [[CrossRef](#)]
5. Castkova, K.; Kastyl, J.; Sobola, D.; Petrus, J.; Stastna, E.; Riha, D.; Tofel, P. Structure–Properties Relationship of Electrospun PVDF Fibers. *Nanomaterials* **2020**, *10*, 1221. [[CrossRef](#)]
6. Liu, Y.Z.; Zhang, H.; Yu, J.X.; Huang, Z.Y.; Wang, C.; Sun, Y. Ferroelectric P(VDF-TrFE)/POSS nanocomposite films: Compatibility, piezoelectricity, energy harvesting performance, and mechanical and atomic oxygen erosion. *RSC Adv.* **2020**, *10*, 17377–17386. [[CrossRef](#)]
7. Liu, Y.Z.; Hao, Z.W.; Yu, J.X.; Zhou, X.R.; Lee, P.S.; Sun, Y.; Mu, Z.C.; Zeng, F.L. A high-performance soft actuator based on a poly(vinylidene fluoride) piezoelectric bimorph. *Smart Mater. Struct.* **2019**, *28*, 055011. [[CrossRef](#)]
8. Cai, J.; Hu, N.; Wu, L.; Liu, Y.; Li, Y.; Ning, H.; Liu, X.; Lin, L. Preparing carbon black/graphene/PVDF-HFP hybrid composite films of high piezoelectricity for energy harvesting technology. *Compos. Part A Appl. Sci. Manuf.* **2019**, *121*, 223–231. [[CrossRef](#)]
9. Dong, L.; Xiong, Z.; Liu, X.; Sheng, D.; Zhou, Y.; Yang, Y. Synthesis of carbon quantum dots to fabricate ultraviolet-shielding poly(vinylidene fluoride) films. *J. Appl. Polym. Sci.* **2019**, *136*, 47555. [[CrossRef](#)]
10. Wu, L.; Yuan, W.; Hu, N.; Wang, Z.; Chen, C.; Qiu, J.; Ying, J.; Li, Y. Improved piezoelectricity of PVDF-HFP/carbon black composite films. *J. Phys. D: Appl. Phys.* **2014**, *47*, 135302. [[CrossRef](#)]
11. Liu, Y.; Huang, Z.; Gao, Y. A Three-Dimensional and Bi-objective Topological Optimization Approach Based on Piezoelectric Energy Harvester. *Appl. Sci.* **2020**, *10*, 6772. [[CrossRef](#)]
12. Lee, S. Carbon nanofiber/poly(vinylidene fluoride-hexafluoro propylene) composite films: The crystal structure and thermal properties with various drawing temperatures. *Fibers Polym.* **2013**, *14*, 441–446. [[CrossRef](#)]
13. Tran, M.Q.; Ho, K.K.C.; Kalinka, G.; Shaffer, M.S.P.; Bismarck, A. Carbon fibre reinforced poly(vinylidene fluoride): Impact of matrix modification on fibre/polymer adhesion. *Compos. Sci. Technol.* **2008**, *68*, 1766–1776. [[CrossRef](#)]
14. Yang, Y.; Centrone, A.; Chen, L.; Simeon, F.; Alan Hatton, T.; Rutledge, G.C. Highly porous electrospun polyvinylidene fluoride (PVDF)-based carbon fiber. *Carbon* **2011**, *49*, 3395–3403. [[CrossRef](#)]
15. Elashmawi, I.S.; Alatawi, N.S.; Elsayed, N.H. Preparation and characterization of polymer nanocomposites based on PVDF/PVC doped with graphene nanoparticles. *Results Phys.* **2017**, *7*, 636–640. [[CrossRef](#)]

16. Thomas, P.; Satapathy, S.; Dwarakanath, K.; Varma, K.B.R. Dielectric properties of poly(vinylidene fluoride)/CaCu₃Ti₄O₁₂ nanocrystal composite thick films. *Express Polym. Lett.* **2010**, *4*, 632–643. [[CrossRef](#)]
17. Rao, K.S.; Senthilnathan, J.; Liu, Y.-F.; Yoshimura, M. Role of Peroxide Ions in Formation of Graphene Nanosheets by Electrochemical Exfoliation of Graphite. *Sci. Rep.* **2015**, *4*, 4237. [[CrossRef](#)] [[PubMed](#)]
18. Barlow, A.J.; Popescu, S.; Artyushkova, K.; Scott, O.; Sano, N.; Hedley, J.; Cumpson, P.J. Chemically specific identification of carbon in XPS imaging using Multivariate Auger Feature Imaging (MAFI). *Carbon* **2016**, *107*, 190–197. [[CrossRef](#)]
19. Militello, M.C.; Gaarenstroom, S.W. Graphite-Filled Poly(vinylidene fluoride) (PVdF) by XPS. *Surf. Sci. Spectra* **1999**, *6*, 141–145. [[CrossRef](#)]
20. Armelao, L.; Barreca, D.; Bottaro, G.; Gross, S.; Gasparotto, A.; Maragno, C.; Tondello, E.; Zattin, A. Introduction to XPS Studies of Metal and Metal-oxide Nanosystems. *Surf. Sci. Spectra* **2003**, *10*, 137–142. [[CrossRef](#)]
21. Knipe, S.W.; Mycroft, J.R.; Pratt, A.R.; Nesbitt, H.W.; Bancroft, G.M. X-ray photoelectron spectroscopic study of water adsorption on iron sulphide minerals. *Geochim. Cosmochim. Acta* **1995**, *59*, 1079–1090. [[CrossRef](#)]
22. Bhunia, R.; Ghosh, D.; Ghosh, B.; Hussain, S.; Bhar, R.; Pal, A. Free-standing flexible nanocrystalline-ZnO-impregnated polyvinylidene fluoride composite thin films. *J. Compos. Mater.* **2015**, *49*, 3089–3101. [[CrossRef](#)]
23. Bokobza, L.; Bruneel, J.-L.; Couzi, M. Raman spectroscopy as a tool for the analysis of carbon-based materials (highly oriented pyrolytic graphite, multilayer graphene and multiwall carbon nanotubes) and of some of their elastomeric composites. *Vib. Spectrosc.* **2014**, *74*, 57–63. [[CrossRef](#)]
24. Peña-Álvarez, M.; del Corro, E.; Langa, F.; Baonza, V.G.; Taravillo, M. Morphological changes in carbon nanohorns under stress: A combined Raman spectroscopy and TEM study. *RSC Adv.* **2016**, *6*, 49543–49550. [[CrossRef](#)]
25. Martins Ferreira, E.H.; Moutinho, M.V.O.; Stavale, F.; Lucchese, M.M.; Capaz, R.B.; Achete, C.A.; Jorio, A. Evolution of the Raman spectra from single-, few-, and many-layer graphene with increasing disorder. *Phys. Rev. B* **2010**, *82*, 125429. [[CrossRef](#)]
26. Constantino, C.J.L.; Job, A.E.; Simoes, R.D.; Giacometti, J.A.; Zucolotto, V.; Oliveira, O.N.; Gozzi, G.; Chinaglia, D.L. The Investigation of alpha → beta Phase Transition In Poly(Vinylidene Fluoride) (PVDF). In Proceedings of the IEEE 2005 12th International Symposium on Electrets, Salvador, Bahia, Brazil, 11–14 September 2005; pp. 178–181.
27. Elashmawi, I.S.; Gaabour, L.H. Raman, morphology and electrical behavior of nanocomposites based on PEO/PVDF with multi-walled carbon nanotubes. *Results Phys.* **2015**, *5*, 105–110. [[CrossRef](#)]
28. Cai, X.; Lei, T.; Sun, D.; Lin, L. A critical analysis of the α , β and γ phases in poly(vinylidene fluoride) using FTIR. *RSC Adv.* **2017**, *7*, 15382–15389. [[CrossRef](#)]
29. Constantino, C.J.L.; Job, A.E.; Simões, R.D.; Giacometti, J.A.; Zucolotto, V.; Oliveira, O.N.; Gozzi, G.; Chinaglia, D.L. Phase Transition in Poly(Vinylidene Fluoride) Investigated with Micro-Raman Spectroscopy. *Appl. Spectrosc.* **2005**, *59*, 275–279. [[CrossRef](#)]
30. Bodkhe, S.; Rajesh, P.S.M.; Kamle, S.; Verma, V. Beta-phase enhancement in polyvinylidene fluoride through filler addition: Comparing cellulose with carbon nanotubes and clay. *J. Polym. Res.* **2014**, *21*, 434. [[CrossRef](#)]
31. Kabir, E.; Khatun, M.; Nasrin, L.; Raihan, M.J.; Rahman, M. Pure β -phase formation in polyvinylidene fluoride (PVDF)-carbon nanotube composites. *J. Phys. D: Appl. Phys.* **2017**, *50*, 163002. [[CrossRef](#)]
32. da Silva, A.B.; Wisniewski, C.; Esteves, J.V.A.; Gregorio, R. Effect of drawing on the dielectric properties and polarization of pressed solution cast β -PVDF films. *J. Mater. Sci.* **2010**, *45*, 4206–4215. [[CrossRef](#)]
33. Xia, W.; Zhang, Z. PVDF-based dielectric polymers and their applications in electronic materials. *IET Nanodielectrics* **2018**, *1*, 17–31. [[CrossRef](#)]
34. Gregorio, R.J.; Ueno, E.M. Effect of crystalline phase, orientation and temperature on the dielectric properties of poly(vinylidene fluoride) (PVDF). *J. Mater. Sci.* **1999**, *34*, 4489–4500. [[CrossRef](#)]
35. Li, J.; Meng, Q.; Li, W.; Zhang, Z. Influence of crystalline properties on the dielectric and energy storage properties of poly(vinylidene fluoride). *J. Appl. Polym. Sci.* **2011**, *122*, 1659–1668. [[CrossRef](#)]
36. Gomes, J.; Serrado Nunes, J.; Sencadas, V.; Lanceros-Mendez, S. Influence of the β -phase content and degree of crystallinity on the piezo- and ferroelectric properties of poly(vinylidene fluoride). *Smart Mater. Struct.* **2010**, *19*, 065010. [[CrossRef](#)]

37. Zhang, L.; Meng, B.; Xia, Y.; Deng, Z.; Dai, H.; Hagedorn, P.; Peng, Z.; Wang, L. Galloping triboelectric nanogenerator for energy harvesting under low wind speed. *Nano Energy* **2020**, *70*, 104477. [[CrossRef](#)]
38. Sun, W.; Ding, Z.; Qin, Z.; Chu, F.; Han, Q. Wind energy harvesting based on fluttering double-flag type triboelectric nanogenerators. *Nano Energy* **2020**, *70*, 104526. [[CrossRef](#)]
39. Heo, D.; Chung, J.; Kim, B.; Yong, H.; Shin, G.; Cho, J.-W.; Kim, D.; Lee, S. Triboelectric speed bump as a self-powered automobile warning and velocity sensor. *Nano Energy* **2020**, *72*, 104719. [[CrossRef](#)]
40. Ibrahim, A.; Ramini, A.; Towfighian, S. Triboelectric energy harvester with large bandwidth under harmonic and random excitations. *Energy Rep.* **2020**, *6*, 2490–2502. [[CrossRef](#)]

Publisher’s Note: MDPI stays neutral with regard to jurisdictional claims in published maps and institutional affiliations.



© 2020 by the authors. Licensee MDPI, Basel, Switzerland. This article is an open access article distributed under the terms and conditions of the Creative Commons Attribution (CC BY) license (<http://creativecommons.org/licenses/by/4.0/>).

Chapter 7. PVDF Fibers Modified by Nitrate Salts

7.1 Motivation of the article

The motivation for this study stems from the need to comprehensively understand the structural properties and behavior of PVDF electrospun fibers when nitrate salts are introduced as additives. While the inclusion of various salts in polymers has been previously explored, and there has been some experimentation with electrospun fibers enhanced by salts, the specific effects of nitrate salts on PVDF fibers remain unexamined. The incorporation of additives into polymers is a pivotal strategy for tailoring their properties to meet specific application requirements. In the context of PVDF, a versatile polymer with significant industrial and scientific applications, the introduction of nitrate salts presents an unexplored avenue for enhancing its structural, chemical, and electrical properties. Despite the extensive research on PVDF and its composites, the specific effects of nitrate salt additives on PVDF fibers, particularly those prepared via electrospinning, remain largely unexamined. This research paper seeks to address this gap by systematically investigating the impact of various nitrate salts on PVDF fibers. Through a comprehensive suite of characterization techniques, including SEM-EDX (scanning electron microscopy with energy dispersive X-ray spectroscopy), DSC (differential scanning calorimetry), XPS, FTIR, Raman spectroscopy, and electrical measurements, the study aims to elucidate the nuanced changes in crystalline phase concentrations and electrical properties induced by these additives.

7.2 Conclusion on the article

The addition of various nitrate salts significantly influences the properties of PVDF fibers. One primary observed effect is on the concentration of crystalline phases. Compared to pure PVDF, salts containing calcium and magnesium cations notably increase the β -phase content, whereas zinc nitrate results in a β -phase content similar to that of pure PVDF. Regardless of the salt used, the γ -phase is almost entirely eliminated. Additionally, zinc nitrate exhibits unique optical properties, showing increased transmittance at higher wavelengths within the visible spectrum, suggesting potential applications in components where incident light is crucial.

In conclusion, the measured electrical properties generally correlate with the electronegativity of the nitrate salt cation. Calcium shows a similar ratio of covalent to semi-ionic bonds and dielectric constant as PVDF, as measured by XPS, while magnesium and zinc form a distinct group with a noticeably lower dielectric constant. These findings provide a foundation for further research and enhance our understanding of PVDF fiber composites.

7.3 Applicant's contribution

The applicant is responsible for the entire XPS analysis (measurement, interpretation and visualisation) which is a sizable part of this paper.

7.4 Article 7

The paper "*PVDF Fibers Modification by Nitrate Salts Doping*" was published in July 2022 in "*Polymers*" journal (IF: 5.0; Q1) and to date (02.06.2024) has 32 citations.

Article

PVDF Fibers Modification by Nitrate Salts Doping

Dinara Sobola^{1,2,3}, Pavel Kaspar², Klára Částková^{4,5}, Rashid Dallaev², Nikola Papež², Petr Sedlák^{2,4}, Tomáš Trčka^{2,*}, Farid Orudzhev³, Jaroslav Kaštyl⁴, Adam Weiser¹, Alexandr Knápek⁶ and Vladimír Holcman²

- ¹ Academy of Sciences ČR, Institute of Physics of Materials, Žitkova 22, 616 62 Brno, Czech Republic; sobola@ipm.cz (D.S.); aweiser@ipm.cz (A.W.)
 - ² Department of Physics, Faculty of Electrical Engineering and Communication, Brno University of Technology, Technická 2848/8, 616 00 Brno, Czech Republic; kasparp@feec.vutbr.cz (P.K.); rashid.dallaev@vutbr.cz (R.D.); Nikola.Papez@vutbr.cz (N.P.); sedlakp@feec.vutbr.cz (P.S.); holcman@feec.vutbr.cz (V.H.)
 - ³ Department of Inorganic Chemistry and Chemical Ecology, Dagestan State University, St. M. Gadjeva 43-a, 367015 Makhachkala, Russia; farid-stkha@mail.ru
 - ⁴ Central European Institute of Technology BUT, Purkyňova 123, 612 00 Brno, Czech Republic; klara.castkova@ceitec.vutbr.cz (K.Č.); jaroslav.kasty@ceitec.vutbr.cz (J.K.)
 - ⁵ Department of Ceramics and Polymers, Faculty of Mechanical Engineering, Brno University of Technology, Technická 2, 616 69 Brno, Czech Republic
 - ⁶ Institute of Scientific Instruments of the Czech Academy of Sciences, Královopolská 147, 612 64 Brno, Czech Republic; knapek@isibrno.cz
- * Correspondence: trcka@feec.vutbr.cz; Tel.: +420-54114-6011



Citation: Sobola, D.; Kaspar, P.; Částková, K.; Dallaev, R.; Papež, N.; Sedlák, P.; Trčka, T.; Orudzhev, F.; Kaštyl, J.; Weiser, A.; et al. PVDF Fibers Modification by Nitrate Salts Doping. *Polymers* **2021**, *13*, 2439. <https://doi.org/10.3390/polym13152439>

Academic Editor: Francisco Javier Espinach Orús

Received: 30 June 2021

Accepted: 21 July 2021

Published: 24 July 2021

Publisher's Note: MDPI stays neutral with regard to jurisdictional claims in published maps and institutional affiliations.



Copyright: © 2021 by the authors. Licensee MDPI, Basel, Switzerland. This article is an open access article distributed under the terms and conditions of the Creative Commons Attribution (CC BY) license (<https://creativecommons.org/licenses/by/4.0/>).

Abstract: The method of inclusion of various additives into a polymer depends highly on the material in question and the desired effect. In the case of this paper, nitride salts were introduced into polyvinylidene fluoride fibers prepared by electrospinning. The resulting changes in the structural, chemical and electrical properties of the samples were observed and compared using SEM-EDX, DSC, XPS, FTIR, Raman spectroscopy and electrical measurements. The observed results displayed a grouping of parameters by electronegativity and possibly the molecular mass of the additive salts. We virtually demonstrated elimination of the presence of the γ -phase by addition of $Mg(NO_3)_2$, $Ca(NO_3)_2$, and $Zn(NO_3)_2$ salts. The trend of electrical properties to follow the electronegativity of the nitrate salt cation is demonstrated. The performed measurements of nitrate salt inclusions into PVDF offer a new insight into effects of previously unstudied structures of PVDF composites, opening new potential possibilities of crystalline phase control of the composite and use in further research and component design.

Keywords: PVDF; nitrate salt; XPS; XRD; Raman spectroscopy; FTIR; EDX; permittivity

1. Introduction

Composite polymer materials have attracted a lot of attention from the scientific community. One of the most prominent polymers in question is polyvinylidene fluoride (PVDF), because of its high chemical and physical resistance and biocompatibility. PVDF thin films and their properties have been explored by a number of authors [1–3]. The fibrous form of the polymer carries different properties and possibilities. That said, special care must be taken in their manufacture, because the preparation process of fibers can be difficult to achieve safely and reliably [4]. The process that is most commonly used in the present to create suitable fibers is electrospinning, providing the best control over the parameters of the resulting material, with diameter of the fiber, inclusions and crystalline phases being among them [5,6]. Many properties of PVDF stem from the concentration of crystalline phases and as such they are one of the most important topics of conversation when the structural, chemical and electrical properties of these fibers are concerned [7,8].

Even though it is possible to affect the composition phase-wise just by proper selection of electrospinning properties, there is a limit to how much control can be exerted over

the phase formation process. To surpass that limit and to change the related properties of the fibers even further, other materials can be included into the polymer during the manufacture [9–11].

The novelty of this work lies with the thorough investigation of the structural properties and behavior of polyvinylidene fluoride electrospun fibers with nitrate salt inclusions. In this paper, the focus is on nitrate salts as an additive. While their introduction into polymers is not a new topic [12], and there has been some experimentation with electrospun fibers enhanced with salts [13], the overall effect of nitrate salts on PVDF fibers has not been explored yet.

The content of the present work includes PVDF fibers preparation by electrospinning and the samples characterization by several complementary techniques, based on different physical principles in order to obtain reliable data. The research was conducted with an emphasis on the comparison of and PVDF fibers with $\text{Ca}(\text{NO}_3)_2$, $\text{Mg}(\text{NO}_3)_2$ and $\text{Zn}(\text{NO}_3)_2$ salts.

2. Materials and Methods

The polyvinylidene fluoride (Sigma Aldrich, St. Louis, MO, USA) material being used in the measurements described below was prepared as fibers ($M_w = 275,000 \text{ g} \times \text{mol}^{-1}$) by electrospinning from 15 wt % PVDF solution in a blend of dimethylsulfoxide (Sigma Aldrich, St. Louis, MO, USA) and acetone (Sigma Aldrich, St. Louis, MO, USA) with a volume ratio of 7/3. The calcium, magnesium and zinc nitrates (in their hydrated form) (Lach-Ner, Neratovice, Czech Republic) were dissolved in the blending solvent in 8 wt% to the solid polymer before the PVDF dissolution. This solution was then electrospun under a constant voltage of 50 kV into fibers forming a mat with thickness of 25 μm .

Electrospinning was performed on an equipment 4-SPIN (Contipro, Dolní Dobrouč, the Czech Republic) at a feeding rate of $20 \mu\text{L} \times \text{min}^{-1}$ using a thin needle with a diameter of 1.067 mm (17 G). The rotation collector has been covered with an aluminum foil to gather the resulting fibers at a speed of 2000 rpm for 30 min, with the distance between the needle tip and the collector being kept at 20 cm. The resulting non-woven fiber mats were left to dry overnight at laboratory temperature. The diameter of the fibers created by this method was in the range from 300 to 700 nm.

X-ray photoelectron spectroscopy (XPS) was conducted to determine types of chemical bonds of the samples on AXIS Supra device (Kratos Analytical Ltd., Manchester, UK), with the results being captured under an emission current of 15 mA and resolution of 20 for wide spectra and 80 for the element-specific spectra. The resulting spectra were fitted in the CasaXPS software (version 2.3.23, Kratos Analytical Ltd., Manchester, UK) using Gaussian-Lorentzian line shape.

FTIR data were acquired in order to analyze phase composition of the samples on a Bruker device (Billerica, MA, USA) in transmission mode over 512 iterations with a resolution of 1 cm^{-1} .

X-ray powder diffraction (XRD) analysis was performed for confirmation of the crystalline structure of the samples on Rigaku SmartLab 3 kW device (Rigaku, Tokyo, Japan) in the Bragg–Brentano configuration. The resulting diffraction patterns were obtained between 10° and 25° (2θ) with $\text{Cu K}\alpha$ radiation.

The Raman spectroscopy results were taken for analysis of structural features of the samples by a WITec alpha300 R (WITec, Ulm, Germany) device at an excitation wavelength of 532 nm and the laser power of 10 mW. The obtained signal was reconstructed over 20 accumulations with the integration time of 10 s.

Energy-dispersive X-ray spectroscopy (EDX) was performed to follow the homogeneity of elements distribution and was conducted at an acceleration voltage of 15 kV in order to provide an overview of the elements distribution at the surface of the fibers samples. The electron microscope used was a Tescan LYRA3 (Tescan, Brno, Czech Republic) with an X-Max50 EDS detector from Oxford Instruments.

The measurement of dielectric properties, as parameters that define samples functionality, was carried out on a Novocontrol Alpha Analyzer device (Novocontrol Technologies, Montabaur, Germany) in the frequency range of 1 to 100,000 Hz.

Data from optical spectroscopy were obtained to study transmittance of the samples on a 3-channel (200–450 nm, 400–750 nm, 700–1000 nm) Spectrometer Ocean Optics JAZ-3 (Dunedin, FL, USA) using Ocean Optics software (OceanView, Dunedin, FL, USA). The resulting data were averaged from 20 scans each over 31 ms integration period.

Differential scanning calorimetry (DSC) measurements were performed to define crystallinity on DSC 204 F1 (NETZSCH, Selb, Germany) at a heating rate of $10\text{ }^{\circ}\text{C} \times \text{min}^{-1}$ from $25\text{ }^{\circ}\text{C}$ to $200\text{ }^{\circ}\text{C}$ under an argon flux $20\text{ mL} \times \text{min}^{-1}$.

Every measurement was performed five times for every sample for good data reliability. With the exception of DSC, all of the measurements used were carried out under room temperature.

3. Results and Discussion

Results from the C1 spectra of XPS measurement of the materials show the presence of standard bands expected for PVDF (Figure 1) [14]. In the pure and the enhanced PVDF fibers the most prominent peak is the C–O/CH₂ and this peak stays almost the same in all the materials. The FC–OH and C–O bands are greater in the pure PVDF, and smaller in the three doped materials. CF₂ is the smallest in the pure material, but together with C–C/C–H they differ within each of the sample. According to literature [15], the points of deliquescence are 56% for Mg(NO₃)₂·6H₂O and Ca(NO₃)₂·4H₂O, 42% for Zn(NO₃)₂·6H₂O. It explains dominant amount of H–O–C bonds for PVDF fibers with Zn(NO₃)₂ (Figure 2b).

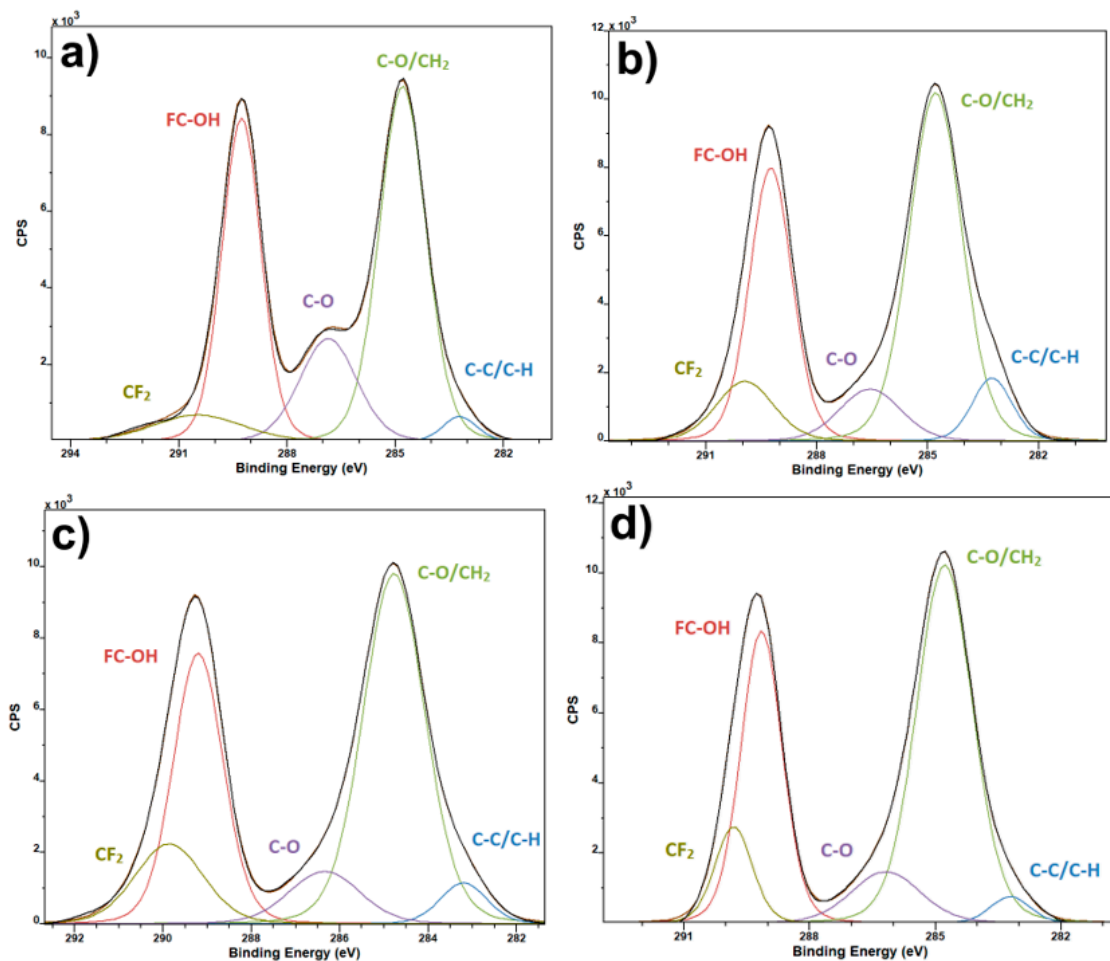


Figure 1. XPS C1 spectra of pure PVDF fibers (a) and PVDF fibers with Ca(NO₃)₂ (b), Mg(NO₃)₂ (c) and Zn(NO₃)₂ (d).

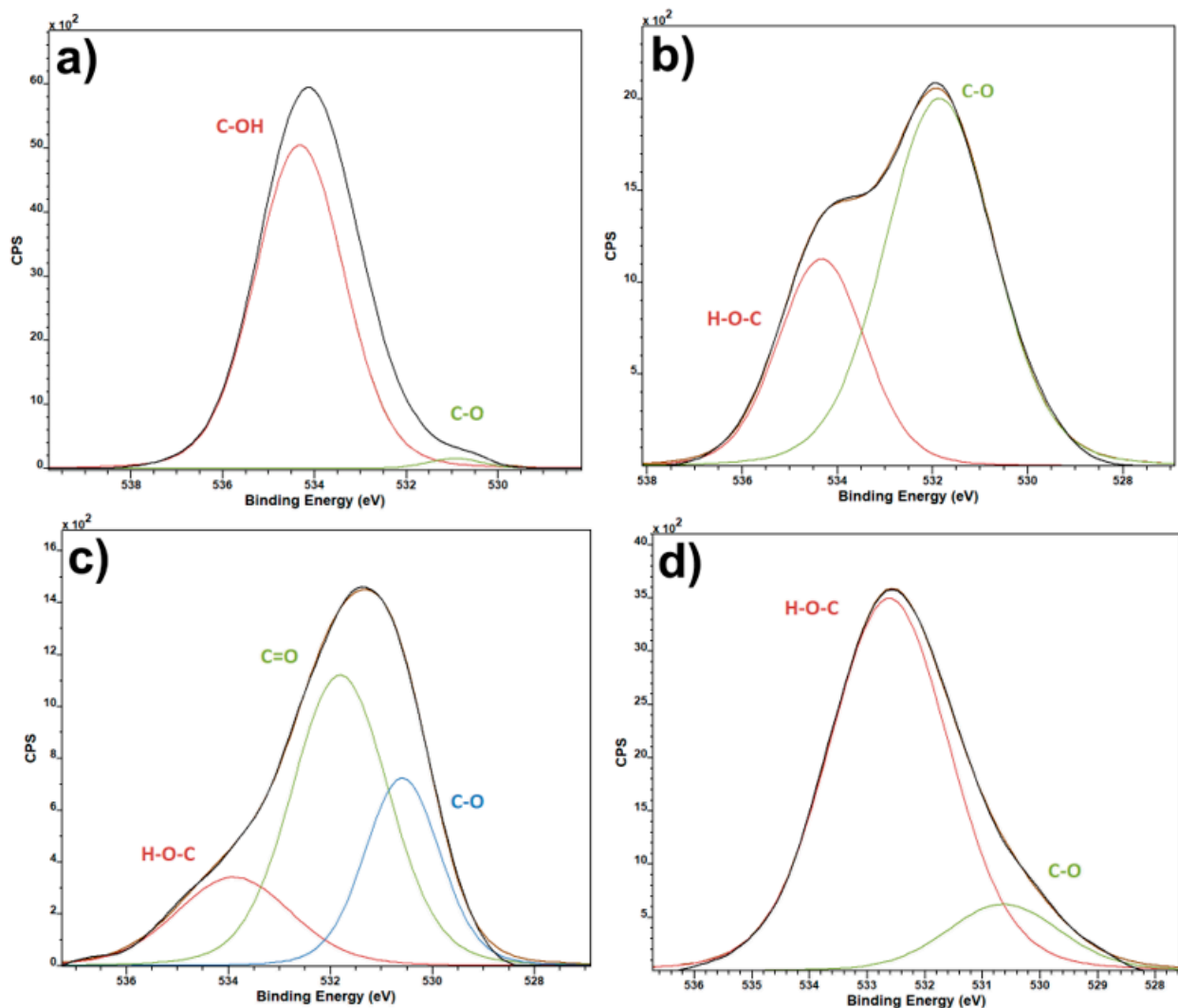


Figure 2. XPS O1 spectra of pure PVDF fibers (a) and PVDF fibers with $\text{Ca}(\text{NO}_3)_2$ (b), $\text{Mg}(\text{NO}_3)_2$ (c) and $\text{Zn}(\text{NO}_3)_2$ (d).

O1 spectra (Figure 2) of pure PVDF samples and salt-enhanced ones show one interesting fact, that the PVDF with calcium and magnesium salts have much higher relative content of C-O bonds, than zinc salt and pure PVDF. This points to presence of CO_2 in the materials, as there seems to be no other reason for such an increase in the C-O bonds. The only time that such a contamination could occur is during the electrospinning process due to high reactivity of the two elements. The CO_2 presence is not intended, and the salts in the composite are much more reactive than CO_2 , being the reason for its presence in the samples. The salts have an effect on the chemical bonds and crystalline composition of the resulting fiber. As it will be shown below, the crystallinity of PVDF with calcium and magnesium salts is lower, which make possible CO_2 capture [16].

F1 spectra (Figure 3) are interesting namely because of the indication of covalent and semi-ionic bond presence. Pure PVDF has a high ratio of semi-ionic to covalent bonds. This does not change much in the calcium salt variant, but the ratio is almost even in the magnesium and zinc salt variants. This can be likely ascribed to the electronegativity of the elements in question. Calcium electronegativity is lower compared to the other two salt elements, which causes the ratio of covalent and semi-ionic bonds to remain almost the same as pure PVDF, when compared to the other two salts.

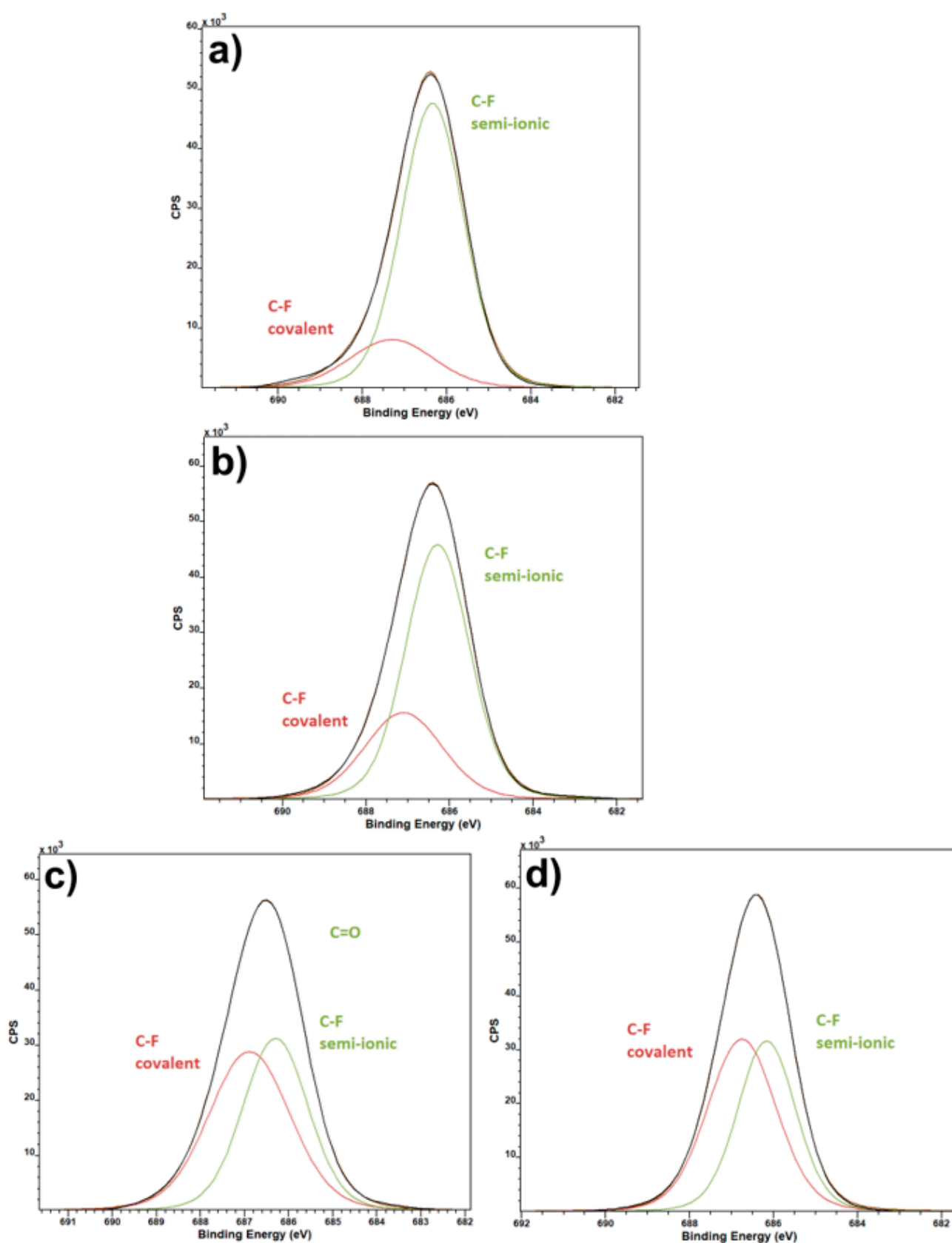


Figure 3. XPS F1s spectra of pure PVDF fibers (a) and PVDF fibers with $\text{Ca}(\text{NO}_3)_2$ (b), $\text{Mg}(\text{NO}_3)_2$ (c) and $\text{Zn}(\text{NO}_3)_2$ (d).

Unique elements spectra (Figure 4) serve as a check for the presence of the specified salts in the intended samples. Since it is virtually impossible to tell whether or not the salts

are present by eye, or even by scanning electron microscopy, XPS spectra of the unique elements were used as a confirmation that the required elements have made their way from the electrospinning solution into the final fiber product.

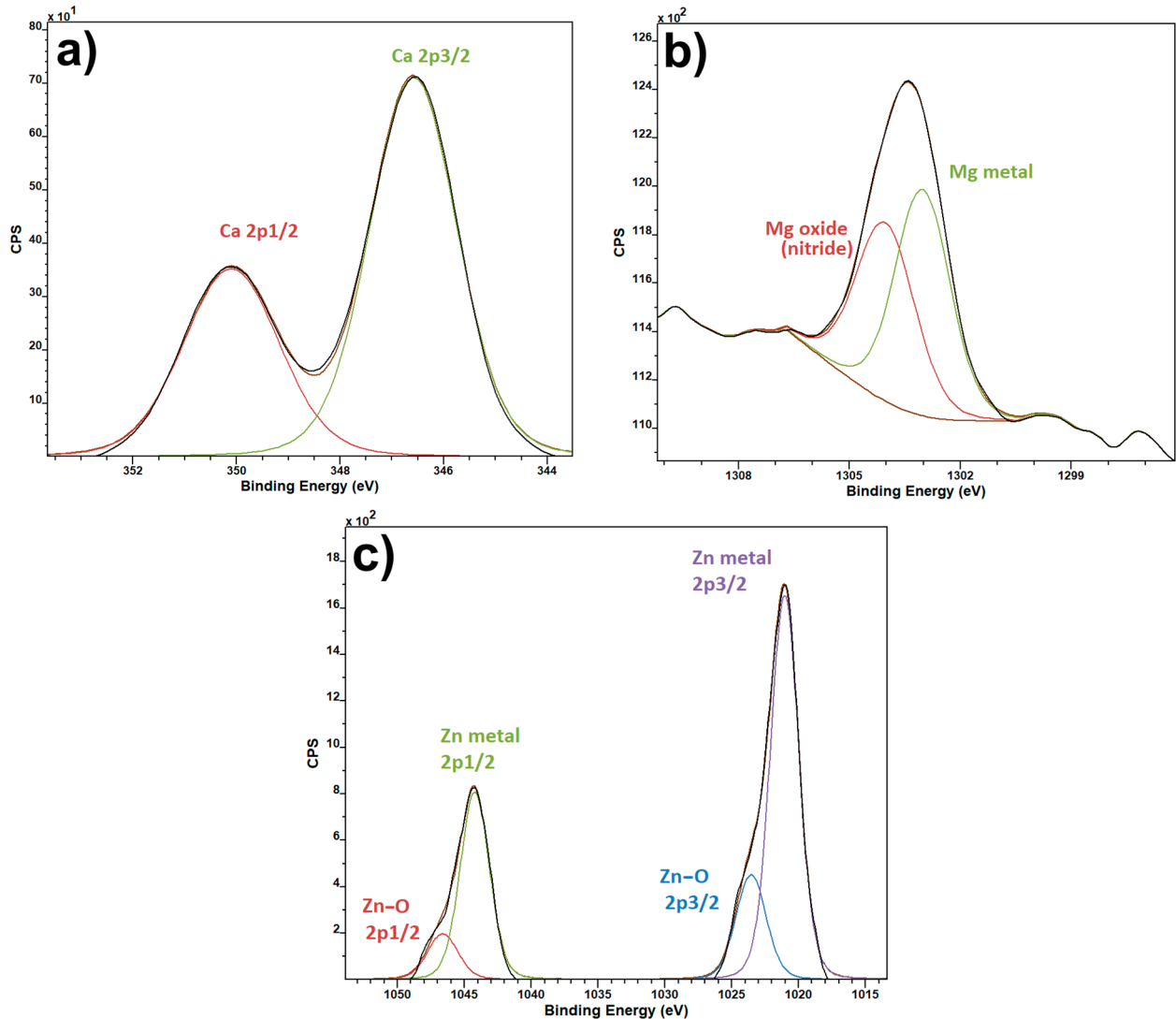


Figure 4. XPS spectra of unique salt elements: Ca2p for PVDF fibers with $\text{Ca}(\text{NO}_3)_2$ (a), Mg1s for PVDF fibers with $\text{Mg}(\text{NO}_3)_2$ (b) and Zn2p for PVDF fibers with $\text{Zn}(\text{NO}_3)_2$ (c).

To gain a more in-depth look into the presence and concentration of crystalline phases, FTIR measurement was performed (Figure 5). Peaks at 510 cm^{-1} represent both the β and γ phases, but as is the case for all of the peaks combining multiple phases, it is not possible to discern the concentration of individual phases from them. A small peak at 600 cm^{-1} is sometimes assigned to the β phase [17–20], but some specialized authors argue that it should not be so, as this band commonly shows up in many samples, including those with pure α phase, due to more pronounced peak at 613 cm^{-1} [21]. Peaks at 840 cm^{-1} are commonly assigned to both β and γ phases. Peaks at 885 and 1401 cm^{-1} represent all three phases combined. The peak located at 1074 cm^{-1} is usually assigned to the β phase, but it is not reliable as a characteristic peak for this crystalline phase, as references to other phases can be found at this wavelength as well. Lastly, from the combined peaks, the one located at 1074 cm^{-1} represents both the β and γ phases. Peaks characteristic for specific phases are 1233 cm^{-1} representing γ phase, and peaks located at 437 , 840 , 1276 and 1431 cm^{-1} represent β phase, which is the reason for their size.

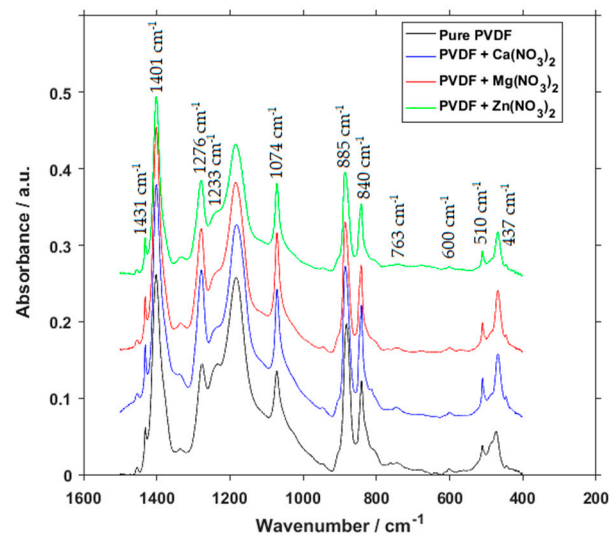


Figure 5. FTIR spectra of pure PVDF fibers and PVDF fibers with $\text{Ca}(\text{NO}_3)_2$, $\text{Mg}(\text{NO}_3)_2$ and $\text{Zn}(\text{NO}_3)_2$.

At the first glance we can see that there is only a small difference between individual spectra. If we are to look at the characteristic peaks, however, we find, that in comparison to pure PVDF, the compounds with salts have little to no characteristic peaks for γ phase. Especially the 1233 cm^{-1} most often used for determination of γ phase concentration [22] is so small that it is virtually zero. When the precision of FTIR is taken into account, the presence of γ phase can be considered to be negligible.

Calculation of phase composition was performed according to X. Cai, et al. [21]

$$F_{EA} = \frac{I_{EA}}{\left(\frac{K_{840}}{K_{763}}\right) I_{763} + I_{EA}} \cdot 100\% \quad (1)$$

$$F(\beta) = F_{EA} \cdot \frac{\Delta H_{\beta'}}{\Delta H_{\beta'} + \Delta H_{\gamma'}} \cdot 100\% \quad (2)$$

$$F(\gamma) = F_{EA} \cdot \frac{\Delta H_{\gamma'}}{\Delta H_{\beta'} + \Delta H_{\gamma'}} \cdot 100\% \quad (3)$$

Here F_{EA} is the common amount of the electroactive phases (β and γ);

I_{EA} is the absorbance at 840 cm^{-1} ;

I_{763} is the absorbance at 763 cm^{-1} ;

K_{840} is the absorption coefficient at the wave number 840 cm^{-1} , equal to $7.7 \cdot 10^4\text{ cm}^2 \cdot \text{mol}^{-1}$;

K_{763} is the absorption coefficient at the wave number 763 cm^{-1} , equal to $6.1 \cdot 10^4\text{ cm}^2 \cdot \text{mol}^{-1}$;

$\Delta H_{\beta'}$ is the height differences at absorbance spectra between the peak around at 1275 cm^{-1} and the valley around at 1260 cm^{-1} ;

$\Delta H_{\gamma'}$ is the height differences at absorbance spectra between the peak around at 1234 cm^{-1} and the nearest valley around at 1225 cm^{-1} .

Calculation themselves show the relative fraction of phases for pure PVDF to be 13.45% for α , 82.52% for β and 4.03% for γ . This changes into 7.71% for α , 92.29% for β and virtually 0 for γ in the case of $\text{Ca}(\text{NO}_3)_2$, 4.25% for α , 95.75% for β and 0 for γ in the case of $\text{Mg}(\text{NO}_3)_2$, and 14.70% for α , 85.30% for β and again 0 for γ in the case of $\text{Zn}(\text{NO}_3)_2$. Recent theoretical research [23] confirmed the β phase formation due to interactions between polymer chains and the interstitial water of the hydrated salts through hydrogen bonds formation. Electrostatic forces caused repelling of negative charges of

the polymer molecules, which is the reason for the stretching of the macromolecules and transformation into an all-trans-configuration.

Samples of pure PVDF and PVDF mixed with additives in the form of three different salts have been measured by Raman spectroscopy (Figure 6). From the typical expected peaks of PVDF we can find those in all four material compositions at 840 cm^{-1} belonging to β - and γ - phases, and at 1430 cm^{-1} representing the CH_2 bending vibrations of all three phases, but which are usually attributed to the β - and γ -phases as well, and a composite band around 2974 cm^{-1} most commonly attributed to CH_2 symmetric stretching associated with the β -phase [24]. The change in the dimensions of peaks belonging to the β -phase of PVDF, which is the one that varies the most throughout the samples, corresponds with FTIR measurements of crystalline phase concentrations.

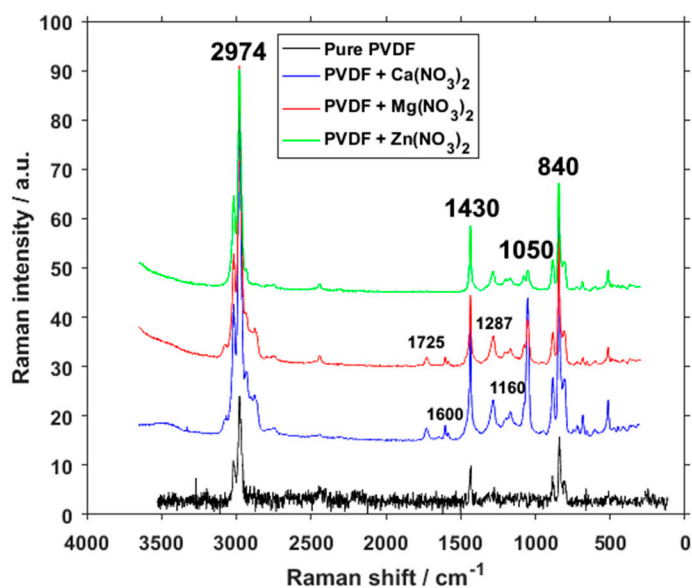


Figure 6. Raman spectra of pure PVDF fibers and PVDF fibers with $\text{Ca}(\text{NO}_3)_2$, $\text{Mg}(\text{NO}_3)_2$ and $\text{Zn}(\text{NO}_3)_2$.

The band at 1050 cm^{-1} that is only present in the salt-enhanced polymer belongs to a $\nu_1\text{-NO}_3^-$ group vibration [25]. Peaks at around 1170 cm^{-1} can be assigned to the β -phase [26], and since they are larger in calcium and magnesium salts, that would correspond to the concentration of phases as gained from FTIR. Peaks at around 1160 and 1287 cm^{-1} could be attributed to C–O and C=O bonds in the organic compounds [27]. A higher presence of C–O and C=O bonds can also be seen on O1 XPS spectra (Figure 2). Since the salts themselves do not contain any carbon and this peak is missing within the pure PVDF, their presence suggests either an adsorbed CO_2 during the electrospinning process under high voltage, chemical bond between the salts and PVDF fibers, or even a possibility of PVDF hydroxylation [28]. Because these peaks are present in two different sample series, however, it is highly unlikely that they were caused by a random error or simple contamination of the source solution.

The two small peaks present at calcium and magnesium salt additives at around 1600 and 1725 cm^{-1} are bending water peaks [29], likely caused by the water absorption of these two materials, and the O–H bending peak respectively. The absence of these peaks in the spectrum of zinc salt corresponds with the water-absorption ability, which is lower in zinc salts than in magnesium and calcium ones.

Several places of interest have been revealed in the spectra taken by the XRD measurement (Figure 7). The most notable is located at 18° , representing the α phase, and a second at 21° , representing a combination of the α and β phases [30]. In the pure sample, the peak at 18° is still visible, but it virtually disappears in the salt-doped PVDF fibers. This

change in peaks shows a clear shift towards a very high concentration of the β phase at the expense of other phases, which corresponds with the data gained from the FTIR.

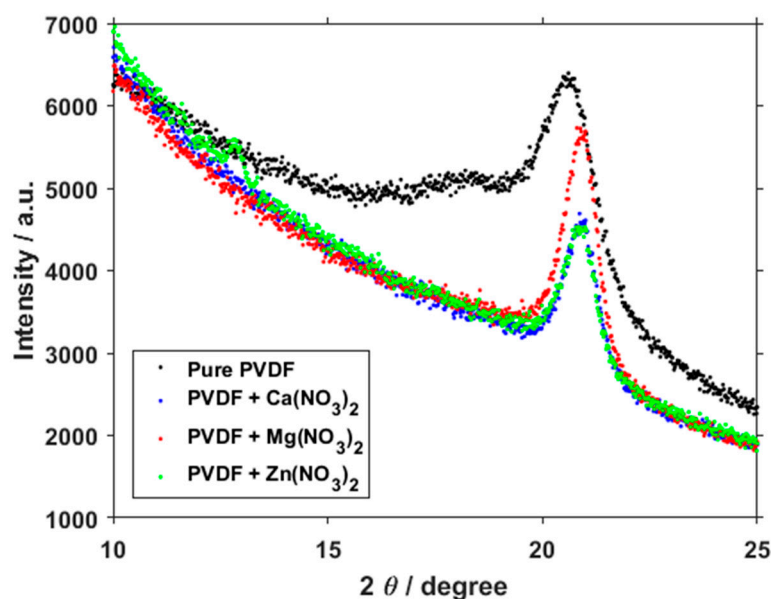


Figure 7. Focused XRD spectra of PVDF fibers and PVDF fibers with $\text{Ca}(\text{NO}_3)_2$, $\text{Mg}(\text{NO}_3)_2$ and $\text{Zn}(\text{NO}_3)_2$.

During the electrospinning process there is always the remote possibility that the inclusions will aggregate into one location and will not be distributed throughout the material. This would, naturally, affect the resulting material in a detrimental way. EDX measurement was performed to find out whether this sub-optimal distribution pattern occurred. Figure 8 shows SEM images of the samples and then EDX measurements of the same location focused on the unique element in the nitrate salts. Even though the signal-to-noise ratio is not optimal, the unique element images show the dispersion of the element in question throughout PVDF fibers, supporting the claim that this method of fiber preparation can indeed distribute the inclusions successfully and evenly.

Figure 9 shows the dielectric measurement performed on pure PVDF samples and samples with $\text{Ca}(\text{NO}_3)_2$, $\text{Mg}(\text{NO}_3)_2$ and $\text{Zn}(\text{NO}_3)_2$. They all follow generally the same trends, but there are some differences. The first thing that is immediately visible is that the pure PVDF and PVDF with $\text{Ca}(\text{NO}_3)_2$ have highly similar progressions in the dielectric constant measurements for both real (ϵ_r') and imaginary (ϵ_r'') values. This similarity is even greater in the real part of conductivity (σ'), and they are virtually the same in the imaginary part (σ''). This pairing correlates with the electronegativity of calcium and the ratio of semi-ionic and covalent bonds in Figure 3. It is originated from electrostatic interactions between the PVDF polymer chain and dissolved hydrate metallic salts caused by hydrogen bonding between the CF_2 and the salt cation [31]. More interesting progressions can be seen in the PVDF fibers containing $\text{Mg}(\text{NO}_3)_2$ and $\text{Zn}(\text{NO}_3)_2$. The curve of the real dielectric constant for the magnesium salt intersects the one for zinc salt between 10^2 Hz and 10^3 Hz, which is all the more visible in the graph depicting dielectric loss. What is somewhat unexpected, however, is that conductivity of PVDF with and without added salts is almost identical, with only minor differences that would likely not be noticeable in most practical uses.

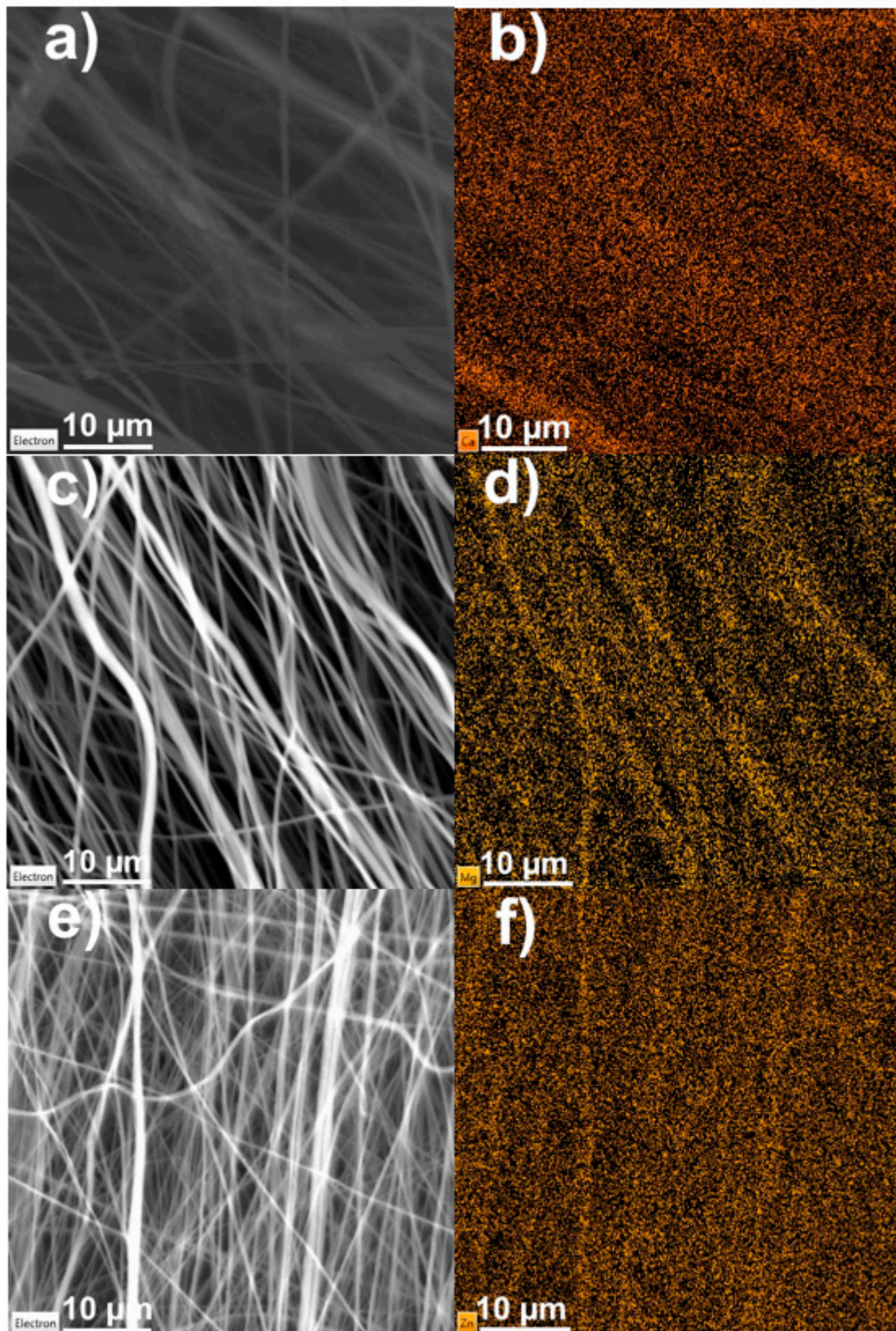


Figure 8. SEM and EDX images of salt-enhanced PVDF fibers, electron image and unique elements: (a,b) $\text{Ca}(\text{NO}_3)_2$, (c,d) $\text{Mg}(\text{NO}_3)_2$ and (e,f) $\text{Zn}(\text{NO}_3)_2$.

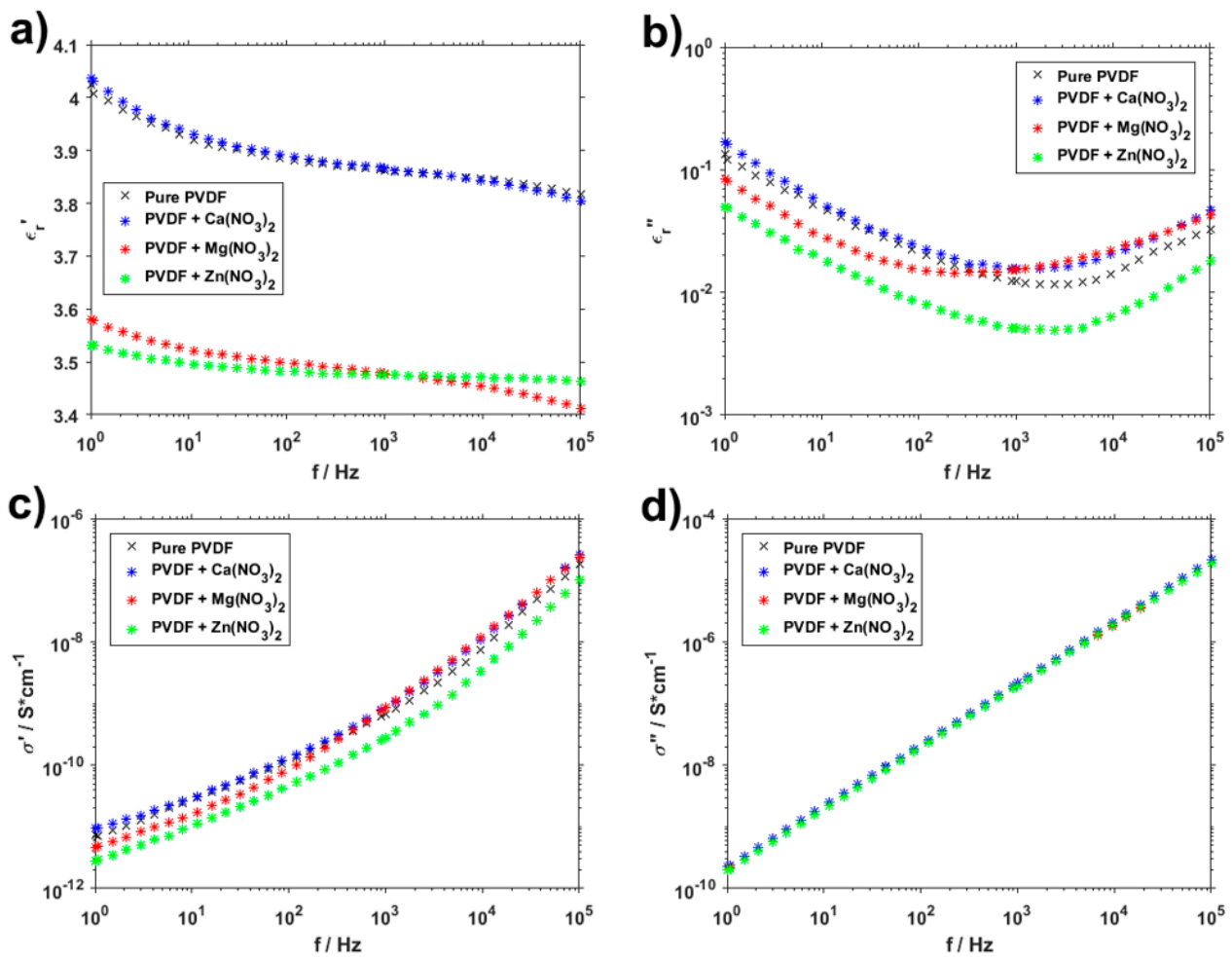


Figure 9. Real (a) and imaginary (b) permittivity and real (c) and imaginary (d) conductivity of pure PVDF fibers and PVDF with $\text{Ca}(\text{NO}_3)_2$, $\text{Mg}(\text{NO}_3)_2$ and $\text{Zn}(\text{NO}_3)_2$.

To obtain a more complex idea about the properties of PVDF fibers, optical spectroscopy has been performed on the materials. Though it is one of the less used methods to describe PVDF composites, it can provide more of an insight into their potential use. Pure PVDF has been used as a benchmark to compare the materials enriched by salts to. Figure 10 shows visual and near infrared transmittance spectra of the materials. While the spectra of salt-enhanced PVDF seem to have much higher absorption in lower wavelengths, zinc salt starts to be more transparent for the incident light over the course of wavelength increase, and eventually reaches the transmittance values of pure PVDF in near-infrared ranges. This makes the zinc salt optically interesting, and it might be possible to find use for the PVDF fibers enriched by $\text{Zn}(\text{NO}_3)_2$ in components actively using light for their operation.

A hydrophobicity measurement was taken to obtain information about the interaction of the material with aqueous substances, because such an interaction is both expected, and in the case of potential use in biology and chemistry, required. From the results in Table 1, it can immediately be seen that the pure PVDF material and all of its enhancements with salts are highly hydrophobic. While that is not entirely unexpected, what is more interesting is the fact that even after the addition of the salts the hydrophobicity does not change all that much. When considering the deviations, the average values of measured angles are very close to one another. As salts are usually used to alter hydrophobicity of a material [32], this lack of significant difference is somewhat puzzling. Out of all the three salts, the zinc salt behaves in the most distinctive manner, but that can be seen in the permittivity or optical spectroscopy measurement as well.

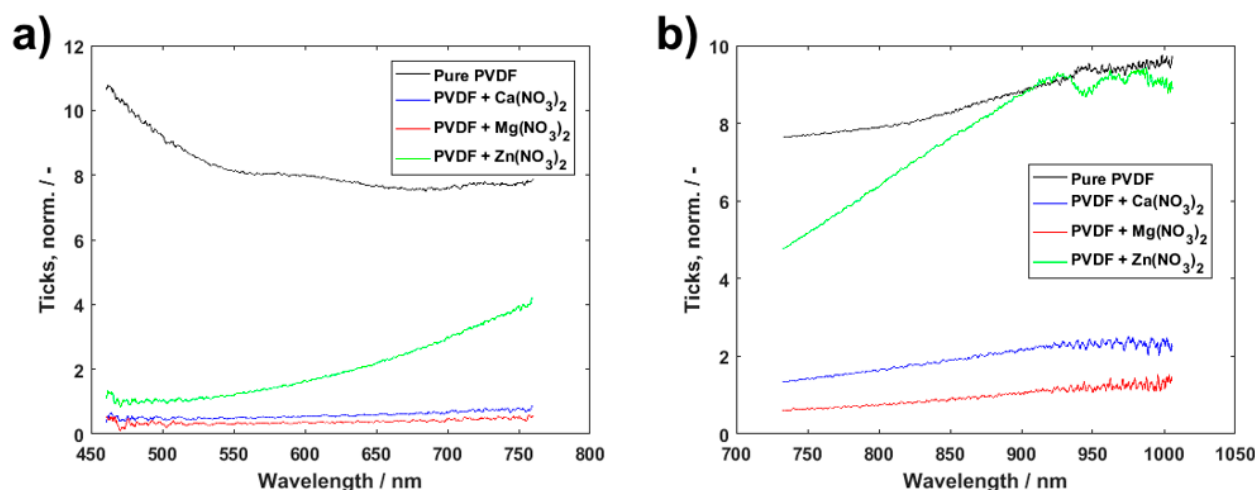


Figure 10. Transmittance spectra of pure PVDF fibers and those with $\text{Ca}(\text{NO}_3)_2$, $\text{Mg}(\text{NO}_3)_2$ and $\text{Zn}(\text{NO}_3)_2$ in visual (a) and near-infrared (b) range.

Table 1. Average, median and standard deviations for hydrophobicity measurement of pure PVDF fibers and PVDF with $\text{Ca}(\text{NO}_3)_2$, $\text{Mg}(\text{NO}_3)_2$ and $\text{Zn}(\text{NO}_3)_2$.

	Average/ $^\circ$	Median/ $^\circ$	Std. Dev./ $^\circ$	Std. Dev./%
PVDF	127.1	127.6	7.6	6.0
PVDF with $\text{Ca}(\text{NO}_3)_2$	124.1	125.2	11.9	9.6
PVDF with $\text{Mg}(\text{NO}_3)_2$	131.3	131.4	4.6	3.5
PVDF with $\text{Zn}(\text{NO}_3)_2$	135.9	135.9	7.8	5.8

To obtain the crystallinity percentage of the measured material, the DSC method has been employed. Spectra gained by this evaluation (Figure 11) can be used to calculate the total sample enthalpy and then the crystalline phases (X_c) of the PVDF in different polymer mixtures:

$$X_c = \frac{\Delta H_f}{\Delta H_f^* \varphi} 100\% \quad (4)$$

where ΔH_f is the enthalpy of fusion, calculated from the heating DSC curve, ΔH_f^* is the heat of fusion of perfect crystalline PVDF obtained from literature [33], in this case 104.7 J/g, and φ is the weight fraction of PVDF in the samples. The obtained resulting percentage of crystallinity was 64.58% for $\text{Ca}(\text{NO}_3)_2$, 61.01% for $\text{Mg}(\text{NO}_3)_2$ and 73.46 for $\text{Zn}(\text{NO}_3)_2$. Once again, the zinc salt behavior is the most distinct out of the three measured salts.

The hydrogen bonds play an important role in the crystallization of the polymers. These bonds could be considered as electrostatic interaction. The presence of the hydrogen atoms changes in alignment and the distance between the dipoles. The ionic interactions of the polymer with the hydrated salt as well as the hygroscopic properties of the additive are the reasons for the hydrogen bonding [34]. It effects the crystallinity which grows with the electronegativity of the nitrate salt cation.

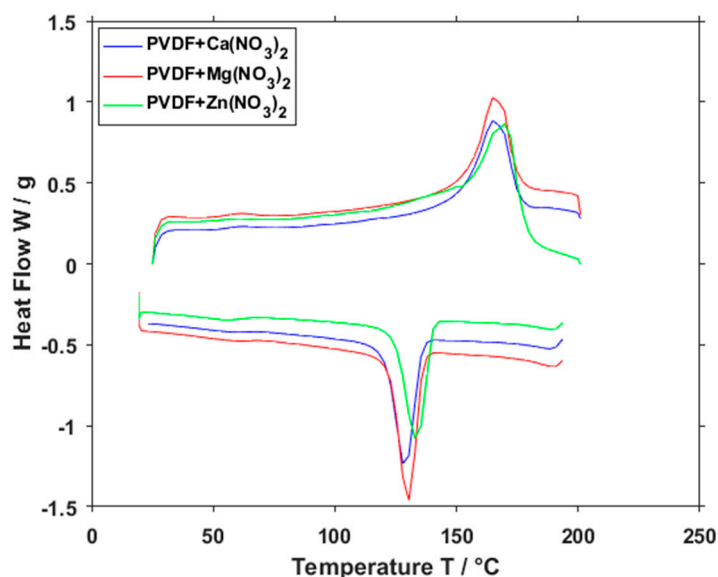


Figure 11. DSC curve of PVDF fibers with $\text{Ca}(\text{NO}_3)_2$, $\text{Mg}(\text{NO}_3)_2$ and $\text{Zn}(\text{NO}_3)_2$.

4. Conclusions

The addition of various nitrate salts has a noticeable and measurable effect on many properties of polyvinylidene fluoride fibers. One of the main observed properties was the concentration of crystalline phases. When compared to pure PVDF, salts containing calcium and magnesium cations had their β -phase content increased by a large amount, while zinc nitrate has a comparable β -phase content as pure PVDF. Any salt addition, however, virtually eliminated the presence of the γ -phase altogether. Zinc nitrate also has distinctive optical properties with a measured increased transmittance towards the higher wavelengths of the visual spectrum and further, showing a potential for components where incident light plays a key role. The measured electrical properties tend to follow the electronegativity of the nitrate salt cation, where calcium exhibits a similar ratio of covalent to semi-ionic bonds, measured by XPS, and dielectric constant, as PVDF, while magnesium and zinc form a group of their own with the dielectric constant being visibly lower. The data obtained from several different measurements have been documented to create a basis for further research and to widen knowledge about the properties of polyvinylidene fluoride fiber composites.

Author Contributions: Conceptualization, D.S., K.Č. and P.K.; methodology, K.Č., R.D., T.T., A.W. and F.O.; software, P.S., T.T. and J.K.; validation, R.D., J.K. and A.K.; formal analysis, R.D., N.P. and V.H.; investigation, N.P., A.W. and V.H.; resources, P.S. and K.Č.; data curation, K.Č., N.P., P.S. and A.W.; writing—original draft preparation, P.K., D.S. and F.O., writing—review and editing, K.Č., P.K. and D.S.; visualization, T.T., A.K. and V.H.; supervision, P.S., J.K., A.K. and F.O.; project administration, K.Č. All authors have read and agreed to the published version of the manuscript.

Funding: The research described in this paper was financially supported by the Internal Grant Agency of Brno University of Technology [Grant No. FEKT-S-20-6352] and the Grant Agency of Czech Republic under project No. 19-17457S. A part of the work was carried out with the support of CEITEC Nano Research Infrastructure [grant ID LM2015041, MEYS CR, 2016–2019], CEITEC Brno University of Technology. We also acknowledge the Czech Academy of Sciences (RVO:68081731).

Institutional Review Board Statement: Not applicable.

Informed Consent Statement: Not applicable.

Data Availability Statement: The research data are available upon request from authors.

Conflicts of Interest: The authors declare no conflict of interest.

References

1. Roopa, T.; Murthy, H.N.; Harish, D.; Jain, A.; Angadi, G. Properties of PVDF films stretched in machine direction. *Polym. Polym. Compos.* **2021**, *29*, 198–206. [[CrossRef](#)]
2. Arshad, A.N.; Wahid, M.H.M.; Rusop, M.; Majid, W.H.A.; Subban, R.H.Y.; Rozana, M.D. Dielectric and Structural Properties of Poly(vinylidene fluoride) (PVDF) and Poly(vinylidene fluoride-trifluoroethylene) (PVDF-TrFE) Filled with Magnesium Oxide Nanofillers. *J. Nanomater.* **2019**, *2019*, 1–12. [[CrossRef](#)]
3. Ruan, L.; Yao, X.; Chang, Y.; Zhou, L.; Qin, G.; Zhang, X. Properties and Applications of the β Phase Poly(vinylidene fluoride). *Polymers* **2018**, *10*, 228. [[CrossRef](#)]
4. McKeen, L.W. Fluoropolymers. In *Fatigue and Tribological Properties of Plastics and Elastomers*; Elsevier: Kidlington, UK, 2016; pp. 291–315.
5. Wu, C.-M.; Chou, M.-H.; Zeng, W.-Y. Piezoelectric Response of Aligned Electrospun Polyvinylidene Fluoride/Carbon Nanotube Nanofibrous Membranes. *Nanomaterials* **2018**, *8*, 420. [[CrossRef](#)]
6. Castkova, K.; Kasty, J.; Sobola, D.; Petrus, J.; Stastna, E.; Riha, D.; Tofel, P. Structure-properties relationship of electrospun pvdf fibers. *Nanomaterials* **2020**, *10*, 1221. [[CrossRef](#)] [[PubMed](#)]
7. Mokhtari, F.; Shamshirsaz, M.; Latifi, M. Investigation of β phase formation in piezoelectric response of electrospun polyvinylidene fluoride nanofibers: LiCl additive and increasing fibers tension. *Polym. Eng. Sci.* **2016**, *56*, 61–70. [[CrossRef](#)]
8. Mokhtari, F.; Shamshirsaz, M.; Latifi, M.; Asadi, S. Comparative evaluation of piezoelectric response of electrospun PVDF (polyvinylidene fluoride) nanofiber with various additives for energy scavenging application. *J. Text. Inst.* **2016**, *108*, 906–914. [[CrossRef](#)]
9. Al Abdullah, K.; Batal, M.A.; Hamdan, R.; Khalil, T.; Zaraket, J.; Aillerie, M.; Salame, C. The Enhancement of PVDF Pyroelectricity (Pyroelectric Coefficient and Dipole Moment) by Inclusions. *Energy Procedia* **2017**, *119*, 545–555. [[CrossRef](#)]
10. Kaspar, P.; Sobola, D.; Částková, K.; Knápek, A.; Burda, D.; Orudzhev, F.; Dallaev, R.; Tofel, P.; Trčka, T.; Grmela, L.; et al. Characterization of polyvinylidene fluoride (Pvdf) electrospun fibers doped by carbon flakes. *Polymers* **2020**, *12*, 2766. [[CrossRef](#)] [[PubMed](#)]
11. Kaspar, P.; Sobola, D.; Částková, K.; Dallaev, R.; Šťastná, E.; Sedlák, P.; Knápek, A.; Trčka, T.; Holcman, V. Case study of polyvinylidene fluoride doping by carbon nanotubes. *Materials* **2021**, *14*, 1428. [[CrossRef](#)]
12. Wissbrun, K.F.; Hannon, M.J. Interaction of inorganic salts with polar polymers. II. Infrared studies of polymer-inorganic nitrate systems. *J. Polym. Sci. Polym. Phys. Ed.* **1975**, *13*, 223–241. [[CrossRef](#)]
13. Prasad, G.; Sathiyathan, P.; Prabu, A.A.; Kim, K.J. Piezoelectric characteristics of electrospun PVDF as a function of phase-separation temperature and metal salt content. *Macromol. Res.* **2017**, *25*, 981–988. [[CrossRef](#)]
14. Akashi, N.; Kuroda, S. Protein immobilization onto poly(vinylidene fluoride) microporous membranes activated by the atmospheric pressure low temperature plasma. *Polymer* **2014**, *55*, 2780–2791. [[CrossRef](#)]
15. Fernadéz, V.; Sotiropoulos, T.; Brown, P. *Foliar Fertilization: Scientific Principles and Field Practices*; Statewide Agricultural Land Use Baseline: Honolulu, HI, USA, 2013; Volume 1, p. 112.
16. Ghodsi, A.; Fashandi, H.; Zarrebini, M.; Abolhasani, M.M.; Gorji, M. Highly effective CO₂ capture using super-fine PVDF hollow fiber membranes with sub-layer large cavities. *RSC Adv.* **2015**, *5*, 92234–92253. [[CrossRef](#)]
17. Bormashenko, Y.; Pogreb, R.; Stanevsky, O.; Bormashenko, E. Vibrational spectrum of PVDF and its interpretation. *Polym. Test.* **2004**, *23*, 791–796. [[CrossRef](#)]
18. Patro, T.U.; Mhalgi, M.V.; Khakhar, D.V.; Misra, A. Studies on poly(vinylidene fluoride)-clay nanocomposites: Effect of different clay modifiers. *Polymer* **2008**, *49*, 3486–3499. [[CrossRef](#)]
19. Baji, A.; Mai, Y.-W.; Li, Q.; Liu, Y. Electrospinning induced ferroelectricity in poly(vinylidene fluoride) fibers. *Nanoscale* **2011**, *3*, 3068. [[CrossRef](#)] [[PubMed](#)]
20. Thakur, P.; Kool, A.; Bagchi, B.; Hoque, N.A.; Das, S.; Nandy, P. In situ synthesis of Ni(OH)₂ nanobelt modified electroactive poly(vinylidene fluoride) thin films: Remarkable improvement in dielectric properties. *Phys. Chem. Chem. Phys.* **2015**, *17*, 13082–13091. [[CrossRef](#)] [[PubMed](#)]
21. Cai, X.; Lei, T.; Sun, D.; Lin, L. A critical analysis of the α , β and γ phases in poly(vinylidene fluoride) using FTIR. *RSC Adv.* **2017**, *7*, 15382–15389. [[CrossRef](#)]
22. Gregorio, R. Determination of the α , β , and γ crystalline phases of poly(vinylidene fluoride) films prepared at different conditions. *J. Appl. Polym. Sci.* **2006**, *100*, 3272–3279. [[CrossRef](#)]
23. Sarkar, R.; Kundu, T.K. Hydrogen bond interactions of hydrated aluminum nitrate with PVDF, PVDF-TrFE, and PVDF-HFP: A density functional theory-based illustration. *Int. J. Quantum Chem.* **2020**, *120*, e26328. [[CrossRef](#)]
24. Constantino, C.J.L.; Job, A.E.; Simões, R.D.; Giacometti, J.A.; Zucolotto, V.; Oliveira, O.N.; Gozzi, G.; Chinaglia, D.L. Phase Transition in Poly(Vinylidene Fluoride) Investigated with Micro-Raman Spectroscopy. *Appl. Spectrosc.* **2005**, *59*, 275–279. [[CrossRef](#)]
25. Brooker, M.H. Raman and i.r. spectra of zinc, cadmium and calcium nitrate: A study of the low temperature phase transitions in calcium nitrate. *Spectrochim. Acta Part. A Mol. Spectrosc.* **1976**, *32*, 369–377. [[CrossRef](#)]
26. Yaqoob, U.; Uddin, A.S.M.I.; Chung, G.-S. The effect of reduced graphene oxide on the dielectric and ferroelectric properties of PVDF-BaTiO₃ nanocomposites. *RSC Adv.* **2016**, *6*, 30747–30754. [[CrossRef](#)]

27. Huang, N.; Short, M.; Zhao, J.; Wang, H.; Lui, H.; Korbelik, M.; Zeng, H. Full range characterization of the Raman spectra of organs in a murine model. *Opt. Express* **2011**, *19*, 22892. [[CrossRef](#)] [[PubMed](#)]
28. Xu, Y.; Lin, Y.; Lee, M.; Malde, C.; Wang, R. Development of low mass-transfer-resistance fluorinated TiO₂-SiO₂/PVDF composite hollow fiber membrane used for biogas upgrading in gas-liquid membrane contactor. *J. Memb. Sci.* **2018**, *552*, 253–264. [[CrossRef](#)]
29. Seki, T.; Chiang, K.-Y.; Yu, C.-C.; Yu, X.; Okuno, M.; Hunger, J.; Nagata, Y.; Bonn, M. The Bending Mode of Water: A Powerful Probe for Hydrogen Bond Structure of Aqueous Systems. *J. Phys. Chem. Lett.* **2020**, *11*, 8459–8469. [[CrossRef](#)]
30. Yu, L.; Wang, S.; Li, Y.; Chen, D.; Liang, C.; Lei, T.; Sun, D.; Zhao, Y.; Wang, L. Piezoelectric performance of aligned PVDF nanofibers fabricated by electrospinning and mechanical spinning. In Proceedings of the 2013 13th IEEE International Conference on Nanotechnology (IEEE-NANO 2013), Beijing, China, 5–8 August 2013; IEEE: Beijing, China, 2013; pp. 962–966. [[CrossRef](#)]
31. Fortunato, M.; Chandraiahgari, C.R.; De Bellis, G.; Ballirano, P.; Sarto, F.; Tamburrano, A.; Sarto, M.S. Piezoelectric Effect and Electroactive Phase Nucleation in Self-Standing Films of Unpoled PVDF Nanocomposite Films. *Nanomater* **2018**, *8*, 743. [[CrossRef](#)]
32. Francisco, O.A.; Glor, H.M.; Khajepour, M. Salt Effects on Hydrophobic Solvation: Is the Observed Salt Specificity the Result of Excluded Volume Effects or Water Mediated Ion-Hydrophobe Association? *ChemPhysChem* **2020**, *21*, 484–493. [[CrossRef](#)]
33. Merlini, C.; Barra, G.M.O.; Medeiros Araujo, T.; Pegoretti, A. Electrically pressure sensitive poly(vinylidene fluoride)/polypyrrole electrospun mats. *RSC Adv.* **2014**, *4*, 15749–15758. [[CrossRef](#)]
34. Dhakras, D.; Borkar, V.; Ogale, S.; Jog, J. Enhanced piezoresponse of electrospun PVDF mats with a touch of nickel chloride hexahydrate salt. *Nanoscale* **2012**, *4*, 752–756. [[CrossRef](#)] [[PubMed](#)]

Chapter 8. Analysis of PVDF/NMP/[EMIM][TFSI] Solid Polymer Electrolyte

8.1 Purpose of the article

The development of advanced polymer electrolytes is crucial for enhancing the performance and stability of various electrochemical devices. PVDF known for its exceptional chemical, thermal, and electrical stability, along with its unique piezoelectric and pyroelectric properties, offers significant potential in this area. However, the impact of thermal treatment on the morphology and properties of PVDF-based solid polymer electrolytes (SPEs) remains insufficiently explored. In this study, the PVDF/NMP/[EMIM][TFSI] electrolyte was investigated, focusing on how different thermal treatment conditions influence its surface morphology, phase composition, chemical composition, and depth profiling. Utilizing advanced characterization techniques such as SEM, Raman spectroscopy, FTIR, DSC, XPS, SIMS, the aim is to provide a comprehensive understanding of the morphological changes induced by thermal treatments. This research not only seeks to elucidate the relationship between thermal treatment conditions and the resultant morphological properties of PVDF-based SPEs but also aims to contribute valuable insights for optimizing their performance in practical applications. The findings could pave the way for the development of more efficient and stable polymer electrolytes, thereby advancing the field of electrochemical energy storage and conversion technologies.

8.2 Conclusion on the article

FTIR spectra analysis confirmed the dominance of the β -phase, consistent with Raman spectroscopy results. Both techniques showed stable peak positions, suggesting good miscibility between the PVDF matrix and the ionic liquid [EMIM][TFSI] in the solvent NMP (N-methyl-pyrrolidone). DSC analysis indicated a decrease in PVDF crystallinity as solvent evaporation increased.

XPS analysis showed an increase in elements F, N, and S, and a decrease in C with higher solvent evaporation rates. For samples with higher evaporation rates, the C1s spectrum resembled that of the ionic liquid, indicating a surface composition closer to the ionic liquid, as corroborated by Raman mapping at the 741 cm^{-1} band.

Given the previously published data showing that the DC conductivity of the SPE increases with heat treatment intensity and becomes comparable to that of the ionic liquid, it is concluded that ion transport occurs predominantly on the surfaces of the spherulites and within the amorphous regions.

8.3 Applicant's contribution

The applicant is responsible for the SIMS (Secondary Ion Mass Spectrometry) analysis in this paper.

8.4 Article 8

The paper "*Surface Analyses of PVDF/NMP/[EMIM][TFSI] Solid Polymer Electrolyte*" was published in August 2021 in "*Polymers*" journal (IF: 5.0; Q1) and to date (02.06.2024) has 16 citations.

Article

Surface Analyses of PVDF/NMP/[EMIM][TFSI] Solid Polymer Electrolyte

Petr Sedlak ^{1,*}, Dinara Sobola ^{1,2} , Adam Gajdos ¹, Rashid Dallaev ¹ , Alois Nebojsa ³ and Petr Kubersky ⁴ 

¹ Faculty of Electrical Engineering and Communications, Brno University of Technology, Technicka 10, 616 00 Brno, Czech Republic; sobola@feec.vutbr.cz (D.S.); xgajdo12@stud.feec.vutbr.cz (A.G.); xdalla03@stud.feec.vutbr.cz (R.D.)

² Institute of Physics of Materials, Academy of Sciences CR, Zizkova 22, 616 62 Brno, Czech Republic

³ Central European Institute of Technology (CEITEC), Brno University of Technology, Purkynova 123, 612 00 Brno, Czech Republic; nebojsa@fme.vutbr.cz

⁴ Research and Innovation Centre for Electrical Engineering (RICE), Faculty of Electrical Engineering, University of West Bohemia, Univerzitni 8, 301 00 Plzen, Czech Republic; kubersky@fel.zcu.cz

* Correspondence: sedlakp@vut.cz; Tel.: +420-54114-6021

Abstract: Thermal treatment conditions of solid polymer polymer electrolyte (SPE) were studied with respect to their impact on the surface morphology, phase composition and chemical composition of an imidazolium ionic-liquid-based SPE, namely PVDF/NMP/[EMIM][TFSI] electrolyte. These investigations were done using scanning electron microscopy, Raman spectroscopy, Fourier transform infrared spectroscopy, differential scanning calorimetry as well as X-ray photoelectron spectroscopy and time-of-flight secondary ion mass spectroscopy. A thoroughly mixed blend of polymer matrix, ionic liquid and solvent was deposited on a ceramic substrate and was kept at a certain temperature for a specific time in order to achieve varying crystallinity. The morphology of all the electrolytes consists of spherulites whose average diameter increases with solvent evaporation rate. Raman mapping shows that these spherulites have a semicrystalline structure and the area between them is an amorphous region. Analysis of FTIR spectra as well as Raman spectroscopy showed that the β -phase becomes dominant over other phases, while DSC technique indicated decrease of crystallinity as the solvent evaporation rate increases. XPS and ToF-SIMS indicated that the chemical composition of the surface of the SPE samples with the highest solvent evaporation rate approaches the composition of the ionic liquid.

Keywords: solid polymer electrolyte; imidazolium ionic liquids; poly-(vinylidene fluoride); crystallinity; solvent evaporation; Raman spectroscopy; Fourier transform infrared spectroscopy; X-ray photoelectron spectroscopy; secondary ion mass spectroscopy



Citation: Sedlak, P.; Sobola, D.; Gajdos, A.; Dallaev, R.; Nebojsa, A.; Kubersky, P. Surface Analyses of PVDF/NMP/[EMIM][TFSI] Solid Polymer Electrolyte. *Polymers* **2021**, *13*, 2678. <https://doi.org/10.3390/polym13162678>

Academic Editor: Claudio Gerbaldi

Received: 7 July 2021

Accepted: 9 August 2021

Published: 11 August 2021

Publisher's Note: MDPI stays neutral with regard to jurisdictional claims in published maps and institutional affiliations.



Copyright: © 2021 by the authors. Licensee MDPI, Basel, Switzerland. This article is an open access article distributed under the terms and conditions of the Creative Commons Attribution (CC BY) license (<https://creativecommons.org/licenses/by/4.0/>).

1. Introduction

Solid polymer electrolytes (SPEs) could be easily and safely prepared as flexible thin films in desirable sizes with good electrochemical stability and good mechanical properties [1–5]. SPEs are increasingly used as electrolytes in preference to liquid electrolytes for electrochemical devices for the storage of electric energy [6,7] or sensing [8–12], as well as other applications. Several authors have described methods for fabricating electrochemical gas SPE-based sensors on a flexible substrate which are inexpensive and easily mass produced [8,13,14]. However, these printed gas sensors may show a certain drawbacks in a low selectivity, a low consistency of performance in short-time and long-time periods [13]. These weaknesses represent an important motivation for current research in the development of improved SPEs [14].

Generally, SPEs are solid or gel mixtures consisting of a salt dispersed in a polymer host that conducts ions through the polymer chains [15]. Alongside the most commonly studied polymer host polyethylene oxide (PEO) [4,16], polyvinylidene fluoride (PVDF)

provides chemical, thermal and electrical stability, as well as unique piezoelectric and pyroelectric properties [5,17,18]. Among crystal phases types, three of them (α , β , and γ) are allowed to be steady in PVDF matrix as results of the mutual repulsion of fluorine atoms and its linear structure [19]. In polymer electrolytes, ion transport occurs predominantly in the amorphous region where the segmental motion of polymer chains becomes faster, thus the co-occurrence of crystalline and amorphous phases in PVDF-based SPEs fundamentally affects the ionic conductivity [17,19,20]. Besides techniques such as blending, addition of additives, etc. [17,18], the incorporation of an ionic liquid (IL) in the polymer matrix represents another approach that could modify overall electrochemical and mechanical properties [21]. For example, the crystallinity of polymer electrolyte is affected by the interaction of anion and cation of IL with the positive and negative polymer chains of PVDF, respectively [22,23]. It should also be noted that the electrical and mechanical properties of ionic liquids can be tailored according to their functional requirements [2,20]. These effects on crystallization and other properties of SPEs are related to the amount of IL in the polymer electrolyte [21,24–26].

Besides the IL content, thermal treatment is another way to change the properties of PVDF-based electrolytes [19,27]. Under various thermal conditions, the solvent evaporates differently from polymer mixtures and the evaporation rate has a significant influence on a degree of crystallinity that affects the morphology, chemical composition as well as ionic conductivity of the polymer electrolytes, as demonstrated on PVDF/[BMIM][TFSI] mixtures (with dimethyl formamide as solvent) [28] as well as on PVDF/[EMIM][BF₄] mixtures (with NMP as solvent) [14] or even on pure PVDF with various solvents [29]. Gregorio et al. [29] showed that PVDF/NMP solutions contain predominantly the β -phase at temperatures below 100 °C, while α -phase begins to form above this temperature. Furthermore, the amount of α -phase increases as temperature is increased; however, even at 140 °C there is still a large amount of β -phase present.

This work describes research into the effects of thermal treatment conditions on the morphology of PVDF/NMP/[EMIM][TFSI] electrolyte in terms of surface morphology, phase composition, chemical composition and depth profiling using scanning electron microscopy (SEM), Raman spectroscopy, Fourier transform infrared (FT-IR), differential scanning calorimetry (DSC), X-ray photoelectron spectroscopy (XPS) and secondary ion mass spectroscopy (SIMS). Thermal treatment conditions were chosen to prepare the SPE layers in a wide range in the morphology and to get a good adhesion between the SPE layer and ceramic substrate. This paper builds on earlier research which described the effect of thermal treatment conditions on AC/DC conductivity and also current fluctuations of PVDF/IL-based solid polymer electrolyte [18] as well as on the characterization of PVDF/NMP/[EMIM][TFSI] based amperometric sensors [30–33].

2. Materials and Methods

2.1. Sample Preparation

The samples were prepared on an electrode platform deposited on a ceramic substrate using lift-off technology. The thickness of the golden interdigital (comb-like) electrodes varied in the order of tenths of micrometers, while the widths of the fingers and gaps were 25 μm . The solid polymer electrolyte is a mixture of three basic components: (i) 1-ethyl-3-methylimidazolium bis(trifluoromethylsulfonyl)imide ([EMIM][TFSI], Merck, Darmstadt, Germany) as ionic liquid, (ii) poly-(vinylidene fluoride) (PVDF, Lyon, Sigma-Aldrich, France) as polymer matrix, (iii) N-methyl-pyrrolidone (NMP, VWR, Fontenay-sous-Bois, France) as a solvent. The ionic liquid, polymer matrix and solvent were combined in a weight ratio 1:1:3 and mixed using a magnetic stirrer at 70 °C. Then, the blended mixture in amount of 1.5 mg was deposited by drop coating on the electrode platform, and the substrate with the SPE layer was held at a certain temperature for a specific time using a hot plate to get different microstructures and porosities in the SPE layer, i.e., to achieve different crystalline forms of the PVDF. Thermogravimetric analyses of this mixture performed previously [34] showed two well-separated processes (110 °C

and 425 °C) due to the excellent thermal stability of PVDF and the ionic liquid, and the relatively low boiling point of the solvent (NMP). In this study, the four different conditions of the SPE layer preparation: (a) 80 °C for 90 s, (b) 120 °C for 90 s, (c) 120 °C for 210 s and (d) 160 °C for 600 s were predominantly chosen with regard to two factors: (i) preparation as much variation as possible in the structure and morphology of the SPE layer (associated with the particular temperature level and also with the crystallization rate of the PVDF in NMP), (ii) achievement a good adhesion between the SPE layer and the alumina substrate (associated with empirically chosen specific times for the particular temperature level). Because the thermal treatment conditions were chosen in the vicinity of the first decomposition process of the previously published thermogravimetric curve of the electrolyte [35], another issue is the residual content of the solvent (NMP) in the resultant SPE layer for different thermal treatment conditions. Standard test method for decomposition kinetics by thermogravimetry (E 1641, American Society for Testing Materials) was carried out for such estimation. Four test specimens were taken from the original mixture of electrolyte and heated through their decomposition region (25–250 °C), each of them at a different heating rate (1, 2.5, 5, and 10 °C/min). The specimen mass was recorded as a function of temperature. This standard test method allowed to estimate the mass loss of the solvent (NMP) from the electrolyte as follows: 5.5%, 32%, 58% and 100% for the following conditions (a) 80 °C 90 s, (b) 120 °C 90 s, (c) 120 °C 210 s and (d) 160 °C 600 s, respectively.

2.2. Scanning Electron Microscopy (SEM)

SEM images were acquired by Scanning Electron Microscope LYRA3 (TESCAN, Brno, Czech Republic) under acceleration voltage 10 kV.

2.3. Raman Spectroscopy

This non-destructive spectroscopic technique offers information about the molecular structure and the local chemical environments. It is also useful for studying subtle changes in electrolyte materials [35,36]. Raman spectra were collected using the confocal Raman imaging system Alpha 300 R (WITec, Ulm, Germany) with a 50 mW and 532 nm irradiation laser at 50× objective magnification. Integration time was 2 s.

2.4. Fourier Transform Infrared Spectroscopy

Attenuated total reflection Fourier-transform infrared spectroscopy (ATR-FTIR) is one the most used FTIR techniques since it requires minimal sample preparation for analysis and exhibits better performance. In our case, the standard FTIR was not able to distinguish the modes, while ATR-FTIR has higher measurement accuracy in the case of multicomponent samples with low reflectance signals. A Fourier infrared microscope Hyperion 3000 KIT (Bruker, Ettlingen, Germany) was used to study the phase composition. The spectra were collected in the range from 800 cm^{-1} to 4000 cm^{-1} . The lower limit of the spectra is defined by the Ge crystal used.

2.5. Differential Scanning Calorimetry

To describe the crystallinity of SPEs, the differential scanning calorimetry (DSC) measurements were done on DSC 204 F1 (NETZSCH, Selb, Germany) at a heating rate of 10 °C/min in temperature range from 20 °C up to 200 °C under an argon flux 20 mL/min.

2.6. X-ray Photoelectron Spectroscopy

Samples were investigated using an AXIS Supra X-ray photoelectron spectrometer (Kratos Analytical, Manchester, UK), with the emission current used to capture the data set at 15 mA. During the measurement process, a resolution of 80 was used to acquire wide spectra and 20 for element spectra. The angle of photoelectron take-off was 90°. The obtained XPS spectra correspond to the 6–7 nm depth analysis due to the inelastic mean free path of photoelectrons in organic compounds at kinetic energy of ~1 keV.

2.7. Secondary Ion Mass Spectroscopy (SIMS)

The SIMS technique is one of the leading surface chemical analysis and imaging techniques providing molecular and elemental information in the field of material science [37]. It consists of bombarding the sample surface with an ion beam (called primary ions) and analysing the ions generated by bombardment (secondary ions). The apparatus used in our case was a TOF.SIMS 5 (Iontof, Münster, Germany) which is a system with a time of flight mass analyser that separates the ions in a field-free drift path according to their velocity. The resulting erosion speed differs depending on various factors such as material type or sputtering energy. All measurements were done in the negative mode since the samples mostly contain non-metals. The duration of the analysis for each sample was 6–10 h (from which 2–5 h are sputtering only with 2 keV Cs ions). The depth of the craters exceeds 5 μm .

3. Results and Discussion

Figure 1 shows the surface of the investigated polymer electrolytes dominated by spherulites, i.e., rounded micrometric particles. Apart from the morphology of the SPEs after different preparation conditions in the middle of the SPE, Figure 1 also shows particle size distribution histograms. Each histogram is determined from analyses of four SEM images with a viewfield of 100 μm on our SEM Lyra 3 (Tescan, Brno, Czech Republic). The average diameter of SPE particles increases with preparation temperature from $\sim 3.08 \mu\text{m}$ up to $\sim 15.12 \mu\text{m}$. Thus, the lower the temperature, the greater is the porosity of SPE. The porosity of the prepared layers is tightly bound to the crystallization phase, as was pointed out experimentally on mixture of the polymer (PVDF) and the solvent (NMP) [29]. The diameter of the spherulites has a non-uniform distribution across the electrolyte surface, with the spherulites in the middle of the prepared layer being larger than at the edges.

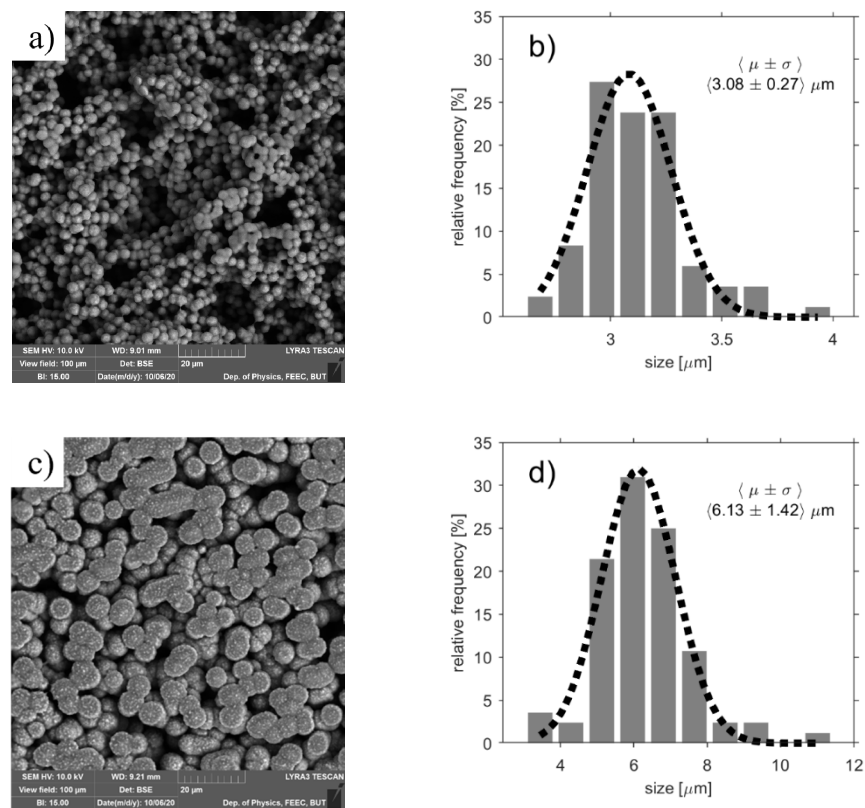


Figure 1. Cont.

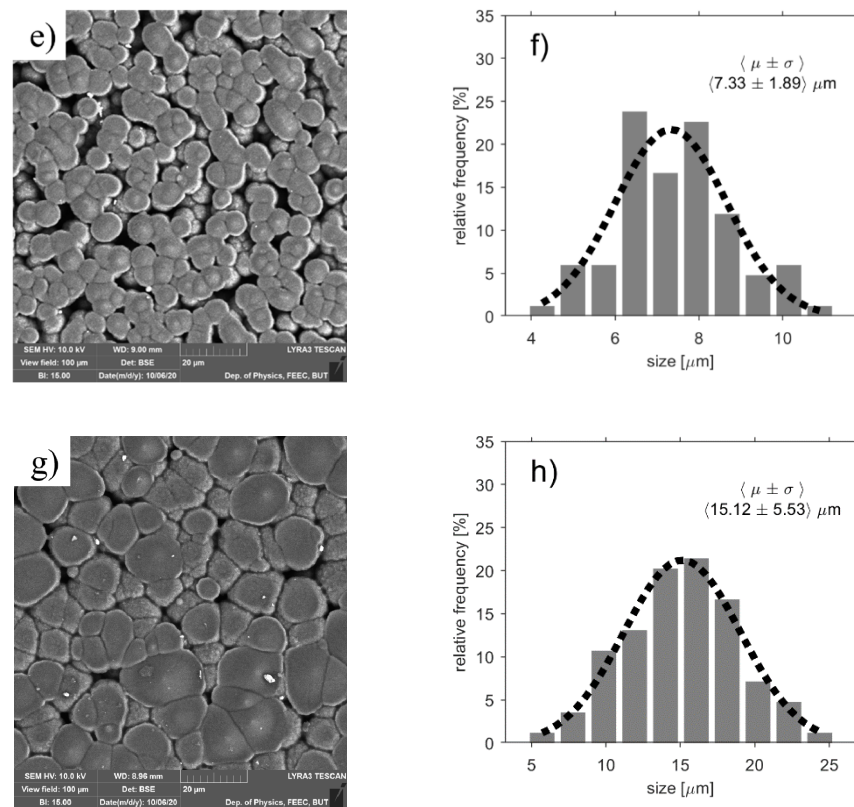


Figure 1. Scanning electron microscope (SEM) images and particle size distribution histograms of the studied SPEs after different preparation conditions: (a,b) 80 °C for 90 s (c,d) 120 °C for 90 s (e,f) 120 °C for 210 s (g,h) 160 °C for 600 s.

3.1. Raman Spectroscopy

Raman spectra from ionic liquid, PVDF and the average of each sample are presented in Figure 2. The average spectra were used for characterization because the sample consists of spherulites with different sizes and the spectra could be dependent on the acquisition point. The average data were extracted from an area of $40 \times 40 \mu\text{m}$ to study the Raman spectra of the samples.

Figure 2 shows the Raman spectra of the ionic liquid, PVDF as well as the four studied SPEs. Grey lines with squares and cyan lines with triangles represent significant peaks connected to the ionic liquid and PVDF respectively. The strongest Raman signals, which the solid polymers exhibit, are found in the CH stretching region ($2800\text{--}3050 \text{ cm}^{-1}$) dominated by a very strong peak line at 2977 cm^{-1} which belongs to symmetric mode of CH_2 group [38]. The side peak at line 3014 cm^{-1} connected to β -phase asymmetric CH_2 stretching [39] becomes more distinguishable as the temperature of SPE preparation increases. Other PVDF related lines are 513 cm^{-1} (β -phase, CF_2 scissoring), 796 cm^{-1} (α -phase, CH_2 rocking), 811 cm^{-1} (γ -phase, CH_2 wagging), 840 cm^{-1} (β , CH_2 rocking and CF_2 stretching mode), 882 cm^{-1} ($\alpha + \beta + \gamma$, CC symmetric and asymmetric stretching, CC symmetric stretching and CH_2 twisting) and 1432 cm^{-1} (CH_2 twisting + wagging) [38–41]. The observed band at 840 cm^{-1} is common for both β -phase and the γ -phase, however, the dominance of this peak refers only to β -phase [41–44], which was formed due to electrostatic interaction with IL.

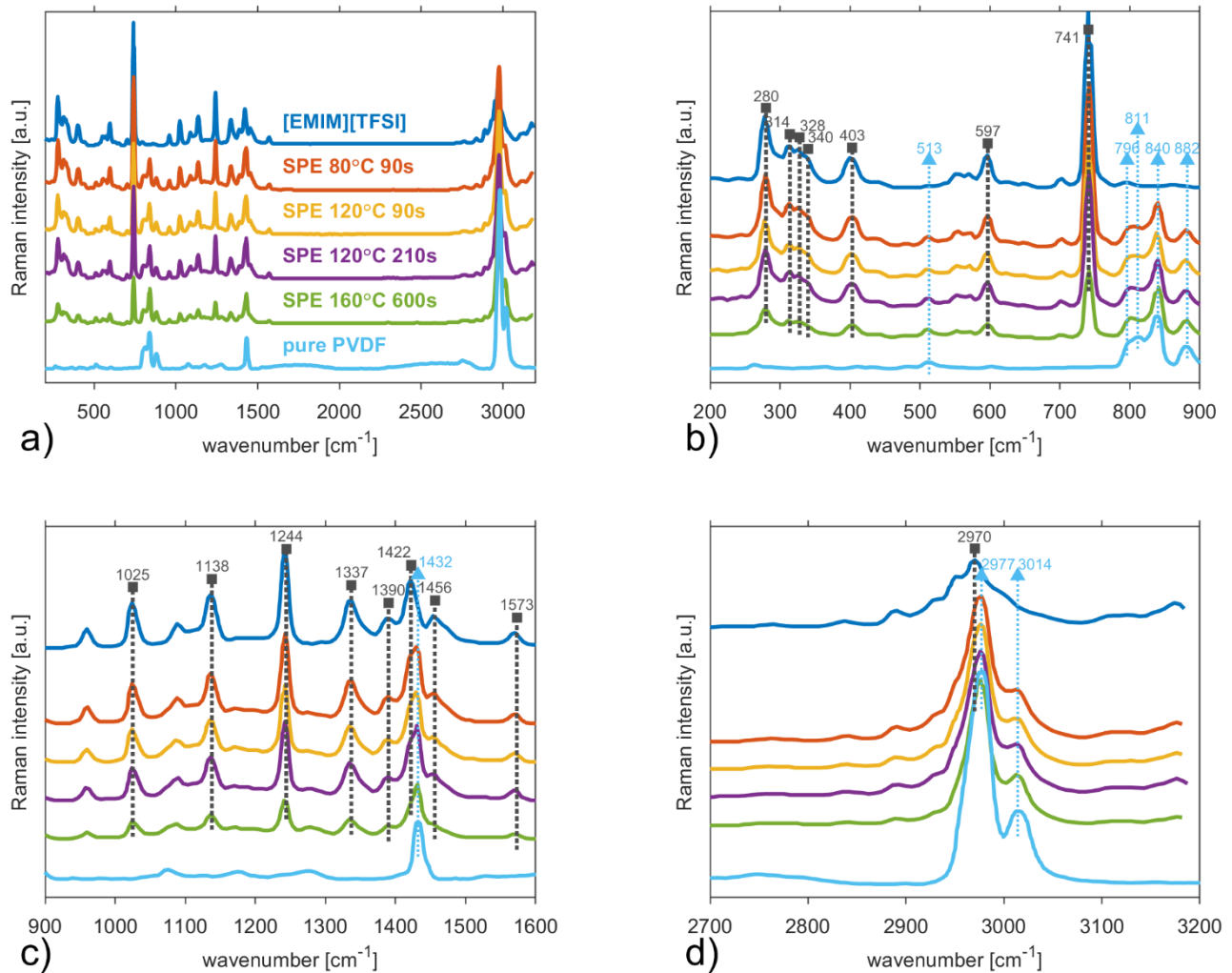


Figure 2. Raman spectra of ionic liquid [EMIM][TFSI], solid polymer electrolytes after four treatment conditions and PVDF in (a) full spectral range 200–3200 cm^{-1} , (b) spectral range 200–900 cm^{-1} , (c) spectral range 900–1600 cm^{-1} , and (d) spectral range 2700–3200 cm^{-1} . Grey lines and squares represent significant peaks connected to ionic liquid. Cyan lines and triangles are connected to PVDF peaks ($\blacktriangle\blacktriangleleft\blacktriangleright$).

Concerning the ionic liquid [EMIM][TFSI], a ring H–C–C–H symmetric bending, CF_3 symmetric bending as well as contributions from two conformers of the [TFSI] anion [45,46] contribute to the second strongest Raman peak observed at line 741 cm^{-1} . Further, CF_3 symmetric bending (280 cm^{-1}), S–C stretching (314, 328, and 340 cm^{-1}), SO_2 antisymmetric bending (597 cm^{-1}), SO_2 symmetric stretching (1138 cm^{-1}) and a SO_2 antisymmetric stretching with contributions from the CF_3 symmetric stretching (1244 cm^{-1}) are noticeable vibrations from [TFSI] anion. Other strong Raman peaks are assigned to $\text{CH}_2(\text{N})/\text{CH}_3(\text{N})$ C–N stretching (1337, 1390, 1422, and 1456 cm^{-1}). These bands are in good agreement with published studies [45–48].

Raman mapping allows localization of PVDF phase and IL distribution. Detailed mapping was carried out using a Zeiss EC Epiplan-Neofluar DIC objective with magnification 100 \times . The scan area was 45 \times 45 μm with 90 lines and 90 points per line. Integration time was 5 sec. Excitation wavelength was 532 nm and laser power 5 mW. Formation of spherulitic texture during PVDF crystallization with the presence of IL was described earlier by polarization optical microscopy and by analysis based on the kinetics of crystallization [21]. These spherulites are composed of highly ordered lamellae which were previously confirmed by observation of a Maltese cross as fact of birefringences [49].

Figure 3 shows Raman maps for peaks 741 cm^{-1} and 840 cm^{-1} as well as normalized spectra corresponding to an area of small white squares for all types of studied SPEs. According to Raman mapping of band 741 cm^{-1} in Figure 3a–d, the ionic liquid is concentrated at the edges and on the surface of the spherulites. The lamellae of the PVDF are connected by amorphous regions, which is characterized by the spectrum dominated by [EMIM][TFSI] bands as illustrated in Figure 3e for the white circle located between spherulites (Figure 3d). Thus, blue and green lines in Figure 3e are Raman spectra of the same sample (SPE $160\text{ }^{\circ}\text{C}$ 600 s) measured at two different locations to demonstrate a semi-crystalline structure of spherulites (white square) and amorphous regions between spherulites (white circle). The normalized Raman spectra to the 741 cm^{-1} line shows in Figure 3e that the band of β -phase of PVDF (840 cm^{-1}) increases with the intensity of solvent evaporation in SPE during the preparation process, and indicates that the fraction of β -phase also grows. This peak becomes more dominant over other phases, the γ -phase (811 cm^{-1}) especially becomes insignificant, even to the α -phase (796 cm^{-1}). The samples processed at the same temperature but different times do not show dramatic changes to the shape of Raman spectrum. The sample prepared at $120\text{ }^{\circ}\text{C}$ for 210 s was studied under 1 V. The spectroscopy confirmed that changes occur for IL bands and not for the PVDF bands. Dependence of IL bands on electron density is confirmed by ionic type conductivity. This observation is in direct agreement with our previous study where we showed [18] that the ionic conductivity is coupled to the ionic liquid, which modifies the conductivity of the polymer matrix (PVDF).

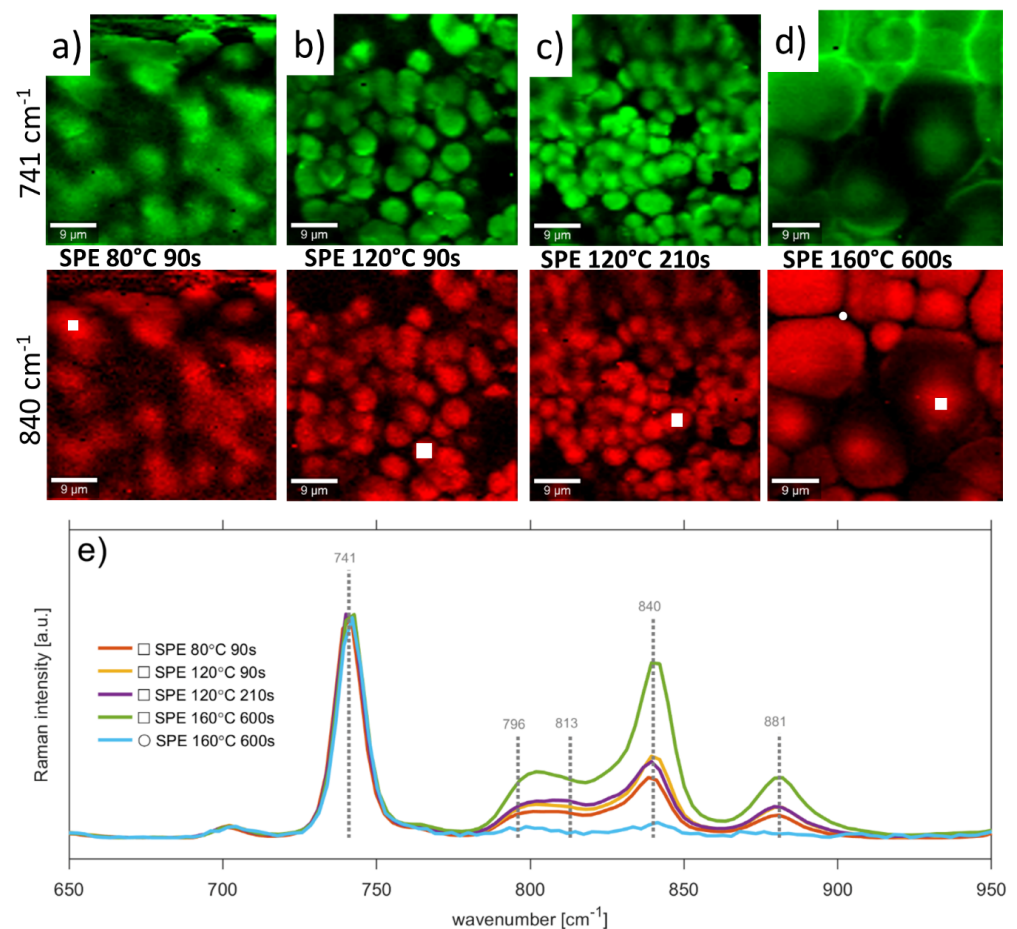


Figure 3. Raman maps for peaks 741 cm^{-1} (ionic liquid), 840 cm^{-1} (PVDF) for SPEs prepared at (a) $80\text{ }^{\circ}\text{C}$ 90 s (b) $120\text{ }^{\circ}\text{C}$ 90 s (c) $120\text{ }^{\circ}\text{C}$ 210 s and (d) $160\text{ }^{\circ}\text{C}$ 600 s (e) normalized Raman spectra corresponding to area of small white squares and white circle on SPEs. Peaks were normalized at 741 cm^{-1} . White squares are located on spherulites, while circle is located between them (amorphous region).

3.2. Fourier Transform Infrared Spectroscopy

ATR-FTIR spectra in Figure 4a show that the C–H stretching region ($2800\text{--}3300\text{ cm}^{-1}$) is not as dominant as in the results obtained by Raman spectroscopy. In order to separate the substrate signal, the ATR-FTIR of the ceramic substrate are also presented. Peaks at the same position for the samples and the substrate were not considered in this work. ATR-FTIR spectra in Figure 4b show the presence of exclusive peaks for γ -phase ($\sim 1232\text{ cm}^{-1}$) and β -phases ($\sim 1276\text{ cm}^{-1}$, 1431 cm^{-1}) of PVDF [50,51]. The peak at 840 cm^{-1} belongs to both γ - and β -phases [52], while peaks at 880 cm^{-1} and 1401 cm^{-1} are assigned to α -, β - and γ -phases [51]. Unfortunately, the characteristic bands of the α -phase [51] (854 , 975 , 1149 , 1209 , 1383 and 1423 cm^{-1}) are weak or located below (410 , 489 , 532 , 614 , 763 , 795 cm^{-1}) the lower limit of our apparatus, which is given by the Ge crystal used. Thus, the fractions of a particular PVDF phase cannot be estimated by the generally accepted approach [51,53–55] based on the α -phase peak at 763 cm^{-1} . In order to calculate the relative percentage of γ - and β -phases we consider the number of electroactive phases consist only of γ - and β -phases (100%) and use the peak to valley method [51]: valley of $\sim 1276\text{ cm}^{-1}$ and peak of 1260 cm^{-1} for β -phase and valley of $\sim 1232\text{ cm}^{-1}$ and peak of 1225 cm^{-1} for γ -phase. Table 1 shows relative percentage of γ - and β -phases for all samples.

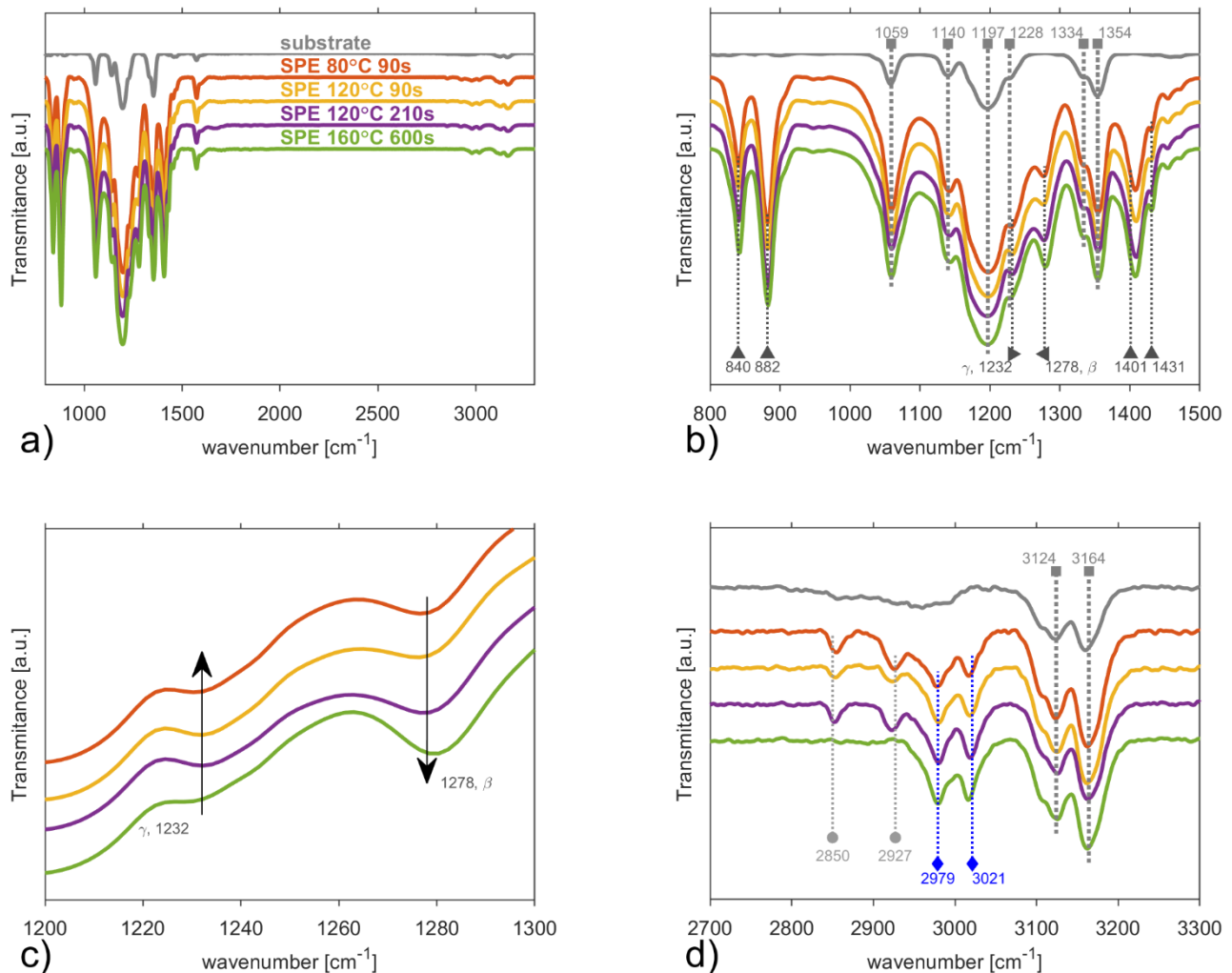


Figure 4. ATR-FTIR spectra of the solid polymer electrolytes after four treatment conditions and substrate in (a) the full spectral range $800\text{--}1430\text{ cm}^{-1}$, (b) the spectral range $800\text{--}1500\text{ cm}^{-1}$, (c) the spectral range $1200\text{--}1300\text{ cm}^{-1}$ of exclusive γ -phase and β -phase peaks, and (d) the spectral range of C–H stretching region $2700\text{--}3300\text{ cm}^{-1}$. Light grey squares represent peaks connected to the substrate. Grey triangles (\blacktriangle \blacktriangledown) are connected to PVDF peaks. Blue diamonds represent ionic liquid peaks. Grey circles are assumed to be connected to the solvent NMP.

Table 1. Relative percentage of γ - and β -phases in sample considering number of electroactive phases consisting only of γ - and β -phases (100%).

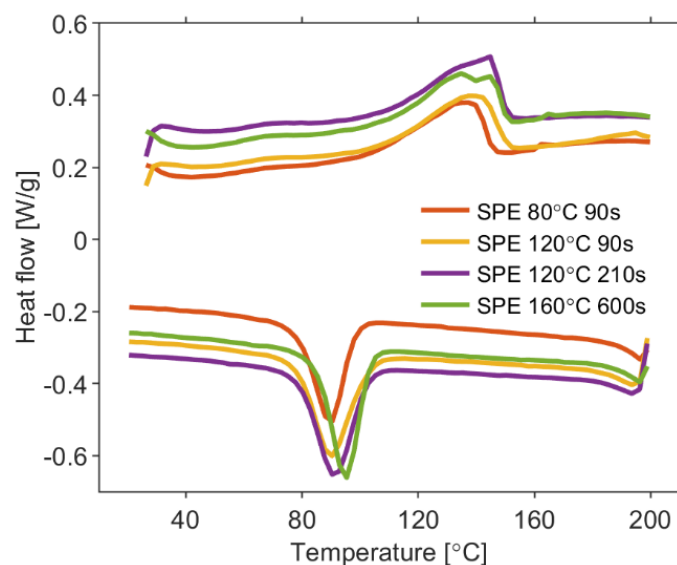
Sample	SPE 80 °C 90 s	SPE 120 °C 90 s	SPE 120 °C 210 s	SPE 160 °C 600 s
β -phase, %	84.11	56.23	73.03	98.80
γ -phase, %	15.89	43.77	26.97	1.20

Electrostatic interaction between the ionic liquid and the PVDF polymeric chains leads to crystallization of PVDF into the electroactive β -phase. Increasing the temperature leads to a shift of vibration modes from $\sim 1276\text{ cm}^{-1}$ (for SPE 80 °C 90 s) to $\sim 1279\text{ cm}^{-1}$ (SPE 160 °C 600 s) and from $\sim 1230\text{ cm}^{-1}$ (for SPE 80 °C 90 s) to $\sim 1232\text{ cm}^{-1}$ (for SPE 160 °C 600 s). This shift to higher wavenumbers can be attributed to the size effect of the crystallites [56] and the firm interaction of the polymer matrix with the IL cation (more precisely, between CF_2 groups of PVDF with the imidazolium ring) [57,58]. The higher intensity of SPE preparation conditions (temperature and time) leads to the higher evaporation rate of NMP [18,34] as well as to an increase of the PVDF β -phase in the SPE, as indicated in Table 1 which is in full agreement with other experimental studies [28].

FTIR spectra of the C–H stretching region ($2800\text{--}3300\text{ cm}^{-1}$) are shown in Figure 4d. Ionic liquid is represented by two characteristic peaks of $(\text{N})\text{CH}_3$ at 2979 cm^{-1} [59] and $\text{C}(2)\text{--H}$ 3018 cm^{-1} [60], which are present for all samples. The peaks of C–H vibration at $\sim 2921\text{ cm}^{-1}$ ($-\text{CH}_3$) at 2853 cm^{-1} ($-\text{CH}_2-$) could be assigned to aliphatic carbon–hydrogen stretching in methyl and methylene groups of NMP [61] and are not observed for the sample (SPE 160 °C 600 s) [62–64]. The disappearance of these two peaks could be explained by the removal of NMP in the last sample.

3.3. Differential Scanning Calorimetry

DSC analysis were carried out on all types of the solid polymer electrolytes to investigate their relative crystallinity. Figure 5 shows the DSC curves where the melting temperature around 140 °C and the crystallization temperature around 90 °C are observed for each electrolyte under investigation. These temperatures increase as solvent evaporation rate increases for particular preparation conditions of SPE. The temperature difference between melting and crystallization is connected to the kinetics of crystallization, i.e., polymer chains reorganization and recrystallization [27].

**Figure 5.** DSC thermogram of PVDF/NMP/[EMIM][TFSI] electrolytes of four treatment conditions.

Assuming pure PVDF to be 100%, the relative crystallinity, γ_c , is determined by formula [65]

$$\gamma_c = \frac{\Delta H_f}{\Delta H_{f0} \times \varphi} \times 100 [\%], \quad (1)$$

where ΔH_f , the enthalpy of fusion, was determined as area below melting peaks, ΔH_{f0} represents the heat of fusion for the pure crystalline PVDF (for this case 104.7 J/g [27]) and φ denotes the weight fraction of PVDF in a mixture. The relative crystallinity was estimated to be 92.64% for SPE 80 °C 90 s, 73.24% for SPE 120 °C 90 s, 57.51% for SPE 120 °C 210 s and 44.55% for SPE 160 °C 600 s. The PVDF/NMP/[EMIM][TFSI] electrolytes under the test exhibited lower γ_c as intensity of solvent evaporation increases during the preparation process. Thus, the SPE prepared at conditions 160 °C for time 600 s is the most amorphous.

3.4. X-ray Photoelectron Spectroscopy

All types of the solid polymer electrolytes were subjected to XPS measurement, which provides an estimate of the surface elemental compositions and chemical structures in the samples. An incorrect referencing of the binding energy scale may mislead the interpretation of the data, thus we were cautious about the conclusions drawn from XPS characterization [66]. All XPS binding energies were corrected using the C1s line of (C–C/CH₃) at 284.6 eV. Figure 6a shows wide range XP spectra for all samples where the expected elements (in PVDF, NMP and ionic liquid) F, N, O, S, and C were detected and confirmed that the mixtures of ionic liquid, polymer matrix and did not produce a new binding energy.

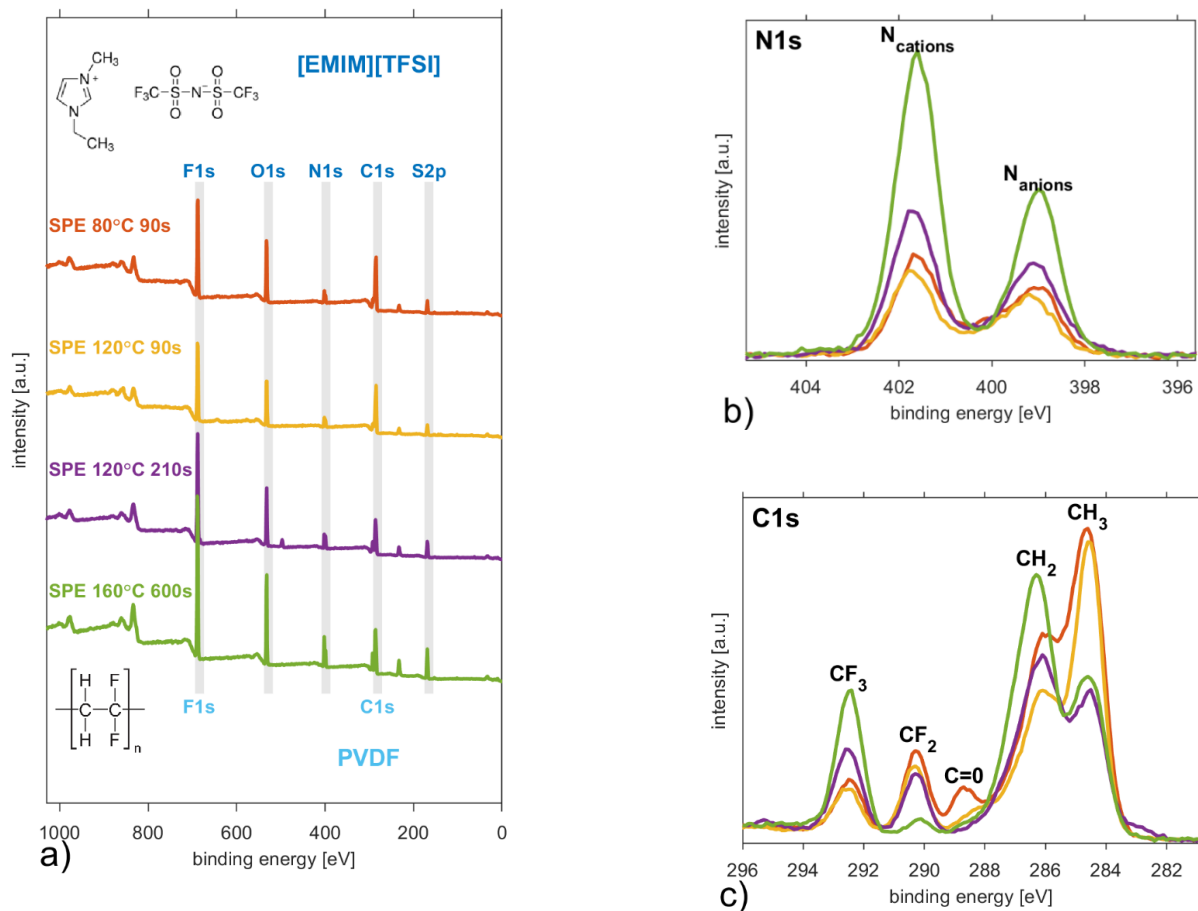


Figure 6. (a) survey XP spectrum, (b) N1s XP spectrum and (c) C1s XP spectrum of the solid polymer electrolytes prepared in four treatment conditions.

While the F1s and O1s peaks contain a single narrow peak with a full width at half maximum below 1.8 eV, the others (S2p, N1s and C1s) contain distinguishable components. XPS S2p spectra contain only a characteristic doublet peak of the TFSI anion [67,68]. Figure 6b shows how XPS N1s spectra are split into two recognisable peaks, where the larger one at 401.7 eV is related to N located at the [EMIM] cation ring and the smaller one at 399.1 eV corresponds to the N anions [69]. Their relative peak surface ratio changes from 1:1.18 (SPE 80 °C 90 s) up to 1:1.75 (SPE 160 °C 600 s), but it never gains the value characteristic for pure ionic liquid [EMIM][TFSI] 1:1.90 published elsewhere [70].

Figure 6c shows that the SPEs have four specific peaks at 292.4 eV (CF₃), 290.3 eV (CF₂), 286.1 eV (C–N/CH₂) and 284.6 eV (C–C/CH₃). The relatively low boiling point of the solvent NMP [18,34] results in a decrease of NMP content in the SPE mixture and the disappearance of the specific peak at 288.7 eV (C=O) [71,72], which is distinguishable only in the case of the SPE layer prepared at 80 °C for 90 s. Table 2 illustrates the solvent evaporation as the relative chemical compositions change with the thermal and time conditions in the preparation process of different SPEs. The relative amount increases for elements F, N, and S, while it decreases for C as the solvent evaporation rate grows. The relative concentrations of each element were calculated by taking into account the corresponding relative sensitivity factors [73] of our apparatus. Furthermore, the relative intensities of specific peaks become insignificant at 292.4 eV (CF₂) and decrease at 284.6 eV (C–C/CH₃) in comparison to the CF₃ peak. The shape of the C1s XP spectrum becomes more similar to the C1s spectrum of pure ionic liquid [EMIM][TFSI] [70] as more solvent is evaporated. Figure 6c illustrates that the chemical composition of the surface is closer to the composition of the ionic liquid as spherulites grow due to solvent evaporation during the preparation process. This confirms our observations obtained from Raman spectroscopy about ionic liquids being on the surfaces of the spherulites.

Table 2. Relative chemical compositions determined by XPS.

Sample	Element Content [%]				
	S2p	C1s	N1s	O1s	F1s
SPE 80 °C 90 s	3.28	54.15	5.75	16.02	20.79
SPE 120 °C 90 s	3.44	53.24	5.68	14.91	22.72
SPE 120 °C 210 s	5.97	45.02	9.25	14.96	24.80
SPE 160 °C 600 s	6.94	37.53	11.12	17.91	26.50

3.5. Secondary Ion Mass Spectroscopy

To illustrate the change of the relative concentration of elements over depth, time-of-flight secondary ion mass spectroscopy (ToF-SIMS) was applied to examine the surface of the samples. The negative ToF-SIMS spectra of all the samples exhibit expected peaks which are in agreement with the negative spectra of the ionic liquid [74–76] and PVDF [77]. Figure 7a shows that the negative ToF-SIMS spectra are dominated by F[−] ($m/z = 19$) and O[−] ($m/z = 16$). Other intensive peaks are characteristic peaks for PVDF (C₂[−], CF₂[−]) or smaller fragments of the [TFSI][−] anion, such as CF₃[−] at $m/z = 69$, CF₃SO₂N[−] at $m/z = 147$, NSO₂[−] at $m/z = 78$ and SO₂NSO₂[−] at $m/z = 142$. The relative intensity of ion fragments of [TFSI][−] moiety from a sample surface is assumed to be almost unchanged [76] considering the temperatures of the particular preparation process of the SPEs.

Figure 7b indirectly illustrates the depth profiles of ionic liquid from the surface of particular SPEs on normalized depth profiles of the single-bond fraction (CF₃SO₂N[−]) of [TFSI][−] anion ($m/z = 280$), which was not detected due to the setting limitations in our measurements. Depth profiles are normalized with respect to total count at a specific sputter time. Figure 7b indicates that the concentration of ionic liquid in SPEs grows with the intensity of the thermal treatment. The depth profiles are the results of integral information over an area of 100 × 100 μm² where the average diameters of the spherical particles are from ~3.08 μm up to ~15.12 μm.

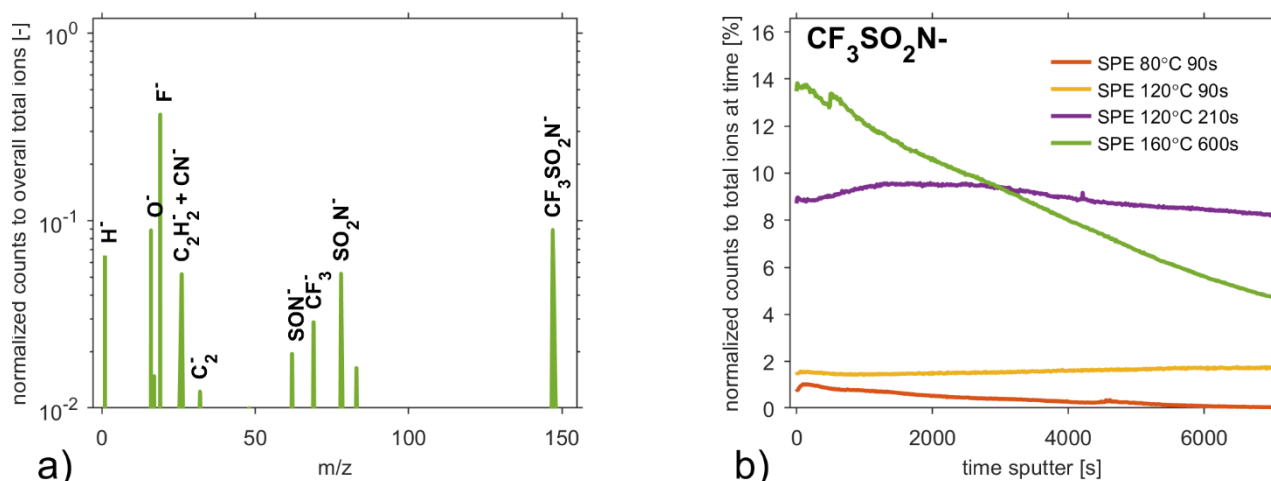


Figure 7. (a) Normalized negative ToF-SIMS spectrum taken from a SPE 160 °C 600 s. Counts are normalized to the total sum of counts across the spectrum. Normalized intensities below 0.01 are ignored. (b) Normalized depth profiles of $\text{CF}_3\text{SO}_2\text{N}^-$ anion to total ions at the specific sputter time for all SPEs. Depth profiles are normalized with respect to the total count at specific sputter time. The spectrum and profiles are obtained by employing Cs^+ ions as a primary projectile with a kinetic energy of 2 keV.

4. Conclusions

This work investigates how thermal treatment conditions of PVDF/NMP/[EMIM][TFSI] electrolyte affect its surface morphology, phase composition and chemical composition. The ionic liquid, polymer matrix and solvent were mixed in a weight ratio 1:1:3. After deposition by drop casting on the electrode platform, mixtures were held at (i) 80 °C for 90 s, (ii) 120 °C for 90 s, (iii) 120 °C for 210 s and (iv) 160 °C for 600 s, to get four types of solid polymer electrolyte. These electrolytes consist of spherulites whose average diameter increases with the preparation temperature. Raman mapping shows that the spherulites have a semicrystalline structure and the area between them is amorphous. The crystalline structure is of PVDF α -, β - and γ -phases. Normalized Raman spectra also showed that the peak band of β -phase of PVDF (840 cm^{-1}) increases with the intensity of solvent evaporation in the SPE during the preparation process. In other words, the crystallinity is connected to the preparation conditions of the SPE thermal treatment.

Analysis of FTIR spectra confirmed the results obtained from Raman spectroscopy that β -phase becomes more dominant over other phases. Comparison of these two spectroscopic techniques shows that the positions of particular peaks remained relatively unchanged indicating that polymer matrix (PVDF) and ionic liquid [EMIM][TFSI] have good miscibility in solvent NMP.

DSC described the decrease of the PVDF crystallinity in PVDF/NMP/[EMIM][TFSI] electrolytes as intensity of solvent evaporation increases during the preparation process.

Relative chemical compositions investigated by XPS increase for elements F, N, and S, while they decrease for C as the solvent evaporation rate grows. For SPE samples with a higher solvent evaporation rate, the shape of the C1s XP spectrum is comparable to the C1s spectrum of the ionic liquid, thus, we could conclude that the chemical composition of the surface is closer to the composition of the ionic liquid as was also observed by Raman mapping at band 741 cm^{-1} .

Taking into account the already published fact that the DC conductivity of the SPE increases with the intensity of the heat treatment and this DC conductivity becomes comparable to the DC conductivity of the ionic liquid, it can be concluded that ion transport takes place predominantly on the surfaces of the spherulites as well as in amorphous regions.

Author Contributions: P.S. and P.K. initiated the research. P.S. supervised the project. P.K. prepared the samples. A.G. performed SEM measurements and evaluation. D.S. provided the measurement and the analyses by Raman spectroscopy and XPS. A.N. provided FTIR measurements. R.D. provided SIMS measurements. P.S. wrote the paper with contributions from P.K. and D.S. All authors have read and agreed to the published version of the manuscript.

Funding: The research described in this paper was financed by the grant 18 19104S of the Czech Science Foundation (GACR).

Institutional Review Board Statement: Not applicable.

Informed Consent Statement: Not applicable.

Data Availability Statement: The datasets measured and analyzed during the current study are available from the corresponding author on reasonable request.

Conflicts of Interest: The authors declare no conflict of interest.

References

1. Ye, Y.S.; Rick, J.; Hwang, B.J. Ionic liquid polymer electrolytes. *J. Mater. Chem. A* **2013**, *1*, 2719–2743. [[CrossRef](#)]
2. Correia, D.M.; Fernandes, L.C.; Martins, P.M.; García-Astrain, C.; Costa, C.M.; Reguera, J.; Lanceros-Méndez, S. Ionic Liquid–Polymer Composites: A New Platform for Multifunctional Applications. *Adv. Funct. Mater.* **2020**, *30*, 1909736. [[CrossRef](#)]
3. Josef, E.; Yan, Y.; Stan, M.C.; Wellmann, J.; Vizintin, A.; Winter, M.; Johansson, P.; Dominko, R.; Guterman, R. Ionic Liquids and their Polymers in Lithium–Sulfur Batteries. *Isr. J. Chem.* **2019**, *59*, 832–842. [[CrossRef](#)]
4. Austin Suthanthiraraj, S.; Johnsi, M. Nanocomposite polymer electrolytes. *Ionics* **2017**, *23*, 2531–2542. [[CrossRef](#)]
5. Xia, W.; Zhang, Z. PVDF-based dielectric polymers and their applications in electronic materials. *IET Nanodielectr.* **2018**, *1*, 17–31. [[CrossRef](#)]
6. Kammoun, M.; Berg, S.; Ardebili, H. Flexible thin-film battery based on graphene-oxide embedded in solid polymer electrolyte. *Nanoscale* **2015**, *7*, 17516–17522. [[CrossRef](#)]
7. Park, J.; Ahn, D.B.; Kim, J.; Cha, E.; Bae, B.S.; Lee, S.Y.; Park, J.U. Printing of wirelessly rechargeable solid-state supercapacitors for soft, smart contact lenses with continuous operations. *Sci. Adv.* **2019**, *5*, eaay0764. [[CrossRef](#)]
8. Kuberský, P.; Srovy, T.; Hamáček, A.; Nešpůrek, S.; Srova, L. Towards a fully printed electrochemical NO₂ sensor on a flexible substrate using ionic liquid based polymer electrolyte. *Sens. Actuators B Chem.* **2015**, *209*, 1084–1090. [[CrossRef](#)]
9. Luo, B.; Xiao, M.; Huang, X.; Hu, H.; Knibbe, R.; Wang, S.; Lyu, M.; Wang, L.; Sun, D. An Integrated Strategy towards Enhanced Performance of the Lithium–Sulfur Battery and its Fading Mechanism. *Chem. A Eur. J.* **2018**, *24*, 18544–18550.
10. Luo, R.; Li, Q.; Du, B.; Zhou, S.; Chen, Y. Preparation and Characterization of Solid Electrolyte Doped With Carbon Nanotubes and its Preliminary Application in NO₂ Gas Sensors. *Front. Mater.* **2019**, *6*, 113. [[CrossRef](#)]
11. Vonau, C.; Zosel, J.; Paramasivam, M.; Ahlborn, K.; Gerlach, F.; Vashook, V.; Guth, U. Polymer based materials for solid electrolyte sensors. *Solid State Ion.* **2012**, *225*, 337–341. [[CrossRef](#)]
12. Navratil, J.; Kubersky, P.; Sedlak, P.; Hamacek, A. Preparation of Nitrogen Dioxide Sensor Utilizing Aerosol Jet Printing Technology. In Proceedings of the Proceedings of the International Spring Seminar on Electronics Technology, Demanovska Valley, Slovakia, 14–15 May 2020.
13. Korotcenkov, G.; Cho, B.K. Instability of metal oxide-based conductometric gas sensors and approaches to stability improvement (short survey). *Sens. Actuators B Chem.* **2011**, *156*, 527–538. [[CrossRef](#)]
14. Luo, R.; Li, H.; Du, B.; Zhou, S.; Chen, Y. A printed and flexible NO₂ sensor based on a solid polymer electrolyte. *Front. Chem.* **2019**, *7*, 286. [[CrossRef](#)] [[PubMed](#)]
15. Varshney, P.K.; Gupta, S. Natural polymer-based electrolytes for electrochemical devices: A review. *Ionics* **2011**, *17*, 479–483. [[CrossRef](#)]
16. Kang, Y.; Kim, H.J.; Kim, E.; Oh, B.; Cho, J.H. Photocured PEO-based solid polymer electrolyte and its application to lithium-polymer batteries. *J. Power Sources* **2001**, *92*, 255–259. [[CrossRef](#)]
17. Manjunatha, H.; Damle, R.; Pravin, K.; Kumaraswamy, G.N. Modification in the transport and morphological properties of solid polymer electrolyte system by low-energy ion irradiation. *Ionics* **2018**, *24*, 3027–3037. [[CrossRef](#)]
18. Sedlak, P.; Gajdos, A.; Macku, R.; Majzner, J.; Sedlakova, V.; Holcman, V.; Kuberský, P. The effect of thermal treatment on ac/dc conductivity and current fluctuations of PVDF/NMP/[EMIM][TFSI] solid polymer electrolyte. *Sci. Rep.* **2020**, *10*, 21140. [[CrossRef](#)] [[PubMed](#)]
19. Xu, P.; Fu, W.; Hu, Y.; Ding, Y. Effect of annealing treatment on crystalline and dielectric properties of PVDF/PEG-containing ionic liquid composites. *Compos. Sci. Technol.* **2018**, *158*, 1–8. [[CrossRef](#)]
20. Lewandowski, A.; Świdarska, A. New composite solid electrolytes based on a polymer and ionic liquids. *Solid State Ion.* **2004**, *169*, 21–24. [[CrossRef](#)]
21. Chaurasia, S.K.; Singh, R.K.; Chandra, S. Effect of ionic liquid on the crystallization kinetics behaviour of polymer poly(ethylene oxide). *CrystrEngComm* **2013**, *15*, 6022–6034. [[CrossRef](#)]

22. Correia, D.M.; Costa, C.M.; Lizundia, E.; Sabater i Serra, R.; Gómez-Tejedor, J.A.; Biosca, L.T.; Meseguer-Dueñas, J.M.; Gomez Ribelles, J.L.; Lanceros-Méndez, S. Influence of Cation and Anion Type on the Formation of the Electroactive β -Phase and Thermal and Dynamic Mechanical Properties of Poly(vinylidene fluoride)/Ionic Liquids Blends. *J. Phys. Chem. C* **2019**, *123*, 45. [[CrossRef](#)]
23. Correia, D.M.; Barbosa, J.C.; Costa, C.M.; Reis, P.M.; Esperança, J.M.S.S.; De Zea Bermudez, V.; Lanceros-Méndez, S. Ionic Liquid Cation Size-Dependent Electromechanical Response of Ionic Liquid/Poly(vinylidene fluoride)-Based Soft Actuators. *J. Phys. Chem. C* **2019**, *123*, 12744–12752. [[CrossRef](#)]
24. Xing, C.; Zhao, M.; Zhao, L.; You, J.; Cao, X.; Li, Y. Ionic liquid modified poly(vinylidene fluoride): Crystalline structures, miscibility, and physical properties. *Polym. Chem.* **2013**, *4*, 5726–5734. [[CrossRef](#)]
25. Chaurasia, S.K.; Singh, R.K.; Chandra, S. Ionic liquid assisted modification in ionic conductivity, phase transition temperature and crystallization kinetics behaviour of polymer poly(ethylene oxide). *Solid State Ion.* **2014**, *262*, 790–794. [[CrossRef](#)]
26. Pickford, T.; Gu, X.; Heeley, E.L.; Wan, C. Effects of an ionic liquid and processing conditions on the β -polymorph crystal formation in poly(vinylidene fluoride). *CrystEngComm* **2019**, *21*, 5418–5428. [[CrossRef](#)]
27. Cui, Z.; Hassankiadeh, N.T.; Zhuang, Y.; Drioli, E.; Lee, Y.M. Crystalline polymorphism in poly(vinylidene fluoride) membranes. *Prog. Polym. Sci.* **2015**, *51*, 94–126. [[CrossRef](#)]
28. Dong, Z.; Zhang, Q.; Yu, C.; Peng, J.; Ma, J.; Ju, X.; Zhai, M. Effect of ionic liquid on the properties of poly(vinylidene fluoride)-based gel polymer electrolytes. *Ionics* **2013**, *19*, 1587–1593. [[CrossRef](#)]
29. Gregorio, R.; Borges, D.S. Effect of crystallization rate on the formation of the polymorphs of solution cast poly(vinylidene fluoride). *Polymer* **2008**, *49*, 4009–4016. [[CrossRef](#)]
30. Kuberský, P.; Hamáček, A.; Nešpůrek, S.; Soukup, R.; Vik, R. Effect of the geometry of a working electrode on the behavior of a planar amperometric NO₂ sensor based on solid polymer electrolyte. *Sens. Actuators B Chem.* **2013**, *187*, 546–552. [[CrossRef](#)]
31. Kuberský, P.; Sedlák, P.; Hamáček, A.; Nešpůrek, S.; Kuparowitz, T.; Šikula, J.; Majzner, J.; Sedlaková, V.; Grmela, L.; Syrový, T. Quantitative fluctuation-enhanced sensing in amperometric NO₂ sensors. *Chem. Phys.* **2015**, *456*, 111–117. [[CrossRef](#)]
32. Sedlák, P.; Kuberský, P.; Mívalt, F. Effect of various flow rate on current fluctuations of amperometric gas sensors. *Sens. Actuators B Chem.* **2019**, *283*, 321–328. [[CrossRef](#)]
33. Sedlák, P.; Kuberský, P. The Effect of the Orientation Towards Analyte Flow on Electrochemical Sensor Performance and Current Fluctuations. *Sensors* **2020**, *20*, 1038. [[CrossRef](#)] [[PubMed](#)]
34. Nespurek, S.; Mracek, L.; Kubersky, P.; Syrový, T.; Hamacek, A. Ionic liquids in electrochemical gas sensors and transistors. *Mol. Cryst. Liq. Cryst.* **2019**, *694*, 1–20. [[CrossRef](#)]
35. Nair, J.R.; Shaji, I.; Ehteshami, N.; Thum, A.; Diddens, D.; Heuer, A.; Winter, M. Solid Polymer Electrolytes for Lithium Metal Battery via Thermally Induced Cationic Ring-Opening Polymerization (CROP) with an Insight into the Reaction Mechanism. *Chem. Mater.* **2019**, *31*, 3118–3133. [[CrossRef](#)]
36. Jurado-Meneses, N.M.; Delgado-Rosero, M.I.; Meléndez-Lira, M.A. Structural and vibrational studies on composites polymer electrolytes (PEO)10CF₃COONa + x wt.% Al₂O₃. *Rev. Fac. Ing.* **2017**, *2017*, 43–49. [[CrossRef](#)]
37. Schaepe, K.; Jungnickel, H.; Heinrich, T.; Tentschert, J.; Luch, A.; Unger, W.E.S. Secondary ion mass spectrometry. In *Characterization of Nanoparticles: Measurement Processes for Nanoparticles*; Elsevier: Amsterdam, The Netherlands, 2019; pp. 481–509. ISBN 9780128141830.
38. Constantino, C.J.L.; Job, A.E.; Simões, R.D.; Simões, S.; Giacometti, J.A.; Zucolotto, V.; Oliveira, O.N.; Gozzi, G.; Chinaglia, D.L. Phase Transition in Poly(vinylidene fluoride) Investigated with Micro-Raman Spectroscopy. *Appl. Spectrosc.* **2005**, *59*, 275–279. [[CrossRef](#)]
39. Nallasamy, P. Vibrational spectroscopic characterization of form II poly(vinylidene fluoride). *IJPAP* **2005**, *43*, 821–827.
40. Peleš, A.; Aleksić, O.; Pavlović, V.P.; Djoković, V.; Dojčilović, R.; Nikolić, Z.; Marinković, F.; Mitrić, M.; Blagojević, V.; Vlahović, B.; et al. Structural and electrical properties of ferroelectric poly(vinylidene fluoride) and mechanically activated ZnO nanoparticle composite films. *Phys. Scr.* **2018**, *93*, 105801. [[CrossRef](#)]
41. Barnakov, Y.A.; Paul, O.; Joaquim, A.; Falconer, A.; Barnakov, V.Y.; Dikin, D.; Petranovskii, V.P.; Zavalin, A.; Ueda, A.; Williams, F.; et al. Nanoplasmonics: Past, present, and glimpse into future. *Int. J. Smart Nano Mater.* **2011**, *19*, 1–17.
42. Boccaccio, T.; Bottino, A.; Capannelli, G.; Piaggio, P. Characterization of PVDF membranes by vibrational spectroscopy. *J. Memb. Sci.* **2002**, *210*, 315–329. [[CrossRef](#)]
43. Elashmawi, I.S.; Gaabour, L.H. Raman, morphology and electrical behavior of nanocomposites based on PEO/PVDF with multi-walled carbon nanotubes. *Results Phys.* **2015**, *5*, 105–110. [[CrossRef](#)]
44. Kaspar, P.; Sobola, D.; Částková, K.; Knápek, A.; Burda, D.; Orudzhev, F.; Dallaev, R.; Tofel, P.; Trčka, T.; Grmela, L.; et al. Characterization of Polyvinylidene Fluoride (PVDF) Electrospun Fibers Doped by Carbon Flakes. *Polymers* **2020**, *12*, 2766. [[CrossRef](#)] [[PubMed](#)]
45. Kiefer, J.; Fries, J.; Leipertz, A. Experimental vibrational study of imidazolium-based ionic Liquids: Raman and infrared spectra of 1-ethyl-3-methylimidazolium bis(trifluoromethylsulfonyl) imide and 1-ethyl-3-methylimidazolium ethylsulfate. *Appl. Spectrosc.* **2007**, *61*, 1306–1311. [[CrossRef](#)]
46. Rey, I.; Johansson, P.; Lindgren, J.; Lassègues, J.C.; Grondin, J.; Servant, L. Spectroscopic and theoretical study of (CF₃SO₂)₂N-(TFSI)- and (CF₃SO₂)₂NH (HTFSI). *J. Phys. Chem. A* **1998**, *102*, 3249–3258. [[CrossRef](#)]
47. Lassègues, J.C.; Grondin, J.; Holomb, R.; Johansson, P. Raman and ab initio study of the conformational isomerism in the 1-ethyl-3-methyl-imidazolium bis(trifluoromethanesulfonyl)imide ionic liquid. *J. Raman Spectrosc.* **2007**, *38*, 551–558. [[CrossRef](#)]

48. Huang, H.C.; Yen, Y.C.; Chang, J.C.; Su, C.W.; Chang, P.Y.; Sun, I.W.; Hsieh, C.T.; Lee, Y.L.; Teng, H. An ether bridge between cations to extend the applicability of ionic liquids in electric double layer capacitors. *J. Mater. Chem. A* **2016**, *4*, 19160–19169. [[CrossRef](#)]
49. Xu, P.; Fu, W.; Cui, Z.; Ding, Y. Synergistic promotion of polar phase crystallization of PVDF by ionic liquid with PEG segment. *Appl. Surf. Sci.* **2018**, *444*, 480–484. [[CrossRef](#)]
50. Revathi, V.; Dinesh Kumar, S.; Chithra Lekha, P.; Subramanian, V.; Natarajan, T.S.; Muthamizhchelvan, C. Structural, dielectric, and magnetic studies on electrospun magnesium ferrite-polyvinylidene fluoride core-shell composite fibers. *Acta Metall. Sin.* **2014**, *27*, 557–562. [[CrossRef](#)]
51. Cai, X.; Lei, T.; Sun, D.; Lin, L. A critical analysis of the α , β and γ phases in poly(vinylidene fluoride) using FTIR. *RSC Adv.* **2017**, *7*, 15382–15389. [[CrossRef](#)]
52. Castkova, K.; Kasty, J.; Sobola, D.; Petrus, J.; Stastna, E.; Riha, D.; Tofel, P. Structure–properties relationship of electrospun pvdf fibers. *Nanomaterials* **2020**, *10*, 1221. [[CrossRef](#)] [[PubMed](#)]
53. Benz, M.; Euler, W.B. Determination of the crystalline phases of poly(vinylidene fluoride) under different preparation conditions using differential scanning calorimetry and infrared spectroscopy. *J. Appl. Polym. Sci.* **2003**, *89*, 1093–1100. [[CrossRef](#)]
54. Martins, P.; Lopes, A.C.; Lanceros-Mendez, S. Electroactive phases of poly(vinylidene fluoride): Determination, processing and applications. *Prog. Polym. Sci.* **2014**, *39*, 683–706. [[CrossRef](#)]
55. Xu, F.; Zhang, K.; Zhou, Y.; Qu, Z.; Wang, H.; Zhang, Y.; Zhou, H.; Yan, C. Facile preparation of highly oriented poly(vinylidene fluoride) uniform films and their ferro- and piezoelectric properties. *RSC Adv.* **2017**, *7*, 17038–17043. [[CrossRef](#)]
56. Mayerhöfer, T.G. Employing Theories Far beyond Their Limits—Linear Dichroism Theory. *ChemPhysChem* **2018**, *19*, 2123–2130. [[CrossRef](#)]
57. Arya, A.; Sharma, A.L. Structural, microstructural and electrochemical properties of dispersed-type polymer nanocomposite films. *J. Phys. D. Appl. Phys.* **2018**, *51*, 044504. [[CrossRef](#)]
58. Mejri, R.; Dias, J.C.; Hentati, S.B.; Martins, M.S.; Costa, C.M.; Lanceros-Mendez, S. Effect of anion type in the performance of ionic liquid/poly(vinylidene fluoride) electromechanical actuators. *J. Non. Cryst. Solids* **2016**, *453*, 8–15. [[CrossRef](#)]
59. Sa'Adun, N.N.; Subramaniam, R.; Kasi, R. Development and characterization of poly(1-vinylpyrrolidone-co-vinyl acetate) copolymer based polymer electrolytes. *Sci. World J.* **2014**, *2014*, 254215. [[CrossRef](#)] [[PubMed](#)]
60. Cha, S.; Ao, M.; Sung, W.; Moon, B.; Ahlström, B.; Johansson, P.; Ouchi, Y.; Kim, D. Structures of ionic liquid-water mixtures investigated by IR and NMR spectroscopy. *Phys. Chem. Chem. Phys.* **2014**, *16*, 9591–9601. [[CrossRef](#)]
61. Ponzio, E.A.; Echevarria, R.; Morales, G.M.; Barbero, C. Removal of N-methylpyrrolidone hydrogen-bonded to polyaniline free-standing films by protonation-deprotonation cycles or thermal heating. *Polym. Int.* **2001**, *50*, 1180–1185. [[CrossRef](#)]
62. Badruddoza, A.Z.M.; Bhattarai, B.; Suri, R.P.S. Environmentally Friendly β -Cyclodextrin-Ionic Liquid Polyurethane-Modified Magnetic Sorbent for the Removal of PFOA, PFOS, and Cr(VI) from Water. *ACS Sustain. Chem. Eng.* **2017**, *5*, 9223–9232. [[CrossRef](#)]
63. Hong, Y.; Fang, Y.; Sun, D.; Zhou, X. Ionic liquids modified cobalt/ZSM-5 as a highly efficient catalyst for enhancing the selectivity towards KA oil in the aerobic oxidation of cyclohexane. *Open Chem.* **2019**, *17*, 639–646. [[CrossRef](#)]
64. Hao, D.; Wang, X.; Liu, X.; Zhu, X.; Sun, S.; Li, J.; Yue, O. A novel eco-friendly imidazole ionic liquids based amphoteric polymers for high performance fatliquoring in chromium-free tanned leather production. *J. Hazard. Mater.* **2020**, *399*, 123048. [[CrossRef](#)]
65. Sobola, D.; Kaspar, P.; Částková, K.; Dallaev, R.; Papež, N.; Sedlák, P.; Trčka, T.; Orudzhev, F.; Kaštyl, J.; Weiser, A.; et al. PVDF Fibers Modification by Nitrate Salts Doping. *Polymers* **2021**, *13*, 2439. [[CrossRef](#)]
66. Greczynski, G.; Hultman, L. Compromising Science by Ignorant Instrument Calibration—Need to Revisit Half a Century of Published XPS Data. *Angew. Chem. Int. Ed.* **2020**, *59*, 5002–5006. [[CrossRef](#)] [[PubMed](#)]
67. Weber, I.; Kim, J.; Buchner, F.; Schnaidt, J.; Behm, R.J. Surface Science and Electrochemical Model Studies on the Interaction of Graphite and Li-Containing Ionic Liquids. *ChemSusChem* **2020**, *13*, 2589–2601. [[CrossRef](#)] [[PubMed](#)]
68. Göktürk, P.A. X-ray Photoelectron Spectroscopy for Chemical and Electrical Characterization of Devices Extended to Liquid/Solid Interfaces. Ph.D. Thesis, Bilkent University, Ankara, Turkey, 2018.
69. Seo, S.; Park, J.; Kang, Y.C. Chemical Analysis of Ionic Liquids Using Photoelectron Spectroscopy. *Bull. Korean Chem. Soc.* **2016**, *37*, 355–360. [[CrossRef](#)]
70. Höfft, O.; Bahr, S.; Himmerlich, M.; Krischok, S.; Schaefer, J.A.; Kempter, V. Electronic structure of the surface of the ionic liquid [EMIM][Tf 2N] studied by metastable Impact Electron Spectroscopy (MIES), UPS, and XPS. *Langmuir* **2006**, *22*, 7120–7123. [[CrossRef](#)] [[PubMed](#)]
71. Sim, D.M.; Han, H.J.; Yim, S.; Choi, M.-J.; Jeon, J.; Jung, Y.S. Long-Term Stable 2H-MoS₂ Dispersion: Critical Role of Solvent for Simultaneous Phase Restoration and Surface Functionalization of Liquid-Exfoliated MoS₂. *ACS Omega* **2017**, *2*, 4678–4687. [[CrossRef](#)]
72. Yakimchuk, E.; Volodin, V.; Antonova, I. New graphene derivative with N-methylpyrrolidone: Suspension, structural, optical and electrical properties. *Phys. Chem. Chem. Phys.* **2019**, *21*, 12494–12504. [[CrossRef](#)] [[PubMed](#)]
73. Briggs, D. Handbook of X-ray Photoelectron Spectroscopy C. D. Wanger, W. M. Riggs, L. E. Davis, J. F. Moulder and G. E. Muilenberg Perkin-Elmer Corp., Physical Electronics Division, Eden Prairie, Minnesota, USA, 1979. 190 pp. \$195. *Surf. Interface Anal.* **1981**, *3*. [[CrossRef](#)]
74. Souda, R. Phase transition of 1-ethyl-3-methylimidazolium bis(trifluoromethylsulfonyl)imide thin films on highly oriented pyrolytic graphite. *J. Phys. Chem. B* **2009**, *113*, 12973–12977. [[CrossRef](#)] [[PubMed](#)]

-
75. Bundaleski, N.; Caporali, S.; Chenakin, S.P.; Moutinho, A.M.C.; Teodoro, O.M.N.D.; Tolstogousov, A. Ion-induced fragmentation of imidazolium ionic liquids: TOF-SIMS study. *Int. J. Mass Spectrom.* **2013**, *353*, 19–25. [[CrossRef](#)]
 76. Günster, J.; Höfft, O.; Krischok, S.; Souda, R. A time-of-flight secondary ion mass spectroscopy study of 1-ethyl-3-methylimidazolium bis(trifluoromethylsulfonyl)imide RT-ionic liquid. *Surf. Sci.* **2008**, *602*, 3403–3407. [[CrossRef](#)]
 77. Feng, J.; Chan, C.M.; Weng, L.T. Influence of chain sequence structure of polymers on ToF-SIMS spectra. *Polymer* **2000**, *41*, 2695–2699. [[CrossRef](#)]

Conclusion

This habilitation thesis offers comprehensive conclusions for each individual chapter, available within the respective articles and summarized on the introductory pages preceding the articles. Therefore, rather than reiterating these details, it seems more fitting to present a concise, overarching conclusion for the entire thesis. For the detailed conclusion for each chapter the reader can refer to the corresponding article.

Thus, the work was divided into two parts. The first part is theoretical of several comprehensive review articles written and published by the applicant. It begins with an exploration of self-healing polymers and microcapsules (Article 1). The second article (Article 2) delves into the realm epoxy polymers and their applications in electronics. The last two articles in Part 1 (Article 3 and 4) focus on the properties and modifications of polyvinylidene fluoride (PVDF) and its usage of energy harvester. These last two article serve as a natural transition to Part 2, which is entirely dedicated to the experimental results on PVDF obtained over the years by the author and his team. These results have been systematically published in high-impact, open-access journals for maximum visibility. It is also worth mentioning that these experimental findings have garnered significant number of citations in a relatively short time and continue to guide new researchers in the field.

In conclusion, this habilitation thesis encompasses a comprehensive body of theoretical and experimental research focused on various polymer materials, with a primary emphasis on polyvinylidene fluoride (PVDF). Polymers remain an essential and indispensable component of modern society, and the ongoing interest in their development and application is poised to grow continuously. The extensive work presented here highlights the significant effort and dedication invested in advancing polymer science. This thesis stands as a testament to the applicant's contributions to the field, offering valuable insights and innovations that will drive further research and applications in polymer technology.

List of abbreviations

PVDF – polyvinylidene fluoride

XPS - X-ray Photoelectron Spectroscopy

SEM - Scanning Electron Microscopy,

XRD - X-ray Diffraction

SIMS - Secondary Ion Mass Spectroscopy

FTIR - Fourier Transform Infrared Spectroscopy

SEM-EDX - Scanning Electron Microscopy with Energy Dispersive X-ray Spectroscopy

SHMs - Self-healing Materials

ERs - Epoxy Resins

PENG - Piezoelectric Nanogenerators

TENG - Triboelectric Nanogenerator

CNTs - Carbon Nanotubes

DSC - Differential Scanning Calorimetry

SPEs - Solid Polymer Electrolytes

NMP - N-methyl-pyrrolidone

[EMIM][TFSI] - 1-ethyl-3-methylimidazolium bis(trifluoromethylsulfonyl)imide

Micro-courses for education to scanning probe microscopy

Talu S.

Technical University of Cluj-Napoca
Cluj-Napoca, 400020, Cluj county, Romania
E-mail: stefan_ta@yahoo.com

Sobola D.

Brno University of Technology, Faculty of Electrical
Engineering and Communication
Brno, 616 00, Czech Republic
E-mail: sobola@vutbr.cz

Dallaev R.S.

Brno University of Technology, Faculty of Electrical Engineering and Communication
Brno, 616 00, Czech Republic
E-mail: xdalla03@vutbr.cz

Abstract — This paper describes impact of micro-courses to education in the field of the nanoscience. The feature of the subjects which are related to nanoscience is the combination of new modern research methods and the foundations of physics and chemistry. While there are well-developed textbooks to study the fundamentals, it is necessary to refer to freshly written articles of scientists and data from technical sites. Rapidly developing fields demands flexible form of materials to study and an innovative change in the presentation of an online environment. Here we consider education to scanning probe microscopy techniques in terms of micro courses. This type of microscope is became an important tool for three dimensional surface studies with nanoscale resolution.

Keywords — teaching, studying, nanoscience, micro-course

I. INTRODUCTION

The widespread introduction of high technologies and the openness of the learning process are gaining more and more space in the higher education, in order to develop of highly complex knowledge structures, generic skills as well as transferability of knowledge and skills to future professional work [1-3]. The trend of the modern learning process, for the effective assimilation of material along with classical teaching, a strong place is occupied by micro-courses [4].

The micro-course concept is aimed at obtaining and fixing certain knowledge and skills by the student, being an instrument of internal learning. The step-by-step constructed algorithm will allow to optimize the learning tasks to a greater extent, to structure the information contained in this micro-course of microscopy. The volume course of the training material is given in small doses, one topic is one course, which simplifies the control over the assimilation of the educational material. The time allotted for the video lesson or short lecture is from 5-10 minutes, it is the time interval when the concentration is maximum, hence the probability of obtaining a satisfactory result is high. A logically constructed chain consisting of a set of interrelated topics, with the correct design of the curriculum, creates favorable conditions for memorization.

Efficient SPM education involves wide range of activities from operator-level problem solving to training specialist for research activities. Currently, there are a large number of manufacturers of the microscopes. The scope of microscopy provides ample opportunity to study nanostructures. In addition to high-quality and quantitative surface analysis, modern microscopes are equipped with additional devices for modifying and engineering the surface of samples. Students need to understand the advantages and limitations of the applicability of the technologies introduced in the market for SPM microscopes. Considering specificity of this modern field of study, new education methods should be applied in order to fulfill expectations of future employee [5].

II. MOTIVATION FOR IMPLEMENTATION OF MICRO-COURSES

Students will constantly remember what they learned earlier, and receive new information. New information will be placed on a newly formed database and be perceived much more efficiently [2].

The motivation for micro-studying is relevant factors such as: visibility and availability of the material, saving time, choice of the level of training, the opportunity to learn without interrupting work, learning small parts is easier, availability (using different types of communication, regardless of location); no dependence on external circumstances; unlimited viewing; visual memory is involved. As part of the implementation of adaptive learning using micro-course, it is important to cover all the issues: how the program is arranged, the conditions for switching from one module to another, how long it will take. The main aspect is full transparency as you progress through the course of the program, the ability to display progress in the percentage or percentage ratio, which is a stimulating factor in mastering the material.

In one video lesson, a lot of information is concentrated, which is perceived, both visually and by ear, which is very effective. With the video material everyone can learn and everything is basically clear.

III. DESIGN OF MICRO-COURSES IN MICROSCOPY TEACHING

The scanning probe microscopy can be applied to various problems in a wide range of disciplines of the natural sciences, including solid-state physics, semiconductor science and technology [6-8], molecular engineering, polymer chemistry and physics [10, 11], surface chemistry [12-14], surface science [15-17], molecular biology, cell biology [18], and biomedical sciences [9, 10].

SPM is a physical interaction of a fine probe/tip with the surface of the sample to scan the surface and collect data, typically obtained as a two-dimensional grid of data points and displayed as a computer image. Teaching to SPM is complicated by the fact that this area is located at the intersection of scientific fields: engineering, fundamental science, processing of graphics. It is necessary to design the education process for teaching the student to work with the equipment, to understand the physical basis of the surface scanning and accurately process the data for extraction maximum reliable information.

The main principle in the choice of educational material for microscopy, in particular, scanning probe microscopy, is the relevance of topics and their accessibility in the understanding of the material being studied (for examples: probe-sample interface, electronics for detection of the probe-sample interaction, etc.). The concept of quality of activity includes following aspects: easy assimilation of the material; high learning efficiency at relatively low loads; ease of perception of the material. According to [4] the design of micro-coursed should contain following elements: time, objective, content, method and technology.

Modules of micro-education should contain small practical tasks that help in fixing basic and new acquired knowledge. Video course, as a visual way of information transfer, greatly facilitates the learning process and the formation of the knowledge base, which makes it easier to do self-education. With video courses, the students can learn anywhere from their mobile devices: laptops, tablets or smartphones. The video contains a maximum of useful information. To periodically monitor the assimilation of educational material and consolidate the acquired knowledge, a successful methodological tool is testing.

IV. TIME ALLOCATION FOR SPM TEACHING

An important aspect of micro-course design is the distribution of the teaching time across theoretical education and practical activities.

Visual illustration is important for quick perception of information. The use of interactive presentations reduces the operation time of expensive equipment. The alternation of teaching methods: practice in the laboratory, lectures, interactive web pages, can improve the effectiveness of training. Student can pass independently through chosen theoretical parts of education material and it saves the time of the teacher.

Education time in the case of micro-courses implies its most effective use on the principle: better to keep maximum attention for a short time than to absentmindedly observe for a long time. As a result, there is a variation of studying activities during the education process.

Presence of easy-operating microscopes and accessories for demonstration of basic principles makes learning interesting and not time-consuming. Internet resources provide information about processes at the nanoscale level [19, 20] for their easier perception. Available free software (Gwyddion, ImageJ, etc.) have a number of YouTube tutorials which demonstrate data processing. Teaching model based on micro-courses implies that after determine the gaps in knowledge the student can devote more time to incomprehensible problems at any step.

V. AIMS AND OBJECTIVES OF SPM TEACHING

It was mentioned by R. Blonder et al. [21] that atomic force microscopy (which is one member of SPM group) attracted a lot of attention being "excitement of exploring matter at the nanoscale". Besides this possibility of imaging the nano-topography, SPM is important of surface visualization and modification in various scientific files.

One of the main objectives of SPM teaching is explanation of correlation between SPM data and surface properties.

The basic concepts of physics and chemistry of surface in nanoscale should be explained. The aim of SPM teaching using micro courses can cover more than one SPM technique in dependence of specialization field (physics, biology, chemistry, material science). Most set-ups with they native software allows students to carry out following standard procedures: preparation to measurements: exchange of the probe, fix of the sample; measuring the samples: navigation using optical system (could be build-in optical microscope), trying different techniques (atomic force microscopy, scanning tunneling microscopy, scanning near-field optical microscopy, spectroscopy methods, etc.), trying scanning parameters (scanning rate [16], area, direction, etc.); processing of the results: evaluation of spectroscopy data; estimation of the physical values (in case of electrical, mechanical, optical measurements), image processing and extraction quantitative data (statistical data, filtering, fractal analysis [12, 14], etc.)

SPM measurements should also provide insight to features and peculiarities of the other studies in nanometer and angstrom scale. For example, the quality of the received data (images, spectroscopic data, and lithography) is influenced by external and internal noises. External noises include mechanical and acoustic vibrations of the building, ventilation, classroom conversations, electro-acoustic noise (power lines in walls, mobile phones). Internal noise is associated with the presence of mechanical and electrical elements of the microscope and depends on the instrument configuration. As every education, the SPM-teaching has the aim to provide sufficient information support for preparation well-skilled students. For this purpose, the feedback of the students should be considered. Module character of micro-courses makes them flexible and has advantages for improving quality of education.

VI. CONTENT OF MICRO-COURSES FOR SPM TEACHING

Since SPM has a great application potential from ordinary scanning of surface topography to surface modification, it is necessary to make a right choice of the measurement (or engineering) technique. Study of the principles should begin from the physical fundamentals of interaction between probe and sample surface. A set of micro-coursed at this step should

include such concepts as inter-atomic interaction (for atomic-force microscopy), tunneling effect (for scanning tunneling microscopy), wave properties of light (for scanning near-field optical microscopy), etc. On the basis of this background the specific of the suitable type of SPM should be investigated in details: choice of probes, sample preparation, conditions of measurements. Various types of SPM needs its own preparation procedure and demands in order to provide correct and reliable data.

The micro-courses of this level should include study of the probes characteristics, the methods of samples processing before measurements. Following familiarization with the tool and its software applications are aimed to demonstrate the measurements in practice. In spite the similar physical principles, the existing types can differ a lot in operation way.

A number of micro-courses should be concentrated on description of the set-up, software of the microscope, necessary safety instructions. The special areas of this field are evaluation of results and processing of the data. In case of competent approach the important conclusions can be done.

The micro-courses should be oriented on description of possible artifacts of measurements and elimination of their negative effects and at the same time they should teach to extract maximum of useful information about the studied surface (at both visual and numeric style).

VII. ADVANCED METHODS OF SPM TEACHING

Noting the advantages of micro courses for the training of specialists in the field of SPM, it is also worth to mention that micro-courses can be used by students at any stage of education, and also act as an independent single training program.

The integrity and consistency of a teacher's activities combined with the comprehensible hierarchy of the topics provided to students ensure achievement of the desired result. Already at the initial stages of the teaching process, a forecast for further actions and potential corrections can be made. Methods can be divided into following categories:

- Preparation - the use of micro-courses before the start of basic training - involvement into the motivational process (videos, explanation of the fundamental laws on the basis of which the microscope principle is laid down).

- Focusing - is an addition to the basic training (working on specific tasks in the laboratory and processing the data obtained).

- Consolidation - consolidation of the received information, skills and knowledge (through independent work on the instrument).

Micro-courses provide both psychological comfort (stress states are minimized) and create favorable conditions for the educational process with maximum independence in an environment of realizable possibilities (temporal, physical, physiological).

The choice of optimal teaching methods is carried out by taking into account the total amount of all intermediate decisions: principles, goals and specifics of this discipline, as a result of which knowledge transfer, reinforcement of skills, and expected learning outcomes are ensured. In this regard,

micro-courses are very effective for teaching microscopy, their format simplifies knowledge transfer from person to person and delivers information to a user in small pieces that can act as independent elements, while being at the same time integrated into a common training strategy. Micro courses are also advantageous as regards to time and budget, what is especially important given the expensive equipment and the need for preliminary preparation of students for measurements.

VIII. TECHNOLOGY OF SPM EDUCATION

Not only are the content of the course, supported by appropriate methods, but also the technology of the courses preparation of great importance. The fundamental strategy of micro courses is 100% implementation of goals and objectives, consolidation of the material, the introduction of knowledge and skills in the field of nanotechnology. The proper implementation and use of micro-courses are achieved when their form (content) and the way of their introduction (techniques) are conducive to the desire to be trained in techniques of microscopy.

Educational technologies by using methods, forms, tools and techniques are always focused on the implementation of the pedagogical process with a guaranteed result.

The development of a micro-course strategy consists in:

- setting goals with an emphasis on clarity - course content is dosed;
- accessibility – speed and accessibility to any section of the course;
- evaluation - assessment of how well the given information is internalized (by doing of tasks or taking tests);
- multimedia ways of presenting material;
- use of mobile devices;
- breaking into blocks and combining microcourses into a single unit.
- The format of micro-courses taking into account modern technologies provides optimal and rational opportunities for both students and teachers:
- For students:
 - Concentration - the micro-course is presented as a micro lesson (10-15 minutes), during such a short period of time the learning efficiency is at its maximum. It also allows more students to make measurements independently and with high quality.
 - Web Surfing - each lesson of each course has a link to a micro-course, which is a detailed version of this lesson.
 - Budget and time - on the one hand, a person gets the opportunity to pay only for the knowledge he needs, on the other - not to waste time in case the course has not met expectations.
- For teachers:
 - Easy creation of micro-courses - free and fast.

- Informativeness – micro-courses can be edited, improved and adapted to user expectations.
- Income generation - (paid courses).

IX. CONCLUSION

Interdisciplinary fields need special design of education which includes modern technologies. Nanotechnology covers a wide range of engineering and science. Micro-courses are suitable approach to reach high academic level. Here we describe possible application of micro-courses for education to SPM. This methodology could be applied for other parts of education to nanotechnology. Such, single-topic parts of image processing procedures could be independently applied to a number of visualization techniques. Advanced design of micro-course ensures better understanding of the studying material at short time. The micro-courses are supposed to be useful for education of modern fast developing occupations.

Acknowledgment

Research described in the paper was financially supported by the National Sustainability Program under Grant LO1401. For the research, infrastructure of the SIX Center was used.

References

- [1] <https://kurso.ru/blog/e-learning/>.
- [2] E. Tikhomirova, *Live Learning: What is e-learning and how to make it work* / Elena Tikhomirova - M.: Alpina Publisher, 2016. p. 44.
- [3] R. Donnelly, and F. McSweeney, *Applied E-Learning and E-Teaching in Higher Education*, IGI Global: London, UK, 2009, pp. XVII.
- [4] Hong-yan Shen, "Teaching design factors for micro-courses of specialized courses in university". 2017 4th International Conference on Advanced Education Technology and Management Science (Proceedings AETMS 2017). ISBN: 978-1-60595-489-9. Pp. 34-37.
- [5] Ș. Țălu, D. Sobola, and N. Papež, "Analysis and recommendations for education process of experts in the field of scanning probe microscopy". *DEStech Transactions on Social Science, Education and Human Science*, p. 5-9, 2017. ISSN: 2475-0042. Proceedings AETMS 2017 (2017 4th International Conference on Advanced Education Technology and Management Science, September 17-18, 2017, Shenzhen, China). ISBN: 978-1-60595-489-9.
- [6] Ș. Țălu, D. Sobola, S. Solaymani, R. Dallaev, and J. Brüstlová, "Scale-dependent choice of scanning rate for AFM measurements". *DEStech Transactions on Computer Science and Engineering*, p. 453-459, 2018. DOI: 10.12783/dtscse/cnai2018/24197. ISSN: 2475-8841. Proceedings CNAI 2018 (2018 International Conference on Communication, Network and Artificial Intelligence, April 22-23, 2018, Beijing, China). ISBN: 978-1-60595-065-5.
- [7] Ș. Țălu, D. Sobola, N. Papež, R. Dallaev, and P. Sedlák, "Efficient processing of data acquired using microscopy techniques". *DEStech Transactions on Social Science, Education and Human Science*, p. 202-207, 2018. DOI: 10.12783/dtssehs/amse2018/24838. ISSN: 2475-0042. Proceedings AMSE 2018 (2018 2nd International Conference on Advances in Management Science and Engineering, June 24th-25th, 2018, Xi'an, China). ISBN: 978-1-60595-566-7.
- [8] Ș. Țălu, *Micro and nanoscale characterization of three dimensional surfaces. Basics and applications*. Napoca Star Publishing House, Cluj-Napoca, Romania, 2015.
- [9] Ș. Țălu, and S. Stach, "Multifractal characterization of unworn hydrogel contact lens surfaces". *Polym Eng Sci.*, vol. 54(5), pp. 1066-1080, 2014. DOI: 10.1002/pen.23650.
- [10] Ș. Țălu, "Characterization of surface roughness of unworn hydrogel contact lenses at a nanometric scale using methods of modern metrology". *Polym Eng Sci.*, vol. 53(10), pp. 2141-2150, 2013. DOI: 10.1002/pen.23481.
- [11] S. Ramazanov, Ș. Țălu, D. Sobola, S. Stach, and G. Ramazanov, "Epitaxy of silicon carbide on silicon: Micromorphological analysis of growth surface evolution", *Superlattices Microstruct.*, vol. 86, pp. 395-402, 2015. DOI: 10.1016/j.spmi.2015.08.007.
- [12] D. Dallaeva, Ș. Țălu, S. Stach, P. Škarvada, P. Tománek, and L. Grmela. "AFM imaging and fractal analysis of surface roughness of AlN epilayers on sapphire substrates". *Appl. Surf. Sci.*, vol. 312, pp. 81-86, 2014. DOI: 10.1016/j.apsusc.2014.05.086.
- [13] S. Stach, D. Dallaeva, Ș. Țălu, P. Kaspar, P. Tománek, S. Giovanzana, and L. Grmela, "Morphological features in aluminum nitride epilayers prepared by magnetron sputtering", *Mater. Sci.- Poland*, vol. 33, pp. 175-184, 2015. DOI: 10.1515/msp-2015-0036.
- [14] Ș. Țălu, S. Stach, D. Raoufi, and F. Hosseinpanahi. "Film thickness effect on fractality of tin-doped In₂O₃ thin films". *Electron. Mater. Lett. Vol. 11*, pp. 749-757, 2015. DOI: 10.1007/s13391-015-4280-1.
- [15] Ș. Țălu, S. Stach, S. Valedbagi, S.M. Elahi, and R. Bavadi, "Surface morphology of titanium nitride thin films synthesised by DC reactive magnetron sputtering", *Mater. Sci.- Poland*, vol. 33, pp. 137-143, 2015.
- [16] D. Sobola, Ș. Țălu, S. Solaymani, and L. Grmela, Influence of scanning rate on quality of AFM image: Study of surface statistical metrics, *Microsc. Res. Tech.* 80, pp. 1328-1336, 2017. DOI: 10.1002/jemt.22945.
- [17] Ș. Țălu, N. Papez, D. Sobola, A. Achour, and S. Solaymani, "Micromorphology investigation of GaAs solar cells: case study on statistical surface roughness parameters". *J Mater Sci-Mater El.*, vol. 28(20), pp. 15370-15379, 2017. DOI: 10.1007/s10854-017-7422-4.
- [18] Ș. Țălu, I.A. Morozov, D. Sobola, and P. Škarvada, "Multifractal Characterization of Butterfly Wings Scales". *Bull Math Biol.*, vol. 80(11), pp. 2856-2870, 2018. DOI: 10.1007/s11538-018-0490-7.
- [19] NT-MDT. Available <https://www.ntmdt-si.com/resources/spm-principles> (last accessed 10th January 2019).
- [20] nanoHUB Home Page. <https://nanohub.org/> (last accessed: 10th January 2019).
- [21] R. Blonder, E. Joselevich, and S. R. Cohen, "Atomic Force Microscopy: Opening the Teaching Laboratory to the Nanoworld". *Chemical Education Today*, vol. 87(12), pp. 1290-1293, 2010. DOI: 10.1021/ed100963z.

Applicant's CV

Mgr. et Mgr. Rashid Dallaev, Ph.D.

Date of birth: 22.07.1994

Languages: English, Czech, Russian

Phone: +420 777 828 938

E-mail: rashid.dallaev@vut.cz

1. EDUCATION AND QUALIFICATION:

Dagestan State University, Makhachkala, Russian Federation

- 1st master degree "Organic chemistry" (2008-2013),
- 2nd master degree "Analytical chemistry" (2013-2015),
- Doctoral (C.Sc.) study (2016-2017). Field: Condensed matter physics. Unfinished, transferred to BUT

Brno University of Technology, Brno, Czech Republic

- Doctoral (Ph.D.) study (2017-2021). Field: Microelectronics and technology

2. EMPLOYMENT HISTORY:

- Dagestan State University (2011-2012) laboratory assistant
- Brno University of Technology, Brno, Czech Republic (from 2020-2021) technical worker.
- Brno University of Technology, Brno, Czech Republic (from 2021 - present) scientific worker, researcher.

3. PROFESSIONAL PRACTICE, INTERNSHIPS, SOLVED SCIENTIFIC PROJECTS:

Professional skills:

Deposition techniques (ALD, CVD), thin film preparation, ion-beam analysis (ERDA, RBS), materials characterization by XPS, SIMS, SPM, AFM. Polymer materials, PVDF.

Internships abroad:

- Sweden, Uppsala university. Period: 10.20.2020 → 25.11.2020
Doctoral internship. The purpose of the stay was investigation of hydrogen impurities in AlN thin films prepared by atomic layer deposition method using ion beam analyses (NRA, ERDA, RBS).
- Ljubljana, Slovenia. Joseph Stefan Institute. Period: 06.06.2022-06-06 → 12.12.2022
Postdoctoral mobility within MEMOV II project. The purpose of the stay was investigation of hydrogen concentration in solid materials such as nitinol (alloy of titanium and nickel) and highly oriented pyrolytic graphite (HOPG) using IBA (ion beam analysis) methods.

Participation in research projects in Czech Republic:

- Advanced characterization of materials for sensors and electric power generators (FEKT-S-20-6352). Start: 03.01.2020, End: 02.28.2023.

Teaching experience:

- Laboratory classes of physics for czech and foreign (in English) bachelor students. (7 years)
- Lectures, numerical and computer exercises in physics for foreign students (2 years). In English.

Research activities for last 5 years:

The bulk of my research expertise lies in materials science field. During my scientific career I have had full access to the state-of-the art cleanrooms of CEITEC Nano Research Infrastructure. CEITEC is a modern research center equipped with a great number of advanced tools for materials fabrication and characterization with which I had to work on a regular basis (XPS, AFM, SEM, FTIR, SIMS etc.). Furthermore, I gained additional experience during my stays abroad at such renowned research facilities as Tandem Laboratory (Uppsala University, Sweden) and Joseph Stefan University (Ljubljana, Slovenia) where I worked with techniques utilizing high-energy particle accelerator to study materials composition. My early research endeavors had to do with deposition techniques for obtaining thin layers of semiconductive materials and their following characterization. Lately, however, my interests have expanded to include various polymeric materials, their synthesis, modifications and characterization.

SCIENTIFIC METRICS

H-index: 14;
Scientific publications: 38;
Citation count (Scopus): 622;
Attended conferences (offline and online): 22;
Peer reviews: 10

INTERNATIONAL COOPERATION

During my scientific career at BUT I spent a good amount of time abroad whether on long-term stays or conferences. During my time abroad I worked closely with foreign colleagues in state-of-the art laboratories (e.g. Tandem laboratory in Sweden) to produce high quality results which were subsequently published. I also work on a long-term basis with assoc. Prof. Ștefan Țălu from Romania, our cooperation had produced numerous publications in the last several years.

LINKS

SCOPUS: <https://www.scopus.com/authid/detail.uri?authorId=57201461813>

WoS: <https://www.webofscience.com/wos/author/record/1948134>

ORCID: <https://orcid.org/0000-0002-6823-5725>

RG: <https://www.researchgate.net/profile/Rashid-Dallaev>